



Saurashtra University

Re – Accredited Grade 'B' by NAAC
(CGPA 2.93)

Chauhan, Chetankumar K., 2011, “*Growth and Characterization of struvite and related crystals*”, thesis PhD, Saurashtra University

<http://etheses.saurashtrauniversity.edu/id/879>

Copyright and moral rights for this thesis are retained by the author

A copy can be downloaded for personal non-commercial research or study, without prior permission or charge.

This thesis cannot be reproduced or quoted extensively from without first obtaining permission in writing from the Author.

The content must not be changed in any way or sold commercially in any format or medium without the formal permission of the Author

When referring to this work, full bibliographic details including the author, title, awarding institution and date of the thesis must be given.

Saurashtra University Theses Service
<http://etheses.saurashtrauniversity.edu>
repository@sauuni.ernet.in

© The Author

**GROWTH AND CHARACTERIZATION OF STRUVITE
AND RELATED CRYSTALS**

**Thesis submitted to the
SAURASHTRA UNIVERSITY**

For

**The award of the degree of
DOCTOR OF PHILOSOPHY**

in

PHYSICS

by

CHETANKUMAR KANUBHAI CHAUHAN

(M. Sc., M.Ed.)

Guided by

Dr. M. J. Joshi

Professor

Department of Physics,

Saurashtra University,

Rajkot – 360 005

October 2011

Statements Under O.Ph.D. 7 of Saurashtra University

The contents of this thesis is my own work carried out under the supervision of ***Dr. M. J. Joshi*** and leads to some contributions in Physics supported by necessary references.

(Chetankumar K. Chauhan)

This is to certify that the present work submitted for Ph. D. Degree in Physics of the Saurashtra University, Rajkot, by ***Mr. Chetankumar Kanubhai Chauhan*** has been the result of about five years of work under my supervision and is a valuable contribution in the field of “Solid State Physics and Materials Science”.

(Dr. M. J. Joshi)
Professor
Department of Physics
Saurashtra University
Rajkot, 360 005

अन्ति सन्तं न जहात्यन्ति सन्तं न पश्यति !
देवस्य पश्य काव्यं न ममार न जीर्यति !!

अथर्ववेद १० - ८ - ३२

Let us visualize,

The poetic creation of God.

He is so near,

Nobody can leave Him.

He is so near,

Nobody can see Him.

Even though His poetic creation,

Never dies or decays...!

Atharva Veda 10 – 8 – 32

Dedicated
to
My Beloved Family

ACKNOWLEDGEMENT

First and foremost the author is heartily thankful to the **Almighty God** for the abundant blessings and special providence fell through his work. The author expresses his deep sense of gratitude and sincere thanks to his enthusiastic guide **Dr. Mihir J. Joshi**, Professor, Department of Physics, Saurashtra University, Rajkot, who introduced him to the field of "*Crystal Growth*" particularly, in the multidisciplinary research work on urinary type struvite crystals which requires integrating data, theories, methodologies, perspectives, and concepts from multiple disciplines like physics, chemistry, material science, mineralogy, life sciences, botany, *ayurveda*, pharmacology, and medicine as well. **Dr. Joshi** has not only guided him in the most profound manner with continuous encouragement, inspiration and love with close family touch during entire course of the work but also enlightened the author through his wide knowledge of intelligence and has certainly played a major role to inculcate authors scientific career and in a true sense shaped author as a true researcher...! Author appreciates all his contributions of time, ideas, and constructive comments, to make Ph.D. experience fruitful and stimulating.

The author is highly indebted to **Prof. Hiren H. Joshi**, Head, Physics Department, Saurashtra University, Rajkot, and the former head of the Department **Prof. K. N. Iyer** for their keen interest and providing the necessary facilities to work at the Crystal Growth Laboratory in the Department of Physics.

The author expresses his sincere thanks to other faculty members of the Physics Department **Prof. H. P. Joshi**, **Prof. D. G. Kuberkar**, **Dr. G. J. Baldha**, **Dr. K. B. Modi** and **Dr. J. A. Bhalodia**, for their kind help and cooperation during the experimental work.

The author wishes to express his gratitude to **Prof. B. S. Shah**, **Prof. B. J. Mehta**, **Dr L. K. Maniar**, **Dr R. M. Vaishnav**, **Dr S. G. Nene**, **Dr R. J. Bhayani** for providing motivation to do research work at the very initial stage and also whole hearted wishes and encouragements during the entire work.

The author expresses his gratitude towards **Dr A. D. B. Vaidya** (Kasturba Health Society, ICMR Advanced Center for Reverse Pharmacology in Traditional Medicine, Mumbai), **Prof. Vrinda Thakar** (Bioscience Department, Rajkot) for fruitful discussions for the experimental work in the early stage and **Prof. H. S. Joshi** (Chemistry Department, Rajkot) for various experimental help.

The author is thankful to **Smt. Jayanti S. Ravi, Commissioner of Higher Education**, Commissionerate of Higher Education (CHE), Gandhinagar, Gujarat for providing not only the encouragement to carry out extensive research work but also providing motivation to participate in the international conferences and felicitate by providing a certificate of appreciation. The author is also thankful to the **Department of Education**, Government of Gujarat, for providing NOC to participate the international conferences abroad.

The author is also thankful to the University Grants Commission (**UGC**), New Delhi, Department of Science and Technology (**DST**), New Delhi and Council of Scientific and Industrial Research (**CSIR**), New Delhi for providing financial assistance to participate in the international conferences **ICMAT-2009** at **Singapore**, **ICCG-2010** at **Beijing** and **ICMAT-2011** at **Singapore**, respectively.

The author is grateful to his senior research colleagues of “Crystal Growth Laboratory” namely **Dr. V. S. Joshi** (Principal, Science College, Petlad), **Dr. R. M. Dabhi** (Virani High-school, Rajkot), **Dr. K. C. Joseph** (St Xavier’s School, Jamnagar), **Dr. B. B. Parekh** (Pt. Deendayal Petroleum University, Gandhinagar), **Dr. S. R. Suthar** (Science College, Mehsana), **Dr. H. J. Pandya**, **Dr. S. J. Joshi** (Head, Physics Department, Bahauddin Science College, Junagadh), **Mr. D. J. Dave** (M. N. Virani Science College, Rajkot), **Dr. K. D. Parikh** (M. P. Shah Arts and Science College, Surendranagar) and also the present co-workers **Mr. Poorvesh M. Vyas**, **Ms. Kashmira J. Tank**, **Ms. Sonal R. Vasant**, **Mr. Rakesh R. Hajiyani**, **Mr. Ravindra Gohel**, **Mr. Ravi Mansuria** and **Mr. Hiren Jani**, for their friendly support and kind cooperation throughout the research work. The author wishes his special gratitude to his senior colleague **Dr. Bharat B. Parekh** for designing the experiments in the early initial stages. Author also expresses his thanks to workshop staff as well as non-teaching staff and the office staff of the Physics Department for their kind cooperation.

The author also extends his sincere thanks to **Dr. R. A. Agarwal**, Principal, H. & H. B. Kotak Institute of Science, Rajkot for providing motivation during the course of work. Author is also thankful to former incharge Principals, **Mr. H. P. Buch** and **Mr. N. T. Chotaliya** – especially for providing motivation to participate at ICMAT-2009 and also for helping to solve the troubleshooting in his PC during the course of work. Author is also thankful to his colleagues in Physics Department, H. & H. B. Kotak Institute of Science, namely, **Dr. R. K. Trivedi**, **Dr. K. H. Jani**, **Dr. P. B. Vala**, **Mr R. B. Rupapara**, **Ms M. J. Modi**,

Mr. V. K. Lakhani, Mr N. Y. Vyas, Mr V. M. Sanghani, Mr. R. G. Ramanuj and Mr. J. N. Dave for their encouragements. Author also extends thanks to **Mr. D. J. Bhatt**, Librarian for providing library and extension facilities and all the colleagues at H. & H. B. Kotak Institute of Science, Rajkot.

The author also expresses his heartfelt gratitude towards the parents of his guide – **Mr. Janakrai Joshi (Dadaji)** and **Ba** for their wholehearted blessings. Author can not forget the moral support provided by his Guide's better-half **Mrs. Shilpa M. Joshi**, and daughter **Ms Krutika M. Joshi** and the whole family of his guide for the moral support and the affection throughout the work.

Finally, Last but not least, author would like to express his love and appreciation to his near and dear family members - a powerful source of inspiration and energy, to whom this thesis is dedicated, for their years of sacrifices and lots of prayers. The author heartily expresses his gratitude to his beloved parents **Mr. Kanubhai L. Chauhan** and **Late Hansaben Chauhan**. Especially a big thanks to his wife **Mrs. Vaishali Chauhan** and son **Drumil** who have supported his desire to embark on a Ph. D. and provided unending moral support, great patience at all the times and love, without which it was difficult to culminate this research work. Author shall endeavour to make up for all the lost vacations as well as week-ends ...! Author is also thankful to his both sisters and brother in law - **Sonal & Hemendrakumar, Bharti & Parimalchandra** and his cute niece **Bhavya** for providing inspiration and also for bearing his un-availability and negligence towards them throughout the work. Author is also thankful to his sisters for gifting him a nice Laptop and a portable hard disk to carry out work uninterruptedly.

Completion of this research work and the writing of this thesis on a part time basis has been a real challenge for the author without sacrificing day to day classroom teaching and laboratory work, and also any administrative work assigned by the college principal and higher authorities at CHE, Gandhinagar.

Perhaps, if author forgot someone to acknowledge... so, just in case: thank you to whom it concerns...! For any errors or inadequacies that may remain in this work, of course, is the solely responsibility of author.

Chetankumar K. Chauhan

Rajkot.

October 2011.

Content

Chapter Number	Name of Chapter	Page Number
	<i>Certificate</i> (<i>Statements Under O.Ph.D. 7 of Saurashtra University</i>)	(i)
	<i>Acknowledgement</i>	(iv)
	<i>Abbreviations</i>	(viii)
	<i>Abstract</i>	(x)
I	General Introduction	1
II	Brief Review on Urinary Calculi	28
III	Crystal Growth Technique	113
IV	Characterization Techniques	162
V	Growth and Characterization of Struvite	202
VI	Growth Inhibition Study of Struvite	245
VII	Vickers Micro-hardness and Etching Study of Struvite	308
VIII	Growth and Characterization of Struvite Family Crystals	361
IX	Conclusions	398
Annexure 1	Research Paper Publication	412
Annexure 2	Research Paper Presentation	414
Annexure 3	Research Papers	417

Abbreviations

ADP	Ammonium Dihydrogen Phosphate
AFM	Atomic Force Microscopy
AHA	Aceto-Hydroxamic Acid
AKI	Acute Kidney Injury
AMPH	Ammonium Magnesium Phosphate Hexahydrate
ANN	Artificial Neural Network
ANOVA	ANalysis Of Variance
AR	Analytical Reagent
ASTM	American Society for Testing and Materials
ATR	Attenuated Total Reflectance
BMI	Body Mass Index
BPH	Benign Prostatic Hypertrophy
BSM	Binocular Stereoscopic Microscopy
CKD	Chronic Kidney Disease
CNMNC	Commission on New Minerals, Nomenclature and Classification
COD	Calcium Oxalate Dehydrate
COLA	Cystine, Ornithine, Lysine, and Arginine
COM	Calcium Oxalate Monohydrate
COT	Calcium Oxalate Trihydrate
CSTR	Continuously Stirred Tank Reactor
CT	Computed Tomography
DDTA	Derivative Differential Thermal Analysis
DETA	Dielectric Thermal Analysis
DMA	Dynamic Mechanical Analysis
DRIFTS	Diffuse Reflectance Infrared Fourier Transform Spectroscopy
DSC	Differential Scanning Calorimetry
DSI	Depth-Sensing Indentation
DSM/NC	Differential Scanning Micro / Nano Calorimetry
DTA	Differential Thermal Analysis
DTG	Derivative Thermo-Gravimetry
EDAX	Element Distribution Analysis
Eds	Emergency Departments
EDTA	Ethylene Diamine Tetra Acetic Acid
EGA	Evolved Gas Analysis
EGD	Evolved Gas Detection
EHL	Electro-Hydraulic Lithotripsy
ESWL	Extracorporeal Shock Wave Lithotripsy
FT-IR	Fourier Transform Infrared Spectroscopy
HA	Hydroxyapatite
ICTAC	International Confederation for Thermal Analysis and Calorimetry

IMA	International Mineralogical Association
ISE	Indentation Size Effect
IUPAC	International Union of Pure and Applied Chemistry
IVP	Intravenous Pyelogram
IVU	Intravenous Urogram
JCPDS	Joint Committee of Powder Diffraction Standards
KDP	Potassium Dihydrogen Phosphate
KUB	A Plain X-Ray Of Kidneys, Ureter, and Bladder
LCR	Inductance, Capacitance and Resistance
MRI	Magnetic Resonance Imaging
MSUM	Mono-Sodium Urate Monohydrate
NHANES	National Health and Nutrition Examination Surveys
OPN	Osteopontin
PCNL	Percutaneous Nephrolithotomy
PEO	Polyethylene Oxide
PLS	Partial Least Squares
PMPH	Potassium Magnesium Phosphate Hexahydrate
PSR	Proportional Specimen Resistance
RBC	Red Blood Cells
RTA	Renal Tubular Acidosis
SEM	Scanning Electron Microscopy
SG	Specific Gravity
SMPH	Sodium Magnesium Phosphate Heptahydrate
SMS	Sodium Meta-silicate
SOM	Sodium Oxalate Monohydrate
SS	Supernatant Solutions
STA	Simultaneous Thermal Analyzer
SWW	Synthetic Wastewater
TD	Thermo- Dilatometry
TDI	Tolerable Daily Intake
TGA	Thermo-Gravimetric Analysis
THAM	Tris-Hydroxymethylene-Aminomethane
TMA	Thermo Mechanical Analysis
Tof-SIMS	Time-Of-Flight Secondary Ion Mass Spectrometry
UTI	Urinary Tract Infection
WBC	White Blood Cells
WHO	World Health Organization
XRD	X-Ray Diffraction
XRF	X-Ray Fluorescence Spectrometry

Abstract

The thesis entitled, "GROWTH AND CHARACTERIZATION OF STRUVITE AND RELATED CRYSTALS", representing an elaborated report of the author's research work is covered in following nine chapters.

Chapter : I : General Introduction

This chapter gives the general introduction to the subject and explains the objectives and the significance of the study. In this chapter occurrence of struvite crystals, crystal structure and physical properties of struvite crystals are briefly explained. Struvite is a component of urinary calculi, the *in vivo* growth and pathophysiology is discussed. Various types of crystallization of struvite and its applications are briefly reviewed.

Chapter : II : Brief Review on Urinary Calculi

This chapter describes a brief review on urinary calculi. It gives the general introduction to the human urinary system and its functioning in brief. It describes the terms like nephrolithiasis, urolithiasis, urinary calculi, i.e., kidney stones. It also describes the epidemiology of the urolithiasis. Various crystalline components of urinary calculi, general pathophysiology and etiology of urinary calculi, general biological events and risk factors leading to the formation of urinary calculi, symptoms, diagnosis and management (techniques for treatment) are explained in brief.

Chapter : III : Crystal Growth Technique

This chapter presents brief out line of various crystal growth techniques and especially focuses on the gel growth technique, which was used for the present study. The gel growth technique is one kind of modified version of solution growth technique. In the gel growth technique, growth occurs due to

reaction between two solutions in a gel medium or achieving super-saturation by diffusion in gel medium. Slow and controlled diffusion of reactants in gels can mimic the condition in a body in a broad sense. Bio-crystallization usually occurs in the slow and steady process in the soft tissues, cavities or vessels. Single diffusion gel growth technique provides the simplified *in vitro* model of the highly complex growth of urinary calculi *in vivo*. Growth of crystals with different morphologies is commonly found in bio-crystallization. In the gel growth technique, by changing the growth conditions, crystals with different morphologies and sizes can be obtained. The main advantage is that the crystals can be observed practically in all stages of their growth. Different types of gels, gelling mechanism, structure of silica hydro gel and its properties are discussed. It also covers the description of different types of gel growth methods, growth mechanism, nucleation control and Liesegang rings. A brief review of the urinary type crystals grown by gel method is given. At the end of the chapter advantages as well as limitations are explained in brief.

Chapter : IV : Characterization Techniques

This chapter describes different experimental techniques used to characterize the grown crystals. These techniques are powder X-ray diffraction (XRD), Fourier Transform Infrared Spectroscopy (FTIR), Thermal studies including Thermo Gravimetric Analysis (TGA), Differential Thermal Analysis (DTA) and Differential Scanning Calorimetry (DSC); and dielectric study.

Chapter : V : Growth and Characterization of Struvite

This chapter deals with the growth and characterization of struvite crystals. Struvite crystals were grown by single diffusion gel growth technique

in silica hydro gel medium, which provides the simplified *in vitro* model of the highly complex growth of urinary calculi *in vivo*. In the present study, the silica gel was chosen as it remains stable and does not react with the diffusing solutions within it or with the product crystal formed. Struvite crystals of different morphologies such as rectangular, prismatic, elongated dendritic, dendritic, needle and star types were grown depending on different growth parameters such as, the specific gravity of Sodium metasilicate (SMS) solutions, the concentrations of reacting solutions and the gel pH. The crystals were characterized by powder XRD, FT-IR, Thermal analysis and dielectric study. The kinetic parameters were evaluated by applying the Coats and Redfern relation to the thermo-gram of struvite. Also, thermodynamic parameters were calculated by applying well known formulae. The results are discussed.

Chapter : VI : Growth Inhibition Study of Struvite

This chapter describes the growth inhibition study of struvite crystals. Struvite type urinary calculi can grow rapidly forming 'staghorn-calculi', which is more painful urological disorder. Therefore, it is of prime importance to study the growth and inhibition of struvite crystals. The *in vitro* growth inhibition or dissolution study is important to understand the *in vivo* process where the growths of calculi continue to occur with the supply of nutrients through urine and the inhibition process has to be achieved. In the gel growth, nutrients are constantly supplied to the growing crystals and the dissolution or inhibition is to be checked. Hence, *in vitro* single diffusion gel growth technique was used to study the growth and inhibition behavior of struvite crystals in the presence of herbal extracts like *Boerhaavia diffusa* Linn,

Commiphora wightii and *Rotula aquatica* Lour as well as in the presence of the fruit juice of *Citrus medica* Linn. It also explains in details the inhibitory effects of these extracts and the fruit juice of *Citrus medica* Linn. The details of the studies will be discussed in this chapter. This study incorporated multidisciplinary interests and may be used for formulating the strategy for prevention or dissolution of urinary stones.

All these herbal extracts and the juice of *Citrus medica* Linn proved to be good inhibitors of struvite crystals. Herbal extracts in higher concentration brought fragmentation of the crystals, which is very important because the small pieces of stones can easily be flushed out through urinary tract. The growth inhibition of struvite crystals produced by *Citrus medica* Linn proved the citrate inhibition theory as the *Citrus medica* Linn contain citric acid.

Chapter : VII : Vickers Micro-hardness and Etching Study of Struvite

This chapter deals with Vickers micro-hardness as well as the etching study of struvite crystals. Struvite single crystals of platelet type morphology with smooth faces were selected for Vickers micro-indentation hardness study by varying loads from 5 to 125 gram. The variation of Vickers micro-hardness with applied load suggested that the micro-hardness increased with load with certain variations. The Kick's law was also verified and the value of work hardening coefficient n was found. The phenomenon of reverse Indentation Size Effect (reverse ISE) was observed in case of struvite crystals. The experimental data were analyzed using different theoretical models like Hays and Kendall's model and Proportional Specimen Resistance (PSR) model to obtain load independent hardness of the struvite crystals. The values of yield stress and elastic stiffness constant were calculated. This Vickers micro-

hardness study and related mechanical properties may provide useful information to fracture the struvite stones and the power required to fracture in Extracorporeal Shock Wave Lithotripsy (ESWL).

In the second part of the chapter, the dislocation etching study of struvite crystals was discussed. Since the citric acid is a good inhibitor of the growth of urinary stones as well as urinary crystals and, therefore, it was chosen as an etchant to etch the crystalline face of struvite. The chemical etching was carried out for different temperatures from 30° C to 70° C. The etchant produced crystallographically oriented triangular etch pits on triangular surface, i.e., {1 1 1} face of the crystal. The width of the etch pits increased with the increase in the temperature of the etchant. The estimation of kinetic and thermodynamic parameters has been carried out.

Chapter : VIII : Growth and Characterization of Struvite Family crystals

This chapter deals with the growth and characterization of following two struvite family crystals.

- (1) Potassium Magnesium Phosphate Hexahydrate (PMPH) or struvite-K. The crystals of struvite-K are rich in potassium and similar to struvite in crystal structure. It is the potassium equivalent to struvite $\text{NH}_4\text{MgPO}_4 \cdot 6\text{H}_2\text{O}$. The chemical formula of struvite-K or PMPH is $\text{KMgPO}_4 \cdot 6\text{H}_2\text{O}$. Struvite-K crystals were also noticed as a component of urinary calculi in the animals fed with the high-level cottonseed meal diet.
- (2) Sodium Magnesium Phosphate Heptahydrate (SMPH) or struvite-Na. The crystals struvite-Na are rich in sodium and similar to struvite in crystal structure. It is the sodium equivalent to struvite $\text{NH}_4\text{MgPO}_4 \cdot 6\text{H}_2\text{O}$. The chemical formula of struvite-Na or SMPH is $\text{NaMgPO}_4 \cdot 7\text{H}_2\text{O}$.

These struvite family crystals were grown by single diffusion gel growth technique in silica hydro gel medium. These crystals were characterized by powder XRD, FT-IR, TGA, DTA, DSC and dielectric study. The kinetic and thermodynamic parameters were evaluated from thermo-gram.

Chapter : IX : Conclusions

This chapter gives an over all view of the results and general conclusions. Also, the scope of the future work is discussed.

Chapter I

General Introduction

Topic Number	Topic	Page Number
1.1	Introduction	2
1.2	Struvite – As a Mineral	3
1.3	Occurrence of Struvite	5
1.4	Crystallographic Study of Struvite	6
1.5	Applications of Struvite	7
1.6	Struvite – As a Crystalline Component of Urinary Calculi	9
1.7	<i>In-Vivo</i> Growth: Pathophysiology of the Formation of Struvite	11
1.8	Crystallization of Struvite	13
1.9	Objectives of the Present Study	20

1.1 Introduction

Struvite, Ammonium Magnesium Phosphate Hexahydrate [(AMPH) - $(\text{NH}_4)\text{MgPO}_4 \cdot 6(\text{H}_2\text{O})$], is one of the fascinating inorganic phosphate minerals. Struvite is widely investigated by scientists and researchers for several reasons. The most important reason is the fact that struvite is one of the components of the urinary stones. Struvite occurs as crystallites in urine and grows as a type of kidney stone. Struvite forms in humans as well as in animals as a result of urinary tract infection with urolithic microorganisms that split urea and cause persistently alkaline urine. Due to the occurrence of struvite as urinary sediments and calculi in humans as well as in animals, it requires much attention in its crystal growth and related studies of chemical and physical properties. Moreover, these stones can grow rapidly forming “staghorn-calculi”, which is more painful urological disorder. It has also high degree of recurrence. Therefore, it is of prime importance to study the growth inhibition of struvite crystals. Another reason is that struvite precipitation occurs spontaneously in sewage and wastewater treatment plants, which generates problems of scale deposits in areas such as pipes and recirculation pumps. At the same time, struvite is considered as a potentially marketable product as an alternative fertilizer. Moreover, it may be used as raw material for the production of phosphorus.

In the present chapter a brief review of struvite is given in terms of the mineralogical and crystallographical studies, occurrence of struvite and its applications in various fields, the role as a component of urinary calculi, pathophysiology of the formation and crystallization. The objectives and the significance of the present study are given at the end of this chapter.

1.2 Struvite – As a Mineral

Minerals are naturally-occurring crystalline substances with a definite chemical composition and physical properties. Struvite is the mineralogical name of Ammonium Magnesium Phosphate Hexahydrate crystals. However, some critics might claim that because struvite frequently has somewhat dubious anthropogenic origins, it fails to meet the ‘sniff test’ (i.e., the strict definition) for a mineral. But struvite is also found in non-anthropogenic settings too. Table 1.1 depicts the mineralogical data [1-9] of struvite and figure 1.1 shows the photographs of the struvite mineral obtained from various localities [2,10]. Struvite tends to occur as yellow to brownish pyramidal crystals. If it is white when found then it tends to become yellow upon the exposure to light.

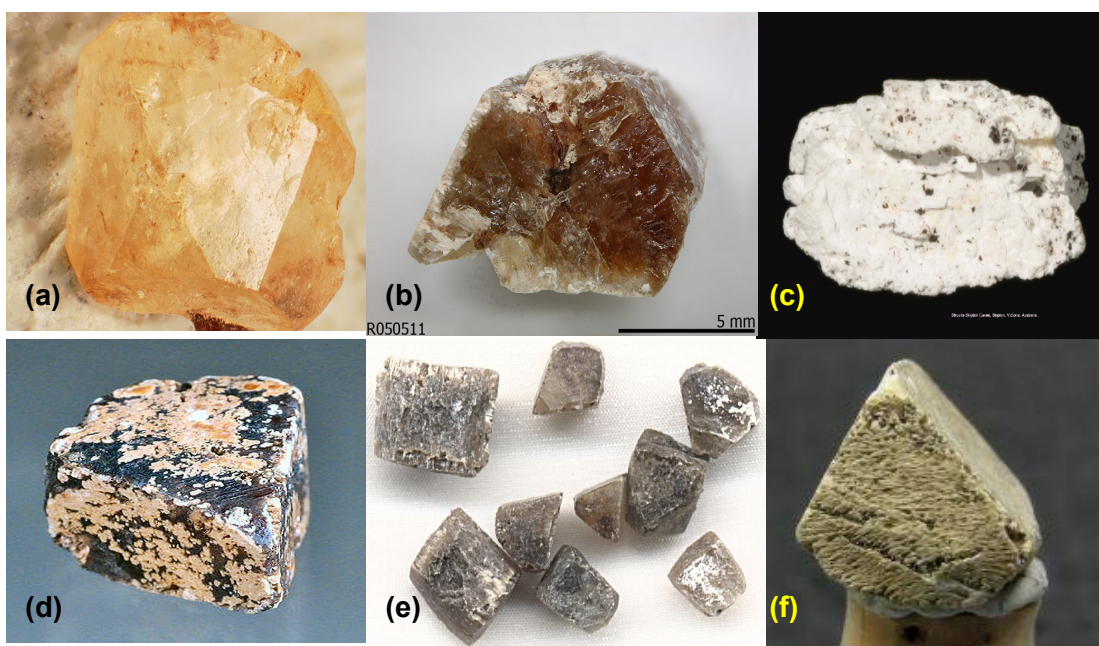


Figure : 1.1 Struvite Mineral Photographs [2]

[(a) A nice yellow struvite crystal without matrix from Skipton Caves, (b) Colorless struvite with a brown tint from Hamburg, Germany (c) decomposed struvite decomposing to white, chalk-like Newberyite (d) Yellow-brown tabular struvite crystal from Nicolaikirche, Hamburg, Germany (e) Braunschweig, Germany (f) Struvite crystal from St Nikolai church, Hamburg, Germany]

Table : 1.1 : Mineralogical Data of Struvite [1-9]

General Information	
Chemical Formula	(NH ₄)MgPO ₄ .6(H ₂ O) : The Commission on New Minerals, Nomenclature and Classification of the International Mineralogical Association (CNMNC-IMA) approved formula
Molecular Weight	245.41 gram
Composition	12.62 % phosphorus, 9.90 % magnesium, 5.71 % nitrogen, 65.20% Oxygen, 6.57 % Hydrogen by weight
Locality / Distribution	(i) Hamburg, Germany [4], (ii) Skipton lava caves, Australia [5] (iii) Niah Great Cave, Sarawak, Malaysia, (iv) Reunion Island, Indian Ocean [4], (v) Paoha Island, Mono Lake, California [6], (vi) Mt Antero, Colorado, USA [7], (vii) Gcwihaba Cave, Botswana, (viii) Staritrg mine, Kosovo [8], (ix) Kettle Lake, North Dakota, USA [9] etc...
Classification	
Dana Classification	40.01.01.01 : (40) Hydrated Phosphates (40.01) where A ⁺⁺ B ⁺⁺ (XO ₄) · n (H ₂ O) (40.01.01) Struvite Group: on the basis of structural similarities (40.01.01.01) Struvite : individual mineral species
Strunz Classification	08.CH.40 (08) Phosphates, Arsenates, Vanadates (08.C) Phosphates without Additional Anions, with H ₂ O (08.CH) With large and medium-sized cations, RO ₄ :H ₂ O < 1:1
Physical Properties	
Luster	Vitreous
Diaphaneity	Transparent, Translucent, Opaque
Colour	Colourless, White (dehydrated), Yellowish white, Brownish white
Cleavage	{100} perfect
Habit	Euhedral to platy Crystals
Density	1.71 g / cm ³
Solubility in Water	Sparingly soluble in water
In Air	Dehydrates in dry and warm air
Other Properties	Piezoelectric, Pyroelectric, Gemstone Rare, Bio-Mineral.

1.3 Occurrence of Struvite

The struvite mineral may be termed as a 'cave' mineral, since this mineral is generally found either in caves or lakes. Some of the main reasons of occurrence of the struvite in nature are, (i) Lakes with relatively low water stage and consequent elevated water salinity, (ii) Disappearance of water from some of the lakes and wetlands in the world, (iii) Visitations by large populations of migratory waterfowl to the lakes, and also (iv) Microbial activity may be related to the formation of struvite mineral in nature.

The main localities of the struvites are as mentioned in table 1.1. Moreover, struvite has been found in association with organic matter decomposition, for example, in barns and cemetery soils, in old graveyard and in guano deposits, in human urinary sediments, manures and sediments rich in organic remains [11,12]. Moreover, struvite has been found on the surface of old ivory and on the fossilized teeth of a mammoth.

Struvite is sometimes an unwanted mineral. Struvite is occasionally found in a variety of canned seafood, including canned tuna, salmon, shrimp, crab meat, lobster, and sardines, where its appearance is that of small glass slivers. It does not present a health hazard, but no one wants to eat a bunch of crystals with one's food. In wastewater treatment systems it presents a bigger problem. Struvite is frequently produced in specific areas of wastewater treatment plants such as in sludge liquors pipes, centrifuges, belt presses, and heat exchangers [13]. Moreover, struvite is an important constituent of urinary calculi in humans and animals. Surprisingly, struvite has also been found in a human lung [14]. Struvite is a common mineral found in enteroliths, i.e., intestinal calculi, in horses and zebras [15,16].

1.4 Crystallographic Study of Struvite

The crystal structure of struvite was reported from the single crystal X-ray diffraction (XRD) data by Whitaker and Jeffery [17]. Moreover, Ferraris et al [18] carried out neutron diffraction study for the accurate determination of water molecules in struvite. Struvite crystallizes in the orthorhombic system with unit cell parameters $a = 6.941 \pm 0.002 \text{ \AA}$, $b = 6.137 \pm 0.002 \text{ \AA}$, $c = 11.199 \pm 0.004 \text{ \AA}$ [17]. The space group is $Pmn2_1$. There are two molecules in a unit cell of a struvite. As shown in figure 1.2 the struvite crystal structure consists of three structural units, namely, (i) PO_4 tetrahedron, (ii) $\text{Mg} \cdot 6\text{H}_2\text{O}$ octahedron and (iii) NH_4 groups held together by hydrogen bonding [17,18].

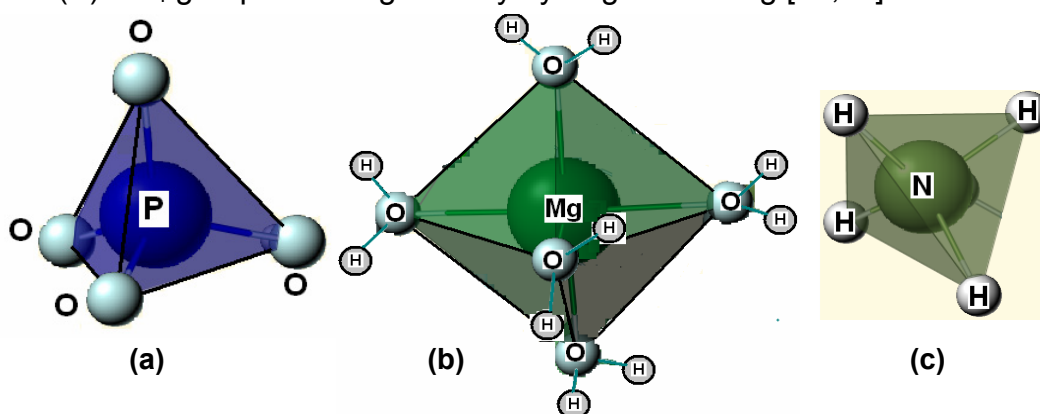


Figure : 1.2 Structural Units of Struvite
(a) Tetrahedra PO_4 , (b) Octahedra $\text{Mg} \cdot 6\text{H}_2\text{O}$ and (c) NH_4 groups

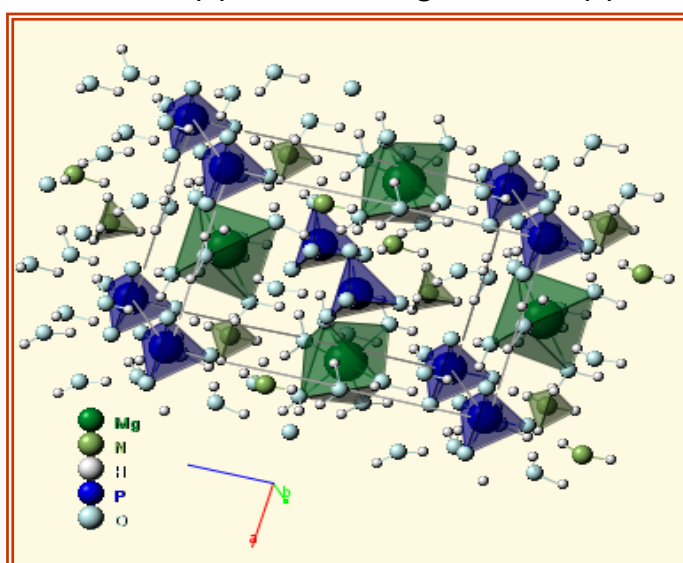


Figure : 1.3 Struvite Crystal Structure [17, 18, 19]

The PO₄ tetrahedron is regular with a mean phosphorous – oxygen bond length of 1.5370 ± 0.0011 Å and the Mg.6H₂O octahedron is distorted with mean magnesium – water oxygen bond length of 2.0711 ± 0.0011 Å. The mean water oxygen – hydrogen bond length is 0.778 ± 0.014 Å. By analyzing thermal vibrations Whitaker and Jeffery [17] found the mean corrected bond lengths as 1.5431 Å, 2.0810 Å and 0.792 Å respectively. The crystal structure of struvite is as shown in figure 1.3.

1.5 Applications of Struvite

Struvite has many applications. Some of the main applications are as follows:

- (i) Struvite has been proposed as active component in setting surgical cements by Driessens et al [20].
- (ii) In future, long term space habitation on the moon or mars will require constant food and water supply. Recently, Thompson et al [21] suggested that struvite, the precipitate formed in urine, can be used as a nutrient source for the growth of crops. The supernatant remaining after precipitation is a water source that must be reclaimed in order to maintain a constant water supply.
- (iii) The composition of struvite makes it a potentially marketable product for the fertilizer industry. Struvite contains the essential nutrients that plants need, therefore, it can be used as a fertilizer. Since the struvite is being recycled product from water waste, it is known as ‘green fertilizer’.
- (iv) All life forms require phosphorus in the form of phosphate, which has an essential role in RNA and DNA and in cellular metabolism. In many countries, phosphorus, being a plant nutrient, is in deficiency in the soil and hence farmers add phosphate-based fertilizers to increase

agricultural yields. Struvite can be used as a high quality, slow-release, non-burning fertilizer in horticulture and agriculture due to its solubility characteristics, without the danger of damaging plant roots.

- (v) Ghosh et al [22] carried out several comparative studies with struvite, urea, formaldehyde, ammonium nitrate and ammonium sulphate on crops, which proved that struvite responded better (even double) than superphosphates.
- (vi) Crystallization of struvite has been identified as an effective way of recovering nitrogen and phosphorous from waste water [23].
- (vii) Struvite shows up in decomposed dead bodies. Struvite thus has some importance as a forensic tool because it can be used to determine the approximate date of a burial [24].
- (viii) When struvite powder is heated in an air atmosphere it loses crystal structure. This amorphous struvite-related substance crystallizes back into struvite at room temperature, when soaked in ammonium ion-containing aqueous solution. The struvite powder transforms at 36.5°C and in 72 hours, into the human bone mineral, when it is immersed in solutions having similar alkali (Na and K) and alkaline earth (Ca) ions such as those of body fluids [25].
- (ix) According to the hypothesis made by Handschuh and Orgel [26], struvite was important for the origins of life. They reported that struvite may have precipitated from evaporating seawater on the primitive earth, and may have been important for prebiotic phosphorylation. Moreover, authors emphasized that struvite would have provided the major intracellular inorganic ions, other than chloride, for primitive cells.

1.6 Struvite – As a Crystalline Component of Urinary Calculi

Majority of the calculi are composed of calcium salts, oxalates and phosphates. Among the phosphates, magnesium phosphates, namely, ammonium magnesium phosphate hexahydrate, i.e., struvite, and magnesium hydrogen phosphate trihydrate, i.e., newberyite, have been reported to occur as constituents in renal calculi [27-31] not only in adults but also in children [32,33]. Struvite calculi have afflicted mankind from thousands of years. A struvite stone was found in the pelvis of 7000 year old Egyptian mummy during excavation representing the oldest known urolith [34]. Struvite is also known as 'urine sand', 'triple phosphate stone', 'phosphatic stone', 'infection stone' or 'urease stone'. The term triple phosphate stems from early chemical analyses of the stones which demonstrated the presence of calcium, magnesium, ammonium, and phosphate (i.e., three cations and one anion). Since the struvite stones occur mainly due to urinary tract infections, they are described as infection stones. The term urease stone is used to describe struvite calculi, because the presence of urease-producing microorganisms like bacteria and yeasts are requisite to their formation.

Worldwide, struvite compose 30% of all kidney stones in humans [35]. In contrast to humans, struvite stones account for 75% of urinary calculi found in the animals like dogs and cats [36]. Diamond et al [37] observed that struvite stones are more common in the children of Europe than in the United States. Struvite stones are associated with the development of chronic kidney disease (CKD), and these patients require special attention. Nathan Saucier et al [38] confirmed a significantly greater risk of CKD in patients with a diagnosis of struvite stone disease. Modern crystallographic analyses have

shown that in some cases struvite stones are found as a mixture of struvite and carbonate-apatite. Altogether, struvite stones are found more frequently in women and in persons older than 50 years [35]. Priestley and Dunn [39] reported that 41% of the patients have 5-year survival rate with untreated unilateral struvite stones. Figure 1.4 shows the photographs of the struvite kidney stones [40-42].



Figure : 1.4 Struvite Type Kidney Stones [40-42]

Pure struvite stones are usually off-white to light brown in color with a rough textured surface. When sectioned, the interior of the stone contains white concentric rings and, occasionally, the interior contains white porous granulated material. Admixed struvite/apatite stones are usually light brown in color with a coarse granular surface. The interior is normally intermixed with white and light brown layers. Struvite stones are radio opaque and radiographs show struvite stones as large, gnarled, and laminated. Struvite stones have a characteristic X-ray appearance with branching like horn of deer. These are fast growing stones that grow to fill up the naturally occurring cavities in the kidney to take on a “staghorn” appearance. Struvite stones may grow rapidly over a period of weeks to months and, if not adequately treated, can develop into a branched calculus that involves the entire renal pelvis and calyces. Furthermore, these large staghorn calculi can cause renal obstruction and significant damage to the involved kidney. These stones are difficult to remove and often require extensive surgery.

Struvite stones are often one of the most troublesome stones for patients as well as physicians. A patient with struvite stones should be assumed to have a progressive disease which cannot be ignored. Even after seemingly successful elimination of stones with lithotripsy or percutaneous nephrolithotomy, careful medical follow-up is needed.

Patients with infected staghorn calculi, who do not receive any treatment, have about a 50% chance of losing the kidney [43,44]. Sometimes kidney removal prior to transplantation is necessary. Ghumman et al [45] carried out renal stone analysis with the Time-of-flight secondary ion mass spectrometry (ToF-SIMS) technique, which gives information about all elements present in a specimen, and showed that in some cases struvite stones were found with some additional minerals like Na⁺ and K⁺.

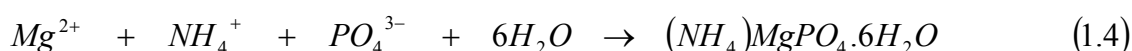
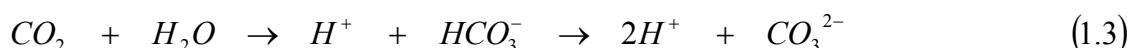
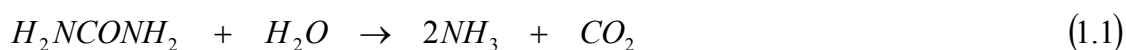
1.7 *In-Vivo* Growth: Pathophysiology of the Formation of Struvite

The pathophysiology of struvite urolithiasis is different from that of other forms of urolithiasis. Struvite stones are most commonly, but not always, occur with urinary tract infections. Struvite forms in humans as well as in animals as a result of urinary tract infection with urolithic microorganisms that split urea and cause persistently alkaline urine [30, 46-48]. Since women are more susceptible to urinary tract infections, struvite stones occur more often in women than men with a ratio of 2:1. It has also high degree of recurrence [49].

The stone formation requires supersaturated urine. Super-saturation also depends on urinary pH, ionic strength, solute concentration and complexations [50]. Crystallization begins with supersaturation leading to nucleation, followed by crystal growth and aggregation.

Struvite calculi develop, when three conditions coexist: (i) the alkaline urine (i.e. pH > 7.2), (ii) the presence of urea or ammonia in the urine and (iii) the higher concentration of minerals in the urine. This leads to magnesium ammonium phosphate and carbonate apatite crystallization. Infection with urea splitting bacteria leads to a production of ammonia and alkalinization of the urine. The produced ammonia generates magnesium ammonium phosphate crystals. Various urease producing micro-organisms hydrolyze urea to ammonium and raises urine pH [29]. As the urine pH increases, phosphate becomes more available to contribute to struvite crystal formation and struvite becomes less soluble. As the concentrations of phosphate, magnesium, and ammonium rise in urine, a supersaturation occurs contributing to crystal growth and urolith formation.

The conversions of urea to ammonia, ammonia to ammonium, acidification from carbon dioxide, and general reactions of the formation of struvite are as follows:



The reaction sequences as presented in the above equations show the pathophysiology of the formation of struvite crystals. Equation (1.4) is the most general equation of the formation of struvite *in vivo* conditions, which shows that for the formation of the struvite, the NH_4^+ , PO_4^{3-} and Mg^{2+} ions must be present in the urine. However, this equation exhibits a simplified chemistry involved in struvite formation. As it has already been discussed,

struvite forms as a consequence of a urinary tract infection by urease producing micro-organisms. This urease splits urea and produces ammonia as shown in equation (1.1). Further hydrolysis of the ammonia takes place, which produces NH_4^+ ions and increases urine pH and gives neutral or alkaline urine according to equation (1.2). Higher intake of phosphate (usually from Proteins) and magnesium-based food and lower intake of water gives rise to the PO_4^{3-} and Mg^{2+} ions in the supersaturated urine, which leads to the conditions of formation of struvite according to equation (1.4).

Though the urine of a healthy person is under-saturated with regard to struvite, the conditions provoked by urease producing micro-organisms and the urine complex composition, the precipitation of struvite occurs. Under such conditions it often precipitates together with apatites and the sediment can easily be attached to the particles of organic matter formed as a consequence of the infection. This mechanism favors the crystal deposition and aggregation, so that struvite stones grow rather quickly. Matsumoto and Funaba [51] reported that Tamm–Horsfall glycoprotein - a urine protein, can not enhance struvite crystallization.

1.8 Crystallization of Struvite

Solution chemistry of magnesium, ammonium and phosphate in ionic state plays a predominant role in struvite crystallization. Imtiaj Ali et al [52] reported a thermodynamic model relating to all the complexes of magnesium, ammonium and phosphate using gPROMS process software. Thermodynamic model response showed that both solution pH and free ion concentration of dissolved species play most significant role in struvite crystallization. Studies on crystallization of struvite are widely carried out by various scientists and

researchers for the reasons as depicted in the figure 1.5. Various techniques and processes were experimented to date by researchers either at laboratory – pilot level or at full-scale level.

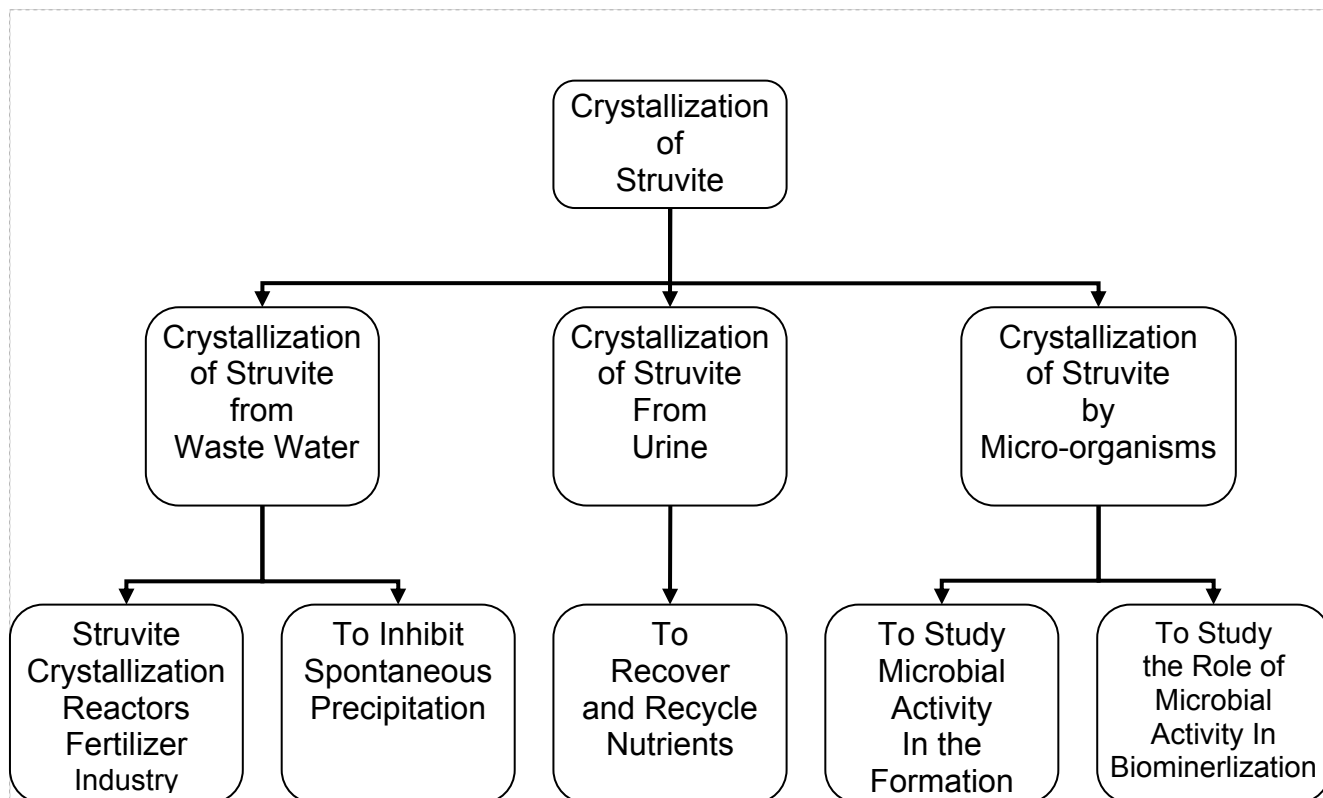


Figure : 1.5 Studies on Crystallization of Struvite

Crystallization of struvite represents an interesting technique to recover phosphorus from wastewater [53] or urine [54,55] or manure [56,57]. Ivancic et al [58] carried out the experiments of spontaneous precipitation of struvite and studied the influence of the initial reactant concentrations, ageing time and temperature on the composition and morphology of struvite. They tried to find the difference in the solubility and dissolution kinetics of dendrites and rod-like crystals of struvite. Boistelle and Abbona [59] carried out the study on conditions like concentration and pH for preparation of single crystals of struvite at 25 °C from ammoniacal solutions equi-molar with respect to magnesium - phosphate ions and discussed mechanisms of nucleation.

1.8.1 Crystallization of Struvite from Waste Water

Crystallization of struvite can be applied for several purposes, such as to prevent scaling problems [60], as well as to remove phosphate [61] or nitrogen [62,63]. Recent publications show an increasing interest in struvite precipitation as a technology for phosphorus recovery taking into account the economic impact of increasing energy costs and limited natural phosphorus resources [64-66]. Thus, struvite crystallization is widely studied as a technique to remove phosphorus [67] and nitrogen from wastewater effluents and simultaneously generate a valuable as well as sustainable product for the fertilizer industry. There exists considerable interest in recycling phosphorus as struvite based on philosophical, environmental, economical and commercial reasons. Struvite crystallization reactors have been used at laboratory, pilot and full scale and have shown great potential in removing and recovering phosphorus as struvite crystals [68]. In 2004 an international conference on 'Struvite - its role in phosphorus recovery and recycling' was organized by Cranfield University School of Water Sciences, which showed that there was a very wide interest in struvite recovery, with scientific research underway in many countries across the world [69]. Many researchers are continuously engaged in finding the new methods of struvite crystallization such that the nutrients may be recycled effectively, efficiently and economically. Struvite precipitation occurs spontaneously in wastewater treatment plants under conditions that are influenced by many factors including concentration of Mg^{2+} , NH_4^+ , and PO_4^{3-} ions, pH and temperature. Corre et al [70] found that the presence of Ca ions in solution has a significant impact on struvite crystallization in terms of size, shape, and purity of the

product recovered. They found that increasing calcium concentration reduces the crystal size and inhibits the struvite growth, or affects struvite crystallization and leads to the formation of an amorphous substance rather than crystalline struvite.

Electrochemical precipitation of struvite also appeared as an alternative method to recover *P*, *N*, and *Mg* from waste waters. Recently, Wang et al [71] demonstrated the feasibility of electrochemical deposition for recovering pure struvite from waste streams at a neutral pH value, which could be easily realized at a lower voltage in laboratory condition. This method could also realize both the high phosphate removal efficiency in solution and the highly pure content of struvite.

On the other hand, some researchers also carried out investigation to inhibit spontaneous precipitation of struvite from wastewater. The effect of citrate and phosphocitrate ions on the kinetics and the morphology of the spontaneous precipitation of struvite in synthetic wastewater (SWW) supersaturated solution was investigated by Kofina et al [72]. Both citrate and phosphocitrate ions in SWW supersaturated with respect to struvite were found to be effective inhibitors. Recently, Du Xian-Yuan et al [73] reported the formation of struvite crystals in a simulated food waste aerobic composting process.

1.8.2 Crystallization of Struvite from urine

Urine-separation toilets are a possible route for achieving maximum recovery and recycling of urine nutrients not contaminated by hazardous compounds such as heavy metals. Lind et al [74] presented a technique for the crystallization of struvite by adding small amount of *MgO* to the natural

human urine. Recently, Ronteltap [75] presented a technique for struvite formation from hydrolyzed urine by using continuously stirred tank reactor (CSTR). The process in CSTR was shown to be a reliable stable process that does not require any pH control. The reactor showed very stable operation conditions and high removal efficiencies. The main advantage of using urine as a source for struvite precipitation is that no pH adjustment is needed. This allows for a stable running of the reactor without operation issues for a longer period of time, provided magnesium is supplied sufficiently.

1.8.3 Crystallization of Struvite by Micro-organisms

Micro-organisms are capable of forming a diverse array of minerals [76]. The phenomenon of bio-mineralization was well documented [77,78]. It has been suggested that microbial activity could be related to the formation of rocks and sediments in nature. The formation of struvite crystals by bacteria was first described by Robinson [79]. Many studies proved the role of micro-organism in the formation of struvite crystals [79-81].

As it is well known that the urease producing bacteria in the urinary tract infection induce certain urinary stone formations, i.e., struvite type. These stones are not totally crystalline in nature but rather consists of an agglomeration of bacteria, organic matrix and struvite crystals. Crystal formation is related to the ability of the bacteria to affect an increase in the urine pH. Moreover, another equally important bacterial role lies in their formation of a 'biofilm', which later on becomes the organic matrix constituent for the stone. Results of *in vitro* study indicate that the crystals are formed more readily if grown within the bacterial biofilm than the surrounding urine. It has been proposed that supersaturation, due in part to a bacterial induced pH

increase and in part to the metal binding tendency of the biofilm, leads to crystal formation via gel growth mechanism within the biofilm itself [82].

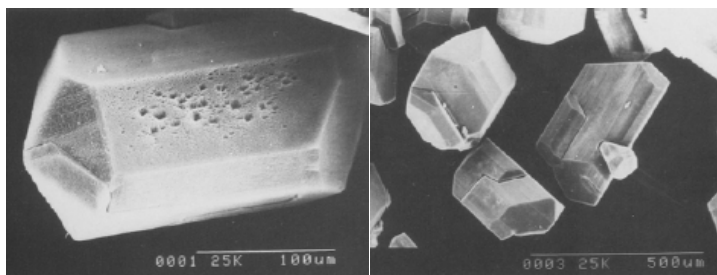


Figure 1.6 : Grown Struvite Crystals in the Gel Medium [83]

Rivadeneyra et al [81] showed that soil and fresh water bacteria contribute to the formation of struvite under suitable conditions in natural habitats. Figure 1.6 shows the scanning electron micrograph of the struvite crystals produced by bacteria in vitro [83].

The formation of struvite by bacteria has been widely documented for *Brucella* [84], *Staphylococcus aureus* [80], *Pseudomonas calciprecipitans* [85], *Proteus mirabilis* [46, 86,87], *Ureaplasma urealyticum* [88], *Myxococcus xanthus* [89] and strains of the genera *Pseudomonas*, *Flavobacterium*, *Acinetobacter*, *Yersinia*, *Corynebacterium*, *Azotobacter* [81] and *Bacillus pumilus* [90].

The effect of *Proteus mirabilis* biofilm formation on struvite crystals has been reported by McLean et al [91]. The struvite crystallization due to urease activity and pH elevation above neutrality, was preceded by the deposition of organic matter on the glass surface, followed by the appearance of micron level crystals. The crystals formation within a biofilm at low dilution rates took on a characteristic twinned or 'X-shaped' struvite habit indicating rapid growth. However, those growing outside the biofilm gave tabular habit suggesting slower growth rate. When in the macro-environment the authors varied the

flow rate of artificial urine (initial pH 5.8) in the glass flow cell from 2 mL/h to 4 mL/h, the struvite crystal not associated with biofilms dissolved within 10 minutes, however, the crystals within the *P. mirabilis* biofilm withstood flow rates up to 200 mL/h, which might be due to the maintenance of an alkaline Mg-saturated micro-environment within the biofilm.

Chen et al [92] demonstrated the seed-mediated synthesis of unusual struvite hierarchical superstructures using Bacterium in *Proteus mirabilis*/urea aqueous solution. The results of the study indicate that only rod-like or prism-like struvite crystals are formed without seed crystals or using magnesium phosphate seed crystals in *Proteus mirabilis*/urea solutions or utilizing ammonium carbonate instead of urea and the bacterium in the absence or presence of dittmarite $[(\text{NH}_4)\text{MgPO}_4 \cdot \text{H}_2\text{O}]$ seed crystals. This suggests that the bacterium, urea and the dittmarite seed crystals all play important roles in directing the struvite superstructures.

Recently, Prywer and Torzewska [93] studied the crystallization process of struvite crystals induced by *Proteus mirabilis*. The crystallization process occurred at conditions mimicking the real urinary tract infection. The authors explained their results on the basis of polar properties of struvite crystals. This feature of struvite crystals is very important in the case of binding additives which may either enhance or inhibit crystallization process. It seems also that the differences in the polarity of opposite faces of c-axis may play important role in directing the struvite mesoscopic arrangement. The same authors also have described curcumin, the pigment extracted from the roots of turmeric, exhibited the effect against *Proteus mirabilis* inhibiting the activity of urease and consequently decreasing the efficiency of struvite

growth. Therefore, curcumin belongs to phytoterapeutic components and suggests the alternative with reference to the antibiotic therapy.

1.9 Objectives of the Present Study

Since the study of the present researcher is based on urinary type struvite and related crystals, it requires to cross the traditional boundary of the physics subject. The work carried out by the author is not only limited to growth and characterization of struvite and related crystals, but it also covers the growth inhibition studies of struvite crystals to check the inhibitory effect of some herbal extracts as well as that of the citrus fruit juice. So, this interdisciplinary research work requires integrating data, theories, methodologies, perspectives, and concepts from multiple disciplines like physics, chemistry, material science, mineralogy, life sciences, botany, ayurveda, pharmacology, and medicine. The objectives envisaged to be achieved during the course of present research work are as follows:

- To grow urinary type struvite crystals with different morphologies by single diffusion gel growth technique, which provides simplified *in vitro* model of the highly complex growth of urinary calculi *in vivo*.
- To characterize the grown struvite crystals using techniques like powder X-ray diffraction (XRD), Fourier Transform Infrared Spectroscopy (FT-IR), Thermo-gravimetric Analysis (TGA), Differential Thermal Analysis (DTA) and Differential Scanning Calorimetry (DSC) and dielectric study.
- To carry out growth inhibition study of struvite crystals in the presence of herbal extracts such as *Boerhaavia diffusa* Linn., *Commiphora wightii* and *Rotula aquatica Lour* as well as in the presence of the fruit juice of *Citrus*

medica Linn. This study will hopefully suggest some potent inhibitors for struvite crystals, which will have therapeutic implications.

- To study the mechanical property, viz., micro-hardness, of struvite crystals, for that Vickers micro-indentation hardness test will be carried out. To estimate the load independent hardness of struvite crystals by applying theoretical models such as Hays and Kendall's model and Proportional Specimen Resistance (PSR) model. The micro-hardness study is expected to be helpful for Extracorporeal Shock Wave Lithotripsy (ESWL), where the estimation of power required for smashing the calculi changes from one type of calculi to other calculi.
- To carry out the dislocation etching study of struvite crystals surfaces using citric acid as an etchant and to estimate the kinetic and thermodynamic parameters for the motion of the ledges of the dislocation etch pits. Citric acid is a good inhibitor of most of the urinary type crystals. By selecting it as an etchant, it will throw light on the nature of preferential dissolution of struvite surfaces at dislocations.
- To grow and characterize analogous system crystals to struvite, such as, struvite-K and struvite-Na, which contains potassium and sodium, respectively. These crystals are not studied significantly and in literature only a few reports are available.

References

1. <http://webmineral.com/data/Struvite.shtml>
2. <http://www.mindat.org/min-3811.html>
3. J. W. Anthony, R. A. Bideaux, K. W. Bladh, M. C. Nichols, "*Handbook of Mineralogy*", Vol. 4, Mineral Data Publishing, , Tucson, Arizona (2000).
4. C. Palache, H. Berman, C. Frondel, "*The System of Mineralogy of J. D. Dana and E. S. Dana*", Vol. 2, 7th edition, John Wiley and Sons, New York (1951).
5. W. D. Birch, D. A. Henry, "*Phosphate Minerals of Victoria*", Sp Pub 3, Mineral. Soc. Victoria, Melbourne (1993).
6. J. F. Cooper, G. E. Dunning, *Calif. Div. Mines Geol. Miner. Inf. Serv.*, **22** (1969) 44.
7. M. I. Jacobson, *Mineral. Rec.*, **10** (1979) 339.
8. V. Bermanec, S. Scavnicar, V. Zebec, *Mineral. Petrol.*, **52** (1995) 197.
9. J. J. Donovan, E. C. Grimm, *The Holocene*, **17** (2007) 1155.
10. http://www.gimizu.de/kabinett/pics_7/7_069.jpg
11. H. Robinson, *Proc. Camb. Phil. Soc.*, **6** (1889) 360.
12. R. V. Gaines, H. C. W. Skinner, E. E. Foord, B. Mason, A. Rosenzweig, "*Dana's New Mineralogy*", 8th Edition, John Wiley and Sons, New York, (1997).
13. J. D. Doyle, S. A. Parsons, *Water Res.*, **6** (2002) 3925.
14. M. W. Porter, *Am. Mineral.*, **9** (1924) 93.
15. M. G. Blue, R. W. Wittkopp, *J. Am. Vet. Med. Asso.*, **179** (1981) 79.
16. L. D. Lewis, "*Feeding and Care of the Horse*", 2nd Edition, Wiley - Blackwell Publishing Ltd, Oxford (1995).

17. A. Whitaker, J. W. Jeffery, *Acta Cryst.*, **B26** (1970) 1429.
18. G. Ferraris, H. Fuess, W. Joswig, *Acta Cryst.*, **B42** (1986) 253.
19. http://webmineral.com/jpowd/JPX/jpowd.php?target_file=Struvite.jpj
20. F. C. Driessens, M. G. Boltong, R. Wenz, J. Meyer, *Key Eng. Mater.*, **284** (2005) 161.
21. M. S. Thompson, S. S. Guest, J. G. Camacho, *Proc. of the 11th Inter. Conf. on Eng., Sci., Constr., and Oper. in Chall. Environ.*, Long Beach, CA (2008).
22. G. K. Ghosh, K. S. Mohan, A. K. Sarkar, *Nutr. Cycling Agroecosyst.*, **46** (1996) 71.
23. P. W. A. Perera, Z. Y. Han, Y. X. Chen, W. X. Wu, *Biomed. Environ. Sci.*, **20** (2007) 343.
24. A. A. Sicree, *Newslett. for Gem and Miner. Soc. of the Virginia Peninsula*, **36** (2009) 3.
25. G. Kurtulus, A. Cunezt Tas, 15th Biomedical Engineering Meeting (BIYOMUT 2010), 21 – 24 April 2010, Antalya, p. 48.
26. G. J. Handschuh, L. E. Orgel, *Science*, **179** (1973) 483.
27. N. Q. Dao, M. Daudon (Eds.) *"Infrared and Raman Spectra of Calculi"*, Elsevier, Paris (1997).
28. F. Abbona, R. Boistelle, *J. Cryst. Growth*, **46** (1979) 339.
29. F. Deng, J. M. Ouyang, *Mater. Sci. Eng.*, **C26** (2006) 688.
30. F. L. Coe, J. H. Parks, J. R. Asplin, *New Engl. J. Med.*, **327** (1992) 1141.
31. M. Mandel, N. Mandel, *"Analysis of Stones"*, In *"Kidney Stones: Medical and Surgical Management"*, Eds. F. L. Coe, M. J. Favus, C. Y. C. Pak, J. H. Parks, G. M. Preminger, Lippincott- Raven Pub., Philadelphia (1996).

32. M. Biocic, M. Saraga, A. C. Kuzmic, Z. Bahtijarevic, D. Budimir, J. Todoric, M. Ujevic, *Coll. Antropol.*, **27** (2003) 745.
33. H. Kuvezdic, A. Tucak, N. Peric, D. Prlic, I. Zoric, R. Galic, *Coll. Antropol.*, **27** (2003) 71.
34. S. G. Shattock, *Trans. Path. Soc. Lon.*, **56** (1905) 275.
35. M. Meng, M. L. Stoller, T. Minor, "Struvite and Staghorn Calculi", Website of e-medicine by WebMD - <http://emedicine.medscape.com/article/439127-diagnosis>, (2009).
36. B. F. Schwartz, M. L. Stoller, *Uro. Clin. N. Am.*, **26** (1999) 765.
37. D. A. Diamond, A. M. Rickwood, P. H. Lee, J. H. Johnston, *Urology*, **43** (1994) 525.
38. N. A. Saucier, M. K. Sinha, K. V. Liang, A. E. Krambeck, A. L. Weaver, E. J. Bergstralh, X. Li, A. D. Rule, J. C. Lieske, *Am. J. Kidney Dis.*, **55** (2010) 61.
39. J. T. Priestley, J. H. Dunn, *J. Urol.*, **61** (1949) 194.
40. <http://www.herringlab.com/photos>
41. http://www.lithostat.com/Kidney_Stone_Photos/Photo22-Struvite.aspx
42. <http://homepages.nyu.edu/~rabenr01/struvite.htm>
43. A. Wojewski, T. Zajackowski, *Int. Urol. Nephrol.*, **5** (1974) 249.
44. M. Singh, R. Chapman, G. C. Tresidder, Y. J. Bland, *Br. J. Urol.*, **45** (1973) 581.
45. C. A. A. Ghumman, A. M. C. Moutinho, V. Vassilenko, O. M. N. D. Teodoro, *Abstract Book, 5th Eur. Topical Conf. on Hard Coatings*, Caparica, Portugal (2008).
46. D. P. Griffith, *Kidney Int.*, **13** (1978) 372.

47. A. Hesse, D. Heimbach, *World J. Urol.*, **17** (1999) 308.
48. S. J. Ross, C. A. Osborne, J. P. Lulich, D. J. Polzin, L. K. Ulrich, L. A. Koehler, K. A. Bird, L. L. Swanson, *Vet. Clin. North Am. (Small Anim. Pract.)*, **29** (1999) 231.
49. E. Takasake, *Urol. Int.*, **30** (1975) 585.
50. M. Menon, B. G. Parulkar, G. W. Drach, "Urinary Lithiasis, Etiology, Diagnosis, and Medical Management", In: "Campbell's Urology", Vol 3, Ed. P. C. Walsh, 7th edition, WB Saunders Co., Philadelphia (1998).
51. K. Matsumoto, M. Funaba, *Biochim. Biophys. Acta*, **1780** (2008) 233.
52. I. Ali, P. A. Schneider, N. Hudson, *J. Indian Inst. Sci.*, **85** (2005) 141.
53. N. Marti, A. Bouzas, A. Seco, J. Ferrer, *Chem. Eng. J.*, **141** (2008) 67.
54. M. Ronteltap, M. Maurer, W. Gujer, *Water Res.*, **41** (2007) 977.
55. J. Wilsenach, C. Schuurbiens, M. C. M. van Loosdrecht, *Water Res.*, **41** (2007) 458.
56. I. Celen, J. R. Buchanan, R. T. Burns, R. B. Robinson, D. R. Raman, *Water Res.*, **41** (2007) 1689.
57. R. Schuiling, A. Andrade, *Environ. Technol.*, **20** (1999) 765.
58. V. Ivancic, J. Kontrec, D. Kralj, L. Brecevic, *Croat. Chem. Acta*, **75** (2002) 89.
59. R. Boistelle, F. Abbona, *Cryst. Res. Technol.*, **20** (1985) 133.
60. J. D. Doyle, S. A. Parsons, *Water Sci. Technol.*, **49** (2004) 177.
61. P. Battistoni, G. Fava, P. Pavan, A. Musacco, F. Cecchi, *Water Res.*, **31** (1997) 2925.
62. M. Altinbas, I. Oztruk, A. F. Aydin, *Water Sci. Technol.*, **45** (2002) 189.
63. R. Laridi, J. C. Auclair, H. Benmoussa, *Environ. Tech.*, **26** (2005) 525.

64. L. Shu, P. Schneider, V. Jegatheesan, J. Johnson, *Bioresour. Technol.*, **97** (2006) 2211.
65. M. Carballa, W. Moerman, W. Windt, H. Grootaerd, W. Verstraete, *J. Chem. Technol. Biotechnol.*, **84** (2009) 63.
66. A. L. Forrest, K. P. Fattah, D. S. Mavinic, F. A. Koch, *J. Environ. Eng.*, **134** (2008) 395.
67. K. S. Le Corre, E. Valsami-Jones, P. Hobbs, S. A. Parsons, *Crit. Rev. Environ. Sci. Technol.*, **39** (2009) 433.
68. Y. Ueno, M. Fujii, *Environ. Technol.*, **22** (2001) 1373.
69. *SCOPE Newsletter*, **57** (2004) Website:<http://www.ceep-phosphates.org/Files/Newsletter/Scope%20Newsletter%2057%20Struvite%20conference.pdf>
70. K. S. Le Corre, E. Valsami-Jones, P. Hobbs, S. A. Parsons, *J. Cryst. Growth*, **283** (2005) 514.
71. C. C. Wang, X. D. Hao, G. S. Guo, M. C. M. Loosdrecht, *Chem. Eng. J.*, **159** (2010) 280.
72. A. N. Kofina, K. D. Demadis, P. G. Koutsoukos, *Cryst. Growth Des.*, **7** (2007) 2705.
73. X. Du, J. Liu, G. Huang, Y. Li, *Chem. Res. Chinese Uni.*, **26** (2010) 210.
74. B. Lind, Z. Ban, S. Bydén, *Bioresour. Technol.*, **73** (2000) 169.
75. M. Ronteltap, M. Maurer, R. Hausherr, W. Gujer, *Water Res.*, **44** (2010) 2038.
76. H. A. Lowenstam, *Science*, **211** (1981) 1126.
77. T. J. Beveridge, *Annu. Rev. Microbiol.*, **43** (1989) 147.
78. T. J. Beveridge, J. D. Meloche, W. S. Fyfe, R. G. E. Murray, *Appl. Environ. Microbiol.*, **45** (1983) 1094.

79. H. Robinson, *Proc. Cambr. Phil. Soc.*, **6** (1989) 360.
80. J. Beavon, N. G. Heatley, *J. Gen. Microbiol.*, **31** (1962) 167.
81. M. A. Rivadeneyra, R. Cormenzana, G. Cervigon, *Geomicrobiol. J.*, **3** (1983) 151.
82. L. Clapham, R.J.C. McLean, J.C. Nickel, J. Downey, J.W. Costerton, *J. Crystal. Growth*, **104** (1990) 475.
83. M. A. Rivadeneyra, I. Perez-Garcia, A. Ramos-Cormenzana, *Curr. Microbiol.*, **24** (1992) 343.
84. F. Huddleson, O. B. Winter, *J. Infect. Dis.*, **40** (1927) 476.
85. H. Shinano, M. Sakai, *Bull. Jpn. Soc. Sci. Fish.*, **41** (1975) 913.
86. S. P. Lerner, M. J. Gleeson, D. P. Griffith, *J. Urol.*, **141** (1989) 753.
87. R. J. C. McLean, J. C. Nickel, K. J. Cheng, J. W. Costerton, *Crit. Rev. Microbiol.*, **16** (1988) 37.
88. L. Grenabo, J. Brorson, H. Hedelin, S. Pettersson, *J. Urol.*, **132** (1984) 795.
89. S. Silva, N. Bernet, J. Delgenes, R. Moletta, *Chemosphere*, **40** (2000) 1289.
90. B. Nelson, J. Struble, G. McCarthy, *Can. J. Microbiol.* **37** (1991) 978.
91. R. J. McLean, J. R. Lawrence, D. R. Korber, D. E. Caldwell, *J. Urol.*, **146** (1991) 1138.
92. L. Chen, Y. Shen, A. Xie, F. Huang, W. Zhang, S. Liu, *Cryst. Growth Des.*, **10** (2010) 2073.
93. J. Prywer, A. Torzewska, *Cryst. Res. Technol.*, **45** (2010) 1283.

Chapter II

Brief Review on Urinary Calculi

Topic Number	Topic	Page Number
2.1	Introduction	29
2.2	Human Urinary System and Kidney Function	31
2.3	Urinary Calculi	35
2.4	Epidemiology	36
2.5	Crystalline Components of Urinary Calculi	40
2.6	General Pathophysiology of Urinary Calculi	51
2.7	Etiology of Urinary Calculi	56
2.8	Symptoms of Urinary Calculi	72
2.9	Diagnosis of Urinary Calculi	74
2.10	Management of Urinary Calculi	88
2.11	Prevention of Urinary Calculi	95
2.12	<i>In Vitro</i> Growth Inhibition	96

2.1 Introduction

*The excruciating pain
that I am going thru
because of you,
oh my dear Kidney Stone !
Kept you safe
inside of me
for these whole long
four years, just like
one of my own
oh my dear Kidney Stone !
Feeling like a sharp knife
cutting me open and carving
it inside
your name all inside me
oh my dear Kidney Stone !
Ah ! ! ! How ungrateful of you
to give me all this horrible pain
I should have dumped you
long time ago
If I would have known
all this then
oh my dear Kidney Stone !
Some say it feels like giving birth
and some say losing virginity
but I don't really give a
Damn !
I would like to lose you
lose you right now
oh you painfully not so dear
Kidney Stone...*

Khalid Hameed

The formation of urinary calculi, usually known as, renal stone or kidney stone is a serious, debilitating problem in all societies throughout the world. In medical language, the condition of having kidney stones is termed as nephrolithiasis, urolithiasis or ureterolithiasis, where the root word 'lith' means a stone. More specifically, Nephrolithiasis, urolithiasis and ureterolithiasis are the medical terms used to describe the different locations of the stones occurring in the Kidney, urinary tract and ureter, respectively. The term urinary calculi are synonymous with uroliths, kidney stones, renal calculi or crystals. To keep things simple, however, the term "Urinary calculi" is used throughout the thesis.

In India, the earliest Sanskrit documents like the *Vedas*, the *Puraṇas* and the *Samhitās* also described urinary calculi and their remedies [1]. The *Charak Samhitā* contains sufficient but scattered matter pertaining to anatomy, physiology and pathology of urinary calculi (*Mutravaha aṣhmari*) as well as the diagnosis and treatment of its disorders. The *Sushruta Samhitā* is the pioneer text in surgery and it contains more descriptive explanations as far as the anatomy and physiology of *Mutravaha aṣhmari* is concerned. The third chapter *Aṣhmari Nidāna* of *Sushruta Samhitā* provides a scientific description of types, characteristics, etiology and symptoms of urinary calculi, where as the seventh chapter *Aṣhmari Chikitsita Sthanam* explains the treatment of urinary calculi [2,3].

This chapter describes a brief review on urinary calculi, which covers various points related to urinary calculi like function of urinary system, types of kidney stones and epidemiology of urinary calculi all over the world. Various crystalline components of urinary calculi, pathophysiology as well as etiology

of urinary calculi including risk factors leading to the formation of urinary calculi and symptoms are briefly explained. At last the present techniques for diagnosis and management (line of treatment) of urinary calculi are discussed in brief.

2.2 Human Urinary System and Kidney Function

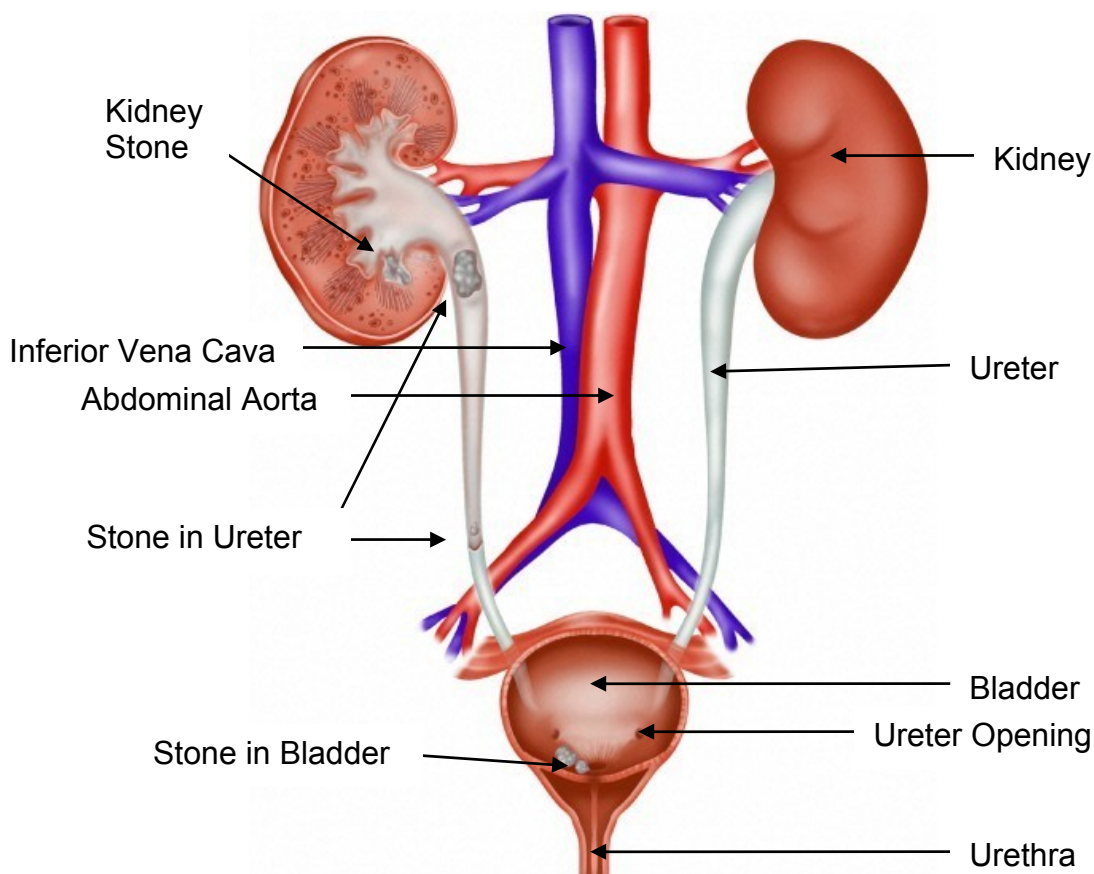


Figure : 2.1 Human Urinary System [4]

The urinary tract, or system, consists of two kidneys, two ureters, bladder and urethra. Figure 2.1 shows the human urinary system [4]. The system keeps or eliminates substances depending on the body's current needs. Each kidney continuously produces urine. Ureters are the tubes connecting each kidney to the bladder. A bladder is a triangle-shaped expandable, hollow muscular bag type organ in the lower abdomen that serves as a reservoir of urine. Normally the bladder can hold 250 - 450 cc of

urine. The bladder's elastic walls expand to store the incoming urine until it is eliminated from the body via another fibro-muscular tube called the urethra. Urethra varies from male to female. The male urethra is more complicated than the female urethra. The male urethra is usually 18 – 20 cm long and functions as a conduit for urine as well as seminal fluid. The male urethra is divided into three sections: prostatic urethra, membranous urethra, and spongy (penile) urethra. The upper portion, the prostatic urethra, passes through the prostate gland. Whereas female urethra is only 4 cm long. It begins at the internal urethral orifice at the neck of the bladder, roughly 5 cm behind the middle of the pubic symphysis. It runs downwards and forwards embedded in the anterior wall of vagina, traverses urogenital diaphragm and end at the external urethral orifice in the vestibule of vagina.

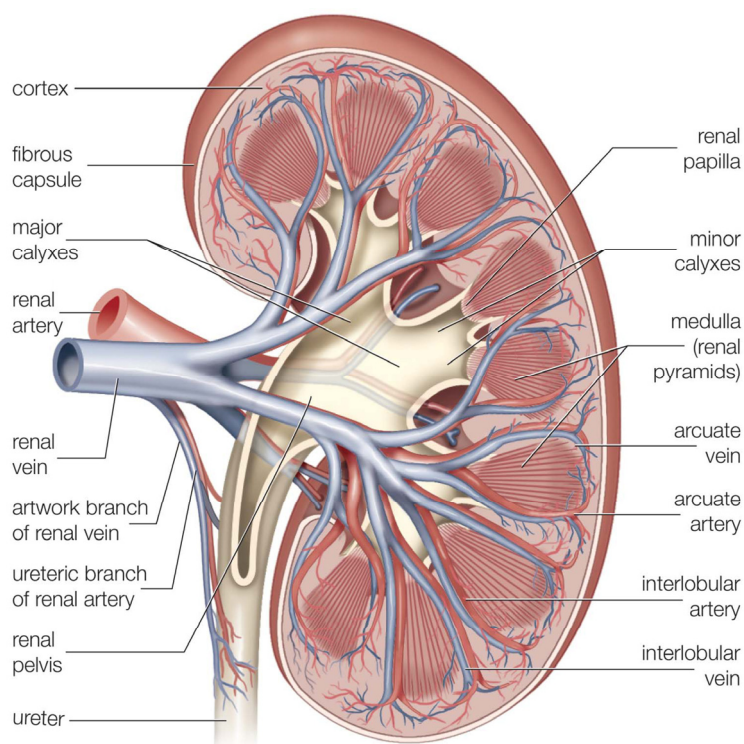


Figure : 2.2 Cross Section of Human Kidney [5] (Source: Encyclopedia Britannica)

The kidneys are the main incredibly well-functioning organs of the urinary system. Figure 2.2 shows the cross sectional art of right Kidney [5].

The kidneys are two bean-shaped, fist –sized, reddish-brown organs on each side of spine located deep behind the abdomen below the ribs and toward the middle of the back. They are about 12.5 cm long and 7.5 cm wide. Grossly, the structure of the kidney consists of the cortex, medulla (inner and outer zones of outer medulla and papilla or inner medulla), pyramids, renal calyces and pelvis. Each kidney receives blood through a branch of the aorta, called the renal artery. Blood flows from the renal artery into progressively smaller arteries, the smallest being the arterioles. From the arterioles, blood flows into glomeruli, which are tufts of microscopic blood vessels called capillaries. Blood exits each glomerulus through an arteriole that connects to a small vein. The small veins join to form a single large renal vein, which carries blood away from each kidney.

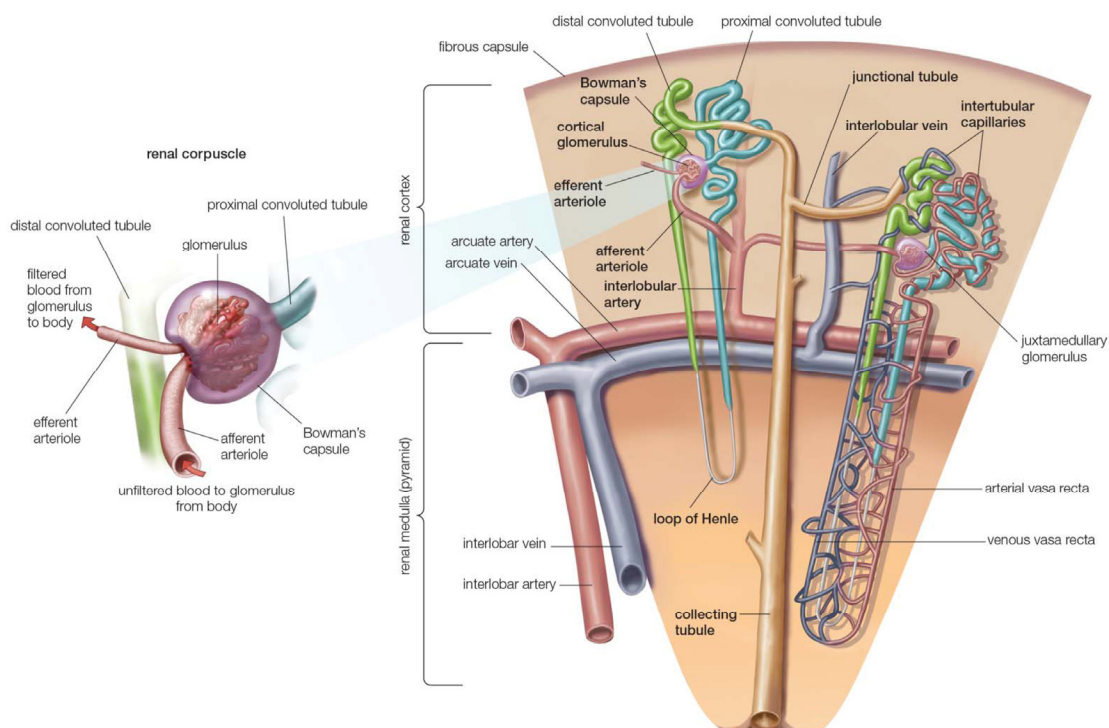


Figure: 2.3 Renal Malpighian Corpuscle and Nephron [6] (Source: *Encyclopedia Britannica*)

The process of urination begins in the kidneys. Figure 2.3 shows the renal malpighian corpuscle, which constitutes the beginning of the structural

and functional unit of the kidney i.e. nephron [6]. Nephrons are microscopic functional filtration units that filter the blood and produce urine. Each kidney contains about one million nephrons. Each nephron contains a filtering system known as a glomerulus; and a tube through which filtered fluid travels. Each glomerulus is a network of tiny blood vessels surrounded by a membrane enclosed in a funnel-like bowl-shaped structure called Bowman's capsule. A third part of the nephron is a collecting duct that drains urine from the tubule. Each tubule has three interconnected parts: the proximal convoluted tubule, the loop of Henle, and the distal convoluted tubule. The kidneys consist of an outer part cortex and an inner part medulla. All glomeruli are located in the cortex, while tubules are located in both the cortex and the medulla. The urine drains from the collecting ducts of many thousands of nephrons into a cup like structure calix. Each kidney has several calices, all of which drain into a single central chamber renal pelvis. Urine drains from the renal pelvis of each kidney into a ureter.

The primary function of the kidneys is to maintain the proper balance of water and minerals including electrolytes in the body. The kidneys remove extra water and dispose toxic substances from the blood by converting it to urine. The kidneys play a role in controlling the acid-base balance in the body, regulating electrolyte balance as well as helping to control blood pressure. Another function of the kidneys is to produce hormones such as erythropoietin, which regulates the production and release of red blood cells from the bone marrow.

Body fluid is a pivotal element in digestion, circulation, elimination, and regulation of body temperature. A critical function of the urinary system is the

maintenance of normal composition and volume of body fluid; this is accomplished by glomerular filtration, tubular reabsorption, and tubular secretion of soluble and filterable plasma components. By such means, urine contains water, electrolytes, minerals, hydrogen ions, end products of protein metabolism such as urea, uric acid, and creatinine.

2.3 Urinary Calculi

A urinary calculus, generally known as kidney stone, is a solid mineral like crystalline material that accumulates in the urinary tract when one or more calculogenic (crystal-forming) substances separate from the supersaturated urine. Urinary calculi (Plural of calculus) result from the growth of crystals into a larger lump of aggregates or stones [7]. Urinary calculi are compounds made up of salts, minerals, and other things found in urine and usually develop in the kidneys. However, they can form anywhere in the urinary tract. They grow slowly over several months or years. The composition of kidney stones may vary from person to person. Kidney stones vary greatly in size. Some are as small as a grain of sand or as large as a pearl or as big as golf balls. Sometimes it may fill the entire renal pelvis. They may be smooth, round, or jagged, spiky or asymmetrical. Most stones are yellow to reddish brown in colour. Passing of a kidney stone through a ureter or the urethra may be painless or may cause severe pain, depending on the size of the stone. When urinary calculi are quite tiny, they may pass unnoticed with the urine. Often calculi grow too large to pass easily through the urinary tract as well as some stones have rough or sharp edges, it can be quite painful when they pass through the urinary tract. In some cases, when kidney stones cannot pass on their own, a medical management is required. If untreated, it may

lead to substantial damage and in extreme case severe renal impairment or failure. Early detection of the occurrence of stone is beneficial in treatment.

2.4 Epidemiology

Urinary stone is one of the oldest and common afflictions of humans and remains a major public health burden. A large number of people are suffering from urinary stone problem all over the globe. Not only the humans but animals and birds also suffer from the urinary stone problem.

Generally, three terms, i.e., incidence, prevalence, and lifetime prevalence, are frequently used in the epidemiological studies of urolithiasis. The incidence of stone disease is defined as the number of new stone patients in a given population over a defined period of time (usually a year). The prevalence is defined as the number of stones present in a screened population at a particular point in time. Finally, the lifetime prevalence is defined as the presence of a stone at any point in a patient's history.

Urolithiasis is a global problem spanning all geographic regions with an estimated annual incidence of 1%, prevalence of 3–5% and a lifetime risk of 15–25%. Once afflicted, urolithiasis tends to be recurrent in the majority of cases [8]. Recurrence rates after the first stone episode are 14%, 35%, and 52% at 1, 5, and 10 years, respectively. Approximately 50% of patients with previous urinary calculi have a recurrence within 10 years [9]. In a recent study the recurrence rates are estimated at about 10% per year, totaling 50% over a 5–10 years period and 75% over 20 years [10].

The incidence of urolithiasis varies in different countries. The risk of developing urinary calculi in adults appears to be higher in the western hemisphere than in the eastern hemisphere, although the highest risks of

20.1% have been reported in Saudi Arabia. It has been reported that the incidence rates of urolithiasis are 5–9% in Europe, 12% in Canada, 13–15% in the USA [11,12]. The incidence rate increases to 20–25% in the Middle East, because of increased risk of dehydration in hot climates [13]. According to the data of a nationwide survey on urolithiasis in Japan between 1965 through 1987, 5.4% of the population may be expected to develop a urinary calculus at least once in their life time [14].

The occurrence in some areas is so alarming that they are known as ‘Stone Belts’ [15]. The areas of high incidence of urinary calculi include British islands, Scandinavian countries, Central Europe, Northern Australia, Mediterranean countries. The Afro-Asian stone-forming belt stretches from Sudan, Egypt, Saudi Arabia, United Arab Emirates, Iran, Pakistan, India, Myanmar, Thailand, and Indonesia to the Philippines. In these areas of the world, the disease affects all age groups, from less than 1 year to more than 70 years old, with a male-to-female ratio of 2 : 1 [16].

Urolithiasis is a common disorder responsible to substantial human suffering and economic cost to society. Studies conducted over the last half century, suggest that the incidence has been steadily increasing [17,18]. Using data from the National Health and Nutrition Examination Surveys (NHANES) carried out by Centers for Disease Control and Prevention (CDC), USA, Stamatelou et al [18] demonstrated that the lifetime prevalence of a history of kidney stones among adults in the USA increased significantly by 37% between two periods, namely, 1976 to 1980 and 1988 to 1994. Recently, Brown [19] reported that the patients with urinary calculi account for nearly 1 million visits to emergency departments (EDs) in the United States annually.

Correspondingly, in one study the economic impact in the USA was estimated as US \$ 2.1 billion (based on 2003) per year [20] and in another study as US \$ 5.3 billion per year [21]. It has been found that in recent years there is an increase in the treatment and the money involved with urinary stone problems. In the last 10 years, the diagnosis of urolithiasis was increased approximately by a 50% [22].

In Germany there are approximately 7,50,000 cases of urolithiasis per year [23]. Recent reports suggest a continuing upward trend in stone rates in Germany. For example, between 1979 and 2000, the incidence increased nearly threefold (0.54–1.47%), with a resulting rise in prevalence from 4.0 to 4.7% among the population as a whole. Among German men aged 50–64 years, the prevalence was even higher at 9.7%, and over 40% of the stone formers were recurrent [17].

Studies in UK suggest that there has been a gradual increase in the annual incidence and a decrease in the age of onset of the urolithiasis perhaps due to the result of change in lifestyle and diet [24].

Based on epidemiological studies in Swedish stone patients, there was an expected recurrence rate of 70% after 10 years when those patients were considered who had formed at least 2 stones before the follow-up period [25].

As India comes under the stone belt region, urolithiasis affects about 2 million people every year and the incidence is comparatively low in southern India as compared to other parts of the country. In India, the "stones belt" occupies parts of Maharashtra, Gujarat, Rajasthan, Punjab, Haryana, Delhi and states of north-east [26]. Fewer occurrences of urinary calculi are found in southern India, which may be due to regular dietary intake of tamarind. A

recent study conducted by Ansari et al [27] at the All India Institute of Medical Sciences (AIIMS), New Delhi for upper urinary tract calculi; it was found that pure calcium oxalate is the most frequent stones. Prevalence of urolithiasis is high in many parts of India including Gujarat and Rajasthan [28-33]. The Saurashtra and Kutch region of Gujarat has higher prevalence of urinary stones. In India, 12% of the population is expected to have urinary stones, out of which 50% may end up with loss of kidneys or renal damage. Also, nearly 15% of the population of northern India suffers from kidney stones [34]. Singh et al [30] reported that the rate of incidence of urolithiasis, particularly staghorn calculi in Manipur is very high. Review of literature in urolithiasis in the recent past indicates that in India, there is an increased prevalence of the urolithiasis in north-western region [35]. Rao et al [36] reported a gradual increase of urolithiasis cases in Purnia division, situated in the northeastern part of Bihar during 1999-2001.

The epidemiologic studies have also shown a progressive increase in the incidence of pediatric urolithiasis over the last few decades, referred to as a "stone wave" [37]. VanDervoort et al [38] reported a fivefold increase in the prevalence of pediatric urolithiasis in North American children in the last decade. The incidence varies by region, but urolithiasis is most common in the southeastern region of the USA, where the states of Virginia, North Carolina, Georgia, Tennessee, and Kentucky are described collectively as the North American "stone belt" [39].

Recently, in the era of globalization, due to the use of melamine-tainted milk, milk powder as well as milk based food products such as cookies, candies and chocolates led to an emerging epidemic of nephrolithiasis and

acute kidney injury (AKI) among the people including children took place in East Asia, particularly in China, Taiwan, Hong Kong, and Macau [40]. Nearly 2,94,000 young children, most under 36 months of age, were diagnosed with urinary stones induced by melamine-tainted food in the mainland of China during the year 2008 [41].

Although nephrolithiasis is perceived as an acute illness, there has been growing evidence that nephrolithiasis is a systemic disorder that leads to end-stage renal disease [42]. The prevalence of this disease has been increasing among males and females of all ages, indicating a possible environmental cause in addition to genetic predisposition. Furthermore, the incidence of stone disease is increasing worldwide [43]. The lifetime risk of kidney stones is 6% for women and 12% for men [18]. For those with untreated stones, the risk at 5 years for forming another stone is 30% to 40%. Since all the epidemiological data show an increase in incidence and prevalence rates, the prevention and techniques for the medical management of urolithiasis requires further attention.

2.5 Crystalline Components of Urinary Calculi

Although the stone disease has been documented in ancient mankind [44] and indeed was avidly investigated by physicians and surgeons of advanced civilizations thousands of years ago, but much of the scientific analysis that rigorously investigated and accurately determined the components of urinary stone disease was carried out only within the past 200 years [45]. Urinary stone is usually a multiphase material; its compositions are complex and often found in a mixture of multiple mineral constituents. Knowledge of the composition of urinary stone is important because

urolithiasis is a recurrent disease in many people and preventive measures can be taken based on such information. There are several types of urinary calculi that differ in composition and pathogenesis. Major components of the urinary calculi are already listed in the literature [15, 45-47] Majority of the calculi are composed of calcium salts, oxalates and phosphates. Table 2.1 shows the major components of the urinary calculi.

Table : 2.1 : The Crystalline Components of Urinary Calculi

Compounds		Mineralogical Name	Formula
Oxalates	Calcium Oxalate Monohydrate (COM)	Whewellite	$\text{CaC}_2\text{O}_4 \cdot \text{H}_2\text{O}$
	Calcium Oxalate Dihydrate (COD)	Weddellite	$\text{CaC}_2\text{O}_4 \cdot 2\text{H}_2\text{O}$
	Calcium Oxalate Trihydrate (COT)		$\text{CaC}_2\text{O}_4 \cdot 3\text{H}_2\text{O}$
Phosphates	Hydroxyapatite (HA)	Hydroxyapatite	$\text{Ca}_{10}(\text{PO}_4)_6(\text{OH})_2$
	Calcium Hydrogen Phosphate Dihydrate (CHPD)	Brushite	$\text{CaHPO}_4 \cdot 2\text{H}_2\text{O}$
	Unusual form of Calcium Phosphate	Whitlockite	$\text{Ca}_9(\text{Mg,Fe})(\text{PO}_4)_6(\text{PO}_3\text{OH})$
	Tricalcium Phosphate		$\text{Ca}_3(\text{PO}_4)_2$
	Ammonium Magnesium Phosphate Hexahydrate (AMPH)	Struvite	$\text{NH}_4\text{MgPO}_4 \cdot 6\text{H}_2\text{O}$
	Ammonium Magnesium Phosphate Monohydrate	Dittmarite	$\text{NH}_4\text{Mg PO}_4 \cdot \text{H}_2\text{O}$
	Magnesium Hydrogen Phosphate Trihydrate	Newberyite	$\text{MgHPO}_4 \cdot 3\text{H}_2\text{O}$
	Carbonate Apatite	Carbonate apatite	$\text{Ca}_{10}(\text{PO}_4, \text{CO}_3, \text{OH})_6(\text{OH})_2$
	Octacalcium Phosphate	-	$\text{Ca}_8\text{H}_2(\text{PO}_4)_6 \cdot 5\text{H}_2\text{O}$
	Calcium Phosphate	Apatite	$\text{Ca}_5(\text{PO}_4)_3(\text{F,OH,Cl})$
Uric Acid	Uric Acid Anhydrous	Uricite	$\text{C}_5\text{H}_4\text{N}_4\text{O}_3$
	Uric Acid Dihydrate	-	$\text{C}_5\text{H}_4\text{N}_4\text{O}_3 \cdot 2\text{H}_2\text{O}$
Urates	Ammonium Acid Urate	-	$\text{C}_5\text{H}_3\text{N}_4\text{O}_3\text{NH}_4$
	Sodium Acid Urate Monohydrate		$\text{C}_5\text{H}_3\text{N}_4\text{O}_3\text{Na} \cdot \text{H}_2\text{O}$
Cystine			$\text{C}_6\text{H}_{12}\text{N}_2\text{O}_4\text{S}_2$
Purine	Xanthine		$\text{C}_5\text{H}_4\text{N}_4\text{O}_2$
	Melamine-associated urinary stones		$\text{C}_3\text{H}_6\text{N}_6 + \text{C}_5\text{H}_4\text{N}_4\text{O}_3$

The crystalline constituents of urinary calculi in the human are varied. Some of these occur geologically as a mineral, whereas others are found only in animal kingdom. To date over 200 components have been found in calculi; however, the most common constituents of kidney stones are as follows [45]:

2.5.1 Whewellite $\text{CaC}_2\text{O}_4 \cdot \text{H}_2\text{O}$

Calcium oxalate is the most common crystalline constituent of urinary stones. Usually, calcium oxalate occurs as three different phases: Calcium Oxalate Monohydrate (COM), Calcium Oxalate Dihydrate (COD) and Calcium Oxalate Trihydrate (COT). However, majority of them are of COM or COD.

Calcium oxalate monohydrate, also known as whewellite and synonymous with oxacalcite, is named after Professor William Whewell of Cambridge, England. Most calcium stones are formed when the calcium combines with oxalate. Occasionally, calcium may also combine with carbonate or phosphate. Calcium oxalate stones are the most common stone encountered by practicing emergency physicians [48]. All calcium stones are radio-opaque. Whewellite is one of the most common kidney stone minerals. It typically occurs as small, smooth, botryoidal to globular, yellow-green to brown, radially fibrous crystals and is traditionally hard to fragment.

2.5.2 Weddellite $\text{CaC}_2\text{O}_4 \cdot 2\text{H}_2\text{O}$

Calcium oxalate dihydrate (COD), also known as weddellite, is named after James Weddell. Like whewellite, weddellite is a calcium oxalate mineral. It differs from the whewellite in terms of amount of water included in its crystal structure, which gives very different crystal habit. Pure dihydrate stones are usually small and spherical consisting of a tan or yellow cluster of platelets. The platelets are sharp and are arranged in various orientations.

2.5.3 Calcium Oxalate Trihydrate $\text{CaC}_2\text{O}_4 \cdot 3\text{H}_2\text{O}$

Tomazic and Nancollas [49] reported that COT could be a precursor to COM and COD formation. There is supporting evidence that the COT is the first nucleated crystal phase of calcium oxalate. Subsequently, COT is converted to COD and then to COM [50].

2.5.4 Apatite

Hydroxyapatite, or hydroxylapatite, also known as apatite, is named from the Greek word *apatao* meaning “I am misleading”, in allusion to its similarity to other more valuable minerals such as the gems peridot and beryl. Apatite is a common mineral in nature. Chemically it is a complex calcium phosphate with varied, attached molecules of hydroxyl (*OH*), fluorine (*F*), and sometimes other elements. Apatite is the fundamental mineral component in bones and teeth, and when apatite has fluorine in its crystal structure, it is stronger. In kidney stones, the hydroxyl group is predominant, and carbonates (CO_3) substitutes for some of the phosphate, forming a mineral that is relatively poorly crystallized. Apatite often forms the nucleus on which other urinary minerals are deposited.

2.5.5 Brushite $\text{CaHPO}_4 \cdot 2\text{H}_2\text{O}$

Calcium hydrogen phosphate dihydrate, also known as brushite, was named in 1864 by G. E. Moore, in honor of George Jarvis Brush. Brushite is a calcium phosphate compound that is very similar to the common mineral gypsum (calcium sulfate). Brushite is found as a common cave mineral in guano deposits and in phosphorites formed at low pH (acidic) by reaction of phosphate rich solutions with calcite and clay. It is a soft, silky mineral, usually honeybrown and showing a fine radial fibrous structure.

2.5.6 Whitlockite $\text{Ca}_3(\text{PO}_4)_2$

Tricalcium phosphate, or whitlockite, was named in 1940 for Herbert Percy Whitlock, who was a 20th century American mineralogist. Whitlockite is very rarely found in the urinary system and is usually found in prostate stones. It is a calcium phosphate with small amounts of magnesium, $\text{Ca}_9(\text{Mg,Fe})\text{H}(\text{PO}_4)_7$ or $\text{Ca}_9(\text{Mg,Fe})(\text{PO}_4)_6(\text{PO}_3\text{OH})$, and its occurrence may be stabilized by trace amounts of zinc, which perhaps accounts for its predilection for the prostate gland, which has a relatively high zinc content. The mineral is a resinous, brown material.

2.5.7 Struvite $(\text{NH}_4)\text{MgPO}_4 \cdot 6(\text{H}_2\text{O})$

Ammonium Magnesium Phosphate Hexahydrate (AMPH), also known as struvite, is one of the fascinating inorganic phosphate minerals. It was first identified in the 18th century as a crystalline substance. The term “struvite” was introduced in 1845 by George Ludwig Ulex, a Swedish geologist [45]. It was named after geographer and geologist Heinrich Christian Gottfried von Struve of the Russian diplomatic service, consul at Hamburg, Germany.

Struvite is the main component of the infectious urinary stones and is associated with chronic urinary tract infection (UTI) with microorganisms that split urea into ammonium, which further combines with phosphate and magnesium. UTI does not resolve until stone is completely removed. Usually, the formations of struvite type calculi take place when the urine pH is typically greater than 7. Radiographs show that struvite stones are usually large, gnarled, and laminated ones. Struvite stones are among the most difficult and dangerous problems in stone disease because of the potential of life-threatening complications from infections.

Epidemiological studies from various countries continue to report a frequency of struvite stones of between 25% and 38% out of total observed cases with urinary calculi [51,52]. It was reported that struvite was present in 42.9% of stones in women in Sub-Saharan Africa, 13% in South America [51], 28.8% in Algeria [52]. Griffith [53] reported that struvite stones are relatively uncommon in the USA, making up to 15% - 20% of kidney stones. Durgawale et al [54] reported that uroliths obtained by surgical intervention at Krishna Institute of Medical Sciences and Research Centre, Karad, in Maharashtra, were of mixed heterogeneous type with struvite as predominant constituent having 71.2%. Pendse and Singh [55] reported that struvite was present in 78.2% stones out of 56 stones analyzed, which were collected from clinics of Udaipur in Rajasthan.

2.5.8 Dittmarite $NH_4Mg PO_4 \cdot H_2O$

It was named after William Dittmar (1833-1892), Professor of Chemistry, University of Glasgow, Glasgow, Scotland. Dittmarite is found rather infrequently in urinary calculi [56].

2.5.9 Newberyite $MgHPO_4 \cdot 3H_2O$

Magnesium hydrogen phosphate trihydrate, also known as Newberyite, is named in honour of James Cosmo Newbery (1843–1895), who was a 19th century Australian geologist and mineralogist. Newberyite is rare in kidney stones. It was first identified as a crystalline component of a kidney stone in 1956 [57]. It often occurs as tiny isolated globular crystals on the surfaces of apatite–struvite stones. This probably reflects an alteration of struvite to newberyite, or perhaps a change of conditions to more acidic solutions.

2.5.10 Uric acid stones

Usually, uric acid stones are found between 5 to 10% of all stones analyzed in a stone clinic. Uric acid is a product of metabolism. Generally, these stones are associated with urine pH less than 5.5. Uric acid stones are spherical with a smooth yellow-orange surface and nearly radiographically transparent unless mixed with calcium crystals or struvite. Approximately 25% of patients with uric acid stone have gout problem. There are three major factors for the development of uric acid stones, low urine volume, acidic urine pH, and hyperuricosuria.

2.5.11 Cystine Stones

Cystine stones account for only 1 to 3 % of all kidney stones. They form in individuals with a rare inherited metabolic disorder that causes high levels of cystine in the urine. These stones can occur in childhood. Cystine is one of the essential amino acids, which are the building blocks of protein. Cystinuria is an uncommon genetic disorder that causes the kidney to excrete too much cystine type amino acid in the urine. The concentrated cystine leads to the formation of cystine kidney stones. Cystine is relatively insoluble, and appears in normal urine in small amounts that are insufficient to cause supersaturation, crystalluria, or stone formation.

2.5.12 Xanthine $C_5H_4N_4O_2$

Chemically, xanthine is a purine. These stones are extremely uncommon and usually occur as a result of a rare genetic disorder. It can be caused by a deficiency of xanthine oxidase (enzyme necessary for converting xanthine to uric acid), which results in the production of xanthine and hypoxanthine rather than uric acid as an end product of purine metabolism

[58]. Xanthine stones are radiolucent, but can be detected by using computed tomography. Inasmuch as xanthine stones are radiolucent they are frequently mistaken for the more common radiolucent uric acid stone. Usually, these stones tend to be small, round or oval in shape.

2.5.13 Matrix :

Matrix stone is a rare form of urinary calculi made of organic material muco-proteins. Usually they are radiolucent; however the radiologic aspect of these stones depends on the degree of mineral incrustations. The percentage of matrix, by weight, in urinary stones varies. In general, most solid urinary stones have a matrix content of about 3% by weight [59]. Matrix stones are non-crystalline and take on a variety of shapes and colors. The stones are composed of a variety of organic molecules including urinary macromolecules and membrane fragments.

2.5.14 Medication Related Stones

Unusual types of urinary calculi caused by ingestion of inappropriately large doses of medications are Ephedrine stones, Guaifenesin stones, Indinavir stones, Nelfinavir stones, Oxypurinol stones, Silicate stones, Sulfa stones, Topimarate-induced stones, Triamterene stones, Ammonium acid urate stones, Ciprofloxacin induced stones, etc [60].

Ephedrine stones : Ephedrine containing drugs have been used as bronchodilator for asthma, as a cough medicine, as a fat burner for weight loss, energy and sexual enhancement, as a stimulant and euphoria. But, excessive ephedrine intake can cause ephedrine nephrolithiasis and results in radiolucent ephedrine kidney stones. Usually, ephedrine is highly water soluble, however urine alkalinity decreases solubility.

Guaifenesin stones : Guaifenesin (glyceryl guaiacolate) is sold as pills or syrups and most often used as an expectorant, i.e., medication that helps bring up mucus and other material from respiratory tract including the lungs, bronchi, and trachea. Moreover, it is also used for the treatment of asthma, gout, fibromyalgia, to facilitate conception and as analgesic drug. But, excessive guaifenesin intake can cause guaifenesin urolithiasis and results in radiolucent guaifenesin kidney stones.

Indinavir (Crixivan) stones : Indinavir (Crixivan) is an antiretroviral (protease inhibitor) medication used in the treatment of HIV infections. It easily precipitates to form crystals. Due to the gelatinous nature of indinavir stones, they are not visible on plain radiographs. These calculi are difficult to detect by X-ray or CT scan. However, CT scan with contrast may demonstrate the presence of these stones. They are visible on an ultrasound. Indinavir crystals form at a pH of 7. Indinavir crystals are very distinctive, with a fan-shaped or starburst type of appearance. Pure indinavir stones are brown and have a pliable, puttylike consistency. Several other antiretroviral drugs such as ritonavir, nelfinavir, saquinavir, efavirenz and atazanavir have been reported to cause urinary calculi.

Nelfinavir Stone : Similar to indinavir stones, nelfinavir stones are radiolucent. However, in contrast to indinavir calculi, nelfinavir stones are visible on CT scan.

Oxypurinol Stones : The oxypurinol stone is seen in patients using high dose of allopurinol (600 mg/d). These stones are soft, yellow and radiolucent.

Silicate Stone : Silicate urinary calculi occur exclusively in patients taking large amounts of magnesium silicate antacids. They are extremely rare in

humans, but occurs in animals, when they are fed plants grown in sandy areas or water containing high levels of silica. In Japan, 46 adult patients with urinary silicate calculi have been reported in the literature [61].

Sulfa Stones : Sulfamethoxazole-trimethoprim is a commonly employed antibiotic. Sulfonamides, sulfadiazine medication commonly used to treat AIDS. Various sulfa compounds, such as sulfadiazine, acetylsulfasoxazole, acetylsulfamethoxazole, acetylsulfaguanadine and may precipitate in the urine and may lead to formation of sulfa stones. Usually, sulfa-induced calculi were found in the bladder and they are radiolucent on plain radiography.

Triamterene Stones : Triamterene is often used to treat edema as well as hypertension. Triamterene calculi are faintly radiopaque on plain radiography; however, they are detectable with CT scan. Triamterene is most commonly seen as a secondary component of calcium oxalate or uric acid stones, and has been described as a nidus for secondary stone formation. Triamterene calculi cannot be dissolved by pH manipulation and, rather, must be treated with conventional lithotripsy techniques.

2.5.15 Rare types of Urinary Calculi

There are certain rare types of urinary calculi which are summarized briefly as follows :

Urostealith Calculi: They are composed of fatty constituents and occasionally found in urinary concretions, but very rarely composing the entire calculus.

Cholesterol Calculi : They are usually yellow-green in color and are made mostly of hardened cholesterol.

In figure 2.4 photographs of different types of kidney stones are shown courtesy to L. C. Herring laboratory [62].



			
Calcium Oxalate Monohydrate	Calcium Oxalate Monohydrate	Calcium Oxalate Monohydrate	Calcium Oxalate Monohydrate with Apatite
			
Calcium Oxalate Dihydrate	Calcium Oxalate Dihydrate	Calcium Oxalate Dihydrate	Calcium Oxalate Monohydrate with superficial Dihydrate
			
Irregularly Laminated Oxalates & Apatites	Calcium Oxalate Monohydrate irregularly laminated with Apatites	Calcium Oxalate Monohydrate deposited over Apatites	Carbonate Apatite
			
Brushite	Brushite	Brushite	Tricalcium Phosphate with Apatites
			
Struvite	Struvite	Uric Acid	Cystine
			
Xanthine	Calcium Carbonate	2,8-dihydroxyadenine	Cholesterol (Biliary)

Figure : 2.4 Photographs of Kidney Stones [62] [Source: L. C. Herring & Co. Laboratory]

2.6 General Pathophysiology of Urinary Calculi

The physical process of stone formation is a complex cascade of events. Kidney stones result from the growth of crystals into stones [7]. The process of stone formation depends on urinary volume; concentrations of calcium, phosphate, oxalate and sodium ions; concentrations of natural calculus inhibitors and urinary pH [63]. High ion levels, low urinary volume, low pH, and low citrate levels favor the formation of urinary calculi. The pathogenesis of urinary calculi formation is the end result of the following fundamental multi-step physicochemical processes :

Saturation → Supersaturation → Nucleation → Crystal aggregation → Crystal growth → Crystal retention → Stone formation

2.6.1 Supersaturation : The central event in stone formation is supersaturation. The term supersaturation refers to a solution that contains more of the dissolved material than could be dissolved by the solvent under normal circumstances. Supersaturation occurs when the concentration of substances forming urinary calculi increases in urine, or urine volume decreases, as well as the absence or reduction in urinary stone inhibitors occurs in urine. Supersaturation depends on urinary pH, ionic strength, solute concentration, and complexation. The level of supersaturation of a salt is expressed as the ratio between the actual ion-activity product (AP_{salt}) and the solubility product (SP_{salt}). The ion-activity of a salt is calculated from the free ion concentrations and the activity coefficients corresponding to the charge of the ions in the salt. The point at which saturation of a solution is reached, and crystallization begins is commonly known as thermodynamic solubility product (K_{sp}). Urine contains inhibitors of crystallization and can hold large

concentrations of solute above the K_{sp} , a metastable state. If the concentration of solute increases further and a point is reached where it cannot be held in solution, this concentration is known as K_F , which is the point of formation of product in urine [15,64]. Thus, supersaturation of the urine constitutes a driving force within the solution which can lead to crystallization and trigger a series of pathophysiologic events that include nucleation, crystal aggregation, growth, and attachment to epithelia. There are two stages of supersaturation. Once the solubility product exceeds in urine, a metastable process of supersaturation begins, which is followed by slow crystalline growth. This process is accelerated by preexisting crystals. If a critical limit of supersaturation is exceeded (formation product), large scale spontaneous precipitation of crystals occurs.

2.6.2 Nucleation : Urinary supersaturation alone cannot explain the formation of urinary stones. Nucleation is the formation of a solid crystal phase in a solution. It is an essential step in the formation of urinary calculi [65]. Nucleation involves the association of crystalloids in solution to form a submicroscopic particle. There are two types of nucleation; the homogeneous nucleation and the heterogeneous nucleation. The homogeneous nucleation results, when the process occurs spontaneously in a pure solution. Because impurities are always present in human urine, the homogeneous nucleation is unlikely to occur *in vivo*. Heterogeneous nucleation sites in urine can be epithelial cells, red blood cells, cell debris, urinary casts, other crystals and bacteria. The surfaces provided by the impurities can serve as a nidus in the nucleation process, leading to the heterogeneous nucleation. The heterogeneous nucleation will, generally, occur at a lower supersaturation

level than that required for the homogeneous nucleation [15]. The nucleation of crystalline components may occur in the lumens of renal tubules, in the basement membranes of tubule cells, or at both sites, perhaps depending on the type of stone.

2.6.3 Crystal Aggregation : The process in which crystal nuclei bind to each other to form larger particles is called aggregation. The initial nuclei can grow by further addition of desired salts. Aggregation of particles in solution is determined by a balance of forces, some with aggregating effects and some with disaggregating effects. A small inter-particle distance increases the attractive force and favours particle aggregation. Crystal aggregation plays an important role in stone formation.

2.6.4 Crystal Growth : Crystal growth is the next major step of the formation of urinary calculi. In this process atoms or molecules from solution are added to the solid phase of growing crystal in a geometrically precise arrangement. The driving force for crystallization is a reduction in the potential energy of the atoms or molecules when they form bonds to each other. The crystal growth process starts with the nucleation stage. Several atoms or molecules in a supersaturated liquid start forming clusters; the bulk free energy of the cluster is less than that of the liquid. The total free energy of the cluster is increased by the surface energy (surface tension), however, this is significant only when the cluster is small. Crystal growth is determined by the molecular size and shape, the physical properties of the material, the supersaturation levels, the pH of solution, and the defects present in the structure of crystal. The combination of crystal aggregation and crystal growth can explain the genesis of urinary calculi.

2.6.5 Crystal Retention : Another process that may lead to stone formation is crystal retention. None of the previously discussed elements, i.e., crystal precipitation, growth, and aggregation would result in urinary stone formation if the nucleated crystals were flushed out by urinary flow. Crystal retention is, therefore, a key factor. Crystal retention will result if the crystals grow large enough to be trapped in renal tubules.

2.6.6 Role of Promoters and Inhibitors

Urine is having several substances that change or modify the crystal formation [15]. These can further be divided into inhibitors, promoters and complexors. In general, the crystallization of stone-forming salts is due to an abnormal urinary composition that is either higher in crystallization promoters or lower in inhibitors or both [66].

Substances which prevent or reduce the crystallization are called inhibitors. Urinary inhibitors attach to the growth sites on crystals, retarding further growth and aggregation. Inhibitors exert their effects in multiple ways, including inhibition of primary and secondary nucleation and crystal growth and aggregation. Urinary inhibitors may be categorized into multivalent metallic cations, small organic or inorganic anions, or macromolecules.

Promoters promote the growth of crystals and facilitate the formation of urinary calculi. It may be possible that a substance may promote one stage of crystal formation such as growth and inhibits another stage such as aggregation.

Certain substances, which form soluble complexes with lattice ions of specific crystals, decrease the free ion activity of that ion and effectively decrease the state of saturation for that ion system. These substances are

known as complexers. Citrate is the potent complexor of calcium in urine and reduces ionic calcium concentration. Table 2.2 shows the promoters, inhibitors and complexors [15, 64, 66-71].

Table : 2.2 : Urinary Stone Promoters and Inhibitors

Role	Substances in the urine
Promoters	Calcium, Sodium, Oxalate, Uric Acid, Urate, Cystine
Inhibitors	Magnesium, Potassium, Pyrophosphate, Citrate, Glycosaminoglycans (GAGs) kidney proteins such as Nephrocalcin (NC), Osteopontin (OPN), Tamm-Horsfall protein (THP), Muco-protein, Uropontin, Crystal matrix protein, Renal lithostathine, Urinary prothrombin fragment 1, Bikunin (Inter-alpha inhibitor), Calgranulin
Complexor	Citrate is the complexor for calcium ions.

Supersaturation takes place with low urine volume and abnormally high concentration of stone promoters as well as low concentration of stone inhibitors. When the balance of components in the urine is off, or a person is dehydrated, deposition is likely to occur on the walls of the kidneys, the ureter, or the bladder, forming crystals. In most cases, these crystals are removed from the body by the flow of urine, but they sometimes stick to the lining of the kidney or settle in places where the urine flow fails to carry them away. These crystals may aggregate and grow into a stone, ranging in size from a grain of sand to a golf ball. Most of the stones start growing in the kidneys. Some may travel to other parts of the urinary system, such as the ureter or bladder, and grow there. Mineralization in all biological systems has a common theme, in which the crystals and matrix are intertwined. Urinary stones are no

exception; they are polycrystalline aggregates composed of varying amounts of crystallite and organic matrix.

2.7 Etiology of Urinary Calculi

Etiology is the study of causes of disease. The development of stones in the urinary tract is a complex, poorly understood, multifactorial process. The formation of urinary calculi is a final manifestation of a broad range of etiologies and pathogenesis. A number of chemical and physical factors are known to play their roles. Kidney stones develop as a result of a complicated interaction of biologic events that are most likely triggered by genetic susceptibility coupled with dietary factors. Various etiologic factors play important role in the formation of urinary calculi. The primary known causes for the formation of urinary calculi are as follows:

2.7.1 Low Urine Volume

Low fluid intake greatly increases the risk of developing virtually all types of stones [72-74]. Urolithiasis is related to decreased urine volume as well as increased excretion of stone-forming components such as calcium, oxalate, urate, cystine, xanthine, and phosphate. Dehydration may also lead to formation of urinary calculi. When there is too little water in the body, the kidneys conserve water by forming less urine, and as a result the urine they produce is highly concentrated. People who live in hot climates may be susceptible to kidney stones if fluid is lost through perspiration [75].

2.7.2 Changes in the Urinary pH

Urinary pH is a major determinant for kidney stone formation. Changes in the balance of urinary pH can affect stone precipitation. Kamel et al [76] have suggested that urine pH approximately 6.0 reduces the risk of kidney

stone formation. However, the risk of uric acid and calcium stone formation increases progressively at urinary pH < 5.5 and > 6.5, respectively. Generally, some crystals are found exclusively in acidic urine, while the others are found exclusively in alkaline urine. Uric acid, calcium oxalates and cystine stones thrive in acidic urine, whereas calcium phosphate, calcium carbonates and struvite stones thrive in alkaline urine.

An elevated net acid excretion may occur due to increased endogenous acid production or because of dietary influences such as low dietary alkali or the increased consumption of acid-rich foods. Intake of high animal protein is known to reduce urinary pH and may lead to the formation of uric acid stones [77]. This happens due to the generation of protons during the oxidation of sulfur in animal proteins to sulfate [78].

2.7.3 Deficiency of Stone Inhibitors

The urinary constituents such as citrate, magnesium, zinc, glycosaminoglycans, pyrophosphate, various glycol-proteins and enzymes as listed in table 2.2 act as urinary inhibitors. At the physicochemical level, the urinary supersaturation capacity can be increased and crystal formation, growth, and aggregation can be delayed or prevented by micro and macromolecular urinary constituents. Inhibitors act by adsorption on the crystal surface, interfering with the formation of the crystal lattice and retarding the attachment of new ions, thus inhibiting nucleation, and most importantly, growth and aggregation into larger crystals. These compounds may protect against stone formation in various ways like allowing salt in the urine to be at higher-than-normal concentrations without forming crystals, preventing crystal formation, coating the crystals and preventing them for

adhering to the tube surface. Deficiencies in these protective substances therefore cause urinary calculi.

Nephrocalcin (NC), an acidic glycoprotein excreted in human urine, greatly reduce consumption of calcium and oxalate from metastably supersaturated solutions seeded with calcium oxalate crystals, a phenomenon usually referred to as inhibition of crystal growth. Urine and NC suppress self-nucleation *in vitro* by adsorbing to the surface of COM crystals [79,80].

Tamm-Horsfall glycoprotein (THP) inhibits self-aggregation of COM crystals and may therefore be part of the natural defenses against deposition of COM in the kidney [81].

Glycosaminoglycans (GAGs) are well known macromolecular inhibitors found in urine. This growth inhibitor of COM is expected to affect at certain growth sites of crystal surface. The GAGs binds to crystal surfaces in a regular manner than at random, depending on the species. The binding sites are calcium sites on the faces matching negatively charged side groups on the GAG chains. The extensive study has been carried out to investigate the role of GAG in inhibition of COM by using Atomic Force Microscopy (AFM) [82,83].

Osteopontin (OPN), an aspartic acid-rich urinary protein, and citrate, a much smaller molecule, are potent inhibitors of COM crystallization at levels present in normal urine. Recently, extensive studies by James De Yoreo et al [84] on the combination of *in situ* atomic force microscopy (AFM) analyses of the effects of citrate and OPN with molecular modeling have defined both the physical and stereochemical factors responsible for COM inhibition by citrate and OPN.

Low Urine Levels of Citrate (Hypocitraturia) : Citrate (Citrate is the dissociated anion of citric acid) inhibits the growth of urinary calculi [85]. It is the primary agent for removal of excess calcium. Generally, citrate is excreted in normal urine at a mean of about 3.3 mmol/day (640 mg/day) in healthy individuals [86]. Hypocitraturia is defined as citrate excretion of less than 1.67 mmol/day (320 mg/day). Low level of citrate in the urine is a significant risk factor for calcium stones and also uric acid stones. Sometimes the Renal Tubular Acidosis (RTA) results in abnormalities in the acid and alkaline balance in the fluids of body, which causes a reduction of citrate in the urine. To make matters worse, the disorder also causes bone resorption and increases calcium levels in the blood.

Studies on the effects of urinary components, e.g., heparin (a highly-sulfated glycosaminoglycan) [83], phosphocitrate [87,88], nephrocalcin [89], and various surfactants [90] on the growth of calcium oxalate, struvite and hydroxyapatite are widely reported. These studies show a range of effects including inhibition of crystal formation, hydromorph selectivity, habit modification and promotion of the formation of metastable phases.

2.7.4 Use of Certain Medications

Urinary calculi may be induced by a number of medications used to treat a variety of conditions as discussed earlier in the section 2.5.14 of this chapter. These medications may lead to metabolic abnormalities that facilitate the formation of stones. Drugs that induce metabolic calculi include loop diuretics; carbonic anhydrase inhibitors; and laxatives, when abused. The formation of various types of urinary calculi due to overdose of certain medications for long periods have been reported in the literature [91-95].

Medication-induced calculi can be composed of the drug or one of its metabolites, and their formation may be promoted by the urinary supersaturation of these substances. Alternatively, the drug may induce physiologic changes that facilitate the formation of metabolic stones. The incidence of drug-induced urolithiasis is 0.44% [93].

Recently, a new cause of drug-induced acute kidney injury, namely, acute phosphate nephropathy, has been reported by Markowitz and Perazella [94] following the use of oral sodium phosphate bowel purgatives, which has lead to calcium phosphate type urinary calculi.

2.7.5 Excess Calcium in the Urine (Hypercalciuria)

The excessive calcium in the urine is known as hypercalciuria. Hypercalciuria is the most common etiology of urolithiasis in children as well as in adults [27,96]. It is responsible for about 70% of calcium-combining stones. A number of conditions may produce hypercalciuria. The development of hypercalciuria involves interactions between the gastrointestinal tract, bone and kidney, and a complex interplay of hormones, such as parathyroid hormone (PTH), calcitonin, and vitamin D. In a recent study, hypercalciuria is the most common risk factor, rounding about 40%, for the development of urolithiasis in children [97].

The conditions which can contribute to hypercalciuria are as follows:

Overly Efficient Intestinal Absorption of Calcium : In more than half of the cases, the source of excess calcium overload in urine is from the intestine, which may be due to a combination of genetic factors.

Renal Calcium Leak : This is a condition in which the filtering processes in the kidney fail, causing an increase of calcium in the urine.

Increased Intake of Dietary Calcium : Consumption of animal protein from meat, dairy, poultry, or fish increases urinary calcium. An increased level of urinary calcium also increases the risk of stone formation [98-100].

Excessive Chloride : Chloride has a negative charge and calcium has a positive one, so they are often used by the body to balance each other. The presence of excess chloride may lead to excess calcium. Many times it is found that a gene known as CLCN5 (chloride channel 5), which regulates chloride in the urine, is defective in the patients with calcium stones.

Excessive Sodium : Calcium absorption in the kidney tubules follows the absorption of sodium and water. High urinary levels of sodium then results in increased levels of calcium. Defects in the kidney tubules transport system can cause imbalances in sodium and phosphate that result in elevated calcium level in the urine. A high salt diet can also produce this effect.

Disorder : Certain cancers and sarcoidosis (a chronic disorder marked by small lumps on organs) can cause excess calcium.

Medications : Many drugs, including thyroid hormones and loop diuretics (drugs that increase urination), can increase calcium concentration in urine. Stones are an uncommon side effect of these medications.

Idiopathic Hypercalciuria : Idiopathic hypercalciuria (IH) is the most common metabolic abnormality in patients with calcium kidney stones. It is characterized by normocalcemia, absence of diseases that cause increased urine calcium, and calcium excretion that is greater than 250 mg/day in women and 300 mg/day in men [101]. The IH occurs with normal serum calcium and in the absence of any systemic diseases [102].

Figure 2.5 shows the classification of hypercalciuria.

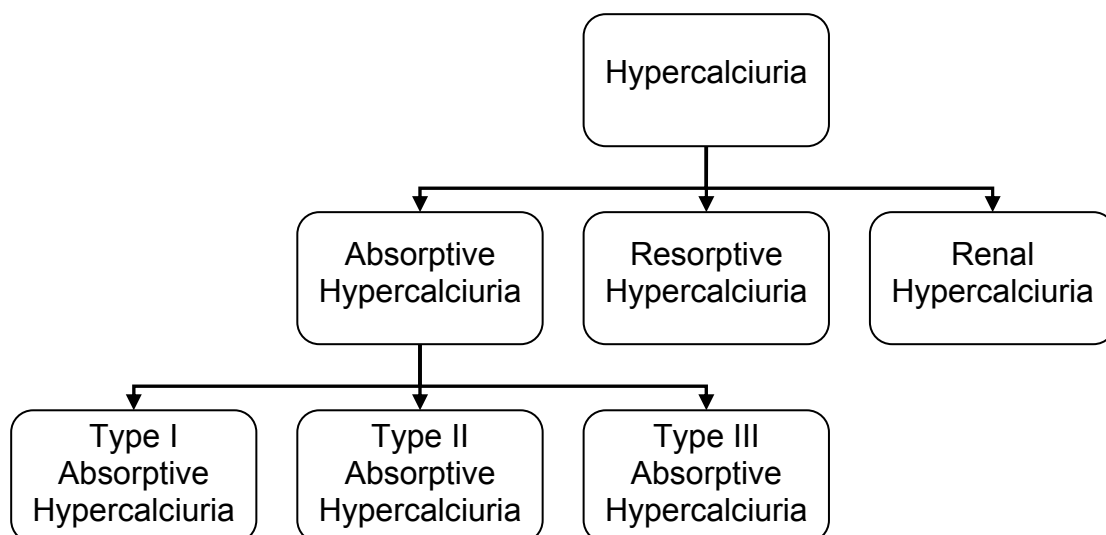


Figure : 2.5 Classification of Hypercalciuria

Absorptive Hypercalciuria : Absorptive hypercalciuria (AH) is a disorder involving the excessive absorption of calcium by the intestines which increases the body's calcium levels and inhibits the functioning of the parathyroid gland. Normal calcium intake averages approximately 900–1000 mg/day. Approximately one-third of this is absorbed by the small bowel and out of that approximately 150–200 mg is obligatorily excreted in the urine [103]. The AH can be subdivided into three parts.

- Type I absorptive hypercalciuria is dietary independent. Patients have elevated urinary calcium levels with a high or low calcium diet.
- Type II absorptive hypercalciuria is dietary dependent and patients will have elevated urinary calcium levels only while consuming a high calcium diet.
- Type III absorptive hypercalciuria is secondary to a phosphate renal leak. The decreased phosphate results in a secondarily increased parathyroid hormone level and an increase in vitamin D production. The increased vitamin D results in increased phosphate, which further

increases calcium absorption, thus it is named as absorptive hypercalciuria.

Resorptive Hypercalciuria : Resorptive hypercalciuria is the result of a rare metabolic disorder, which causes the body to produce too much parathyroid hormone (hyperparathyroidism), causing bone tissue to dissolve. The dissolved tissue creates excessive calcium in the blood that accumulates in the kidneys and produces calcium stones [104].

2.7.6 Excess Oxalate in the Urine (Hyperoxaluria)

The excessive oxalate or oxalic acid in the urine, known as hyperoxaluria, is responsible for about 30% of calcium stones and is a more common cause of stones than excessive calcium in the urine [105]. Oxalic acid combines with calcium to form calcium oxalate which is the most common stone-forming compound. The hyperoxaluria is encountered in 8–50% of kidney stone formers [106].

The conditions which can contribute to hyperoxaluria are as follows :

Primary hyperoxaluria (type I or type II): A rare cause of hyperoxaluria is the inherited condition known as primary hyperoxaluria [107]. Among disorders causing hyperoxaluria, the primary hyperoxaluria is the most severe, ultimately leading to the end-stage renal failure and if untreated, death in most of the patients. It is a hereditary metabolic disorder of amino acid metabolism that leads to increased production and excretion of oxalate (> 40 mg / day) even on oxalate-restricted diets. It is characterized by recurrent nephrolithiasis leading to renal failure [108]. In this condition, the hepatic enzyme that converts glyoxalate to glycine is deficient. As a result, there is increased production of oxalate from glyoxalate. This is an inherited disorder

associated with kidney stones. These conditions are typically present with multiple stones in childhood and may cause renal failure, although presentation in adulthood is also possible [109].

Deficiencies of Pyridoxine (Vitamin B6) : Severe vitamin B6 deficiencies can result in overproduction of oxalic acid. Vitamin B6 deficiency leads to an increase in urinary calculi as a result of elevated urinary oxalate [110].

Short Bowel Syndrome : This disorder is the inability of the intestines to absorb fat and nutrients. In such cases, calcium may bind to unabsorbed fat instead of to oxalates. This leaves excess oxalate, which is absorbed by the intestine and excreted into the kidney.

Dietary Oxalates : Whether eating foods rich in oxalates or taking too much vitamin C plays any major role in hyperoxaluria is unproven. Many foods contain oxalate; however, only a few—spinach, rhubarb, beet greens, nuts, chocolate, tea, bran, almonds, peanuts, strawberries, tomatoes, beans, beets and radishes—appear to significantly increase urinary oxalate levels [111].

Hormones : Androgens (male hormones) are associated with a higher risk for calcium oxalate formation, while estrogens (female hormones) decreased it.

2.7.7 Excessive Calcium in the Bloodstream (Hypercalcemia)

Hypercalcemia is an abnormally high level of calcium in the blood, usually more than 10.5 mg / dL of blood, which also plays an important role in the formation of urinary calculi [112]. Hypercalcemia generally occurs when bones break down and release too much calcium into the bloodstream. This is a process called resorption, which can occur because of following reasons:

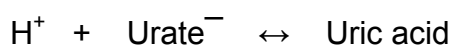
Hyperparathyroidism : Overactive parathyroid glands are the causes of about 5% of calcium stones. And people with this disorder have at least a

20% chance of kidney stones. Women are more likely to have this disorder than men are.

Renal Tubular Acidosis : Renal Tubular Acidosis (RTA) is a disease that occurs when the kidneys fail to excrete acids into the urine, which causes a patient's blood to remain too acidic. It not only increases calcium in the blood stream, but it also reduces citrate levels.

2.7.8 Excessive Amounts of Uric Acid (Hyperuricuria)

Uric acid [$C_5H_4N_4O_3$ - {7,9 dihydro-1H-purine-2,6,8(3H)-trione}] is a weak organic acid and major metabolite of purine nucleotides. Excessive amounts of uric acid, i.e., the hyperuricuria may also play a role in the formation of urinary calculi. Uric acid stones most often form out of high concentrations of uric acid. The two major factors that promote uric acid precipitation are a high urine uric acid concentration and an acidic urine pH, which drives the following reaction toward the right, converting the relatively soluble urate salt into insoluble uric acid.



In some cases, urate (anion of uric acid or the salt formed from uric acid) creates a crystal nidus, around which calcium oxalate crystals form and grow. Such stones tend to be severe and recurrent. Hyperuricuria occurs after eating purine-rich foods or because of uric acid overproduction [113]. A uric acid stone is an end product of purine metabolism.

Generally, urinary uric acid solubility is limited to 96 mg / L in normal urine. In humans with the urinary uric acid excretion of 600 mg / day, generally, exceeding the limit of solubility, is susceptible to precipitation [114]. Moreover, the urine pH is another important factor in uric acid solubility. The

ionization constant of uric acid is 5.35 [114, 115]. Therefore, at the urine pH less than 5.35, the urinary environment becomes supersaturated with sparingly soluble, undissociated uric acid that precipitates to form uric acid stones [116].

2.7.9 Defect in Renal Ammonia Secretion

In some patients very low urine pH is caused by a defect in renal ammonia secretion that results in less buffering of secreted hydrogen ion and lower urine pH. Sakhaee et al [116] suggested that very low urine pH is in some way related to the insulin resistance. Uric acid is insoluble (15 mg / dL) in urine at pH 5.0, but becomes significantly more soluble (150 mg / dL) in urine at pH 7.0. Any combination of low urine pH, concentrated urine, and increased urinary uric acid excretion make one at risk for uric acid stone.

2.7.10 Inappropriate Renal Phosphate Transport

The control and balance of serum phosphate concentration, which is carried out by kidneys, is mandatory to avoid the occurrence of severe metabolic disorders. Inappropriate renal phosphate transport may alter serum phosphate concentration and bone mineralization and as a result increase the risk of urinary calculi [117]. Hypophosphatemia is also associated with bone demineralization and increased risk of occurrence of urinary calculi [118].

2.7.11 Urinary Tract Infections (UTI)

Urinary calculi may also result from long-standing urinary tract infections (UTI), which affects as many as 50% women at least once during their lifetime [119]. Generally, struvite and carbonate apatite type urinary calculi form as a result of UTI. Struvite calculi are formed due to UTI with various urease producing urolithic microorganisms like *Proteus* (most

commonly), *Pseudomonas*, *Klebsiella*, some *Escherichia coli*, and *Staphylococcus* species, that split urea and cause persistently alkaline urine [47,53,113,120].

2.7.12 Genetic Abnormalities

Some other urinary calculi, like cystine and xanthine, are usually due to genetic abnormalities. Cystine stone disease occurs in individuals who have an inherited genetic disorder that causes abnormal transport in the kidney and gastrointestinal system of the four amino acids, namely, cystine, ornithine, lysine, and arginine (COLA). Cystine type urinary calculi arise from excessive cystine excretion [121]. The cystine is the most insoluble in normally acidic urine and thus precipitates, crystallizes and forms stones [122,123]. The cystine is normally absorbed by the kidney. When there is defective absorption, large amounts of this amino acid are excreted in the urine and may crystallize and form large stones.

2.7.13 Vitamin Abnormalities

Vitamin abnormalities, e.g., vitamin A deficiencies, excessive vitamin D, are also responsible for the formation of urinary calculi.

2.7.14 Other Risk Factors of Urinary Calculi

A variety of intrinsic and extrinsic factors influence urolithiasis in individuals. Urolithiasis is a multifactorial disorder arising essentially from an abnormal combination of a number of urinary risk factors. Epidemiologic data, particularly, differences in occurrence rates among populations, strongly suggest that various environmental factors such as diet, climate, geographical factors and fluid consumption play a strong etiologic role [15, 124].

Inherited Factors : Inherited factors account for 45% of all cases of kidney stones. A person with a family history of kidney stones may be more likely to develop stones [125-126]. More than 70% of patients with adequate hereditary disease called renal tubular acidosis develop kidney stones.

Age : Stone occurrence is relatively uncommon before the age of 20 years but peak in incidence occurs in the fourth to sixth decades of life. The prevalence of stone disease increases with age until of 70 years. The incidence of nephrolithiasis exhibits peak between the ages of 20 and 60 years and 50% of stone formers will have a recurrence within 5 years [127]. The intestinal absorption of many nutrients that influence stone formation, such as calcium, may be reduced in the elderly persons [128,129]. In men, the incidence of kidney stones declines markedly after 60 year of age [99,130] suggesting that the pathophysiology of nephrolithiasis is different in the elderly person.

Gender : Urinary calculi are common, with some estimates suggesting that they affect 12% of men and 5% of women in industrialized countries by age of 70 years [131]. Nephrolithiasis typically affects adult men more commonly than adult women, with a male to female ratio of 2 or 3:1 [20]. There are several reasons for high incidence of urinary calculi in men than women. Men generally have a larger muscle mass than women. Hence they have more of the daily breakdown and rebuilding of tissue that result in metabolic waste. And an increase in metabolic waste pre-disposes people to stone formation. Men generally eat more meat than women do.

As mentioned earlier in section 2.2, the male urinary tract is more complicated than the female urinary tract. Occasionally men suffer with

narrowing of penile urethra. The enlargement of the prostate gland, i.e., Benign Prostatic Hypertrophy (BPH) {the condition arise due to the enlargement prostate gland, which makes it difficult to empty the bladder completely, so that some urine remains in the bladder at all times.} and prostatitis (an inflammation of the prostate gland causing acute symptoms such as an urgency to urinate, frequent need to urinate and a very weak stream) are responsible to invite urinary complications. Anatomically, the urethra is larger than the ureter, so most stones that reach the bladder usually pass easily from that point [132].

Race : Disease prevalence varies by race, with the highest prevalence in white men, followed by Asian, Hispanic, and African American men [133].

Geography : Many epidemiological studies have recorded a geographic variability in the prevalence of stone disease. It has been postulated that this variability may be owing to variations in climate and sun exposure [134]. Higher prevalence of stone disease is found in hot, arid, or dry climates such as the mountains, desert, or tropical areas. Uric acid stones are subject to the most pronounced geographical variation. In Scandinavian countries uric acid stones occur with a frequency of not more than 4-5%, while the frequency might be as high as 30-40% in the Mediterranean and Arabic countries [135].

Food Habit Factors : Dietary factors play an important role in kidney stone formation [46,136], because it influences urinary constituents and pH, which may affect stone nucleation and growth [73]. Both malnutrition and obesity increase the risk of urolithiasis. People whose diets are high in animal protein and low in fiber and fluids may be at higher risk for stones [137]. In general, certain foods increase the risk for stones only in people who have genetic or

medical susceptibility. The effects of diet on the formation of urinary calculi may be different for the people of different age groups, because the metabolism of many dietary factors may change with age [138]. Oxalate-rich foods may be a risk factor for formation of calcium oxalate monohydrate calculi.

A diet rich in animal protein is associated with a low urinary pH, which leads to uric acid crystal formation that can act as a heterogeneous nucleant for calcium oxalate crystals [139,140]. The increase in dietary protein also increases the risk of the formation of calcium oxalate stones [141]. Protein consumption in children in Europe and USA is three to five times higher than the recommended intake [142].

Dietary sodium increases the risk of the formation of urinary calculi. Salt intake expands intravascular volume, which can increase urinary calcium level likely by decreasing renal tubular calcium reabsorption. Increase in salt intake can also induce mild systemic metabolic acidosis, which can lower urinary citrate levels, and increases the risk of calcium precipitation [143].

High glucose can also increase the risk of urolithiasis through an increase in urinary oxalate levels [144]. Fructose intake may increase the urinary excretion of calcium, oxalate, uric acid, and other factors associated with kidney stone risk [145]. Fructose intake may also increase insulin resistance, which is associated with the low urinary pH, a major risk factor for uric acid [146]. Sucrose increases the urinary calcium and oxalate concentrations. A lack of dietary fiber is also thought to contribute to stone formation [147].

Use of Melamine-contaminated Food : Use of melamine-contaminated milk products led to melamine nephrotoxicity, which is characterized by nephrolithiasis, acute kidney injury (AKI), or both. It was found that both melamine and cyanua were combined to form insoluble crystals, which results in urinary calculi. Most melamine associated stones were irregular, nubby in shape, and were mainly localized to the renal pelvis [41]. In December 2008, World Health Organization (WHO) published a detailed report on *“Toxicological and Health Aspects of Melamine and Cyanuric Acid”* and considering melamine as one of the risk factors for urolithiasis, set a standard for acceptable human consumption, i.e., Tolerable Daily Intake (TDI) of melamine at 0.2 mg / kg of body mass and gave several recommendations to control the epidemic induced by melamine contaminated food [148].

Soft Drink Habits : The findings of some [149] but not all [150] studies suggest that consumption of soft drinks may increase the risk of forming a kidney stone. The phosphoric acid found in these beverages is thought to affect calcium metabolism in ways that might increase risk of urolithiasis.

Medical Conditions : Many medical conditions, including but not limited to high blood pressure, gout [151], inflammatory bowel diseases [93], hyperparathyroidism [104], tubular acidosis [152], kidney disease, UTI [120], blockage of the urinary tract, chronic diarrhea, being bedridden for a long period, spinal cord injury [153], certain cancers [154], and sarcoidosis [155], put people at higher risk for stones.

Obesity Factor : Recent studies have confirmed that people with overweight and obesity may be at higher risk for urolithiasis [156-158]. The prevalence and incidence of urinary calculi have been reported to be associated with

body weight and body mass index (BMI) [159], although the magnitude of this association is greater in women than in men [160]. Obesity may sometimes cause uric acid stones by producing renal insulin resistance that in turn reduces urinary pH [161].

Stress Factor : Najem et al [162] reported the association between stressful lifestyles and urolithiasis. People who had a major, stressful life experience were more likely to develop stones than those who had not. Stressful lifestyles have been shown to increase lithogenic urinary constituents like calcium, oxalate and uric acid [163]. This increased risk may be due to a hormone called vasopressin, which is released during stress. Among its other functions, vasopressin increases the concentration of urine.

2.8 Symptoms of Urinary Calculi

This chapter starts with the poem – ‘*Ode to a Kidney Stone*’ by Khalid Hameed, which describes the symptoms of the kidney stone disease. The symptoms of urinary calculi disease can some times be excruciating and unbearable pain. It was reported that the presence or absence of symptoms does not significantly alter the presence and extent of urinary deposits in the urinary stone patients [164]. In many cases, kidney stones develop without producing any symptoms. If they become lodged in the ureter, nevertheless, the symptoms can be very severe. Often, they vary depending on the location of stone and then its progress.

- Usually, the first symptom of a kidney stone is extreme pain. Although side pain or flank pain are the most common symptoms in nephrolithiasis, the abdominal pain, back pain, and groin pain are other presenting symptoms encountered in the patients [19]. The pain often

begins suddenly when a stone moves in the urinary tract, causing irritation or blockage. Typically, a person feels a sharp, cramping pain in the back and side in the area of the kidney or in the lower abdomen. Later, pain may spread to the groin, testes, or tip of the penis, depending on the location of obstruction.

- If the stone is in the kidney or upper urinary tract, the pain usually occurs in one flank area.
- If the stone is too large to pass easily, pain continues as the muscles in the wall of the tiny ureter try to squeeze the stone along into the bladder.
- As stone grows or moves, blood may appear in the urine.
- The patient cannot become comfortable and usually stands, sits, paces, or reclines in a vain search for a position that will bring relief.
- It should be noted that the size of the stone does not necessarily predict to the severity of the pain; a very tiny stone with sharp edges or spiky nature can cause intense pain, while a larger round stone may not be as distressing as the spiky small one.
- As the stone moves down the ureter closer to the bladder, one may feel the need to urinate more often or feel a burning sensation during urination.
- Sometimes nausea and vomiting may occur.
- If fever and chills accompany any of these symptoms, an infection may be present.
- Sometimes urine passes with cloudy or foul-smelling.
- Large calculi can cause obstructions anywhere within the urinary tract, eventually causing organ damage and even renal failure.

It is interesting to note that the present author has experience the urinary stone pains.

2.9 Diagnosis of Urinary Calculi

Recurrence of urinary calculi appears to have increased in recent years despite the development of more effective surgical techniques [11,165], emphasizing the importance of laboratory analyses of urinary stones. Investigation of urinary calculi has been an important part of clinical chemistry for more than a century [166]. The majority of routine clinical laboratories only perform a qualitative analysis of the calculus by means of wet chemistry kits or infrared spectroscopy of the whole pulverized calculus, omitting details concerning minority components, percentages of different compounds or internal structure. The information obtained with wet methods or infrared spectroscopy is valuable on setting up therapeutic advice but is not valid for guidance on the concrete etiological causes of the lithiasis [167]. At present it is accepted that no single method provides total information on the structure and composition of the stone, and at least two different methods have to be combined for accurate study of calculi.

Diagnostic steps for urinary calculi :

- By using physical examination and imaging techniques, establish the presence or absence of kidney stones.
- If a kidney stone is present, using imaging techniques, determine whether the stone is obstructing the urinary tract.
- By urine and blood tests, determine the substance forming the crystal so that appropriate treatment and preventive measures can be taken.

- By using the tests for urine and blood chemistries, determine any metabolic abnormalities in patient with recurrent stones.
- Stone analysis may be carried out to determine the stone composition.

2.9.1 Physical Examination :

The physician will press against abdominal areas to know the locations that might indicate the presence of the stone.

2.9.2 Medical History :

A medical history may help predict which crystal has formed the stone.

The physician may need to know the following:

- The physician may ask / collect the previous kidney stone attacks to determine whether first stone or recurrent.
- History, including, family history and dietary history.
- Histories of cancer, sarcoidosis, or small bowel disease.
- The patient should be sure to inform the physician of any medications being taken, including non-prescription substances, particularly high doses of vitamins D or C and calcium-containing antacids.
- Urinary tract infection with organisms possessing urease.

2.9.3 Imaging Techniques :

A number of imaging techniques, including plain abdominal radiography, i.e., X-Rays, ultrasonography, Intravenous Pyelography (IVP), helical Computed Tomography (CT) scanning and Magnetic Resonance Imaging (MRI) can be used to detect urinary calculi in the renal tract.

X-Rays : A standard plain x-ray film of abdomen comprising of the kidneys, ureter, and bladder, commonly referred to as a KUB, may be a first step for identifying urinary calculi, since most of them are opaque on x-rays. Calcium

stones can be identified on x-rays by their white color. X-ray is quick and inexpensive technique that can give the location, size and number of stones present. The use of KUB can result in a much lower radiation burden for the patient. However, small stones less than 2 mm may not be identified. KUB film may be affected by obesity or too much gas in the large intestine. Figure 2.6 shows the location of calculi in x-ray KUB [168].

Table 2.3 shows the radiographic characteristics of urinary calculi. For conventional radiography, a sensitivity of 57% and specificity of 71%, as well as a poor detection rate of 50–70%, are reported [169]. The main disadvantage of a KUB is that overlying bowel gas and bone can obscure the identification of a calculus.



Figure : 2.6 X-ray Film [168]

Table : 2.3 : Radiographic Characteristics of Urinary Calculi

Radiopaque	Poor Radiopaque	Radiolucent
Calcium oxalate monohydrate	Struvite	Uric acid
Calcium oxalate dihydrate	Cystine	Xanthine
Calcium phosphate (different)	Triaterene stone	Matrix calculi
Carbonate		Urate
Brushite		2,8 dihydroxyadenine
		Drug stones like Ephedrine stone, Indinavir stone, Guaifenesin stone, Nelfinavir stone, Oxypurinol stone Sulphonamide

Ultrasonography : This test, generally known as sonography, uses ultrasonic sound waves rather than x-rays to produce pictures of internal organs. The

frequencies used in diagnostic ultrasonography are typically between 1 and 6 MHz. Sonography as an imaging alternative is mainly used for imaging the kidneys and the proximal parts of the ureters. It also can detect the presence of stones and it shows both calcified radiopaque stones and non-calcified radiolucent stones. Ultrasonography may detect all types of renal stones if the stone is larger than 3 to 5 mm. Ultrasound can also detect obstruction in the urinary tract. Ultrasound can be used to obtain information about the presence, size and location of a stone as well as the grade of dilatation and obstruction. It also detects signs of abnormalities likely to increase the probability of stones. But, it is not useful to detect very small stones. The quality of the sonography images depends on many factors that cannot be influenced by the radiologist (e.g., intestinal gas, obesity), and sonography detects only 50–60% of ureteral calculi [170]. Oner et al [171] reported that ultrasonography failed to identify stones in more than 40% of pediatric patients. Nevertheless, it is the preferred imaging method for kidney stone patients who are pregnant since it does not use any ionizing radiation. Moreover it does not use any intravenous contrast agents. Figure 2.7 shows the ultrasound image of calculus [172].

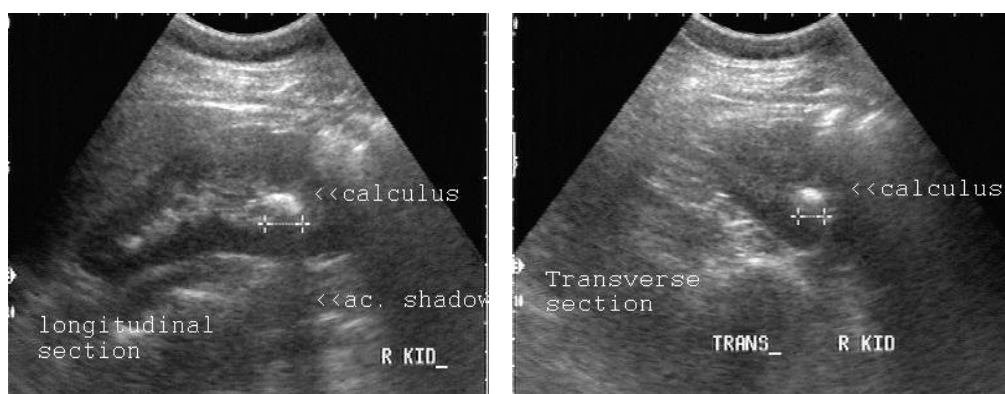


Figure : 2.7 Ultrasound Image of Urinary Calculus [172]

Helical Computer Tomography : A helical (or spiral) Computed Tomography, commonly, known as a CT scan, is a significant advance for diagnosing urinary calculi. Figure 2.8 shows the CT scanner [173] and CT scan image [174].

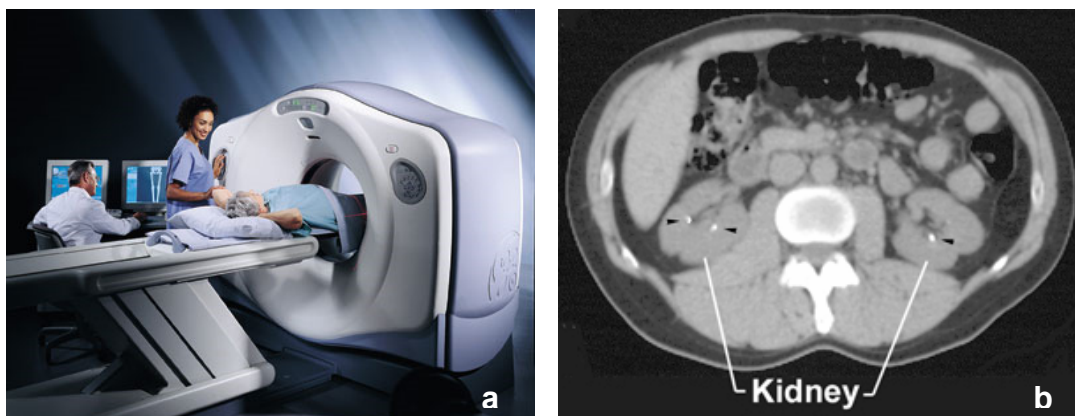


Figure : 2.8 (a) CT Scanner (b) CT scan image of the abdomen showing both kidneys and small calcified stones (arrowheads).

At the present time, helical computed tomography without contrast is the procedure of choice for the initial radiographic investigation. It is now the standard imaging technique for detecting as well as characterizing urolithiasis. The main advantage of CT scan is that it offers rapid and excellent visualization of all opaque and non-opaque stones regardless of their size and location together with additional information about all urinary system. Non-contrast spiral CT seems to be a very effective and reliable imaging tool in the diagnosis of pediatric urolithiasis especially in detection of ureteral stones and stones smaller than 5 mm. Spiral CT is more efficient than ultrasonography [171]. It is noninvasive technique and provides detailed and accurate images. Moreover, the anatomic status of the urinary tract can be clarified and other possible non-stone cause for the patient's symptoms or signs may be identified [175]. In normal radiation dose CT, the sensitivity and specificity are 94–100% and 97%, respectively [176]. Notwithstanding, the main

disadvantage of CT is that it exposes patients to a relatively high radiation dose and the potential effects of the radiation exposure from CT examinations have raised concern among some physicians [177]. However, the mean effective radiation dose for an excretory urography examination is reported as 2.6 mSv (millisievert) {The SI unit of the equivalent dose of radiation is sievert (symbol: Sv), which is named after Rolf Maximilian Sievert - a Swedish medical physicist renowned for work on radiation dosage measurement and research into the biological effects of radiation.} [178], which is less than one third of the effective radiation dose of routinely used CT protocols for the detection of urolithiasis [179] ranging between 8 and 16 mSv. The dose-reduced studies carried out by Niemann et al [180] envisaged that applied maximum effective doses of 0.7–2.8 mSv.

Intravenous Pyelogram (IVP) : An intravenous pyelogram (IVP, also known as intravenous urogram or IVU) is a radiological procedure used to visualize abnormalities of the urinary system, including the kidneys, ureters, and bladder. If no stones show up but the patient has severe pain indicative of urinary calculi, the next step is to proceed to an IVP test.

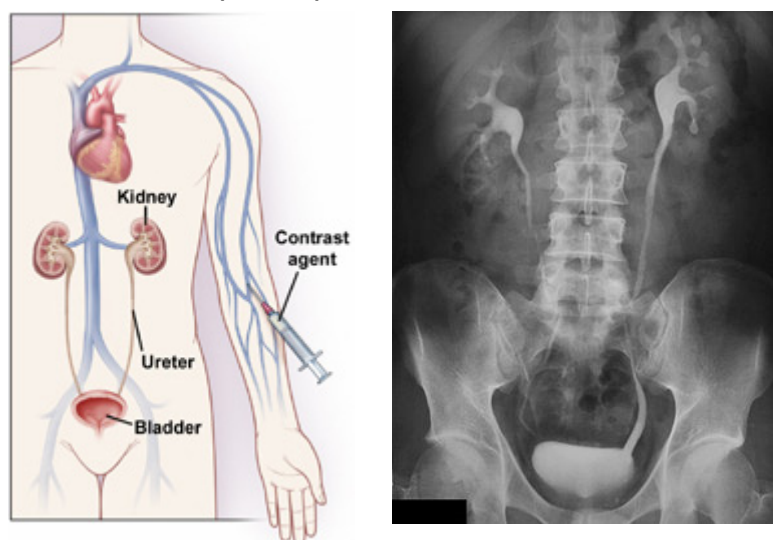


Figure 2.9 (a) Injecting Contrast material into the patient's vein, and (b) IVP Radiograph

In the IVP procedure, the patient is injected with contrast material (a radiopaque dye) and a series of moving X-rays (called fluoroscopy) are taken as the dye travels through the urinary tract. Figure 2.9 shows the injecting contrast material for IVP procedure [181] and IVP radiograph [182]. This procedure is performed to confirm the presence of urinary calculi, although some calculi may be too small to be seen. This test should not be used on patients with kidney failure. There is also a risk for an allergic reaction to standard dyes. IVP is the most cost-effective method for detecting stones to date, but it is invasive and take a very long time if the blockage to the kidney is severe.

Retrograde Pyelogram : It is a procedure in which a cystoscope, which is an endoscopic instrument especially designed for urological use, is inserted into the urethra to visualize the lower urinary tract. The contrast agent is injected directly into this opening and an x-ray is taken to locate the urinary calculi. The flow of contrast (up from the bladder to the kidney) is opposite to the usual flow of urine, hence the name retrograde. This procedure eliminates the risk for an allergic reaction to the contrast agent because the dye does not reach the bloodstream, but it may require anesthesia. It is the most reliable method for visualizing the urinary system and detecting stones. Retrograde pyelography is generally done when IVP or contrast CT scan cannot be done because of renal disease or allergy to intravenous contrast.

Magnetic Resonance Imaging (MRI) : MRI uses three electromagnetic fields, namely, a very strong static magnetic field to polarize the hydrogen nuclei; a weaker time-varying field for spatial encoding; and a weak radio-frequency (RF) field for manipulation of the hydrogen nuclei to produce

measurable signals, collected through an RF antenna. MRI techniques are showing promise for diagnosing urinary tract obstruction, but do not yet accurately reveal non-obstructive or small stones. Unlike x-ray and CT scan, it does not use any harmful ionizing radiation. MRI is an important modality due to its ability to obtain multiplanar images and excellent contrast resolution without the use of ionizing radiation.

2.9.4 Urinalysis (Urine Tests) :

Urine samples are required to evaluate features of the urine, such as its acidity, the presence of red or white blood cells, whether infection is present, presence of any crystals, and elevated or decreased components that inhibit or promote stone formation. Urinalysis helps the clinicians or urologists to know the concentration of sodium, potassium, citrate, chloride, urea, nitrogen, creatinine, pH, calcium, oxalate, phosphate, Glucose, White Blood Cells (WBC), Red Blood Cells (RBC), ketones and bacteria, yeast cells, or parasites if any.

Clean-Catch Urine Sample for Culturing : A kidney stone patient is usually given a collection kit, including filters, to try to catch the stone or gravel as it passes out. A clean-catch urine sample is always required for culturing.

Twenty-Four Hour Urine Collection : A 24-hour urine collection may be needed to measure urine volume, urine pH, i.e., the levels of acidity, calcium, sodium, magnesium, uric acid, oxalate, citrate, and creatinine.

Test for Blood in the Urine : A dipstick for blood in the urine is typically performed when patients appear in the emergency room with flank pain. About a third of kidney stone patients, however, do not show blood in the urine, so other tests are needed.

Testing the Acidity of Urine : Testing whether urine is acid or alkaline helps to identify the specific stone. The levels of acid or alkaline in any solution, including urine, are indicated by the pH scale :

- A pH value of 7.0 is neutral.
- A solution with a low pH (below 7.0) is acidic.
(A low pH favors uric acid and cystine stones.)
- A solution with a high pH (above 7.0) is alkaline.
(A high pH favors calcium phosphate and struvite stones.)

2.9.5 Microscopic Examination

The kidney stones obtained from the sample are examined under a microscope. The crystal morphologies are often specific enough so that the physician is able to identify the substance causing the stone:

- Calcium oxalate crystals are eight-sided (octahedral), while calcium phosphate crystals tend to have irregular shapes.
- Uric acid stones are sometimes described as pear- or diamond-shaped.
- Struvite have very specific shapes commonly described as "coffin lids."

2.9.6 Blood Tests

Blood tests may help determine levels of blood urea nitrogen, creatinine, calcium, phosphate, and uric acid for patients with known or suspected calcium oxalate stones.

Parathyroid Tests : Tests to detect parathyroid hormone levels are needed if the physician suspects hyperparathyroidism.

Tests for Infection : If a test result shows a high white blood cell count, which might indicate infection. But such results could be misleading, since

white cells could also increase in response to the extreme physical stress of a kidney stone attack.

2.9.7 Analysis of Urinary Calculi

Various techniques usually employed for the urinary calculi analysis are as illustrated in figure 2.10.

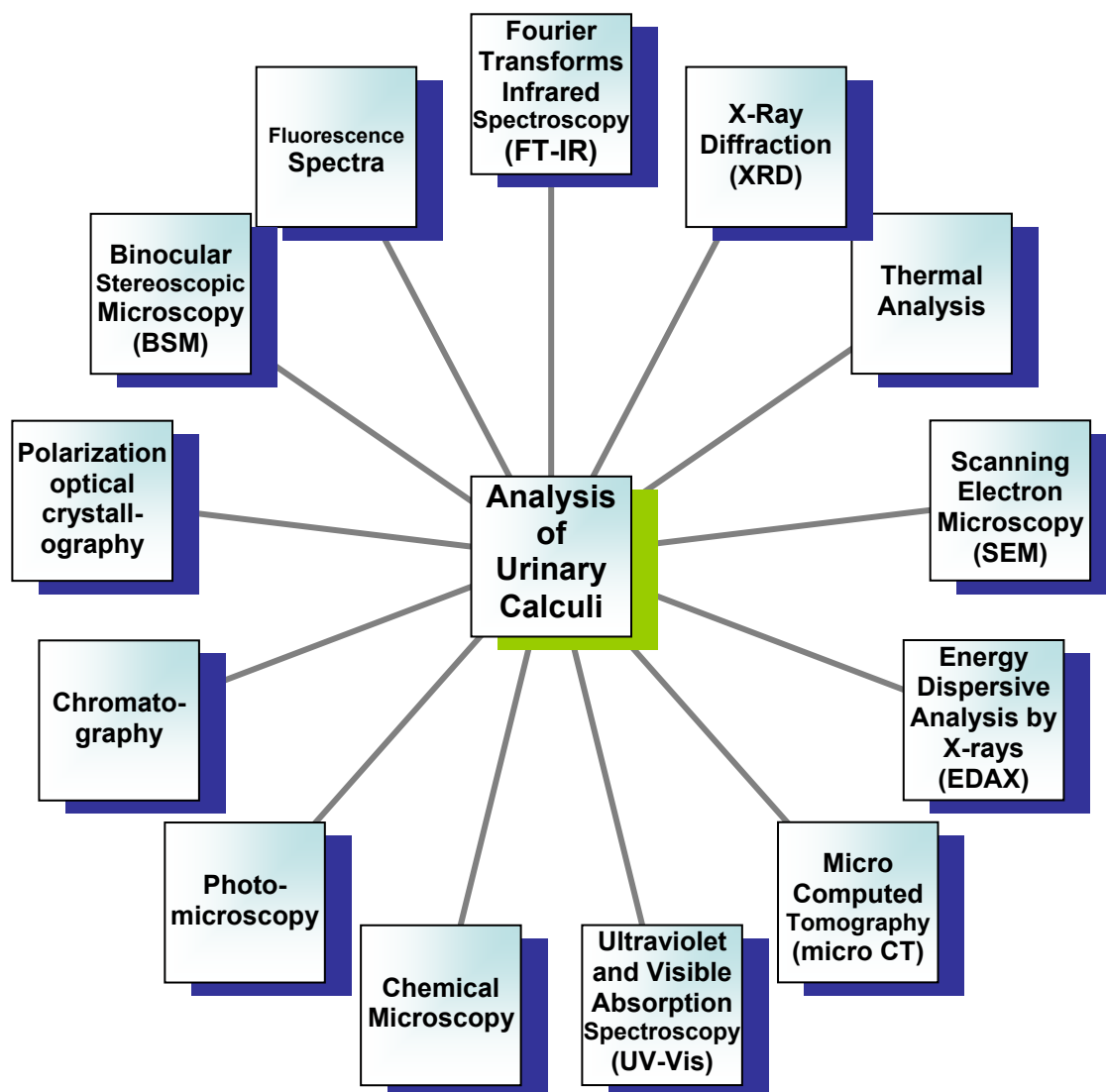


Figure : 2.10 Various techniques for the analysis of urinary calculi

The study of the calculus begins through the direct observation of its external aspect, using a stereoscopic microscope. The surface characteristics are evaluated for color, texture, crystallinity, size, presence of layers, homogeneity, presence of foreign bodies, and any other notable features.

Afterwards, the calculus is sectioned in two parts along a plane as near as possible to its geometric centre, to be able to establish the internal structure. When the calculus is supplied after fragmentation, its all fragments are observed by stereoscopic microscopy to establish its original complete form and as a consequence, its internal structure.

Fourier Transform Infrared Spectroscopy (FT-IR) : The quantity of sample needed for FT-IR can be less than one microgram. If inspection of the superficial and cross-section of the stone reveals a homogeneous appearance, the identification of calculus composition can be performed by powdering the whole stone and taking an average sample for FT-IR study. But if inspection reveals a heterogeneous appearance such as areas of differing colors or textures, lamination or other structural details, it may become necessary to scrape off bits of calculus material from the different regions with a scalpel and perform several identifications by FT-IR. Identification is very simple if a reference spectrum that matches that of the unknown material is found. When an exact reference spectrum match cannot be found, a band by band assignment is necessary to determine the composition of the solid. The main advantages of FT-IR use in the identification of calculi components are the speediness, simplicity and specificity for the identification of rare components and the availability of the instrument. FT-IR technique is less expensive than SEM, and does not require highly qualified technicians.

The FT-IR spectroscopic method was used to investigate urinary calculi [183], it was found that calcium oxalate was the most common constituent with the presence of phases of hydroxyl and carbon apatite. There are reports of upgraded infrared techniques to analyze the urinary calculi, for

instance, the use of partial least squares regression in the analysis program enables better quantitation of stone components [184] by use of Fourier transform infrared spectrophotometer coupled with computer and photoacoustic detector. Spectra analysis was carried out by quantitative analysis program PLS (Partial Least Squares) Quant. Moreover, Volmer et al [185] carried out FT-IR analysis of urinary calculi by use of Golden Gate Single Reflection Diamond Attenuated Total Reflection (ATR) sample holder, a computer library, and an Artificial Neural Network (ANN) for spectral interpretation. FT-IR spectroscopy study of urinary calculi procured from South India has been reported [186,187]. A review is written on the application of infrared and Raman spectroscopy to urinary calculi by Carmona et al [188]. They suggested that some characteristic bands are useful for analytical purpose. Recently, the application of FT-IR and FT Raman spectroscopy in analysis of urinary calculi is reported [189].

X-Ray Diffraction : Unique X-diffraction pattern was explored to characterize and identify different urinary calculi, as early as in 1947 by Prien and Frondel [190]. In 1962 Herring [191] studied 10,000 urinary calculi with x-ray diffraction. The x-ray diffraction is even enabling to determine the proportional rate of particular crystalline components forming the calculus. Moreover, it provides a well organized reliable facility, which can give clinicians reliable results within a few hours [192,193]. Combining crystal-optical and x-ray diffraction methods many urinary calculi have been analyzed with their core and shell examinations separately [194].

The powder XRD technique is also popular to characterize urinary calculi. A difficulty in the identification of different components of mixed urinary

calculi is reported [195]. Moreover the internal standard method and powder XRD has been applied to the quantitative determination of urinary stone constituents. The study has indicated that the XRD analysis, nevertheless, alone can not be regarded as a routine technique for quantitative characterizations for urinary calculi, but the semi-quantitative XRD analysis supplements accurate quantitative elemental data is more suitable for precise determination of true stone composition [196]. Attempts were made to study the urinary calculi constituents by the powder XRD [197]. A mineralogical study was carried out for the calculi collected from the south India by using XRD [186].

Thermal Analysis : The thermal analysis is a popular technique to estimate the presence of water molecules. The presence of different ions and molecules can be estimated easily by the wet chemical methods. The difficulties appear in the differentiation of hydrates of calcium oxalates, not with standing, the thermal technique was found more useful [198]. Thermal study was carried out on various calculi obtained from south India [186,187] employed Differential Scanning Calorimetry (DSC) and identified COM, COD and the mixture of the two urinary calculi. Moreover, Thermogravimetric Analysis (TGA) is an important analytical technique for urinary calculi, which has suggested that some stones had less than 80 % calcium oxalate [199]. It was found that the level of the presence of COM and COD was different in the core region and the surface layer region. Earlier many workers [198-201] have carried out thermal analysis as an alternative method for quantitative determination of the two types of calcium oxalate in urinary stones. The thermo-balance and FT-IR were coupled through a heat transfer line, which

helped to analyze urinary calculi, particularly, in the case of complex mixtures [202].

Scanning Electron Microscopy (SEM) : The SEM provides three outstanding improvements over the optical microscope: it extends the resolution limits so that picture magnifications may be increased up to 30000x to 60000x, it improves the depth-of-field resolution more dramatically, by a factor of approximately 300, and finally, it entails the observation of several surfaces of a sample because of the possibility of rotating the sample in several directions. But in addition to image formation, this instrument may provide elemental analysis of micron-sized areas of the specimen observed when coupled with a special device for energy dispersive X ray microanalysis. SEM provides information about the nature of crystalline compounds, shape of the crystals, internal structure, location of components, crystalline conversions, crystallite size distribution, characteristics of the aggregates and some data about intimate relations between crystals and organic matrix or relationships between different crystalline species [203].

The appearance of urinary calculi by SEM permits identification based on textural grounds [204-206].

Energy Dispersive Analysis by X-rays (EDAX) : The EDAX technique has been employed to investigate the composition of different types of urinary calculi [205,206], viz., calcium oxalate, and / or calcium phosphate containing stones, infection stones, uric acid containing stones, cystine containing stones and containing rare substance (brushite, whitlockite, xanthine, etc) and elements (C, N, O, Na, S, Mg, Al, Si, Cl, K, Ca, Mn, Fe, Ni, Zn). The elemental

analysis of urinary calculi is also reported by Laser Induced Plasma Spectroscopy (LIPS) [207].

Micro Computed Tomography : Clinical laboratory assessment of urinary calculi is typically conducted using destructive methods of analysis. Micro CT is a potential *in vitro* imaging method for the analysis of urinary stone composition and morphology in a nondestructive manner at very high resolution [208,209]. Micro CT gives excellent structural detail within urinary calculi and these results demonstrate the feasibility of identifying and localizing most of the common mineral types found in urinary calculi.

However, it is exhaustive to give complete survey of various stone analysis technique. Louis C. Herring Laboratory [210] performs urinary calculi analysis professionally by using various sophisticated techniques. The predecessor of the present author [211] has analyzed urinary calculi collected after surgery by FT-IR, TGA, SEM, powder XRD and EDAX. Some of the results were presented by Joshi et al [212] using powder XRD technique.

It has been found in the majority of cases that no single technique is capable enough to give complete stone analysis, many times, more than one technique are used.

2.10 Management of Urinary Calculi

In the present time the management of urolithiasis is not only stone removal but also to prevent its recurrence. Medical management or treatment of urinary calculi was once entirely surgical, but recent technological advances allow stones to be treated with less-invasive methods, including Extracorporeal Shock Wave Lithotripsy (ESWL), ureteroscopic and percutaneous procedures. Treatment decisions are based upon suspected

stone type, size, location, renal anatomy, and renal function. A previous study by Tann et al [213] identified that 90% of stones less than 4 mm and 50% of stones 4–7 mm will pass spontaneously while 8 mm and larger stones will rarely pass without intervention. Comprehensive management of urinary calculi necessitates collaborative efforts between various disciplines.

2.10.1 Medications

Physician usually prescribes the drugs such as allopurinol, thiazides, potassium citrate, magnesium citrate and potassium-magnesium citrate depending on the cause of stone formation [214].

2.10.2 Lithotripsy

This procedure is effective for stones in the kidney or upper ureter. It uses an instrument to break the stone into tiny particles that can pass naturally through urine. Lithotripsy is not appropriate for patients with very large stones or other medical conditions. There are various types of techniques available.

2.10.3 Ultrasonic lithotripsy

Ultrasonic lithotripsy uses high frequency sound waves delivered through an electronic probe inserted into the ureter to break up the kidney stone. The fragments are passed by the patient naturally or removed surgically.

2.10.4 Electro-hydraulic Lithotripsy (EHL)

Electro-hydraulic lithotripsy (EHL) uses a flexible probe to break up small stones with shock waves generated by electricity. The probe is positioned close to the stone through a flexible ureteroscope. Fragments can

be passed by the patient or extracted. EHL requires general anesthesia and can be used to break stones anywhere in the urinary system.

2.10.5 Extracorporeal Shock Wave Lithotripsy (ESWL)

"Extracorporeal" means "outside the body" and "lithotripsy" means stone-breaking. All ESWL procedures deliver shock waves from outside the body to break the stones, which are then more easily passed through the ureter and out of the body in the urine. This innovation has eliminated the need for open surgical removal of urinary calculi in the vast majority of patients. ESWL is the most frequently used procedure for most simple stones located in the kidney or upper urinary tract, including struvite stones. It is not used for cystine stones. ESWL is generally not successful for stones larger than three centimeters in diameter.

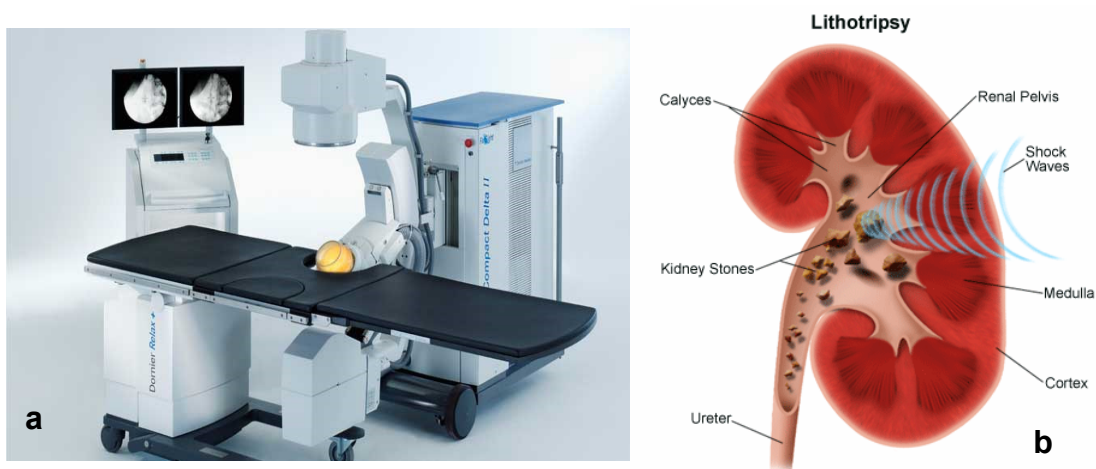


Figure : 2.11 (a) Extracorporeal Shock Wave Lithotripter [215]

(b) Shock waves Break the Urinary Calculus in Kidney [216]

ESWL Procedure : The Lithotripter used for ESWL procedure is as shown in figure 2.11 (a) [215]. Most ESWL procedures use some anesthesia, although they are often done on an outpatient basis. The patient is positioned in a water bath or on a soft cushion. The procedure uses ultrasound to generate shock waves that travel through the skin and body tissues until they hit the

dense stones. The stones are crushed into tiny sand-like pieces (Figure 2.11 b [216]) that usually pass easily through the urinary tract. The shattered stone fragments may cause discomfort as they pass through the urinary tract. In such cases, the doctor may insert a small tube called a stent through the bladder into the ureter to help the fragments pass. This practice, however, has not proved to speed up passage of the stones in most cases and is not used routinely. Success rates range from 50% to 90% depending on the location of the stone and the surgeon's technique and level of experience. Recovery time is short, and most people can resume normal activities in a few days.

Complications of ESWL : The most common complication is blood in the urine, which lasts for a few days after the treatment. To reduce the chances of bleeding, doctors usually advise patients to avoid taking aspirin, which can promote bleeding, for seven to 10 days before the treatment. Bruising and minor discomfort due to the shock waves are common in the back or abdomen. Sometimes the stone is not completely fragmented with one treatment, and then additional treatments may be required. Its safety for small or abnormal kidneys is not fully known. Recently, Xue et al [217] reported through an animal model experiment that ESWL treatment is associated with a high rate of recurrent renal calculi. Shock wave therapy can result in renal epithelial cell injury, which in turn is a most important factor in calculus formation. It is not known if this complication has any long-term consequences. Experts recommend minimizing as much as possible the impact and number of shocks in young people. If more than one treatment is needed, there should be a waiting period of at least 15 days.

2.10.6 Percutaneous Nephrolithotomy (PCNL)

This surgical procedure is performed under local anesthesia and intravenous sedation. Percutaneous means 'through the skin' and lithotomy means 'removal of kidney stones'. It is accomplished through the most direct route to stones through the kidney. Percutaneous nephrolithotomy may be used when ESWL is not available or effective, e.g., if the stone is very large, in an inaccessible location, or is a cystine stone. It is more effective for patients with severe obesity. It appears to be safe for the very elderly and the very young. Long-term effects are unknown. It is also preferred over ESWL for stones that have remained in the ureter for more than four weeks.

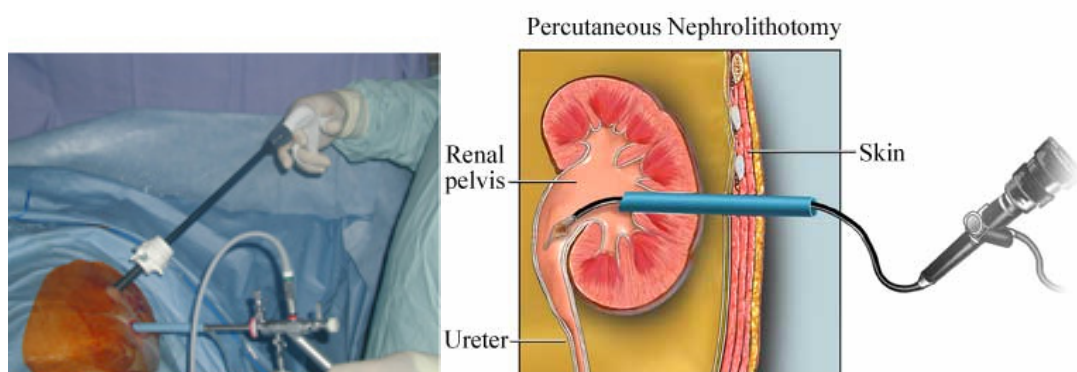


Figure : 2.12 Percutaneous Nephrolithotomy Procedure [218, 219]

PCNL Procedure : As shown in figure 2.12 [218, 219], the surgeon makes a tiny incision in the back and creates a tunnel directly into the kidney. The surgeon then inserts an instrument called a nephroscope through the tunnel. The stone is located and removed. An advantage of percutaneous nephrolithotomy over ESWL is that the surgeon is able to remove the stone fragments directly instead of relying on their natural passage from the kidney. For large stones, some type of energy device (ultrasound, a pneumatic drill-like device, or a special device called a holmium laser lithotripter) may be

needed to break the stone into small pieces. The holmium laser literally melts the stones and can be used on nearly all stone types. Of concern are studies reporting that the holmium laser produces cyanide as a by-product of uric acid stone fragmentation. No poisoning has been reported in any patient after this procedure; nevertheless, the device has an excellent safety record. It should be used sparingly, cautiously with large uric stones until more is understood about this effect. Generally, patients stay in the hospital for five or six days and may need a small tube called a nephrostomy tube left in the kidney during the healing process. Success rates have been reported to be about 98% for kidney stones and 88% for ureteral stones. They are slightly lower in children, although the procedure can be used safely.

Complications of PCNL : Complication rates are about 3% and serious problems are rare. Some scarring occurs, but studies indicate that it does not impair kidney function, even if the patient requires repeat surgery. The procedure also poses a risk for blood loss during and after the procedure, and, in some cases, it can be significant. Other complications encountered are imbalances in the fluid used to irrigate the tunnel, collapsed lung, and injuries to areas outside the kidney but within the operative area, such as the abdomen or chest.

2.10.7 Ureteroscopic Stone Removal

Ureteroscopy may be used for mid- and lower ureter stones. In this procedure no incision is made, but general anesthesia is still required. The surgeon passes a small fiber optic instrument called a ureteroscope through the urethra and bladder into the ureter. The surgeon then locates the stone or stones. Smaller ones are grasped and removed with tiny forceps. Large ones

are shattered with lasers or pneumatic drill-like devices. A small tube, or stent, may be left in the ureter for a few days after treatment to help the lining of the ureter heal. Complication rates range from 10% to 20% with major problems occurring in between 0% and 6%, with the risks being highest in less experienced surgeons and if stones are found in the kidney. The risk for perforation of the ureter is higher the longer the operative time.

2.10.8 Open Surgery (Nephrolithotomy)

Open surgery involves incisions through the patient's flank and into the kidney. The kidneys are cooled down using ice and x-rays are used during the procedure to locate specific areas and the stone. The arteries in the kidney are identified and isolated away from the surgical region. The surgeon locates the collecting system and retrieves the stone. If the surgeon finds any blockage, this is corrected. The surgery is very invasive and is now restricted to the patients with very large or complex stones that cannot be removed using less invasive measures and for very obese patients.

The procedure is not appropriate for the following patients:

- Those with bleeding or clotting disorders.
- Those with untreated widespread infection.
- Those with severe and chronic kidney insufficiency.

Surgery should be reserved as an option for cases where other approaches have failed. Surgery may be needed to remove a kidney stone if ...

- It does not pass after a long period of time and causes constant pain.
- It is too large to pass on its own or is caught in a difficult place.
- It blocks the flow of urine.
- It causes ongoing urinary tract infection.

- It damages kidney tissue or causes constant bleeding.
- It has grown larger.
- Because cystine stones frequently are large and resistant to disruption via shock wave lithotripsy, the surgical treatments are required [220].

Until 30 years ago, surgery was necessary to remove a stone. It was very painful and required a recovery time of 4 to 6 weeks. Today, treatment for stones is greatly improved, and many options do not require major surgery.

2.11 Prevention of Urinary Calculi

Prevention of progressive or recurrent stone formation is best managed by diet, adequate fluid intake, and in some cases, dietary supplements or medications. The modest progress in understanding the pathophysiology has hampered successful development of targeted therapy. Current regimens are based mostly on rational alteration of urinary biochemistry and physical chemistry to lower the risk of precipitation. In terms of pharmacotherapy, there are drugs to successfully improve hypercalciuria, hypocitraturia, aciduria, hyperuricosuria, and hypercystinuria. But due to the space limitation, complete description with exhaustive citation is not possible.

Several authors have written detailed reviews on the etiology, epidemiology, constitutions, theories, characteristics, therapies, medical managements and metabolic factors of urinary stones [15,24,45,56,60,124, 132,134,221,222]. The predecessors of the present author [211,223,224] have written detailed reviews on urolithiasis, therefore, it is avoided in greater details in the present thesis. The author has attempted to mainly include recent studies and the studies carried out mostly in last one decade.

2.12 *In Vitro* Growth Inhibition

The occurrence of urinary calculi is taking place in a dynamic environment in a body where urine is constantly flowing. The growth of urinary calculi in a body is a complex process and depends on many factors. This has already been discussed earlier in this chapter.

Nevertheless, it is important to study the growth of urinary type crystals *in vitro* and study various parameters affecting the growth. The gel growth technique is found the most suitable one to mimic the growth occurring in a body in a simplified manner. This gel growth technique will be discussed in chapter – III.

The *in vitro* growth dissolution and inhibition is again important to study because the normal dissolution differs from it. In the normal dissolution, the stone or urinary crystal is dissolved in a suitable solvent. But in growth dissolution, the dissolution is achieved under the growth condition by maintaining the constant supply of nutrients for the growth. This type of condition mostly desired in a body to dissolve the stone. If the dissolution of stone or crystal is not achieved by the growth is retarded then it is known as inhibition. The gel based *in vitro* growth inhibition study is important as it provides a simple screening model to identify different inhibitors. The inhibitors may be chemical compounds present in urine or different herbal extract solutions or fruit juices for *in vitro* studies. There are large numbers of herbal drugs as well as Ayurvedic drugs available for different therapeutic use [225,226], the possibilities of testing certain selected ones for pilot *in vitro* study is required to be explored. This has lead several researchers to address the issue of urinary stone problem and many other ailments from reverse

pharmacology point of view [227-229]. The reverse pharmacology can be defined as a transdiscipline that initiates drug discovery and development from the traditional knowledge / practice at the beside through robust and objective experimental documentation. The path of reverse pharmacology is cost effective and time saving unlike the long and expensive direct path of drug development from natural products.

Earlier, Natarajan et al [230] employed gel growth of a few urinary stone constituents and studied inhibitory role played by some extracts or juices of natural products in crystal growth.

In the present authors laboratory the earlier workers have studied growth inhibition of different urinary crystals *in vitro* by using gel growth technique with different inhibitors; for instance, growth inhibition of calcium oxalate monohydrate crystals by herbal extracts of *Tribulus terrestris* Linn and *Bergenia ligulata* Linn [231]; brushite by citric acid, lemon juice, artificial reference urine and natural urine [232, 233], by herbal extracts of *Tribulus terrestris* Linn and *Bergenia ligulata* Linn [234] by tartaric acid and tamarind [235], and by unripe mango juice, pomegranate juice and grape juice [223]. The present author has carried out extensive studies on growth inhibition of struvite crystals which will be discussed in chapter VI and published several research papers as listed after the last chapter on page number 412.

References :

1. A. B. Soni, *M.D. Thesis*, Gujarat Ayurveda University, Jamnagar (1999).
2. K. K. Bhishagratna (Editor) "*An English Translation of the Sushruta Samhita*", Calcutta (1911).
3. M. Tewari, H. S. Shukla, *Indian J. Surg.*, **67** (2005) 229.
4. <http://www.dwp.gov.uk/publications/specialist-guides/medical-conditions/a-z-of-medical-conditions/bladder-and-urinary-tract/images-urinary-tract-stones.shtml>
5. <http://www.britannica.com/EBchecked/media/99762/Cross-section-of-the-right-kidney-showing-the-major-blood>
6. <http://www.britannica.com/bps/media-view/107139/1/0/0>
7. D. J. Kok, *Endocrinol. Metab. Clin. N. Am.*, **31** (2002) 855.
8. O. W. Moe, M. S. Pearle, K. Sakhaee, *Kidney Int.*, **79** (2011) 385.
9. J. Sutherland, J. Parks, F. Coe, *Miner. Electrolyte Metab.*, **11** (1985) 267.
10. O. W. Moe, *The Lancet*, **367** (2006) 333.
11. A. Ramello, C. Vitale, M. Marangella, *J. Nephrol.*, **13** (2000) S65.
12. W. G. Robertson, H. Hughes, "*Epidemiology of urinary stone disease in Saudi Arabia*". In "*Urolithiasis*", Ed. R. Ryall, R. Bais, V. Marshall, A. Rofe, L. Smith, V. Walker, Plenum Press, New York, (1994) 453.
13. J. M. Potts, "*Essential Urology: A Guide to Clinical Practice*", Humana Press, Totowa, New Jersey, (2004) 129.
14. O. Yoshida, Y. Okada, *Urol. Int.*, **45** (1990) 104.
15. M. Menon, B. G. Parulkar and G. W. Drach, "*Urinary Lithiasis, Etiology, Diagnosis, and Medical Management*" In: "*Campbell's Urology*", Ed. P. C. Walsh, Vol 3, 7th edition, WB Saunders Co., Philadelphia (1998) 2661.

16. M. López, B. Hoppe, *Pediatr. Nephrol.*, **25** (2010) 49.
17. A. Hesse, E. Brandle, D. Wilbert, K. U. Köhrmann, P. Alken, *Eur. Urol.*, **44** (2003) 709.
18. K. K. Stamatelou, M. E. Francis, C. A. Jones, L. M. Nyberg Jr, G. C. Curhan, *Kidney Int.*, **63** (2003) 1817.
19. J. Brown, *Int. Urol. Nephrol.*, **38** (2006) 87.
20. M. S. Pearle, E. A. Calhoun, G. C. Curhan, *J. Urol.*, **173** (2005) 848.
21. C. S. Saigal, G. Joyce, A. R. Timilsina, *Kidney Int.*, **68** (2005) 1808.
22. A. J. Wein, L. R. Kavoussi, A. C. Novick, A. W. Partin, C. A. Peters (Ed.), *"Campbell-Walsh Urology"*, 9th ed., Saunders-Elsevier, Philadelphia (2007).
23. W. L. Strohmaier, *Der Urologe A*, **39** (2000) 166.
24. W. G. Robertson in *"Eurolithiasis"*, Eds D. J. Kok, H. C. Romijn, P. C. M. S. Verhagen, C. F. Verkoelen, Shaker Publishing, Maastricht, The Netherlands (2001) 9.
25. C. Ahlstrand, H. G. Tiselius, *Urol. Res.*, **18** (1990) 397.
26. D. Raja, Website URL : <http://www.diliprja.com/stone.htm>
27. M. S. Ansari, N. P. Gupta, A. K. Hemal, P. N. Dogra, A. Seth, M. Aron, T. P. Singh, *Int. J. Urol.*, **12** (2005)12.
28. L. B. K. Singh, S. N. Prasad, P. P. Singh, *Asian Med. J.*, **20** (1977) 589.
29. B. N. Colabawalla, *"Incidence of urolithiasis in India"*, In *"Technical Reports Series No 8"*. Indian Council of Medical Research Division of Publication and Information, New Delhi, (1971) 42.
30. P. P. Singh, L. B. K. Singh, S. N. Prasad, M. G. Singh, *Am. J. Clin. Nutr.*, **31** (1978) 1519.

31. A. K. Pendse, A. K. Srivastava, J. L. Kumavat, A. Goyal, R. Ghosh, H. S. Sharma, P. P. Singh, *J. Indian Med. Assoc.*, **82** (1984)151.
32. P. Singh, A. Pendse, V. Rathore, P. Dashora, *Urol. Res.*, **16** (1988) 105.
33. F. Hussain, F. Billimoria, P. Singh, *Int. Urol. Nephrol.*, **22** (1990)119.
34. <http://www.tribuneindia.com/2000/20001102/cth3.htm>.
35. K. R. Haldiya, N. S. Bhandari, M. B. Singh, V. K. Beniwal, J. Lakshmi narayana, *Indian J. Hum. Ecol.*, **10** (1999) 69.
36. T. Rao, S. Bano, M. Das, *Indian J. Community Med.*, **31** (2006) 76.
37. A. P. Sharma, G. Filler, *Indian J. Urol.*, **26** (2010) 516.
38. K. VanDervoort, J. Wiesen, R. Frank, S. Vento, V. Crosby, M. Chandra, H. Trachtman, *J. Urol.*, **177** (2007) 2300.
39. T. Srivastava, U. Alon, *Adolesc. Med. Clin.*, **16** (2005) 87.
40. V. Bhalla, P. Grimm, G. Chertow, A. Pao, *Kidney Int.*, **75** (2009) 774.
41. J. Ding, *Kidney Int.*, **75** (2009) 780.
42. E. Worcester, J. H. Parks, M. A. Josephson, R. A. Thisted, F. L. Coe, *Kidney Int.*, **64** (2003) 2204.
43. O. Yoshida, A. Terai, T. Ohkawa, Y. Okada, *Kidney Int.*, **56** (1999) 1899.
44. A. G. Morris, A. L. Rodgers, *Am. J. Phys. Anthropol.*, **79** (1989) 521.
45. V. A. Master, M. V. Meng, M. L. Stoller, "Stone Nomenclature and History of Instrumentation for Urinary Stone Disease", In "Urinary Stone Disease - The Practical Guide to Medical and Surgical Management" Ed. M. L. Stoller, M. V. Meng, Humana Press, Totowa, New Jersey (2007) 4.
46. C. Y. C. Pak, *Lancet*, **351** (1998) 1797.
47. A. Hesse, D. Heimbach, *World J. Urol.*, **17** (1999) 308.
48. E. M. Worcester, F. L. Coe, *Prim Care.*, **35** (2008) 369.

49. B. B. Tomazic, G. H. Nancollas, *J. of Cryst. Growth*, **46** (1979) 355.
50. B. B. Tomazic, G. H. Nancollas, *J. Colloid Interface Sci.*, **75** (1980) 149.
51. M. Daudon, B. Bounxouei, C. F. Santa, S. S. Leite, B. Diouf, F. F. Angwafoo, J. Talati, G. Desrez, *Prog. Urol.*, **14** (2004) 1151.
52. Z. Djelloul, A. Djelloul, A. Bedjaoui, Z. K. Omar, A. Attar, M. Daudon, A. Addou, *Prog. Urol.*, **16** (2006) 328.
53. D. P. Griffith, *Kidney Int.*, **13** (1978) 372.
54. P. Durgawale, A. Shariff, A. Hendre, S. Patil, A. Sontakke, *Biomed. Res.*, **21** (2010) 305.
55. A. K. Pendse, P. P. Singh, *Urol. Res.*, **14** (1986) 59.
56. N.Q. Dao, M. Daudon (Eds.), *"Infrared and Raman Spectra of Calculi"*, Elsevier, Paris, 1997.
57. K. Lonsdale, D. J. Sutor, *Science*, **154** (1966) 1353.
58. K. Ichida, Y. Amaya, N. Kamatani, T. Nishino, T. Hosoya, O. Sakai, *J. Clin. Invest.*, **99** (1997) 2391.
59. W. Boyce, J. King, *J. Urol.*, **81** (1959) 351.
60. P. S. Lowry, S. Y. Nakada, *"Urinary Stones of Unusual Etiology"* in *"Urinary Stone Disease - The Practical Guide to Medical and Surgical Management"* Ed. M. L. Stoller, M. V. Meng, Humana Press, Totowa, New Jersey (2007) 345.
61. T. Nishizono, S. Eta, H. Enokida, K. Nishiyama, M. Kawahara, M. Nakagawa, *Int. J. Urol.*, **11** (2004) 119.
62. L. C. Herring & Co. Laboratory Website : <http://www.herringlab.com/photos>
63. N. Mandel, *Semin. Nephrol.*, **16** (1996) 364.

64. D. R. Basavaraj, C. S. Biyani, A. J. Browning, J. J. Cartledge, *EAU - EBU update series*, **5** (2007) 126.
65. D. J. Kok, *World J. Urol.*, **15** (1997) 219.
66. M. Marangella, C. Vitale, M. Petrarulo, C. Bagnis, M. Bruno, A. Ramello, *J. Nephrol.*, **13** (2000) S51.
67. E. M. Worcester, *Semin. Nephrol.*, **16** (1996) 474.
68. L. Mo, H. Y. Huang, X. H. Zhu, E. Shapiro, D. L. Hasty, X. R. Wu, *Kidney Int.*, **66** (2004) 1159.
69. B. Dussol, Y. Berland, *Nephrol. Dial. Transplant*, **11** (1996) 1222.
70. J. Liu, J. Chen, T. Wang, S. Wang, Z. Ye, *J. Urol.*, **173** (2005)113.
71. S. N. Pillay, J. R. Asplin, F. L. Coe, *Am. J. Physiol.*, **275** (1998) F255.
72. A. Trinchieri, A. Mandressi, P. Luongo, G. Longo, E. Pisani, *Br. J. Urol.*, **67** (1991) 230.
73. F. Parivar, R. K. Low, M. L. Stoller, *J. Urol.*, **155** (1996) 432.
74. L. A. Ruml, M. S. Pearle, C. Y. Pak, *Urol. Clin. N. Am.*, **24** (1997) 117.
75. W. G. Robertson, M. Peacock, P. J. Heyburn, F. A. Hanes, *Scand. J. Urol. Nephrol. Supplement*, **53** (1980) 15.
76. K. S. Kamel, S. C. Dhadli, M. A. Shafiee, M. L. Halperin, *J. Exp. Biol.*, **207** (2004) 1985.
77. N. A. Breslau, L. Brinkley, K. D. Hill, C. Y. C. Pak, *J. Clin. Endocrinol. Metab.*, **66** (1988) 140.
78. Z. Sabry, S. Shadarevian, J. Cowan, J. Campbell, *Nature*, **206**(1965)931.
79. J. Asplin, S. DeGanello, Y. N. Nakagawa, F. L. Coe, *Am. J. Physiol. - Renal Physiol.*, **261** (1991) F824.

80. Y. Nakagawa, M. Ahmed, S. L. Hall, S. De Ganello, F. L. Coe, *J. Clin. Invest.*, **79** (1987) 1782.
81. B. Hess, Y. Nakagawa, J. H. Parks, F. L. Coe, *Am. J. Physiol.- Renal Physiol.*, **260** (1991) F569.
82. Y. Shirane, Y. Kurokawa, S. Miyashita, H. Komatsu, S. Kagawa, *Urol. Res.*, **27** (1999) 426.
83. Y. Shirane, Y. Kurokawa, Y. Sumiyoshi, S. Kagawa, *Scanning Microsc.*, **9** (1995) 1081.
84. J. J. De Yoreo, S. R. Qiu, J. R. Hoyer, *Am. J. Physiol.-Renal Physiol.*, **291** (2006) F1123.
85. K. Chow, J. Dixon, S. Gilpin, J. P. Kavanagh, P. N. Rao, *Kidney Int.*, **65** (2004) 1724.
86. C. Y. C. Pak, *Am. J. Kidney Dis.*, **17** (1991) 420.
87. J. D. Sallis, N. F.G. Parry, J. D. Meehan, H. Kamperman, M. E. Anderson, *Scanning Microsc.*, **9** (1995) 127.
88. A. Wierzbicki, J. D. Sallis, E. D. Stevens, M. Smith, C. S. Sikes, *Calcified Tissue Int.*, **61** (1997) 216.
89. B. Hess, *Scanning Microsc.*, **5** (1991) 689.
90. H. F. Milhofer, L. Tunik, N. F. Vincekovic, D. Skrtic, V. Babic-Ivancic, N. Garti, *Scanning Microsc.*, **9** (1995) 1061.
91. A. Thomas, C. Woodard, E. S. Rovner, A. J. Wein, *Urol. Clin. N. Am.*, **30** (2003) 123.
92. C. Whelan, B. F. Schwartz, *Urology*, **63** (2004) 175.
93. P. Russinko, S. Agarwal, M. J. Choi, P. J. Kelty, *Urology*, **62** (2003) 748.
94. G. S. Markowitz, M. A. Perazella, *Kidney Int.*, **76** (2009) 1027.

95. B. R. Matlaga, O. D. Shah, D. G. Assimos, *Rev. Urol.*, **5** (2003) 227.
96. K. K. Malhotra, *J. Indian Acad. Clin. Med.*, **9** (2008) 282.
97. F. R. Spivacow, A. L. Negri, E. E. Valle, I. Calviño, E. Fradinger, J. R. Zanchetta, *Pediatr. Nephrol.*, **23** (2008) 1129.
98. J. Hughes, R. W. Norman, *Can. Med. Assoc. J.*, **146** (1992) 137.
99. G. C. Curhan, W. C. Willett, E. B. Rimm, M. J. Stampfer, *N. Engl. J. Med.*, **328** (1993) 833.
100. M. N. Hassapidou, S. T. Paraskevopoulos, P. A. Karakoltsidis, D. Petridis, E. Fotiadou, *J. Human Nutr. Dietet.*, **12** (1999) 47.
101. E. M. Worcester, F. L. Coe, *Semin. Nephrol.*, **28** (2008) 120.
102. J. E. Zerwekh, B. Y. R. Gitomer, C. Y. C. Pak, *Endocrinol. Metab. Clin. N. Am.*, **31** (2002) 869.
103. M. L. Stoller, "Urinary stone disease", In "Smith's general urology", Ed. E. Tanagho, J. McAninch, 16th Ed., McGraw-Hill, New York (2004) 260.
104. S. Corbetta, A. Baccarelli, A. Aroldi, L. Vicentini, G. Fogazzi, C. Vainicher, C. Ponticelli, P. Peccoz, A. Spada, *J. Endocrinol. Invest.*, **28** (2005) 122.
105. J. R. Asplin, *Endocrinol. Metab. Clin. N. Am.*, **31** (2002) 927.
106. F. L. Levy, B. A. Huet, C. Y. C. Pak, *Am. J. Med.*, **98** (1995) 50.
107. E. Leumann, B. Hoppe, *J. Am. Soc. Nephrol.*, **12** (2001) 1986.
108. J. I. Scheinman, *Miner. Electrolyte Metab.*, **20** (1994) 340.
109. A. R. Morton, E. Iliescu, J. Wilson, *Can. Med. Assoc. J.*, **166** (2002) 213.
110. R. Nath, S. Thind, M. Murthy, S. Farooqui, R. Gupta, H. Koul, *Ann. NY. Acad. Sci.*, **585** (1990) 274.
111. L. K. Massey, H. Smith, R. Sutton, *J. Am. Dietet. Assoc.*, **93** (1993) 901.

112. J. S. Rodman, R. J. Mahler, *Urol. Clin. N. Am.*, **27** (2000) 275.
113. F. L. Coe, J. H. Parks, J. R. Asplin, *N. Engl. J. Med.*, **327** (1992) 1141.
114. J. R. Asplin, *Semin. Nephrol.*, **16** (1996) 412.
115. F. L. Coe, A. L. Strauss, V. Tembe, S. L. Dun, *Kidney Int.*, **17** (1980) 662.
116. K. Sakhaee, B. A. Huet, O. W. Moe, C.Y. Pak, *Kidney Int.*, **62**(2002) 971.
117. D. Prie, P. U. Torres, G. Friedlander, *Kidney Int.*, **75** (2009) 882.
118. D. Prie, L. Beck, G. Friedlander, C. Silve, *Curr. Opin. Nephrol. Hypertens.*, **13** (2004) 675.
119. S. R. Chaudhari, A. R. Thakur, P. Nandy, S. Samanta, *Am. J. Infect. Dis.*, **4** (2008) 117.
120. P. Rieu, *Ann. Urol.*, **39** (2005) 16.
121. B. Shekarriz, M. Stoller, *Endocrinol. Metab. Clin. N. Am.*, **31**(2002) 951.
122. Y. Nakagawa, J. R. Asplin, D. S. Goldfarb, J. H. Parks, F. L. Coe, *J. Urol.*, **164** (2000) 1481.
123. C. Y. C. Pak, C. J. Fuller, *J. Urol.*, **129** (1983) 1066.
124. F. L. Coe, "Nephrolithiasis: Pathogenesis and Treatment", Year Book Medical Publishers, Chicago (1978).
125. G. C. Curhan, W. C. Willett, E. B. Rimm, M. J. Stampfer, *J. Am. Soc. Nephrol.*, **8** (1997) 1568.
126. T. Sinha, S. C. Karan, A. Kotwal, *Urol. Res.*, **38** (2010) 17.
127. S. Ljunghall, *Mineral. Electrolyte Metab.*, **13** (1987) 220.
128. J. R. Saltzman, R. M. Russell, *Gastroenterol. Clin. N. Am.*, **27**(1998) 309.
129. S. A. Abrams, *Proc. Nutr. Soc.*, **60** (2001) 283.
130. R. A. Hiatt, L.G. Dales, G. D. Friedman, E. M. Hunkeler, *Am. J. Epidemiol.*, **115** (1982) 255.

131. R. Unwin, O. Wrong, E. Cohen, M. Tanner, R. Thakker, *Lancet*, **348** (1996) 1561.
132. J. S. Rodman, R. E. Sosa, C. Seidman, R. Jones, “*No More Kidney Stones*”, John Wiley & Sons, Hoboken, New Jersey, USA (2007).
133. J. M. Soucie, M. J. Thun, R. J. Coates, W. McClellan, H. Austin, *Kidney Int.*, **46** (1994) 893.
134. J. E. Dalleria, P. S. Chandhoke, “*Epidemiology and Incidence of Stone Disease*”, In “*Urinary Stone Disease - The Practical Guide to Medical and Surgical Management*” Ed. M. L. Stoller, M. V. Meng, Humana Press, Totowa, New Jersey (2007).
135. H. G. Tiselius, *Braz. J. Urol.*, **26** (2000) 452.
136. E. N. Taylor, G. C. Curhan, *Kidney Int.*, **70** (2006) 835.
137. A. Basiri, N. Shakhssalim, A. R. Khoshdel, M. H. Radfar, H. Pakmanesh, *J. Renal. Nutri.*, **19** (2009) 396.
138. E. N. Taylor, M. J. Stampfer, G. C. Curhan, *J. Am. Soc. Nephrol.*, **15** (2004) 3225.
139. R. Siener, A. Hesse, *Eur. J. Nutr.*, **42** (2003) 332.
140. F. Grases, P. Sanchis, J. Perello, A. Bauza, *Int. J. Urol.*, **13** (2006) 252.
141. K. Sternberg, S. Greenfield, P. Williot, J. Wan, *J. Urol.*, **174** (2005) 1711.
142. A. Prentice, F. Branca, T. Decsi, K. F. Michaelsen, R. J. Fletcher, P. Guesry, F. Manz, M. Vidailhet, D. Pannemans, S. Samartin, *Br. J. Nutr.*, **92** (2004) S83.
143. K. Sakhaee, J. A. Harvey, P. K. Padalino, P. Whitson, C. Y. C. Pak, J. *Urol.*, **150** (1993) 310.
144. P. O. Schwille, E. Hanisch, D. Scholz, *J. Urol.*, **132** (1984) 650.

145. E. N. Taylor, G. C. Curhan, *Kidney Int.*, **73** (2008) 207.
146. N. Abate, M. Chandalia, A. Chan, O. W. Moe, K. Sakhaee, *Kidney Int.*, **65** (2004) 386.
147. N. Vyas, R. K. Keservani, S. Jain, R. Raghuvanshi, N. P. Gavatia, A. K. Agrawal, R. K. Kesharwani, *Der Pharmacia Lettre*, **2** (2010) 457.
148. Toxicological and health aspects of melamine and cyanuric acid: A report of WHO expert meeting in collaboration with FAO, supported by Health Canada, Ottawa (2008).
149. J. Shuster, A. Jenkins, C. Logan, *J. Clin. Epidemiol.*, **45** (1992) 911.
150. G. C. Curhan, W. C. Willett, E. B. Rimm, D. Spiegelman, M. J. Stampfer, *Am. J. Epidemiol.*, **143** (1996) 240.
151. H. J. Kramer, H. K. Choi, K. Atkinson, M. Stampfer, G. C. Curhan, *Kidney Int.*, **64** (2003) 1022.
152. T. Watanabe, *Pediatr. Nephrol.*, **20** (2005) 86.
153. M. C. Ost, B. R. Lee, *Curr. Opin. Urol.*, **16** (2006) 93.
154. S. C. Howard, S. Kaplan, B. Razzouk, G. Rivera, J. Sandlund, R. Ribeiro, J. Rubnitz, A. Gajjar, W. Ke, M. Hancock, J. Skoch, S. Roy, M. Hudson, C. Pui, *Leukemia*, **17** (2003) 541.
155. Y. Kato, N. Taniguchi, M. Okuyama, H. Kakizaki, *Int.J. Urol.*, **14**(2007)954.
156. R. C. Calvert, N. A. Burgess, *Curr. Opin. Urol.*, **15** (2005) 113.
157. K. Sarica, B. Eryildirim, F.Yencilek, U.Kuyumcuoglu, *Urol.*, **73**(2009)1003.
158. R. Siener, S. Glatz, C. Nicolay, A. Hesse, *Obes. Res.*, **12** (2004) 106.
159. G. C. Curhan, W. C. Willett, E. B. Rimm, F.E. Speizer, M.J. Stampfer, *J. Am. Soc. Nephrol.*, **9** (1998) 1645.

160. E. N. Taylor, M. J. Stampfer, G. C. Curhan, *J. Am. Med. Assoc.*, **293** (2005) 455.
161. N. M. Maalouf, K. Sakhaee, J. H. Parks, F. L. Coe, B. A. Huet, C. Y. C. Pak, *Kidney Int.*, **65** (2004) 1422.
162. G. R. Najem, J. J. Seebode, A. J. Samady, M. Feuerman, L. Friedman, *Int. J. Epidemiol.*, **26** (1997) 1017.
163. O. Schmucki, R. Asper, C. Zortea, *Urol. Int.*, **39** (1984) 159.
164. Y. M. F. Marickar, A. Salim, A. Vijay, *Urol. Res.*, **38** (2010) 65.
165. T. H. Brikowski, Y. Lotan, M. S. Pearle, *Proc. Natl. Acad. Sci. USA*, **105** (2008) 9841.
166. G. Richet, *Kidney Int.*, **48** (1995) 876.
167. F. Grases, A. Bauza, M. Ramis, V. Montesinos, A. Conte, *Clin. Chim. Acta.*, **322** (2002) 29.
168. http://en.academic.ru/pictures/enwiki/75/KUB_stone.jpg
169. W. P. Springhart, G. M. Preminger, *Curr. Opin. Urol.*, **14** (2004) 95.
170. D. H. Sheafor, B. S. Hertzberg, K. S. Freed, B. A. Carroll, M. T. Keogan, E. K. Paulson, D. M. DeLong, R. C. Nelson, *Radiology*, **217** (2000) 792.
171. S. Oner, A. Oto, S. Tekgul, M. Koroglu, M. Hascicek, A. Sahin, O. Akhan, *JBR-BTR*, **87** (2004) 219.
172. http://www.ultrasound-images.com/renal-calculi.htm#3- D_Ultrasound_image_of_renal_calculus
173. <http://alliedurology.com/assets/images/ctscan.jpg>
174. <http://yoursurgery.com/procedures/stones/images/StonesCT.jpg>
175. D. S. Katz, M. Scheer, J. H. Lumerman, B. C. Mellinger, C. A. Stillman, M. J. Lane, *Urology*, **56** (2000) 53.

176. D. S. Katz, J. Hines, D. Rausch, S. Perlmutter, F. Sommer, J. Lumerman, R. Friedman, M. Lane, *Am. J. Roentgenol.*, **173** (1999) 425.
177. R. J. Zagoria, R. L. Dixon, *Adv. Chronic Kidney Dis.*, **16** (2009) 48.
178. E. Yakoumakis, I. Tsalafoutas, N. Nazos, E. Koulentianos, C. Proukakis, *Br. J. Radiol.*, **74** (2001) 727.
179. M. Cohnen, L. Poll, C. Puettmann, K. Ewen, A. Saleh, U. Modder, *Eur. Radiol.*, **13** (2003) 1148.
180. T. Niemann, T. Kollmann, G. Bongartz, *Am. J. Roentgenol.*, **191**(2008)396.
181. <http://www.childrensurologyofva.com/images/dynamic/U100.jpg>
182. http://en.wikipedia.org/wiki/Intravenous_pyelogram
183. P. A. Bhatt, P. Paul, *J. Chem. Sci.*, **120** (2008) 267.
184. N. Gould, P. C. Hallson, G. P. Kasidas, C. T. Samuell, T. B. Weir, *Urol. Res.*, **23** (1995) 63.
185. M. Volmer, J. C. M. De Vries, H. M. J. Goldschmidt, *Clin. Chem.*, **47** (2001) 1287.
186. E. K. Girija, S. N. Kalkura, P. B. Sivaraman, Y. Yokogawa, *J. Sci. Ind. Res.*, **66** (2007) 632.
187. R. S. Sathish, B. Ranjit, K. M. Ganesh, G. N. Rao, C. Janardhana, *Curr. Sci.*, **94** (2008) 104.
188. P. Carmona, J. Bellanato, E. Escolar, *Biospectrosc.*, **3** (1997) 331.
189. F. S. Manciu, J. R. Govani, W. G. Durrer, L. Reza, L. A. Pinales, *J. Raman Spectrosc.*, **40** (2009) 861.
190. E. L. Prien, C. Frondel, *J. Urol.*, **57** (1947) 949.
191. L. C. Herring, *J. Urol.*, **88** (1962) 545.

192. D. Krausova, *Bull Czech Slovak Crystallogr. Assoc.*, **3** (1996) 148.
193. V. B. Nalbandyan, *Urol. Res.*, **36** (2008) 247.
194. G. Schubert, G. Brien, C. Bick, *Urol. Inst.*, **38** (1983) 65.
195. D. J. Sutor, *British J. Urol.*, **40** (2008) 29.
196. M. A. Wandt, A. L. Rodgers, *Clin. Chem.*, **34** (1988) 289.
197. N. Kumar, P. Singh, S. Kumar, *Indian J. Biochem. Biophys.*, **43** (2006) 226.
198. M. Berényi, D. Frang, J. Légrády, *Int. Urol. Nephrol.*, **4** (1972) 341.
199. Z. Y. Shang, L. Ming, *Zhonghua, Yixue Zazhi (Chinese Medical Journal of China)*, **65** (1985) 474.
200. M. Berenyi, G. Liptay, *J. Thermal. Anal.*, **3** (1971) 437.
201. B. S. Strates, *Experimentia.*, **22** (1966) 574.
202. S. Materazzi, R. Curini, G. D'Ascenzo, A. D. Magri, *Thermochim. Acta*, **264** (1995) 75.
203. S. Charafi, M. Mbarki, A. C. Bauza, R. M. Prieto, A. Oussama, F. Grases, *Int. J. Nephrol. Urol.*, **2** (2010) 469.
204. A. L. Rodgers, Scaillet, M. A. Wandt, In "*Urinary stone : Proceedings of the second International Urinary Stone Conference, Singapore (1983)*", Ed. R. L. Ryall, Churchill Livingstone, New York (1984).
205. R. Agarwal, V. R. Singh, V. Singh, S. U. M. Rao, S. P. Sud, *J. Acoust. Soc. India*, **17** (1989) 194.
206. J. L. Rodríguez-Miñón Cifuentes, E. Salvador, M. L. Traba Villameytide, *Actas Urol. Esp.*, **30** (2006) 57.
207. X. Feng, S. R. Ahmed, M. Mayo, S. Iqbal, *Lasers Med. Sci.*, **20** (2005) 132.
208. C. A. Zarse, J. A. McAteer, A. J. Sommer, S. C. Kim, E. K. Hatt, J. E. Lingeman, A. P. Evan, J. C. Williams, Jr, *BMC Urol.*, **4** (2004) 15.

209. J. C. Williams Jr, J. A. McAteer, A. P. Evan, J. E. Lingeman, *Urol. Res.*, **38** (2010) 477.
210. <http://www.herringlab.com/herringlabs.html>
211. V. S. Joshi, *Ph.D. Thesis*, Saurashtra University Rajkot (2001).
212. V. S. Joshi, M. J. Joshi, "Proc. of Prep. and Charact. of Technologically Important Single Crystals Int. Workshop", NPL, New Delhi, 26-28 February, (2001).
213. E. Tann, P. Silverman, W. Shuman, *Radiology*, **228** (2003) 319.
214. C. Y.C. Pak, *Nephron*, **81** (1999) 60.
215. <http://www.dornier.com/Global/assets/Image/majorVisuals/productCategories/lithotripters/CompactDeltaIIMainVisual.jpg>
216. http://www.reshealth.org/images/greystone/em_1885.gif
217. Y. Q. Xue, D. L. He, X. F. Chen, X. Li, J. Zeng, X. Y. Wang, *J. Urol.*, **182** (2009) 762.
218. http://www.accesssurgery.com/loadBinary.aspx?name=zinn&filename=zinn_c037f014t.jpg
219. <http://www.southcoasturology.com.au/uploads/images/perc.jpg>
220. S. P. Dretler, *J. Urol.*, **139** (1988) 1124.
221. H. Akimoto, E. Higashihara, H. Kumon, Z. Masaki, S. Orikasa, "*Treatment of Urolithiasis*", Springer, Tokyo (2001).
222. C. Y. C. Pak, "*Urolithiasis*", W. B. Saunders Press, Philadelphia (1999).
223. K. C. Joseph, *Ph.D. Thesis*, Saurashtra University Rajkot (2005).
224. B. B. Parekh, *Ph.D. Thesis*, Saurashtra University Rajkot (2005).
225. A. D. B. Vaidya, T. P. A. Devasagayam, *J. Clin. Biochem. Nutr.*, **41** (2007) 1.

226. B. Patwardhan, A. D. B. Vaidya, M. Chorghade, *Curr. Sci.*, **86** (2004)789.
227. A. D. B. Vaidya, *Indian J. Pharmacol.*, **38** (2006) 311.
228. B. Patwardhan, A. D. B. Vaidya, M. Chorghade, S. P. Joshi, *Curr. Bioactive Compounds*, **4** (2008) 201.
229. A. D. B. Vaidya, in “*Ayurveda in Transition*”, Arya Vaidya sala Kotlalkal, Part-I, “The Status of Ayurvedic Paradigm Shifting Environment”, (2010).
230. S. Natarajan, E. Ramachandran, D. Blisin Suja, *Cryst. Res. Technol.*, **32** (1997) 553.
231. V. S. Joshi, B. B. Parekh, M. J. Joshi, A. B. Vaidya, *J. Cryst. Growth*, **275** (2005) e1403.
232. V. S. Joshi, M. J. Joshi, *Indian J. Pure Appl. Phys.*, **41** (2003) 183.
233. B. B. Parekh, M. J. Joshi, *Indian J. Pure Appl. Phys.*, **43** (2005) 675.
234. V. S. Joshi, B. B. Parekh, M. J. Joshi, A. D. B. Vaidya, *Urol. Res.*, **33** (2005) 80.
235. K. C. Joseph, B. B. Parekh, M. J. Joshi, *Curr. Sci.*, **85** (2005) 1232.

Chapter III

Crystal Growth Technique

Topic Number	Topic	Page Number
3.1	Introduction	114
3.2	Crystal Growth Techniques	117
3.3	Gel Growth Technique	123
3.4	Types of Gels	125
3.5	Gelling Mechanism	130
3.6	Structure of Silica Hydro Gel	131
3.7	Classification of Gel Growth Methods	134
3.8	Growth Mechanism	138
3.9	Nucleation Control	141
3.10	Crystal Habit	143
3.11	Liesegang Rings	145
3.12	Crystals Grown by Gel Method	148
3.13	Advantages and Limitations of Gel Growth Technique	150

3.1 Introduction

Free energy barrier is a major burden.

Transformation cannot happen without aid.

The question is what can we do to make it happen.

The answer is something has to nucleate.

In the beginning there was incubation.

The question is "When will we get to steady state?"

Patience will lead to further fluctuation.

Then nuclei will show and grow at a steady rate.

Rolling down the gradient slope.

Gathering buddies along the way.

Which one of them will have hope?

The truth is only the big ones will stay.

Such is the story of nucleation and growth.

Nature has chosen this approach.

– L. I. Preston (2002)

A crystal is a solid material whose constituent atoms, molecules, or ions are arranged in an orderly repeating pattern extending in all three spatial dimensions. A systematic and scientific study of crystals including process of crystallization, internal structure, external morphology, properties and classification of crystals is known as "*Crystallography*". The study of the formation of crystals is covered under the subhead "*Crystal Growth*". The process of crystal formation is known as *crystallization*.

The growth of crystals occurs either in nature or artificially in a laboratory. The Mother Nature grows a variety of crystals in the crust of Earth,

which are mainly the natural mineral crystals including diamond, precious stones and rocks. Mostly these crystals were grown from the molten state by freezing. It is also possible to form crystals directly from a gas without passing through the liquid state; example is, the hoarfrost, i.e., ice crystals which are grown from water vapour in the air. Also, a few mineral substances which are found mainly around volcanoes, where sulphur and ammonium chloride crystals are formed from the gases emitted during eruption. There are other examples of crystals grown in nature, which are famous *Amarnath Shivalinga* of ice in Himalayan cave, large crystals grown around Dead Sea in Israel and gigantic mineral crystals in Naica caves, Chihuahua state of Mexico.

Today, the growth of crystals does not remain the phenomena only occurring in nature, but it has become a well advanced as well as widely used laboratory technique. It is interesting to note that the crystal growth can be regarded as an ancient subject, owing to the fact that the crystallization of salt and sugar was known to the ancient Indian and Chinese civilizations. The subject of crystal growth was treated as a part of crystallography and never had an independent identity until the last century. It is important to note that both structural crystallography and the science of crystal growth emerged from curiosity about the large variety in crystal forms existing in nature. The fundamental aspects of crystal growth had been derived from early crystallization experiments in the 18th and the 19th century [1,2]. Theoretical understanding started with the development of thermodynamics in the late 19th century and with the development of nucleation and crystal growth theories and later on the increasing understanding of the role of transport phenomena in the 20th century. There always has been a requirement of good quality crystals for various

applications. The demand of the modern day science and technology has tempted scientists to synthesize and grow several new varieties of crystals. The requirement for better, cheaper, and larger single crystals has driven extensive research and development in crystal growth. This has brought the field of crystal growth into the lime light. As a result the congeries of crystals is ever expanding day by day.

Crystals are the back bone of today's technological development. Crystals are the unacknowledged pillars of modern technology. The world crystal production was estimated to be more than 20,000 ton per year in the year 1999 [3]. Out of that the largest share of about 60% was from semiconductor materials, for instance, silicon, gallium arsenide, indium phosphate, gallium phosphate, cadmium telluride and its alloys. As can be seen in Figure 3.1, optical crystals, scintillator crystals, and acousto-optic crystals had about equal shares of 10%, whereas laser and nonlinear-optic crystals and crystals for jewelry and watch industry had shares of a few % only.

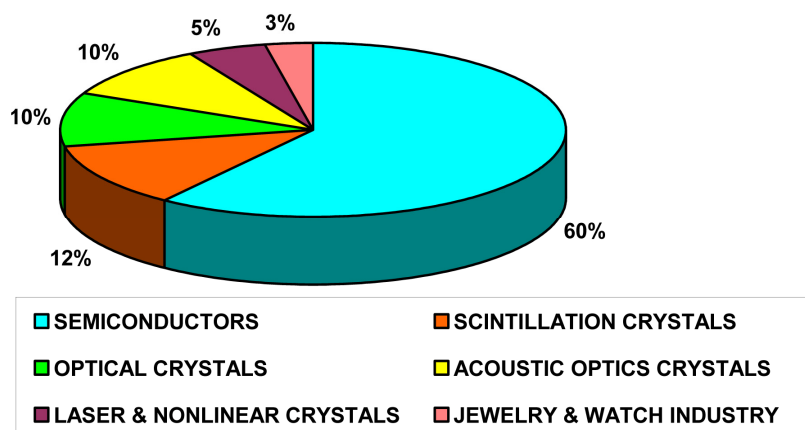


Figure : 3.1 Estimated shares of world crystal production in 1999 [3]

However, over the last decade the demands on synthetic biomaterials have increased significantly with the progress in fields of medicine, material science and engineering, biochemistry, pharmaceuticals and nanotechnology.

Furthermore, crystal growth is divided into five major areas by H. J. Scheel, namely, [4] :

1. Fundamental theoretical and experimental crystal growth studies.
2. Laboratory crystal growth for preparing research samples.
3. Industrial fabrication of single crystals, their characterization and machining
4. Fabrication of metallic / dendritic crystals (e.g. turbine blades).
5. Mass crystallization (salt, sugar, chemicals).

3.2 Crystal Growth Techniques

Crystal growth techniques ranges from a simple inexpensive process to a complex sophisticated expensive process and crystallization time ranges from minutes, hours, days and to months. The process of crystal growth is a controlled change of state, or phase change, to the solid state. This transition may occur from the solid, liquid or vapour state. Hence, depending on the phase transitions involved in the process, the crystal growth methods can generally be classified into three basic categories [5]:

Solid Growth : $S \rightarrow S$ processes involving solid to solid phase transitions.

Melt Growth : $L \rightarrow S$ processes involving liquid to solid phase transitions.

Vapour Growth : $V \rightarrow S$ processes involving vapour to solid phase transitions.

3.2.1 Solid Growth Techniques : The $S \rightarrow S$ processes are not commonly used except for certain metals where strain annealing is effective and certain cases where a crystal structure alters between the melting point and room temperature. These processes include annealing or sintering, strain annealing, deformation growth and polymorphic phase transitions. Single crystals are developed by the preferential growth of a polycrystalline mass, which can be achieved by straining the material and subsequent annealing.

Large crystals of several materials, especially, metals have been grown by this method [6].

3.2.2 Liquid Growth Techniques : The $L \rightarrow S$ processes are many and important also. The growth of crystals from the liquid phase is treated as two categories – (i) Melt Growth and (ii) Solution Growth due to the independent behaviour of melt and solution techniques.

Melt growth is the process of crystallization by fusion (melting) and re-solidification of the pure material. It is the fastest of all crystal growth methods and is widely used for the preparation of large single crystals. Melt growth methods are limited to the materials which melt congruently and having an experimentally viable vapour pressure at its melting point. The material to be grown into crystal form is melted and after that it may progressively cooled to yield the crystalline matter. The normal freezing or directional freezing is a very important process for the crystals which melt congruently without decomposing. When an ingot is gradually frozen from one end to the other, it is said to be frozen normally or directionally. This process comprises of many techniques, which are used world wide for industrial crystallizations, including growth of metals, semiconductor crystals for electronic and computer chip making industries and laser host crystals. Sometimes, the liquid phase contains deliberately added foreign materials as in solution growth or flux growth or liquid phase epitaxy. Bridgman technique and Czochralski technique are the well known melt growth techniques.

The solution growth is also very popular for the growth of numerous crystals for industry. The growth of crystals by precipitation from aqueous solution is the most simple and the oldest technique. In this process, a

saturated solution of the material to be grown into crystal is taken and in an appropriate solvent the crystallization takes place as this solution becomes critically supersaturated. The supersaturation can be achieved either by lowering the temperature of the solution or by slow evaporation. The advantage of the method is that the crystals can be grown from a solution at temperatures well below its melting point, perhaps even at room temperature and, therefore, it turns out to be more applicable in many cases. Solution growth can be broadly classified into high temperature solution growth, hydrothermal method, low temperature solution growth and gel growth.

3.2.3 Vapour Growth Techniques: The $V \rightarrow S$ processes include sublimation, which is strictly speaking a kind of $S \rightarrow V \rightarrow S$ process, and the vapour phase reactions which are used in the epitaxial growth of semiconductors. Sometimes deliberately added gases are helpful as transporting agents for the growing materials. Vapour growth techniques can be adopted for the growth of materials which lack a suitable solvent and sublime before melting at normal pressure. Vapour growth methods have been employed to produce bulk crystals and to prepare thin layers on crystals with a high degree of purity.

The development and refinement of methods of crystal growth to achieve useful products have relied heavily on empirical engineering and on trial and error methods. Crystal growth still remains, by and large, as an art along with a science [7]. A phalanx of crystal growers has developed various crystal growth techniques after their pain staking efforts of years together.

Table 3.1 shows the classification scheme for various growth techniques as summarized by Laudise, which is very important for the neophytes [8,9].

Table : 3.1 : Crystal Growth Techniques

Crystal Growth Techniques			
Mono-component		Poly-component	
A	Solid → Solid (Solid Growth)	A	Solid → Solid (Solid Growth)
	<ol style="list-style-type: none"> 1. Strain annealing 2. Devitrification 3. Polymorphic-phase change 		<ol style="list-style-type: none"> 1. Precipitation from solid solution
B	Liquid → Solid (Melt Growth)	B	Liquid → Solid (Solution Growth)
	<ol style="list-style-type: none"> 1. Conservative <ol style="list-style-type: none"> (a) Directional solidification (<i>Bridgman-Stockbarger</i>) (b) Cooled seed (<i>Kyropoulos</i>) (c) Pulling (<i>Czochralski</i>) 2. Non Conservative <ol style="list-style-type: none"> (a) Zone Melting (<i>horizontal, vertical, float zone, growth on a pedestal</i>) (b) Verneuil (<i>Flame fusion, plasma, arc image</i>) 		<ol style="list-style-type: none"> 1. Growth from Solution (<i>evaporation, slow cooling and temperature differential</i>) <ol style="list-style-type: none"> (a) Aqueous solvents (b) Organic solvents (c) Molten-salt solvents (d) Solvents under hydrothermal (e) Other organic solvents 2. Growth by Reaction <ol style="list-style-type: none"> (a) Chemical reaction (b) Electrochemical reaction
C	Gas → Solid (Vapor Growth)	C	Gas → Solid (Vapor Growth)
	<ol style="list-style-type: none"> 1. Sublimation-condensation 2. Sputtering 		<ol style="list-style-type: none"> 1. Growth by reversible reaction (<i>temperature change, concentration change</i>) <ol style="list-style-type: none"> (a) Van Arkel (<i>hot wire processes</i>) 2. Growth by irreversible reaction <ol style="list-style-type: none"> (b) Epitaxial processes

The designing and development of various crystal growth techniques of the present day is a result of continuous and fruitful modifications occurring since last several decades and still today the modification process is continuing.

Table 3.2 shows the multi-disciplinary nature and complexity of crystal growth processes as explained by Scheel [4].

Table : 3.2 : Multi-Disciplinary Nature and Complexity of Crystal Growth

Multi-Disciplinary Nature of Crystal Growth
<ul style="list-style-type: none"> • Theoretical Physics (especially thermodynamics, non-equilibrium thermodynamics, statistical mechanics) • Solid-State Physics • Crystallography and Crystal Chemistry • Materials Science & Engineering • Chemistry (all fields) including Chemical Engineering • Mechanical & Electrical Engineering (especially hydrodynamics, machine design, process control) • Mineralogy • Metallurgy
Complexity of Crystal Growth
<ul style="list-style-type: none"> • Phase Transformation from Fluid (melt, solution, vapour) to Crystal • Scaling Problem: Control of surface on nm scale in growth system of ~m size, hampers numerical simulation • Complex Structure & Phenomena in Melts and Solutions • Multi-Parameter Processes: Optimize and compromise

Schieber [10] has well explained the required three aspects of crystal growth (i) Theory of nucleation and growth (ii) Experimental crystal growth and (iii) Characterization of crystals. A poem of L. I. Preston describes the competitive nucleation in crystal, which is explained by many authors, in detail [5,11-13]. This has been correctly quoted in a different manner by Gilman [7] in his book *“The Arts and Science of Growing Crystals”* as, “The Systematic production of artificial crystals might be viewed as a new *agriculture* that has begun flourish. It differs from true agriculture in that its products are mostly

inorganic at present, but it has many features common with normal agriculture and promises to have a somewhat comparable effect on society. The new agriculture consists of *growing* solid crystals from a *nutrient* phase (gas, liquid or solid). To start the growth process, the nutrient is often *seeded* with small crystal to be grown, and some workers speak of *repeating the harvest* after a certain length of time.”

Over the years, many successful attempts have been made to describe the art and science of crystal growth, and many review articles, monographs, symposium volumes, and handbooks have been published to present comprehensive reviews of the advances made in this field.

There are many well written books available on subjects like fundamentals of crystal growth [14]; different crystal growth techniques, their theories, characterization and applications [15-21] and understanding the growth mechanism [22]. Even books are available with wonderful photographs of crystals [23]. Whereas, the authors Stangl and Stang [24] have considered the growth of a variety of beautiful crystals as the growth of flowers in a garden, thereby, they have agreed to the concept of Gilman [7].

Various crystal growth techniques have been discussed in detail by several authors [25,26]. The different techniques of each category are found in reviews and books by Faktor and Garrett [27] on vapour growth, Brice [28] on melt growth, Henisch [29] on gel growth, Buckley [30] on solution growth and Elwell and Scheel [1] on high temperature solution growth. A review on the advances in crystal growth techniques are discussed by Mirkin and Moreno [31]. Recently, a “*Handbook of Crystal Growth*” is published [32], which describes the fundamentals of crystal growth and defect formation; bulk

growth from the melt, solution, and vapor; epitaxial growth; crystallization from gels; modeling of growth processes and defects; and techniques of defect characterization.

The predecessors of the present author [33-38] have discussed various growth techniques in detail; therefore, it is avoided in the present thesis. Among various techniques of growing crystals, gel growth technique occupies a prominent place owing to its versatility and simplicity. The present author has employed the gel growth technique to grow struvite and related crystals; therefore, this technique is discussed in some what more elaborately, hereby.

3.3 Gel Growth Technique

The roots of gel growth technique are associated with the earlier observations of the remarkable series of layers due to the phenomenon of periodic precipitation in gel systems in 1896 made by German chemist Raphael Eduard Liesegang [39-41]. A systematic study of crystallization in gels began with Liesegang's famous discovery of the periodic precipitation in gels [39]. His studies described the conditions of nucleation and growth for chromates, halides, phosphates, tartrates with metallic ions such as: Ag^+ , Cu^{2+} , Ca^{2+} , Ba^{2+} , Pb^{2+} , in gelatin, in agar, potassium silicate and macromolecular gels [29]. In its early days the gel was not used as a medium of crystal growth, but only used to study the phenomenon of periodic precipitation in gel. (The phenomenon is known as Liesegang ring and will be discussed later on in section 3.11 of this chapter.) The phenomenon was first explained and named as *Liesegang rings* by Wilhelm Ostwald [42] in 1897. Later on this phenomenon received the attention of Lord Rayleigh [43] because of his curious nature and thereby achieved wide acceptance and

reputation. This has inspired workers like Morce and Pierce [44], Holmes [45], Hatschek [46], Fells and Firth [47], etc. A comprehensive review on the earlier developments of this field has been described by Lloyd [48].

The potential application of gel as a medium for crystal growth was introduced by Fisher and Simons [49-51] in the 1920's. However it did not evoke much interest of crystal growers and remained as an unused work till early 1960's. The rapid developments in semiconducting and laser active materials prompted the search for new materials. This has increased the interests in crystal growth and researchers even turned to the less noticed gel technique. The science of growing crystals in gels has developed since 1920's but after 1970, the gel growth technique became very popular due to the pioneering work of famous experimentalist Henisch [29], who narrated not only the authentic survey of the work carried out in the field, but also explained the various aspects of the gel growth in his famous book on "*Crystal Growth in Gels*". Since then, it has attracted wide interest for growing a variety of crystals. Nowadays this method has been employed to grow not only the inorganic crystals but also to grow biological crystals *in vitro* because of its resemblance with biological environment.

The gel growth technique is a one kind of modified alternative version of solution growth technique. In which the growth occurs due to reaction between two suitable reactants (solutions) in a gel medium or achieving super-saturation by diffusion in gel medium. It is the simplest technique under ambient conditions. This technique is well suited for the crystal growth of compounds, which are sparingly soluble and decompose at fairly low temperatures. Crystals with dimensions of several mm can be grown in a

period of 3 to 4 weeks. Crystal growth by the gel technique has attracted the attention of numerous researchers, as this technique is comparatively simple and can be set up in a laboratory with simple glass-wares and without any need of sophisticated instruments and high temperature furnaces.

The gel growth technique is elaborately described by Henisch [29], Henisch and Hanoka [52], P.S. Raghavan and P. Ramasamy [15] as well as Patel and Venkateswara Rao [53]. An attempt has been made by the present author to review the gel growth technique briefly.

3.4 Types of Gels

Out of four states of matter - solid, liquid, gas and plasma, the three states of matter-solid, liquid and gas are more familiar. Even there are many exotic materials, which are yet not fully understood. Material scientists are trying to understand their structures and properties to derive their useful applications. One of the exotic states of matter is gels. They are neither solids nor liquids. In early stage, gel has been defined as a two component system of a semi solid nature rich in liquid [54]. A gel may also be defined as a semi-solid formulation having an external solvent phase, apolar (organo-gels) or polar (hydro-gel), immobilized within the spaces available of a three dimensional networked structure [55]. Recently, according to IUPAC 2007 recommendations gel is defined as non-fluid colloidal network or polymer network that is expanded throughout its whole volume by a fluid [56]. A characteristic property of gel is that they contain a conspicuously high percentage of solvent and little solid matter. The gel forming substances and solvents stabilize each other in the gel structure. Most gels are mechanically and optically isotropic, except when under strain.

As shown in Table 3.3, gels can be classified according to constituent (matrix) phase, solvent phase and cross-linkages.

Table : 3.3 : Classification of Gels

Classification of Gel		
Constituent Or Matrix Phase	Surfactant Bilayers	
	Polymers	<ul style="list-style-type: none"> • Natural gel • Synthetic gel • Hybrid gel
Solvent Phase	Solid-Liquid	<ul style="list-style-type: none"> • Hydro-gel (Water Solvent) • Organo-gel (Organic Solvent) • Lio-gel (Oily Solvent) • Alco-gel (Alcohol Solvent)
	Solid-Gas	<ul style="list-style-type: none"> • Xero-gel (air) • Aero-gel (air)
	Solid-Solid	<ul style="list-style-type: none"> • Polymer-gel (polymer)
Cross-linkage	Physical Gel (Noncovalently Crosslinked Polymer Networks)	<ul style="list-style-type: none"> • Coulombic Interaction • Hydrogen Bonding • Coordinate Bonding • Hydrophobic Bonding
	Chemical Gel (Covalently Crosslinked Polymer Networks)	<ul style="list-style-type: none"> • Covalent crosslinking

The materials which can be categorized as gels are silica gel, agar (a carbohydrate polymer derived from seaweed), gelatin (a substance closely related to proteins), soft soaps (potassium salts of higher fatty acids), a variety of oleates and stearates, polyvinyl alcohol, various hydroxides in water, and even water-insoluble tetraethoxysilane in the presence of electrolytes and co-solvents (e.g. methanol) and surface active agents [29, 57]. It is also noted that two-component systems, usually known as sols are the materials which are closest to gels in structure, but they resemble liquids more than solids.

The process, through which a network is formed from solution by a progressive change of liquid precursor into a sol, to a gel, is known as sol-gel process. The coagels are hybrid media which consist of small jelly-like particles separated by relative large tracts of liquid phase.

When the dispersion medium (or the swelling agent) is water, then it is called a hydro-gel or aqua-gel having a network of polymer chains that are water-insoluble. Hydro-gels are super-absorbent natural or synthetic polymers. Hydro-gels also possess a degree of flexibility very similar to natural tissues. Moreover, hydro-gels have the ability to sense changes of pH, temperature, or the concentration. On the other hand, an organo-gel is the gel with an organic liquid is used as the dispersion medium instead of water. But in a gel if alcohol is used instead of water as the dispersion medium, it is known as alco-gel. More precisely, alco-gel is the gel in which the swelling agent consists predominantly of an alcohol or a mixture of alcohols.

Aero-gels are made from a sol-gel by carefully evacuating the solvent to leave a fragile polymer network, which is having 90-99% air by volume. Thus, the aero-gel is a gel comprised of a micro porous solid in which the dispersed phase is a gas. Microporous silica, microporous glass and zeolites (microporous aluminosilicate minerals) are common examples of aero-gels. Xero-gel is an open network formed by the removal of all swelling agents from a gel. Examples of xero-gels include silica gel and dried out, compact, macromolecular structures, such as gelatin or rubber.

Gels are materials where polymer chains form the links of a network immersed in a typically liquid environment. The polymer chains are cross-linked at the microscopic level by comparatively stronger chemical (covalent)

bonds or weaker physical bonds; the type of bond is used to label the macroscopic material as a chemical gel or a physical gel, respectively. Both physical gel and chemical gel have distinct macroscopic properties, since their microscopic behaviors of cross-links are different. Since the chemical cross-links prevent the chemical gels from dissolving in its environment solvent, chemical gels behave macroscopically like solids. Such chemical gel structures show higher resistance to slight physicochemical affects and cannot be converted into sols by warming. The gel structure cannot be disrupted except by breakdown of the polymer molecules. However, because of the weaker nature of the cross-linking bonds, physical cross-links are found in a constant cycle of creation and dissolution in physical gels. Therefore, physical gels are sometimes called thermo reversible gels, i.e., the creation and dissolution of cross-links or sol-gel transition are temperature driven and reversible. Such physical gel structures may be disrupted by slight physicochemical effects, which cause sol formation. When it is cooled down the bonds will recombine and the sol once more solidifies into a gel. Agarose (Agarose is a gelling compound extracted from certain red sea weeds of the *Rhodophyceae* group) is the example of the physical gel because the association of its chains is reversible upon heating.

The structure of synthetic and semi-synthetic gel is generally depending on the chemical properties of the basic substances, the relative concentration of the reagents and the solubility conditions during gel formation. The functional reactivity of monomers and their spatial orientation has pronounced effect on cross-linking. The reactions inducing cross-linkages are random processes governed by the laws of statistical probability. These

processes cause voids of dimensions and geometry, which are the characteristic of the type of gel used to form the polymer chains. These voids are known as the *pores of the gel*. Since the gel structure is not a rigid system but a mobile one, more-or-less, fixed network of polymer chains, the terms used in practice are average or effective pore size. The pore size is one of the most important parameters of the molecular phenomena (diffusion, permeability). Pore sizes may be influenced by the conditions of formation, and the solubility relationships of the initial substances and the end product.

There is a distribution of pore sizes within each gel and one gel is distinguished from another by the nature of this distribution. In course of some early experiments on gels, Biltz [58] concluded that hydro-gels are characterized by two types of pores; the *primary* pores are of nearly molecular dimensions and the other ones are much coarser *secondary* pores, which behave as normal capillaries. From the aspect of pore size, Kum and Kunin [59] distinguished two principal types of gel structures, which are micro-reticular (micro-porous) and macro-reticular structures. The more uniform repetition of the cross-links in micro-reticular gels produces smaller pores and renders the gel suitable for the separation of smaller molecules. Micro-reticular gels are obtained if the solubility of the starting substances (monomers) and the end product do not differ greatly, and if the cross-links assume the desired gel structure only gradually, for instances, by increasing the number of cross-links between the polymer chains already fixed. On the other hand, the structure of the macro-reticular gel is rather heterogeneous, the spatial distribution of the matrix being uneven. Their large pores render them suitable for the permeation and separation even of macromolecules.

Most macro-reticular gels are aero-gels; in spite of their high porosity, they are resistant to mechanical effects [60].

One of the most common gels is the silica gel; the synonyms are silica hydro-gel and water of silicate glass. This is prepared from sodium meta-silicate solution. The pores are separated by a solid film of about 2×10^{-5} cm thicknesses. The dimensions of pores depend on the concentration of gel material. The effective pore diameter of silica hydro-gel is of the order of 50 - 100 Å. In order to obtain a gel medium of desired pH, a requisite amount of aqueous sodium meta-silicate solution is normally added to the constantly agitated suitable acid of desired concentration. The acidity of the resulting solution determines the course and the rate of polymerization [53].

Agarose, agar, silica and gellan gum (Gellan gum is a high molecular weight polysaccharide gum produced by a pure culture fermentation of a carbohydrate by *Pseudomonas elodea*, purified by recovery with isopropyl alcohol, dried, and milled) have been successfully used as gel materials to obtain protein crystals. The use of an organic solvent-based gel prepared from polyethylene oxide (PEO) and a polyvinyl alcohol hydro-gel for protein crystallization was investigated by Pietras et al [61]. Chandrasekhar [62] has also discussed the crystal growth from PEO gel.

3.5 Gelling Mechanism

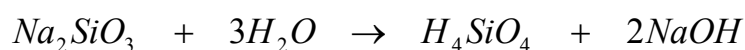
The gelation, i.e. gelling process, can be brought about in many ways, sometimes by the cooling of a sol, by chemical reaction, or by the addition of precipitation agents or incompatible solvents. Gelatin is a good example of a substance, which is readily soluble in hot water and can be gelled by cooling provided that the concentration exceeds about 10%. Formation of gel can be

obtained by the action of two reagents in concentrated solution; preparation of silica gel is an example for this. The process of gelling takes an amount of time, which can vary widely, from minutes to many days, depending on the nature of the materials, its temperature and history [29]. For silica gel, this has been described and documented by Treadwell and Wieland [63]. Silica gel structures depend significantly on the method of preparation. Mechanical properties of fully set gels can vary widely, depending on the density and on the precise conditions during gelling. For the diffusion of reagents through the gel medium, the most important operative parameter is the size of the diffusing particles relative to the pore size in the gel. Another one is the amount of interaction between the solute and internal the gel surfaces. There are varieties of substances, which absorb on silica hydro-gel with particular case [64]. Comparative merits and demerits of gels used for crystal growth are reviewed by Patel and Rao [53].

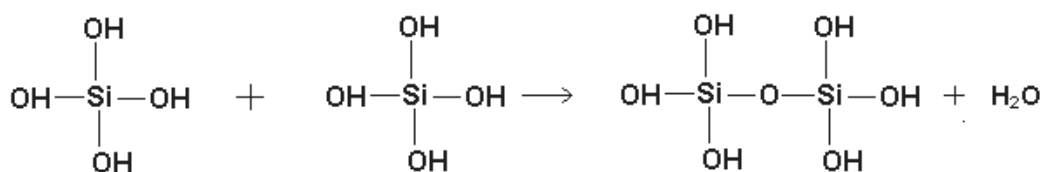
3.6 Structure of Silica Hydro Gel

It is the general observation of the researchers that gels and, in particular, silica gels are the best, very efficient and most versatile media for growing variety of crystals [29, 52, 65-80] and hence silica hydro-gel is the most favorite gel for the crystal growth experiments. Therefore, the study of its gelling mechanism and gel structure carries considerable importance.

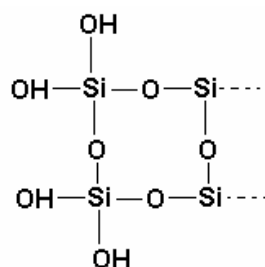
Silica gels are chemical gel because all inter-atomic bonds are covalent. When sodium meta-silicate goes into aqueous solution, mono-silicic acid is produced in accordance with the dynamic equilibrium,



This mono-silicic acid can polymerize with the liberation of water,



This can occur repeatedly and a three dimensional network of Si-O links is established as silica hydro-gel.



As the polymerization process continues, water accumulates on top of the gel surface. This phenomenon is known as *Syneresis*. Much of the water has its origin in the above condensation process, and some may arise from purely mechanical factors connected with a small amount of gel shrinkage. The well-known stability of the silicon-oxygen bonds is responsible for the fact that the polymerization is largely irreversible. It is interesting to note that Kononenko et al [81], studied the characteristics of light scattering in the initial stage of gel formation in silicic acid, which provides valuable information.

The time required for gelation is very sensitive to pH. As the gelation is a gradual process, there is no unique definition for gelation time. It is known that two types of ions are produced during the gelation; H_3SiO_4^- and $\text{H}_2\text{SiO}_4^{2-}$, in relative amount which depends on the hydrogen ion concentration. The latter one, favored by high pH values, is in principle more reactive, but higher charge implies a greater degree of repulsions. The H_3SiO_4^- is favored by moderately low pH values and found to be responsible

for initial formation for long chain polymerization products [82]. Between these chains the cross-linkages are formed in due course and these contribute to the sharp increase of viscosity that signals the onset of gelation. Because of their low mobility, very long chains will cross-link more slowly than short chains. At very low pH values, the tendency towards polymerization is diminished and chain formation is slowed. Gelation time is strongly dependent on temperature [54]. This has been described in detail by Henisch [29].

A weak acid is generally preferred to adjust the pH values, because pH of the set gel changes only slightly with time and, secondly, the mineral acids tend to spoil the growing crystals. It is noteworthy that in less acidic gel solutions the reaction between the acid and sodium meta-silicate occurs with liberation of hydroxyl ions and thus pH of the solution rapidly increases with the process of polymerization, while in highly acidic gel there is no change in pH except due to very little difference in dissociation of acids of different complexities as well as requirements of reaction mechanism. Hence pH has profound influence on the gel structure [69]. Parikh et al [83] reported the effect of gel solution pH on the gel setting time.

Even though crystals can be grown in a variety of gels, the general observation is that silica gel is the best to grow. Better crystallinity of products is the main advantage. It does not need any heating effects. There is no need of additional acid as well as alcoholic substances. Silica gels are irreversible, elastic and resist to deformation. Moreover, silica hydro-gel reduces heterogeneous and secondary nucleations [84]. Also, the gel does not react with crystals grown. It is comparatively cheap.

3.7 Classification of Gel Growth Methods

Crystal growth in gel has been mainly classified into the following five different methods.

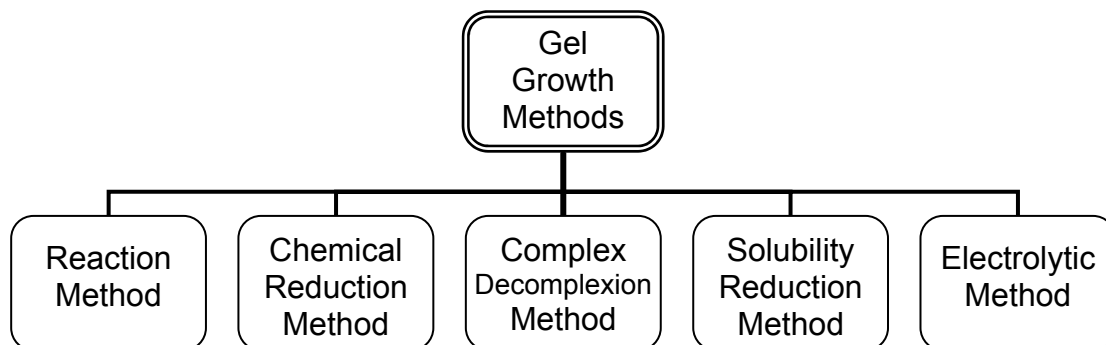
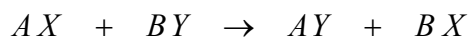


Figure : 3.2 Classification of Gel Growth Methods

3.7.1 Crystal Growth by Reaction

This method is the basis of all methods of gel growth and can be described as crystal growth by chemical reaction. The crystals, which are insoluble or slightly soluble in water and decompose before reaching their melting points, can be conveniently grown by this method. Two basic requirements to grow single crystals by this method are; (i) the reactants used must be soluble in the solvent and the product crystal must be relatively less soluble, and (ii) the gel must remain stable in the presence of the reacting solutions and must not react with these solutions or with the product formed.

Two aqueous solutions of soluble salts are suitably chosen and allowed to diffuse through the gel, so that there can be a slow and controlled segregation of ions and molecules resulting into the precipitation of an insoluble phase as the crystal. The gel affords to limit the number of critical size nuclei and decreases the rate of crystal growth either by controlling the diffusion of reacting ions or by governing the reaction velocity on the surfaces of the growing crystals. Resulting chemical reaction can be expressed as,



Where, A and B are the cations, X and Y are the anions.

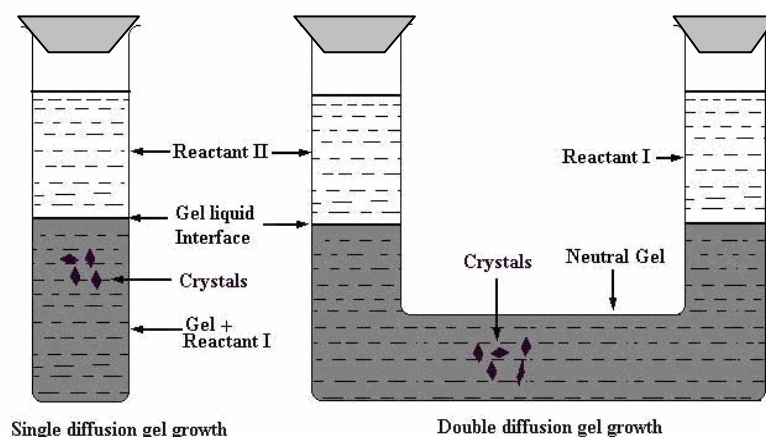


Figure : 3.3 Crystal Growth by Chemical Reaction

This can be achieved by the test tube technique, in which one of the reactants is incorporated in the gel and the other reactant is diffused into it, or by the U-tube technique as shown in Figure 3.3, or its modification in which the two reactants are allowed to react by diffusion into an essentially inactive gel.

There is a variety of crystallization apparatus employed to grow single crystals by this method. The disadvantages of these crystallization apparatus are the depletion of one of the reactants which is inside the gel, the incorporation of reaction waste products by the growing crystals, supporting, handling and cleaning of the apparatus and gel preparation inside the horizontal tube open at both the ends [29].

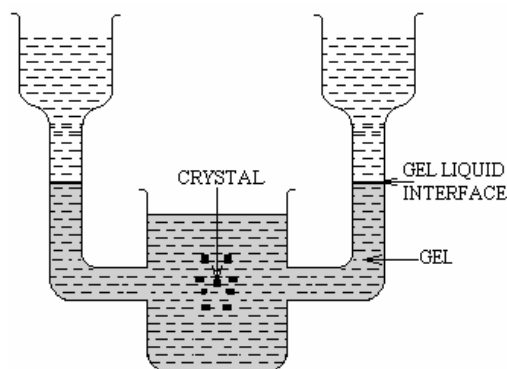


Figure : 3.4 Modified Crystal Growth by Chemical Reaction

An improved design of gel technique used by Patel and Rao [53] is depicted in Figure 3.4, which eliminates all the inconveniences of the previous gel growth techniques and it permits the growth of mixed and doped crystals by multiple diffusion. Several metallic crystals like gold, lead, copper etc. have been grown by this method.

3.7.2 Chemical Reduction Method

This method is suitable for growing only metal crystals from gel media. Hatschek and Simons [85] were the first to report the growth of gold crystals by adding 8 % oxalic acid solution over a set gel containing gold chloride solution. By this particular method crystals of Nickel, Cobalt [86], Selenium, Lead and Copper have been obtained.

3.7.3 Complex Decomplexion Method

This method requires first forming a chemical complex of the material of the crystals to be grown with aqueous solutions of some suitable substance, called complexing agent, in which the former is homogeneously mixable and then providing externally a condition conducive to de-complexing or dissociation of the complex formed. A standard procedure adopted for decomplexion is to increase the dilution steadily, while complex solution is diffused through the gel. Crystal growth by this method was first attempted by O' Connor et al [87] for the growth of cupric halide crystals.

3.7.4 Solubility Reduction Method

This method is applicable to grow single crystals of highly water-soluble substances. The growth of ammonium dihydrogen phosphate (ADP) single crystals by this method has been first reported by Gloker and Soest [88].

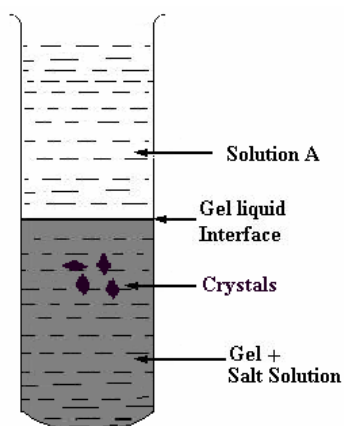


Figure : 3.5 Crystal Growth by Solubility Reduction Method

In this method, the substance to be grown is dissolved in water and is incorporated with the gel forming solution. Then a solution, which reduces the solubility of the substance, is added over the set gel to induce crystallization as in Figure 3.5. For instance, potassium dihydrogen phosphate (KDP) crystals have been grown by adding ethyl alcohol over the gel containing a saturated solution of KDP [89]. Crystals are grown due to the reduction of solubility of KDP in the liquid phase by the diffusing alcohol.

3.7.5 Electrolytic Method

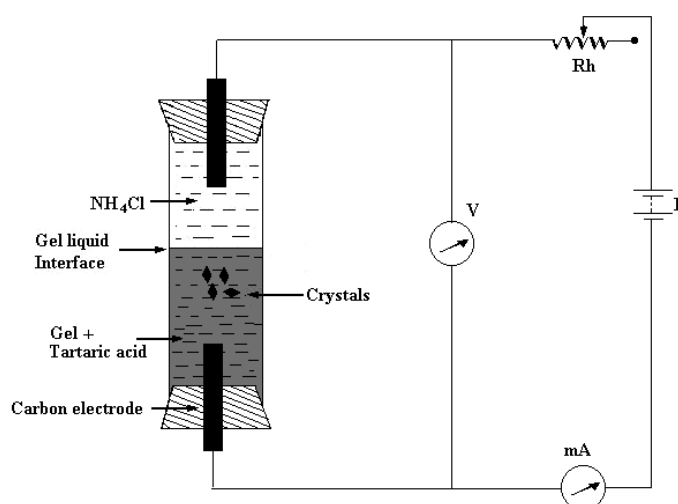


Figure : 3.6 Crystal Growth by Electrolytic Method

The electrolytic method can also be used for the growth of metallic crystals by selecting the gel medium for controlled growth. For this a very low

d.c. electric current, usually of the order of 2-10 mA, is passed through a silica gel charged with suitable acid or electrolytic solution. Details are given in Figure 3.6.

It has been found that the pH of the gel medium, the concentration of the supernatant solution, the current density and the material used as electrode, have considerable influence on the habit of the crystals grown. Muzikar et al [90] have demonstrated the growth of single microcrystals of gold by electrochemical growth in a silica gel. Mohanan Pillai et al [91] grew lead dendrites, while George and Vaidyan [92] grew copper dendrites and silver dendrites and single crystals [93] using the electrolytic technique.

3.8 Growth Mechanism

As silica gels are neither liquid nor solid in nature, there are only a few methods available for quantitative investigations. From the SEM observations of dried silica gels, it has been found that the gel consists of sheet like structures of varying degrees of surface roughness and porosity, forming interconnected cells. Generally, the cell walls are curved. It has been estimated from the SEM images that the cell walls in dense gels (0.4 M Na₂SiO₃) have pores from 0.1μ to 0.5μ and 0.1μ to 4μ in low density (0.2 M Na₂SiO₃) gels. The cell walls are thicker in dense gels. During gelling the pH has a profound influence on the gel structure, changes from a distinctly box like network to a structure consisting of loosely bound platelets which appear to lack cross- linkages and the cellular nature becoming less distinct [94].

In the absence of convection, the only mechanism available for the supply of solute to the growing crystal is diffusion. One may envisage that the solute super-saturation ϕ_{∞} at large distances from the crystal remains

unchanged during growth. However, at the crystal surface ϕ would initially have the same value but would then adjust itself in the course of growth to the lower value ϕ_0 . Hence this is determined by the dynamics of the growth processes.

For different idealized geometries, Frank [95] has developed equations, which give a description of diffusion controlled growth rates. The growth rates calculated by Frank involve the “reduced radius” (S) which for spherical system is defined as $r / (D t)^{1/2}$, where ‘ r ’ is the radius of the crystal, ‘ D ’ is the diffusion constant and ‘ t ’ is the time. The theory presents a simple relation,

$$\phi_{\infty} - \phi_0 = F(S)$$

By measuring ‘ S ’ and knowing the function ‘ F ’ the value of ϕ_0 at any time could be determined. As long as ‘ D ’ does not alter, a constant value of ‘ S ’ implies a constant value of ϕ_0 . The constancy of ‘ S ’ can be checked by plotting r^2 versus t .

However, some limitations exist; one arising from the initial transient period during which steady-state concentration is established, and one arising from exhaustion of available solute. Both factors must be expected to give rise to nonlinearity. In general, there remains substantial uncertainty as to the effect of which the disruption of the gel structure has on the local value of ‘ D ’. This also applies to the effect of pH changes, which occurs during growth. This has been described for various crystals grown in detail by Henisch [29].

Cipanov et al [96] have developed a mathematical model of crystal growth process in gels. Calculations suggest that there is a locality in a gel that provides the best condition for nucleation and growth of crystals. They have compared the model with experimental results. Moreover, theoretical

aspects of the crystal growth in gel medium have been proposed by Desai and Hanchinal [97].

In growth systems, which depend on the diffusion of the reactant through a gel incorporating the other reagent, it has been found that the growth rate is more near the gel solution interface where the concentration gradients are high and away from the interface, the gradients are relatively low. Dislocation density is also different corresponding to the different growth rates. This further suggests that the growth rate itself determines the number of defects grown into the crystal even in the absence of foreign impurities. Occasionally, crystals grown in gels are found to have dislocation densities less than $10^3/\text{cm}^2$. The high degree of perfection of these crystals has been demonstrated by many authors [98,99].

In general, crystals growing in gel either displace the gel as they grow [68] or incorporate [100]. In the case of gel displacing, cusp will be formed around the growing crystals, whereas in the other case, since the crystals incorporate the gel as they grow, final crystals turn turbid instead of being transparent. The cusps like cavities are the regions in which the gel has been split and separated from the growing faces.

In the case of crystals growing in fissures in the gel, a clear boundary between opaque crystal growth in the gel and clear crystal growth in the solution can be seen [101]. In general, the progressive deterioration of crystal quality indicates an increasing incorporation of gel in the passage of time, which eventually leads to the destruction of the perfect facets observed on small crystals.

3.9 Nucleation Control

Nucleation is an important phenomenon in crystal growth and is the precursor of the overall crystallization process. Nucleation is the initiation of a phase change in a small region, such as the formation of a solid crystal from a liquid solution. Even though gel helps in suppressing nucleation, crystals growing in a gel system compete with one another for the solute atoms. This competition limits their size and perfection. It is therefore desirable to suppress nucleation so that only a few crystals are formed. Patel and Rao [53] have described some methods which control nucleation in gel to some extent, those are as follows:

3.9.1 Using Suitable Reactants

Out of various combinations of reactants, which can be used to obtain the required product crystals, only a few are found to be suitable to achieve controlled nucleation. For example, in the case of growth of potassium perchlorate crystals, various reactants were used, however, a combination of potassium chloride and perchloric acid has been found to be suitable for reducing the nucleation density. Reports of many authors confirm the importance of using suitable reactants [98, 102-105].

3.9.2 Using Gels Prepared With Various Acids

After the selection of the best combination of reactants, with particular acid set gel, it is necessary to use the same reactants with various acid set gels in order to reduce the nucleation density and grow larger crystals. Good quality neodymium carbonate crystals have been grown in hydrochloric acid set gels [106]. Moreover, for the growth of potassium perchlorate crystals, Patel and Rao [98] used four mineral acids, namely, perchloric acid,

hydrochloric acid, sulphuric acid and nitric acid; and four organic acids, namely, citric acid, tartaric acid, acetic acid and propionic acid, to set the gel and found the perchloric acid set gel gave the best results.

3.9.3 Changing the Gel Structure

It is possible to change the gel structure and reduce the nucleation density by changing the gel pH [106], gel density and gel ageing [69]. Generally, increasing gel density and gel pH decrease the nucleation density to a certain extent but the final crystals are of poor quality. On the other hand, the gel ageing reduces the nucleation density and hence the total number of crystals without affecting their quality. The decrease of nucleation centers at higher densities of gel as well as the gel aged for longer periods is due to the fact that these two parameters reduce the cell size and consequently the rate of diffusion of ions. The decrease in nucleation density at higher pH values may be due to the improper formation of gel cells [69].

3.9.4 Using Intermediate Neutral Gel

In this method, first the gel is prepared in the usual way containing one of the reactants in the bottom of a test tube. A second gel called the intermediate neutral gel or the reaction gel is formed over the first gel, and the second reactant is then poured over it. The neutral gel will slow down the reaction between the reactants and hence reduce the number of nuclei. This method was used to grow single crystal like cuprous oxide - $\{Cu_2O\}$ [65], calcium carbonate - $\{CaCO_3\}$ [66], neodymium carbonate - $\{Nd_2(CO_3)_3 \cdot nH_2O\}$ and calcium tungstate - $\{CaWO_4\}$ crystals [106]. It has been found that the nucleation density decrease with the height of the intermediate gel [65, 69].

3.9.5 Concentration Programming

In this technique, the concentration of the diffusing reactant is initially kept below the level at which nucleation is known to occur and is then increased gradually in small steps. With very dilute reactants the amount of material diffused through the gel is small and hence smaller is the supersaturation rate. Under these circumstances, a few nuclei are formed. As the concentration is increased further the growth of the existing nuclei is preferred to the formation of additional ones. Crystals grown by this method are more perfect and larger than those grown otherwise. This method has been successfully applied for the growth of many crystals [29,69,100].

3.10 Crystal Habit

Crystals with various habits are important both commercially and also in studying their physical properties. In gel growth, crystals with various habits can be grown by changing concentration of feed solutions, crystallization temperature, adding impurities and using various types of gels. Moreover, in some cases various habits in different regions of gel are also observed.

The habit modification can be obtained by changing concentration of the feed solution. McCauley and Gehrhardt [106] observed that during the growth of neodymium carbonate, a sodium carbonate incorporated gel enhanced the formation of dendrites and spherulites, while a neodymium chloride incorporated gel favored the growth of rhombic plates. Also, Bandhopadhyay and De [102] found that as the strength of feed solution was increased from 0.2 to 0.3 M, the calcium carbonate crystals were of rhombohedral habit and for 0.4 to 0.6 M concentrations the crystals were with the edges having wavy and ripple like features. On further increasing the

strength of feed solution to 1 M or more, a large number of nucleation centers with dendritic growth were observed.

The temperature of the growth has pronounced effect on habit of crystals. For example, in the case of strontium sulphate, all crystals grown at about 35°C exhibited {011} and {102} as their habit faces, whereas the crystals grown at about 20°C developed {022} habit faces in addition to {011} and {102} faces [100]. The habit modification can be observed for various gel structures. Mc Cauley and Roy [66] investigated the growth of calcite crystals and found that the decrease in pH of the gel turned spherulites (pH 10.5) into feathery polycrystalline aggregates (pH 9 to 10.5) and, ultimately, into single crystals of rhombic habits (pH 7 to 9).

Alike to 'solution growth', it is possible to change the crystal habit by adding impurities in the gel growth also. Various habits of calcite were obtained by adding impurities of magnesium, strontium, nickel and barium in different proportions during the growth of these crystals [100]. A similar study was carried out by Rosmalen et al [107] on gypsum crystals.

However, the habit modification is observed by using various types of gels for crystal growth. A comparison of crystals of calcium sulphate dihydrate grown in two different gel media, i.e., sodium silicate gel and bentonite clay gel, showed that the two media clearly affect the crystal habit and surface topography [108].

Interestingly, various crystal habits have been observed at different regions of gel. For lead molybdate growth, there were different regions inside the gel, where lead molybdate crystals of different habits were grown. Near lead nitrate solute, i.e. at the gel-liquid interface, polyhedral pyramidal crystals

were formed. Altogether, octahedral bi-pyramidal crystals and platelets were observed in the central region and near the ammonium molybdate solution, respectively [109]. Nucleation of crystals in gel is also influenced by light [52,110]. Calcium tartrate crystals were observed to have grown more perfectly with irradiation of the gel than in darkness, but copper chloride crystals grown from gel had an adverse effect [111].

3.11 Liesegang Rings

Chemical reactions leading to the formation of precipitates in gels are ideal in sense that the particles of precipitates remain where they are produced and the reagent reach each other only by diffusion. This study is very important, because the chemical reactions in biological media, whether leaving or dead, and in many geological structures are of this type. The diffusion of a soluble substance from an aqueous solution into gel follows the ordinary Fick's diffusion law.

The main feature of chemical reactions is that the diffusion of one reagent into the other contained in the gel produces not only the ordinary chemical change, but also definite mechanical structure. This structure varies with conditions and can be controlled.

Hedges [112] has identified the following four types of structures produced by chemical reaction in gels.

- (i) Precipitates of continuous structure, which consists of small particles uniformly distributed so that the whole mass appears homogeneous.
- (ii) Discrete structures consist of particles of relatively large size, separated by considerable spaces and may contain well-formed crystals.

(iii) Cellular structures comprise of a network of honey-comb like cells of precipitates enclosing clear gel, frequently obtained with a large number of a precipitate.

(iv) Periodic structures contain definite bands or rings of precipitants separated by clear spaces, which often contain the precipitate as discrete structures [113].

The first interesting study of a periodic structure was made by Liesegang in 1896 [39,40]. He covered a glass plate with a layer of gelatin impregnated with potassium chromate and added a small drop of silver nitrate. As a result, silver chromate was precipitated in the form of a series of concentric rings; well develop with regularly varying spacing. These types of fascinating formations are called as *Liesegang rings*.

Several workers have observed that, in many cases, the space between the rings contains a considerable amount of precipitate. Often the rings contain a large number of small particles and the intervening spaces contain a small number of large particles. Hatschek [114] had reported very interesting case of a cadmium sulphide precipitates in silicic acid gel, where the precipitates consisted of alternate pink and yellow bands with the difference in the size of particles. Dhar and Chatterji [115] had recognized that a layer of precipitates was followed by a clear zone in some structures and by a zone of differently dispersed precipitates in others.

Generally, the distance between successive bands of Liesegang rings increases as the diffusion proceeds further. Schleussner [116] had found the spacing to confirm with the geometric series and this conclusion had been confirmed by several other investigators [117,118]. However, a different

nature was observed by Davis [119], when mercurous nitrate was allowed to diffuse into agar gel containing sodium formate, the distance between successive bands was found to decrease. Generally, two types of Liesegang rings have been reported in literature [120]; they are *direct type* and *revert type*. In the direct type, the spacing between successive rings increases with increase in the order of the ring from the gel boundary. Gnanam et al [121] have reported the direct type Liesegang rings of calcite. In contrast to this, the revert type Liesegang rings exhibit the spacing between successive rings decreasing as the order of ring increases from the gel boundary. As shown in Figure 3.7 many parameters may affect the formation of Liesegang rings [113].

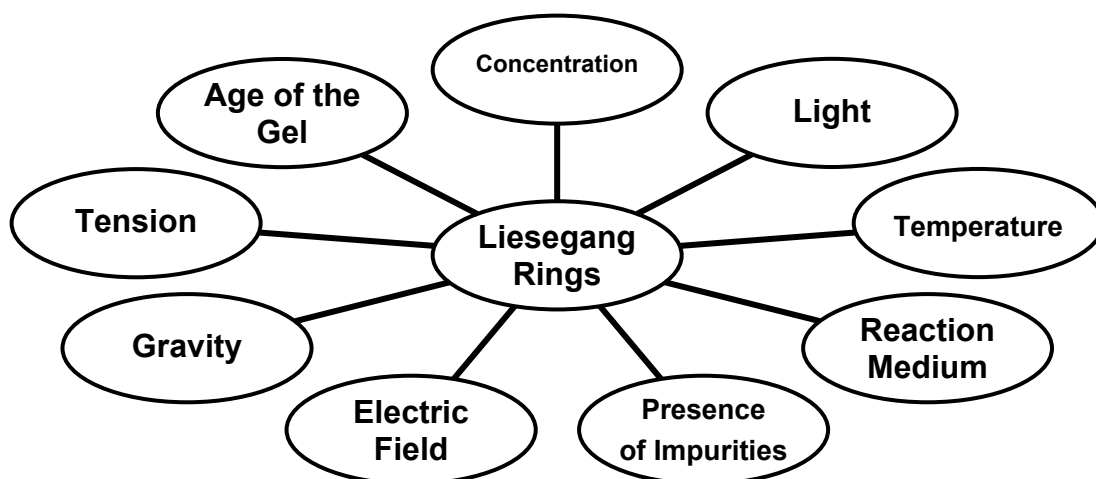


Figure : 3.7 Parameters Affecting the Formation of Liesegang Rings

Many authors have attempted to give explanations of the formation of Liesegang rings by different models, theories and computer simulations. Henisch and Gracia-Ruiz [122] suggested a numerical method to obtain the formation of Liesegang rings. In other study, Henisch and Gracia-Ruiz [123] extended the condition under which two diffusing reagents could form precipitates either continuous or periodic in a gel media. Moreover, several

other theories and models have been suggested by different workers [124-126]. Apart from this, some computer simulation experiments also have been carried out. Bueki et al [127] studied regular Liesegang structure by means of computer simulation. Joseph and Joshi [128] reported the effect of different parameters, for instance, the gel pH, the concentration of reactants, the height of the column of supernatant solutions, on the Liesegang ring formation during the growth of brushite crystals.

3.12 Crystals Grown by Gel Method

Among the various crystallization techniques, crystallization in gels has found wide applications in the fields of biomineralization and macromolecular crystallization in addition to crystallizing materials having nonlinear optical, ferroelectric, ferromagnetic, and other properties. Furthermore, by using this method it is possible to grow single crystals with very high perfection that are difficult to grow by other techniques [78]. The use of gels as growth media has previously been reported in the literature for a wide range of compounds, including both inorganic [29,71,129,130] and organic compounds [131,132] and also proteins [132]. Numerous workers have grown various crystals by the gel growth technique. In the present author's laboratory, his predecessors [33-36,133] have made detailed survey of various crystals grown by the gel techniques, therefore, due to the page constraints, the detailed survey has been avoided here and the concentration is focused on crystal growth of some important biomaterial and particularly urinary type crystals.

Gel is an ideal medium to grow biological crystals since its structure is similar to the mucus in the living organisms. The internal surface of the organs in animals is usually covered with mucus membrane. So, the gel method has

been applied to the study the bio-mineralization, i.e., crystal formation in human body. Most of the phosphate crystals are insoluble in water and decompose before melting. Hence single crystals of such types of compounds can not be grown by either slow evaporation or melt method, but can be conveniently grown by gel method. Gel media prevent convection and crystal sedimentation, and provide an attractive growth environment for optimizing biological crystals.

Nowadays, this method has applied to the study the crystal formation of cholesterol crystals [134-137]. Moreover, the crystallization of biological macromolecules of proteins like thaumatin, pyruvate kinase, lysozyme etc and t-RNA by Cudney et al [80] using silica gel. Biertumpfel et al [138] reported crystallization of some RNA binding proteins using agarose gel. Where as, Lorber et al [139] reported the crystallization of biological macromolecules like proteins and nucleic acids using both the silica and agarose gel. The gel growth technique has been used for several years not only for crystals of small molecules, but also for crystals of proteins [84], for which it is particularly useful since these crystals are often difficult to grow.

The gel method is suitable to mimic the growth of urinary crystals *in vitro*. A urinary stone, however, grows in a continuous flow of urine, i.e., in a dynamic medium. The nutrients for the growth are supplied continuously. The growth of urinary stones can be simulated by a simplified gel based model, where the nutrients are supplied continuously through diffusion in a gel. Notwithstanding, the gel based model is a static model unlike the urinary system, but provides excellent opportunity to grow urinary type crystals and

monitor their growth continuously. The present author has chosen the gel growth technique for the growth of crystals.

Since, the gel method of crystallization provides an ideal and most versatile technique to study crystal deposition diseases, which could lead to better understanding of their etiology, quite significant work has been reported on different kinds of urinary crystals such as, calcium oxalate monohydrate (COM) [140-147], Brushite [73,142,148-153], uric acid crystals [154], hydroxyapatite crystals [155]. Recently, Kanchana and Sekar [156] reported the influence of sodium fluoride on synthesis of hydroxyapatite by the gel method, while Sivakumar et al [157] reported the effect of magnesium on the formation of hydroxyapatite in the silica gel medium.

Recently, a modified gel growth technique has been proposed for the micro-crystal growth and in situ observations, which has been successfully tested for calcium hydrogen phosphate dihydrate micro-crystal growth inhibition in the presence of citric acid [158]. Kanchana et al [159] reported the growth of strontium chromium magnesium hydrogen phosphate (SrCrMHP) crystal in silica gel medium in different growth environments.

However, very few attempts were made to grow struvite crystals by gel method [153,160,161]. The growth of struvite crystals by gel method is explained in chapter V.

3.13 Advantages and Limitations of Gel Growth Technique

The advantages of gel growth technique are as follows:

- As gel growth technique is extremely simple and inexpensive, good quality crystals can be grown even in small laboratories, which do not possess sophisticated instrument.

- By carefully selecting the gel density, pH of the reactants and concentration of the reactants, good quality single crystals with high degree of perfection can be grown at room temperatures.
- Since the crystals are grown at or near room temperature, thermal strains are absent in the gel method.
- Thermodynamic consideration reveals that as the growth proceeds at ambient temperature, the grown crystals would contain relatively less concentration of equilibrium defects.
- Crystals can be observed practically in all stages of their growth.
- The gel framework, which is chemically inert and harmless, acts like a three dimensional crucible in which the crystal nuclei are delicately held in the position of their formation and growth, thereby preventing damage, if any, due to impact with either the bottom or the walls of the container.
- The effects of precipitation are eliminated as all nuclei are spatially separated.
- Growth of crystals with different morphologies is commonly found in bio-mineralization. By changing the growth conditions, crystals with different morphologies and sizes can be obtained.
- Gel medium considerably prevents convection currents and turbulence.
- Gel is soft and it yields a suitable environment for growing crystals.
- Gel matrix suppresses nucleation, reduces the rate of growth, and generally leads to comparatively larger (than that are formed by a similar reaction in water or in molten stage by double decomposition process), higher-quality crystals of enhanced stability.
- Crystallization in gel media also prevents crystal sedimentation.

- The purity of most crystals produced by this method is quite high; crystals generally contain only a few parts per million (atomic) of impurity.
- The growth of single crystals in gel is a self-purifying process, free from thermal strains, which is common in crystals grown from melt.
- The gel method is capable of yielding crystals of high optical perfection and wide range of morphology.
- Gels also provide an efficient protection of samples during handling and transport without affecting their crystallographic analysis.
- The gelation structure provides an ideal medium for the diffusion of reacting ions and can be used to keep the reacting ions separated until reaction is desired. Concentration of the reactants can be easily varied.
- Crystals are suspended in the gel network so that they do not form sediments and can grow free from strain exerted by the container.
- Heterogeneous and secondary nucleations are reduced in the presence of a silica hydro-gel. Silica hydro-gel is compatible with a wide range of salts, polymers, organic solvents, and buffers used for macromolecular crystallization in a pH range from 3 to 10.
- The grown crystals can be harvested easily without damaging the crystals.

Notwithstanding, the above advantages, the gel method has following limitations also:

- Growth period is usually very long.
- Crystal size is generally small, so large crystals cannot be grown.
- When silica gel is used, gel inclusion occurs in some crystals.
- The chance of lattice contamination by impurities from the gel itself is profusely increased.

References

1. D. Elwell, H. J. Scheel, "*Crystal Growth from High-Temperature Solutions*", Academic Press, London (1975).
2. H. J. Scheel, "*Historical Introduction*", in "*Handbook of Crystal Growth*", Ed. D. T. J. Hurle, Vol. 1 Elsevier, Amsterdam (1993).
3. H. J. Scheel, *J. Cryst Growth.*, **211** (2000) 1.
4. H. J. Scheel, "*The Development of Crystal Growth Technology*", in "*Crystal Growth Technology*", Eds. H. J. Scheel, T. Fukuda, John Wiley & Sons Ltd., Chichester (2003).
5. B. R. Pamplin, "*Crystal Growth*", Pergamon Press, Oxford (1975).
6. C. S. Barrat, T. B. Massalski, "*Structure of Metals*", McGraw-Hills, 3rd edn., New York (1966).
7. J. J. Gilman, "*The Art and Science of Growing Crystals*", John Wiley, New York (1963).
8. R. A. Laudise, "*Techniques of Crystal Growth*", in "*Proc. Int. Conf. Cryst. Growth*", Boston, Pergamon Press, Oxford (1966).
9. R. A. Laudise, "*Crystal Growth and Characterization*", in "*Proc. ISSCG-2*", Eds. R. Ueda, J. B. Mullin, North-Holland Pub. Co., Amsterdam (1975).
10. M. Schieber, "*Introductory Remarks in Techniques of Crystal Growth*" in "*Proc. Int. Conf. Crystal Growth*", Boston, Pergamon Press, Oxford (1966).
11. J. A. James, R. C. Kell, "*Crystal Growth*", Ed. B. R. Pamplin, Pergamon Press, Oxford (1975).
12. K. A. Jackson, In "*Growth and Perfection of Crystals*", Eds. R. H. Doremus, B. W. Roberts, D. Turnbull, Wiley, New York (1958).
13. W. A. Tiller, *Acta. Met.*, **5** (1957) 565.

14. J. P. Van Der Eerden, "*Lecture Notes on Fundamentals of Crystal Growth*", World Scientific Publishing, Singapore (1993).
15. P. S. Raghavan, P. Ramasamy, "*Crystal growth Process and Methods*", KRU Publication, Kumbhakonam (2000).
16. B. Chalmers, "*Principles of Solidification*", John Wiley, New York (1964).
17. N. Bardsley, D. Hurle, J. B. Mullin, "*Crystal Growth : A Tutorial Approach*", North-Holland Series in Crystal Growth, Vol. 2, Amstredam (1979).
18. A. V. Shubnikov, A. A. Chernov, N. N. Sheftall, "*Growth of Crystals*", Kluwer Academic Publishers, Dordrecht (1979).
19. A. Majchrowski, "*Single Crystal Growth, Characterization and Applications*", Ed. J. Zielinski, SPIE-International Society for Optical Engineering, Bellingham (1999).
20. K. Byrappa, T. Ohachi (Eds), "*Crystal Growth Technology*", William Andrew Inc., New York (2003).
21. D. T. J. Hurle, "*Handbook of Crystal Growth*", Vol. 1 to 3, Elsevier Science, Amsterdam (1994).
22. T. Nishinaga, K. Nishioka, J. Harada, A. Sasaki, H. Takei, "*Advances in Understanding of Crystal Growth Mechanism*", Elsevier, Amsterdam(1997).
23. A. Holden, P. S. Morison, "*Crystal and Crystals Growing*", MIT Press, Cambridge (1982).
24. J. Stangl, J. Stang, "*Crystals and Crystal Gardens You Can Grow*", The Horn Book Inc., Boston (1990).
25. J. C. Brice, "*Crystal Growth Process*" John Wiley, New York, (1986).
26. A. A. Chernov, "*Modem Crystallography III- Crystal Growth*", Vol. 36, Springer-Verlag, Solid State Series, Berlin (1984).

27. M. M. Faktor, I. Garrett, "Growth of Crystals from Vapour", Chapman and Hall, London (1974).
28. J. C. Brice, "The Growth of Crystals from Liquids", North Holland Publishing Company, Amsterdam (1973).
29. H. K. Henisch, "Crystals in Gels and Liesegang Rings", Cambridge Uni. Press, Cambridge (1988).
30. H. E. Buckley, "Crystal Growth", John Wiley, New York (1951).
31. N. Mirkin, A. Moreno, *J. Mex. Chem. Soc.*, **49** (2005) 39.
32. G. Dhanaraj, K. Byrappa, V. Prasad, M. Dudley, "Hand book of Crystal Growth", Springer, Heidelberg (2010).
33. V. S. Joshi, *Ph.D. Thesis*, Saurashtra University, Rajkot (2001).
34. R. M. Dabhi, *Ph.D. Thesis*, Saurashtra University, Rajkot (2002).
35. B. B. Parekh, *Ph.D. Thesis*, Saurashtra University, Rajkot (2005).
36. S. R. Suthar, *Ph.D. Thesis*, Saurashtra University, Rajkot (2007).
37. D. J. Dave, *Ph.D. Thesis*, Saurashtra University, Rajkot (2011).
38. K. D. Parikh, *Ph.D. Thesis*, Saurashtra University, Rajkot (2011).
39. R. E. Liesegang, *Naturwiss. Wochenschr.*, **11** (1896) 353.
40. R. E. Liesegang, *Phot. Archiv.*, **21** (1896) 221.
41. R. E. Liesegang, *Z. Phys. Chem.*, **23** (1897) 365.
42. W. Z. Ostwald, *Phy. Chem.*, **27** (1897) 365.
43. Lord Rayleigh, *Phil. Mag.*, **38** (1919) 738.
44. H. W. Morse, G. W. Pierce, *Z. Phy. Chem.*, **45** (1903) 589.
45. H. N. Holmes, *J. Phy. Chem.*, **21** (1917) 709.
46. E. Hatschek, *Brit. Assoc. Reports.*, **1919** (1919) 23.
47. H. A. Fells, J. B. Firth, *Proc. Roy. Soc. London*, **112A** (1926) 468.

48. D. J. Lloyd, "The Problem of Gel Structure", in "Colloid Chemistry: Theoretical and Applied"; Ed. J. Alexander, Vol. 1, The Chemical Catalog Co., New York (1926).
49. L. W. Fisher, F. L. Simons, *Am. Mineral.*, **11** (1926) 124.
50. L. W. Fisher, F. L. Simons, *Am. Mineral.*, **11** (1926) 200.
51. L. W. Fisher, *Am. J. Sci.*, **15** (1928) 39.
52. H. K. Henisch, J. Dennis, J. I. Hanoka, *J. Phys. Chem. Solids.*, **26** (1965) 493.
53. A. R. Patel, A. V. Rao, *Bull. Mater. Sci.*, **4** (1982) 527.
54. A. E. Alexander, P. Johnson, *Colloid Science*, Vol. 2, Clarendon Press, Oxford (1949).
55. S. Sahoo, N. Kumar, C. Bhattacharya, S. S. Sagiri, K. Jain, K. Pal, S. S. Ray, B. Nayak, *Des. Monomers Polym.*, **14** (2011) 95
56. R. G. Jones, *Pure Appl. Chem.*, **79** (2007) 1801.
57. V. Caslavaska, P. Gron, *Caries Res.*, **18** (1984) 354.
58. M. Z. Biltz, *Phys. Chem.*, **126** (1927) 356.
59. K. A. Kum, R. Kunin, *J. Polymer Sci.*, **132** (1964) 587.
60. T. Kremmer, L. Bross, "Gel Chromatography Theory, Methodology, Applications", John Willey & Sons, New York (1979).
61. Z. Pietras, H. T. Lin, S. Surade, B. Luisi, O. Slattery, K. M. Pos, A. Moreno, *J. Appl. Cryst.*, **43** (2010) 58.
62. R. Chandrasekhar, *J. Mater. Sci. Lett.*, **19** (2000) 1801.
63. W. D. Treadwell, W. Wieland, *Helv. Chem. Acta*, **13** (1930) 856.
64. K. K. Muller, *Dissertation*, Technische Hochschule, Stuttgart (1939).
65. Z. Blank, W. Brenner, *Nature*, **222** (1969) 79.
66. J. W. McCauley, R. Roy, *Am. Miner.*, **59** (1974) 947.

67. A. R. Patel, S. K. Arora, *J. Mater. Sci*, **11** (1976) 843.
68. A. R. Patel, A. V. Rao, *J. Cryst. Growth*, **38** (1977) 288.
69. A. R. Patel, A. V. Rao, *J. Cryst. Growth.*, **43** (1978) 351.
70. T. Shripathi, H. L. Bhat, P. S. Narayanan, *J. Mater. Sci.*, **15** (1980) 3095.
71. A. F. Armington, J. J. O'Connor, "Crystal Growth in Gels", in "Inorganic Synthesis" Ed. D. H. Busch, Vol. XX, John Wiley, New York, (1980).
72. S. Bhat, P. N. Kotru, *Mater. Sci. Eng.*, **B23** (1994) 73.
73. V. S. Joshi, M. J. Joshi, *Cryst. Res. Technol.*, **38** (2003) 817.
74. E. Ramachandran, S. Natarajan, *Indian J. Pure Appl. Phys.*, **43** (2005) 372.
75. N. Ajeetha, *Bulg. J. Phys.*, **34** (2007) 108.
76. B. Parekh, P. Vyas, S. Vasant, M. J. Joshi, *Bull. Mater. Sci.*, **31** (2008) 143.
77. S. L. Garud, K. B. Saraf, *Bull. Mater. Sci.*, **31** (2008) 639.
78. S. N. Kalkura, S. Natarajan, "Crystallization from Gels" in "Springer Handbook of Crystal Growth" Eds. G. Dhanaraj, K. Byrappa, V. Prasad, M. Dudley, Springer-Verlag, Berlin Heidelberg (2010).
79. D. K. Sawant, H. M. Patil, D. S. Bhavsar, J. H. Patil, K. D. Girase, *Arch. Phys. Res.*, **2** (2011) 67.
80. B. Cudney, S. Patel, A. McPherson, *Acta Cryst.*, **D50** (1994) 479.
81. V. Kononenko, S. Kontovovich, E. Shechukin, *Colloid J.*, **39** (1977) 497.
82. C. J. Plank, *J. Colloid Sci.*, **2** (1947) 413.
83. K. D. Parikh, B. B. Parekh, D. J. Dave, M. J. Joshi, *Indian J. Phys.*, **80** (2006) 719.
84. M. C. Robert, K. Provost, F. Lefauchaux, In "Crystallization of Nucleic Acids and Proteins, a Practical Approach", Eds. A. Ducruix, R. Giege Oxford University Press, Oxford (1992).

85. E. Hatschek, Simon, *Kolloid Z.*, **10** (1912) 265.
86. P. F. Kurz, *Ohio J. Sci.*, **66** (1966) 349.
87. J. J. O'Connor, M. Dipietro, A. Armington, B. Rubin, *Nature*, **212** (1968) 68.
88. D. A. Glocker, I. F. Soest, *J. Chem. Phys.*, **51** (1969) 3143.
89. B. Brezina, J. Havrankova, *Mater. Res. Bull.*, **87** (1971) 537.
90. M. Muzikar, V. Komanicky, W. Fawcett, *J. Cryst. Growth*, **290** (2006) 615.
91. K. M. Pillai, M. Ittyachen, V. Vaidyan, *Natl. Acad. Sci. Lett.*, **3** (1980) 37.
92. M. T. George, V. K. Vaidyan, *Cryst. Res. Technol.*, **15** (1980) 653.
93. M. T. George, V. K. Vaidyan, *J. Cryst. Growth*, **53** (1981) 300.
94. E. S. Halberstadt, H. K. Henisch, H. J. Nickl, E. W. White; *J. Colloid Interface Sci.*, **29** (1969) 469.
95. F. C. Frank, *Proc. Roy. Soc.*, **201A** (1950) 586.
96. A. V. Cipanov, L. L. Goshka, S. I. Kolosov, V. P. Ruzov, *Cryst. Res. Technol.*, **25** (1990) 119.
97. C. C. Desai, A. N. Hanchinal, *Cryst. Res. Technol.*, **22** (1987) 1117.
98. A. R. Patel, A. V. Rao, *J. Cryst. Growth*, **47** (1979) 213.
99. J. J. O'Connor, A. F. Armington, *Mater. Res. Bull.*, **6** (1971) 765.
100. A. R. Patel, H. L. Bhatt, *J. Cryst. Growth*, **18** (1973) 288.
101. H. J. Nickl, H. K. Henisch, *J. Electrochem. Soc.*, **116** (1969) 1258.
102. T. Bandyopadhyay, A. De, *Indian J. Earth Sci.*, **4** (1977) 95.
103. M. Shiojiri, C. Kaito, Y. Saito, M. Murakami, J. Kawamoto, *J. Cryst. Growth*, **43** (1978) 61.
104. Z. Blank, W. Brenner, Y. Okamoto, *Mater. Res. Bull.*, **3** (1968) 555.
105. Z. Blank, W. Brenner, *J. Cryst. Growth*, **11** (1971) 255.

106. J. W. McCauley, H. M. Gehrhardt, Report, Army Mater and Mech. Res. Center TR-70-13 (AD-710236), (1970) 25.
107. G. Rosmalen, W. Marchee, P. Bennema, *J. Cryst. Growth.*, **35** (1976)169.
108. R. D. Cody, H. R. Shanks, *J. Cryst. Growth*, **23** (1974) 275.
109. K. S. Pillai, M. A. Ittyachen, *J. Cryst. Growth*, **39** (1977) 287.
110. J. Dennis, *Ph. D. Thesis*, Pennsylvania State Univ., Pennsylvania (1968).
111. A. F. Armington, M. A. Dipietro, J. O'Connor, *Phys. Sci. Res.*, Paper No. 334, Air Force Cambridge Res. Lab. (Ref. 67-0445), Cambridge (1967).
112. E. S. Hedges, "*Colloids*", Arnold & Co, London (1931).
113. E. S. Hedges, "*Liesegang Rings and Other Periodic Structures*", Chapman & Hall, London (1932).
114. E. Hatschek, *J. Soc. Chem. Ind.*, **30** (1911) 256.
115. N. R. Dhar, A. C. Chatterji, *Kolloid Z.*, **31** (1922) 15.
116. C. A. Schleussner, *Kolloid Z.*, **31** (1922) 347.
117. K. Jableczynski, S. Kobryner, *Bull. of Soc. Chem.*, **39** (1926) 383.
118. R. J. Doyle, H. Ryan, *Proc. Roy. Irish Acad.*, **38B** (1929) 435.
119. H. S. Davis, *J. Amer. Chem. Soc.*, **39** (1917) 1312.
120. K. H. Stern, "*Bibliography of Liesegang Rings*", National Bureau of Standards, Washington (1967).
121. F. D. Gnanam, S. Krishnan, P. Ramasamy, G. S. Laddha, *J. of Colloid Interface Sci.*, **73** (1980) 193.
122. H. K. Henisch, J. M. Grasia-Ruiz, *J. Cryst. Growth*, **75** (1986) 195.
123. H. K. Henisch, J. M. Grasia-Ruiz, *J. Cryst. Growth*, **75** (1986) 203.
124. B. Chopard, P. Luthi, M. Droz, *J. Statistical Phys.*, **76** (1994) 661.
125. D. S. Chernavskii, A. Polezhaev, S. Muller, *Physica D.*, **54** (1991) 160.

126. Y. Brechet, J. S. Kirkaldy, *J. Chem. Phys.*, **90** (1989) 1499.
127. A. Bueki, E. K. Smidroczi, M. Zrinyi, *J. Chem. Phys.*, **103** (1995) 10387.
128. K. C. Joseph, M. J. Joshi, *Indian J. Phys.*, **76A** (2002) 159.
129. A. H. Sharbaugh Sr., A. H. Sharbaugh Jr., *J. Chem. Educ.*, **66** (1989) 589.
130. J. M. García-Ruiz, *J. Cryst. Growth*, **75** (1986) 441.
131. M. Pauchet, T. Morelli, S. Coste, J. Malandain, C. Coquerel, *Cryst. Growth Des.*, **8** (2006) 1881.
132. M. C. Robert, O. Vidal, J. M. García-Ruiz, F. Otálora, In “*Crystallization of Nucleic Acids and Proteins: A Practical Approach*”, Ed. A. Ducruix, R. Giegé, Oxford University Press, New York (1999).
133. S. Joseph, *Ph.D. Thesis*, Saurashtra University, Rajkot (1987).
134. S. N. Kalkura, S. J. Devanarayanan, *J. Mater. Sci. Lett.*, **5** (1986), 741.
135. A. Elizabeth, C. Joseph, M. A. Ittyachen, *Bull. Mater. Sci.*, **24** (2001) 431.
136. T. T. George, K. M. Pillai, *Indian J. Pure Appl. Phys.*, **42** (2004) 465.
137. M. Ammal, K. Geoge, I. Jayakumari, *Cryst. Res. Technol.*, **42** (2007) 876.
138. C. Biertumpfel, J. Basquin, D. Suck, C. Sauter, *Acta Crystallogr.*, **D 58** (2002) 1657.
139. B. Lorber, C. Sauter, A. T. Dietrich, A. Moreno, P. Schellenberger, M. C. Robert, B. Capelle, S. Sanglier, N. Potier, R. Giegé, *Prog. Biophys. Mol. Biol.*, **101** (2009) 13.
140. S. Bisailon, R. Tawashi, *J. Pharm. Sci.*, **64** (1975) 458.
141. M. Deepa, K. R. Babu, V. K. Vaidyan, *J. Mater. Sci.*, **14** (1995) 1321.
142. N. Srinivasan, S. Natarajan, *Indian J. Phys.*, **70B** (1996) 563.
143. J. Kurutz, M. Carvalho, Y. Nakagawa, *J. Cryst. Growth*, **255** (2003) 392.

144. J. Ouyang, S. Deng, X. Li, Y. Tan, T. Bernd, *Sci. China Ser. B Chem.*, **47** (2004) 311.
145. V. S. Joshi, B. B. Parekh, M. J. Joshi, A. B. Vaidya, *J. Cryst. Growth*, **275** (2005) e1403.
146. M. L. Weaver, S. R. Qiu, J. R. Hoyer, W. H. Casey, G. H. Nancollas, J. J. De Yoreo, *J. Cryst. Growth*, **306** (2007) 135.
147. D. Valarmathi, L. Abraham, S. Gunasekaran, *Indian J. Pure Appl. Phys.*, **48** (2010) 36.
148. M. Ohta, M. Tsutsumi, *J. Cryst. Growth*, **56** (1982) 652.
149. T. Iruan, S. N. Kalkura, D. Arivuoli, P. Ramasamy, *J. Cryst. Growth*, **130** (1993) 217.
150. R. Z. LeGeros, J. P. LeGeros, *J. Cryst. Growth*, **13-14** (1972) 476.
151. R. H. Plovnick, *J. Cryst. Growth*, **114** (1991) 22.
152. F. Lefauchaux, M. C. Robert, H. Arend, *J. Cryst. Growth*, **47** (1979) 313.
153. E. Banks, R. Chianelli, F. Pintchovsky, *J. Cryst. Growth*, **18** (1973) 185.
154. S. N. Kalkura, V. K. Vaidyan, M. Kanakavel, P. Ramasamy, *J. Cryst. Growth*, **132** (1993) 617.
155. M. Ashok, N. M. Sundaram, S. N. Kalkura, *Mater. Lett.*, **57** (2003) 2066.
156. P. Kanchana, C. Sekar, *J. Cryst. Growth*, **312** (2010) 808.
157. G. Sivakumar, S. Kalkura, P. Ramasamy, *Mater. Chem. Phys.*, **57** (1999) 238.
158. B. B. Parekh, M. J. Joshi, A. D. B. Vaidya, *Curr. Sci.*, **93** (2007) 373.
159. G. Kanchana, P. Suresh, P. Sundaramoorthi, S. Kalainathan, G. P. Jeyanthi, *J. Miner. Mater. Charact. Eng.*, **7** (2008) 215.
160. T. Iruan, D. Arivuoli, P. Ramasamy, *Cryst. Res. Technol.*, **25** (1990) K104.
161. K. C. Joseph, *Ph. D. Thesis*, Saurashtra University, Rajkot (2005).

Chapter IV

Characterization Techniques

Topic Number	Topic	Page Number
4.1	Introduction	163
4.2	X-ray Diffraction by Powder Method	163
4.3	Infrared (IR) Spectroscopy and FT-IR Spectroscopy	172
4.4	Thermal Studies	185
4.5	Dielectric Studies	194
4.6	Micro-hardness Studies	198
4.7	Etching Studies	198

4.1 Introduction

Nowadays, scientists and engineers have an impressive array of powerful and elegant tools for acquiring quantitative and qualitative information about the composition and structure of matter. There are variety of crystals grown having numerous applications in science and technology. It is always important to characterize these crystals with various angles of interests by different instruments [1].

This chapter describes a brief review of different experimental characterization techniques, which are used by the present author to characterize the grown struvite and related crystals.

4.2 X-ray Diffraction by Powder Method

The use of X-ray techniques in the field of materials qualitative and quantitative analysis is now completing more than its century. While the broad definition of X-ray techniques covers many techniques based on the scatter, emission and absorption properties of X-radiation (X-ray), the two most common are X-ray Fluorescence Spectrometry (XRF) and X-Ray powder Diffractometry (XRD). The powder method derives its name from the fact that the specimen is typically in the form of a microcrystalline powder. Since single crystals are not always available, this method is more suitable for structural determination of various substances. Any material which is made up of an ordered array of atoms gives a particular diffraction pattern. The powder XRD, which is also known as *Debye-Scherrer method* is a non-destructive technique widely used for the characterization of a variety of crystalline materials.

4.2.1 Brief History of the Development of Powder XRD

X-rays were discovered by Wilhelm Conrad Roentgen, the first Nobel laureate in physics, in 1895 [2]. In 1912, Max von Laue, a German physicist and a Nobel laureate, discovered that crystalline substances act as three-dimensional diffraction gratings for X-ray wavelengths similar to the spacing of planes in a crystal lattice. Both the discoveries gave a powerful tool that could see *inside* of crystals and allow investigators for detailed determination of crystal structures. So both the events changed the dimensions of physics, chemistry, crystallography, mineralogy and medicine. After Laue's pioneering research, the field developed rapidly, most notably by the contribution from a pair of father and son physicists, namely, William Henry Bragg and William Lawrence Bragg, respectively. In 1912-1913, the W. L. Bragg developed a well known Bragg's law, which connects the observed scattering with reflections from evenly spaced planes within the crystal [3,4]. Following these discoveries two major fields of materials analysis have developed. One of them is the method of powder XRD, which was devised independently in 1916 by Peter Joseph William Debye, a Nobel laureate, and P. Scherrer [5] in Germany and in 1917 by A. W. Hull [6,7] in United States. In the late 1930s, the powder XRD technique was recognized as a powerful technique for phase identification and chemical analysis. The technique developed steadily and, half a century later, the traditional applications, such as phase identification, the determination of accurate unit-cell dimensions and the analysis of structural imperfections, were well established. There was then a dramatic increase of interest in powder methods during the 1970s, following the introduction by Rietveld in 1967 of his powerful *Rietveld method* for refining

crystal structures from X-ray and neutron powder diffraction data [8,9]. Powder XRD has become an important tool for rapid identification of polymorphs and formed compounds in pharmaceutical industry. Powder XRD opens tremendous possibilities for characterization of materials and stimulates an interdisciplinary dialogue and collaboration among physicists, mineralogists, crystallographers, chemists, pharmacists and material scientist.

4.2.2 X-Ray Diffractometer and Experimental Procedure

Basically, this method involves the diffraction of monochromatic X-ray by a powdered specimen. The instrument used for the method is X-ray diffractometer, which consist of three basic elements, (i) an X-ray tube, (ii) a sample holder, and (iii) an X-ray detector. Figure 4.1 shows the schematic presentation of powder x-ray diffraction (Image Source: PANalytical).

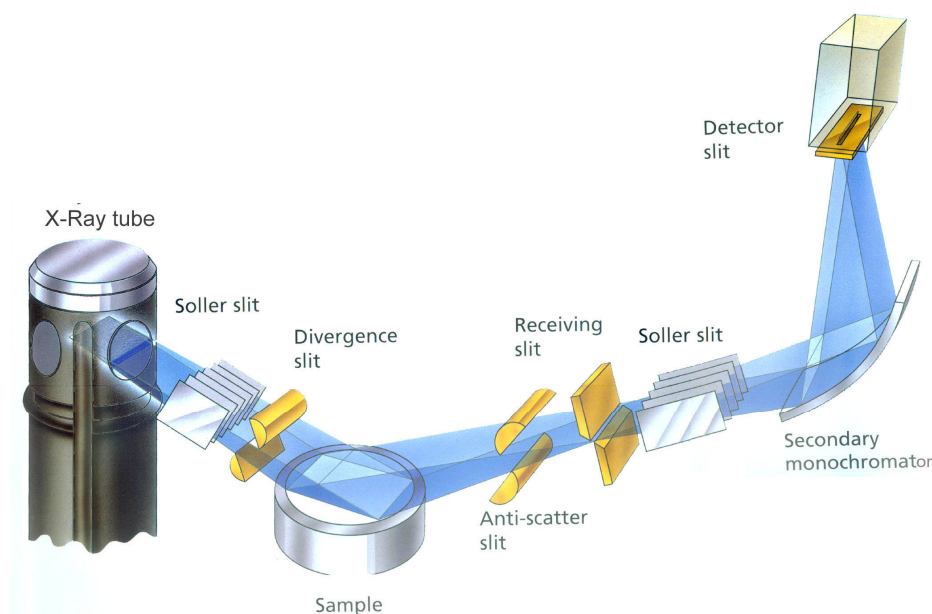


Figure : 4.1 The Schematic Presentation of Powder X-Ray Diffraction

X-rays are generated in a cathode ray tube by heating a filament to produce electrons, accelerating the electrons toward a target by applying a high voltage, and bombarding the target material with electrons. When electrons have sufficient energy to dislodge inner shell electrons of the target

material, characteristic X-ray spectra are produced. These spectra consist of several components, the most common being K_{α} (α -doublet) and K_{β} . K_{α} consists, in part, of $K_{\alpha 1}$ and $K_{\alpha 2}$. $K_{\alpha 1}$ has a slightly shorter wavelength and twice the intensity as $K_{\alpha 2}$. The specific wavelengths are characteristic of the target material. The most common laboratory X-ray tube uses a copper anode, but cobalt and molybdenum are also popular. Table 4.1 shows the wavelengths in Å for various sources. Filtering, by foils or crystal monochrometers, is required to produce monochromatic X-rays needed for diffraction. $K_{\alpha 1}$ and $K_{\alpha 2}$ are sufficiently close in wavelength such that a weighted average of the two is used. Copper is the most common target material for single-crystal diffraction, with CuK_{α} radiation = 1.54184 Å. The basic purpose of the monochromatization is to obtain an experimental pattern from a single, unique wavelength.

Table : 4.1 : Wavelengths in Å for various sources of X-ray tube

Element	Wavelength in Å			
	$K_{\alpha 1}$ (Very Strong)	$K_{\alpha 2}$ (Strong)	K_{α} (Weighted Average)	K_{β} (Weak)
Cu	1.54056	1.54439	1.54184	1.39222
Co	1.78897	1.79285	1.79026	1.62079
Mo	0.70930	0.71359	0.71073	0.63229
Cr	2.28970	2.29361	2.29100	2.08487
Fe	1.93604	1.93998	1.93736	1.75661

A fine powder of the material under investigation should be placed in the sample holder - a small disc like container and its surface carefully flattened. The X-rays are collimated and directed onto the sample.

The fundamental law, which governs the x-ray diffraction phenomenon, is the Bragg's Law and the equation is as follows;

$$n \lambda = 2 d \sin \theta \quad (4.1)$$

where, λ is the wavelength of the x-ray, θ is the scattering angle, and n is an integer representing the order of the diffraction peak. The interaction of the incident X-rays with the crystalline powdered sample produces constructive interference when conditions satisfy Bragg's Law and it gets diffracted in the form of cones, which is exhibited in figure 4.2 [10]. The cones may emerge in all directions, forwards and backwards. A circle of film is used to record the diffraction pattern as shown. Each cone intersects the film giving diffraction lines. The lines are seen as arcs on the film. Each diffraction line is made up of a large number of small spots, each from a separate crystal. Each spot is so small as to give the appearance of a continuous line. If the crystal is not ground finely enough, the diffraction lines appear speckled.

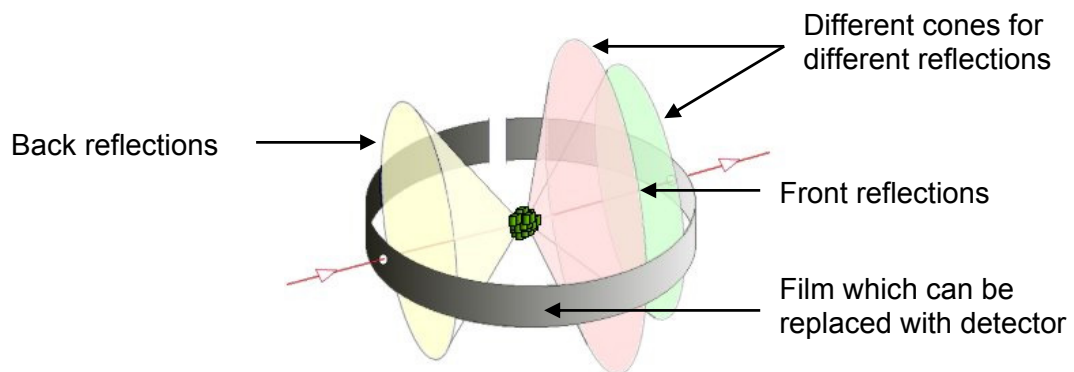


Figure : 4.2 Powder Sample Diffract X-ray Beam in Cones [10]

These diffracted X-rays are then detected, processed and counted. The geometry of an X-ray diffractometer is such that the sample rotates in the path of the collimated X-ray beam at an angle θ while the X-ray detector, mounted on an arm to collect the diffracted X-rays, rotates at an angle of 2θ , which is known as *Bragg-Brentano configuration*. The intensity of diffracted X-rays is continuously recorded as the sample and detector rotate through their respective angles. A peak in intensity occurs when the mineral or crystalline

material contains lattice planes with d-spacing appropriate to diffract X-rays at that value of θ . The instrument used to maintain the angle and rotate the sample is termed a *goniometer*. For typical powder patterns, data is collected at 2θ in the range of angles from $\sim 5^\circ$ to 70° , angles that are preset in the X-ray scan. By scanning the sample through a range of 2θ angles, all possible diffraction directions of the lattice should be attained due to the random orientation of the powdered material. Conversion of the diffraction peaks to d-spacing allows identification of the mineral or crystalline material because each mineral has a set of unique d-spacing. Typically, this is achieved by comparison of d-spacing with standard reference patterns. Resultant diffraction pattern contains a good deal of information of which three parameters are of special interest – (i) the position of the diffraction maxima, (ii) the peak intensities and (iii) the intensity distribution as a function of diffraction angle. Results of the procedure are commonly presented as peak positions at 2θ and X-ray counts (intensity) in the form of a table or an x-y plot, known as *diffractogram*. For determination of unit cell parameters, each reflection must be indexed to specific Miller indices (h, k, l). Nowadays, many types of software are available in market for powder XRD data analysis.

There are three types of powder methods, differentiated by the relative position of the specimen and the film : (i) *Debye-Scherrer Method* - The film is placed on the surface of a cylinder and specimen on the axis of the cylinder. (ii) *Focusing Method* - The film, specimen, and X-ray source are all placed on the surface of a cylinder. (iii) *Pinhole Method* - The film is flat, perpendicular to the incident X-ray beam, and located at any convenient distance.

The powder photographic methods are well described by Azaroff and Buerger [11] as well as Klug and Alexander [12]. The simplest and most inexpensive way of practicing the powder method is to record the X-ray diffraction on photographic film, using a powder camera. A more elaborate way is to detect the diffracted radiation by means of a quantum counter, like Geiger counter. The use of counter diffractometer, and recorder equipment is justified chiefly when one wants to examine different samples rapidly. Such methods also have a real advantage whenever accurately measured intensities are necessary.

4.2.3 Applications of Powder XRD

Powdered XRD has a wide range of applications in material science, geology, environmental science, chemistry, forensic science, and the pharmaceutical industry, etc. This method has been conventionally used for phase identification, quantitative analysis and the determination of structure imperfections. Various types crystalline materials can be characterized by powder XRD, including organic and inorganic materials, minerals, drugs, zeolites, catalysts, metals and ceramics. In the pharmaceutical industries the powder XRD is popular for identification of drug molecule and its polymorphs. The physical states of the materials can be loose powders, thin films, poly-crystalline and bulk materials. By properly using this technique one can yield a great deal of structural information about the material under investigation. For most applications, the amount of information which is possible to extract depends on the nature of the sample microstructure (crystallinity, structure imperfections, crystallite size and texture), the complexity of the crystal structure (number of atoms in the asymmetric unit

cell and unit cell volume) and the quality of the experimental data (instrument performances and counting statistics) [13].

The powder method can be used as a tool to identify crystals, since the powder XRD patterns produced by a crystalline substance is a characteristic of that particular substance. One of the most important uses of the powder method is in the identification of an unknown material. The ASTM (American Society for Testing and Materials) data cards as well as JCPDS (Joint Committee of Powder Diffraction Standards) data files are available for large number of substances for identifications and comparison. Statistical study of the relative orientations of the individual crystals of an aggregate is one of the important secondary uses of the powder method [11,14]. The broad application of powder XRD is summarized as shown in table 4.2 [13].

Table : 4.2 : Applications of Powder XRD [13]

Diffraction Line Parameter	Applications
Peak Position	Unit-cell parameter refinement Pattern indexing Space group determination ($2\theta_0$ / absent reflections) Anisotropic thermal expansion Macro stress: $\sin^2\psi$ method Phase identification (d / I)
Intensity	Phase abundance Reaction kinetics Crystal structure analysis (whole pattern) Rietveld refinement (whole pattern) Search/match, phase identification Preferred orientation, texture analysis
Width / Breadth and Shape	Instrumental resolution function Microstructure: line profile analysis Microstructure (crystallite size, size distribution, lattice distortion, structure mistakes, dislocations, composition gradient) Crystallite growth kinetics Three-dimensional microstructure (whole pattern)
Non-ambient and dynamic diffraction	<i>In situ</i> diffraction under external constraints reaction kinetics.

However, in recent years the applications have been extended to new areas, such as the determination of crystal structures and the extraction of three-dimensional micro-structural properties.

4.2.4 Advantages of Powder XRD :

- It is reliable and powerful tool for crystalline sample identification.
- It is a non-destructive technique.
- Ability to analyze mixed phases.
- For the purpose of simultaneous and quick measurement of the positions and intensities of diffraction lines the diffractometers are advantageous. It is a fast technique (< 20 min) for identification of an unknown sample.
- In most cases, it provides an unambiguous sample determination.
- Simplicity in sample preparation, i.e., required sample preparation is minimal and extensive sample preparation is not needed.
- XRD units are widely available.
- Data interpretation is relatively straight forward.

4.2.5 Limitations of Powder XRD :

- Homogeneous and single phase material is best for material identification.
- Must have access to a standard reference file of compounds.
- Requires tenths of a gram of material which must be ground into a powder.
- The sensitivity of the powder diffraction method is not comparable in sensitivity to the other X-ray-based techniques.
- A phase present in quantities lower than 5% by weight is usually not detected. For mixed materials, detection limit is ~ 2 - 5% of sample.
- Peak overlay may occur and worsens for high angle 'reflections'.
- Can not identify amorphous materials.

- For unit cell determinations, indexing of patterns for non-isometric crystal systems is complicated.
- There may be a chance of misinterpretation during the course of a qualitative analysis procedure.
- No depth profile information.

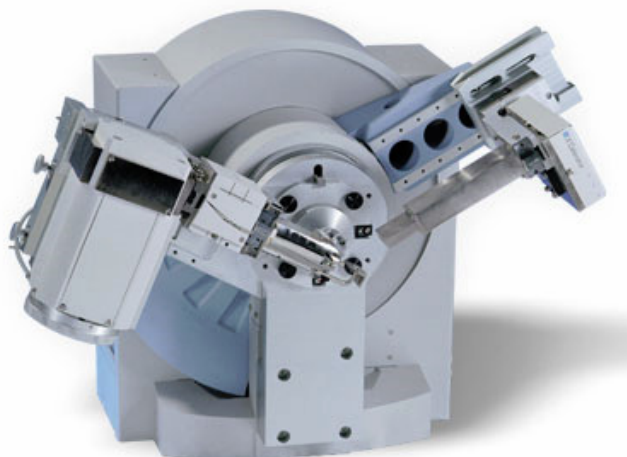


Figure : 4.3 X-ray Powder Diffractometer [15]

In the present work grown struvite and related crystals were analyzed by powder X-ray analysis PHILIPS X'PERT Modular Powder Diffractometer (MPD) system as shown in figure 4.3 [15]. The crystal structures were determined by a computer software Powder-X.

4.3 Infrared (IR) Spectroscopy and FT-IR Spectroscopy

The term 'spectroscopy' is generally used for the analytical techniques based on the interaction of electromagnetic radiation with matter and variation of particular physical quantity with frequency of radiation. In spectroscopy, the measurements of absorbance / transmittance of electromagnetic radiation, due to interaction with sample by molecules that are carried out in a gas or vapour state or dissolved molecules/ions or solid depending upon requirement. Spectroscopy is used for both qualitative and quantitative investigations.

4.3.1 Brief History

The root of the IR spectroscopy is in the discovery of IR radiation by Sir William Herschel in 1800. The first mid-infrared spectrometer was developed by Melloni in 1833 [16]. Infrared spectroscopy emerged as a science with the invention of interferometer by the Nobel Laureate A. A. Michelson in 1890s [17-19]. In 1911 Rubens and Wood presented the first real interferogram. The dispersive infrared spectrometer emerged in the 1940s, but it was still an immature scientific field. But with development of the optical null dispersive spectrophotometer, later that decade, chemical infrared spectroscopy came into widespread use. Dispersive instruments proved the tremendous value of infrared analysis, and soon became the mainstay of organic characterization laboratories. In 1949 Fellgett used an interferometer to measure light from celestial bodies and produced the first Fourier transform infrared spectrum. In the late 1960s due to advent of microcomputers, the Fourier transform became available and the commercial FT-IR spectrometers appeared. The 1966 development of the Cooley-Tukey algorithm [20], which quickly does a Fourier transform, was influential in the popularization of FT-IR spectrometers.

4.3.2 Infrared (IR) Spectroscopy

In infrared (IR) spectroscopy, when IR radiation is incident on a sample, some of the IR radiation is absorbed by the sample and some of it is passed through (transmitted). The resulting spectrum represents the molecular absorption or transmission, creating a molecular fingerprint of the sample. Like a fingerprint no two unique molecular structures produce the same infrared spectrum. This makes IR spectroscopy useful for several types of analysis. It is one of the most powerful analytical techniques, which indicates the

possibility of chemical identifications [21]. Infrared spectroscopy takes the advantage of the fact that molecules absorb specific frequencies that are characteristic of their structure. These absorptions are resonant frequencies, i.e., the frequency of the absorbed radiation matches the frequency of the bond or group that vibrates.

The original IR instruments were of the dispersive type. The individual frequencies of energy emitted from the infrared source were separated by a prism or grating. A grating is a more modern dispersive element which better separates the frequencies of infrared energy. The detector measures the amount of energy at each frequency which has passed through the sample. This results in a spectrum which is a plot of intensity vs. frequency.

4.3.3 IR Spectral Region

The infrared region of the electromagnetic spectrum extends from the red end of the visible spectrum to the microwave region. Infrared spectral region can be divided into three regions; near-infrared, mid-infrared and far-infrared. Table 4.3 gives the details of different infrared spectral regions.

Table : 4.3 : Different Infrared Spectral Regions and its Applications

Spectral Regions	Wave Numbers (cm ⁻¹)	Type of Measurement	Analysis	Applicable Samples
Near-infrared	12,800 - 4000	Diffuse reflectance	Quantitative	Solid or liquid materials
		Absorption	Quantitative	Gaseous mixtures
Mid-infrared	4000 - 200	Absorption	Qualitative	Gaseous, liquid or solid organic compounds. Complex gaseous, liquid or solid mixtures.
		Reflectance	Qualitative	Pure solid or liquid compounds Polymer films, Fibers and rubbers
		Emission	Quantitative	Atmospheric samples
Far-infrared	200 - 10	Adsorption	Qualitative	Pure inorganic or metal-organic species

4.3.4 Types of Molecular Vibrations

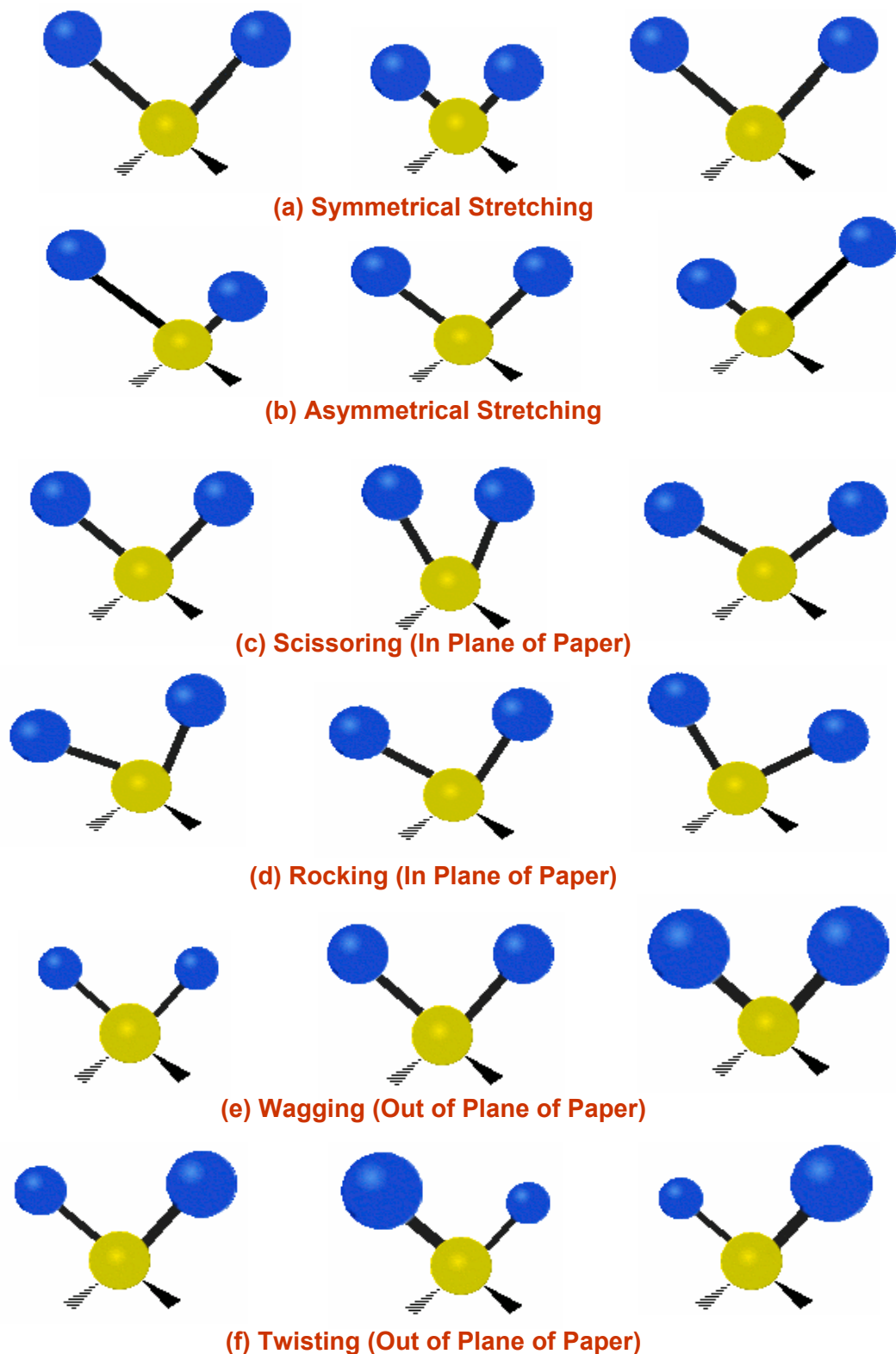


Figure : 4.4 Various stretching and bending modes of vibration in molecule
 Stretching Modes : (a) Symmetrical Stretching (b) Asymmetrical Stretching
 Bending Modes : (c) Scissoring (d) Rocking (e) Wagging (f) Twisting [22]

The covalent bonds of molecules are not rigid, but are more like stiff springs that can be stretched and bent. At ordinary temperatures a molecule can vibrate in many ways, and each way is called a vibrational mode. A molecule composed of N-atoms has 3N degrees of freedom, six of which are translations and rotations of the molecule itself. This leaves 3N-6 degrees of vibrational modes for non-linear molecules, whereas it will be 3N-5 for the linear molecule. Molecular vibrations are falling into two basic categories of stretching and bending. A stretching vibration involves a continuous change in the inter-atomic distance along the axis of bond between two atoms, i.e. change in bond length. However, the bending vibrations are characterized by a change in the angle between two bonds, which are of four types, scissoring (bending), rocking, wagging and twisting in the figure 4.4.

The fundamental vibrational frequency of a diatomic molecular ensemble can be given by the following formula, which can be derived from Hooke's law.

$$\nu = \frac{1}{2 \pi c} \sqrt{\frac{\kappa}{\mu}} = \frac{1}{2 \pi c} \sqrt{\frac{\kappa (m_1 + m_2)}{m_1 \cdot m_2}} \quad (4.2)$$

where, ν is the fundamental vibration frequency in cm^{-1} , c is the velocity of light in cm / s , κ is the force constant of the bond in dyne / cm , and μ is the reduced mass in gram. The reduced mass is $\mu = m_1 \cdot m_2 / (m_1 + m_2)$. Here, m_1 and m_2 are the masses of the component atoms of the chemical bond. Because of the interaction with molecular vibrations, portions of the incident infrared radiation are absorbed at particular wavelengths. The multiplicity of vibrations occurring simultaneously produces a highly complex absorption spectrum, which is a unique characteristic of the overall configuration of the atoms as well. Details of assignments of different frequencies with different

vibrations of bonds, such as H–O, N–H, C=O, C–C, C–H etc are given in detail by many authors [1, 21, 23-25]. Many times it is given in chart and tabular forms to facilitate the user to identify the specific bond vibrations from the frequency in wave numbers, represented in the figure 4.5.

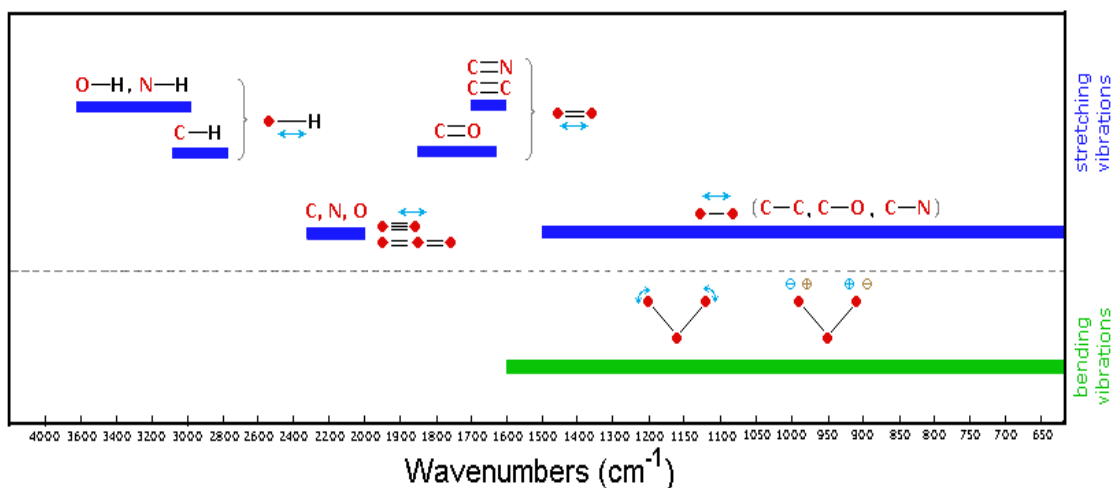


Figure : 4.5 A Simple Chart to Identify Specific Bond Vibrations in Wave Numbers (Blue = Stretching Vibrations; Green = Bending Vibrations) [26]

The general trends of frequency of vibrations are (i) Stretching frequencies are higher than corresponding bending frequencies, since it is easier to bend a bond than to stretch or compress it, (ii) Bonds to hydrogen have higher stretching frequencies than those to heavier atoms, and (iii) Stronger bonds have higher stretching frequencies than weaker bonds.

4.3.5 Fourier Transform Infrared Spectroscopy

Due to the advent of Fourier Transform technology, the scenario is completely changed. Fourier Transform Infrared (FT-IR) spectrometry was developed in order to overcome the limitations encountered with dispersive instruments. The main difficulty was the slow scanning process. A method for measuring all of the infrared frequencies simultaneously, rather than individually, was needed. A solution was developed which employed a very

simple optical device called an interferometer. The interferometer produces a unique type of signal which has all of the infrared frequencies “encoded” into it. The signal can be measured very quickly, usually on the order of one second or so. Thus, the time element per sample is reduced to a matter of a few seconds rather than several minutes. Therefore, FT-IR is the preferred method of infrared spectroscopy.

4.3.6 FT-IR Spectrometer and Experimental Procedure

An FT-IR spectrometer is a spectral instrument that collects and digitizes the interferogram, performs the Fourier transform function on the interferogram and displays the spectrum. FT-IR spectrometer is the advancement of the dispersive spectrometer.

Sample preparation: Samples for FT-IR can be prepared in a number of ways. Sample crystal can be milled with potassium bromide (KBr) to form a very fine powder. This powder is then compressed into a thin pellet which can be analyzed. KBr is also transparent in the IR. Alternatively, solid samples can be dissolved in a solvent such as methylene chloride, and the solution placed onto a single salt plate. The solvent is then evaporated off, leaving a thin film of the original material on the plate. This is called a cast film, and is frequently used for polymer identification. For liquid samples, the easiest is to place one drop of sample between two plates of sodium chloride (salt). Salt is transparent to infrared light. The drop forms a thin film between the plates.

Multiplex types of instruments employ the mathematical tool of Fourier Transform [27]. The Michelson interferometer, which is the heart of the apparatus of FT-IR spectrometer, is as shown in figure 4.6. The creation of today’s FT-IR would not have been possible had it not been for the existence

of the Michelson interferometer. The interferometer requires two mirrors (M_1 and M_2), an infrared light source, an infrared detector, and a beam splitter (B) made-up of half-silvered mirror. Figure 4.7 shows the schematic diagram of FT-IR spectrometer.

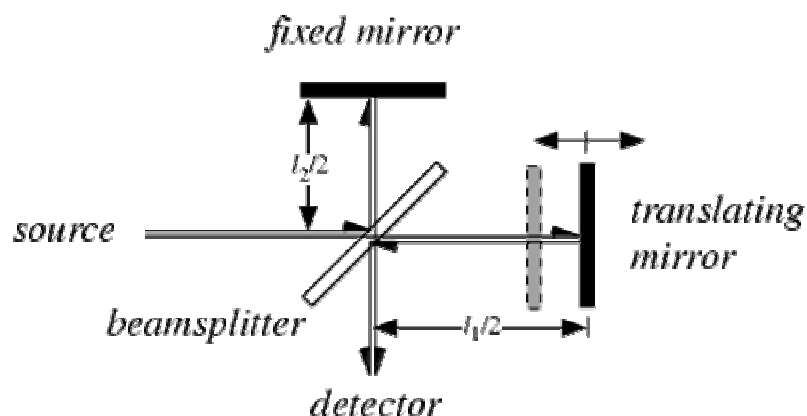


Figure : 4.6 Schematic Diagram of Michelson Interferometer [28]

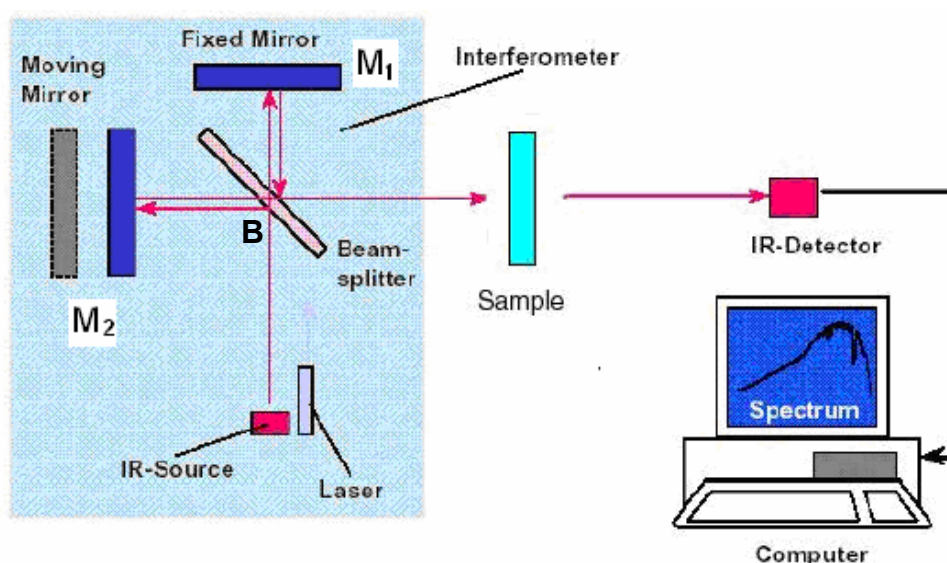


Figure : 4.7 Schematic Diagram of FT-IR Spectrometer

The main components of the FT-IR spectrometers are (1) drive mechanism, (2) beam splitters and (3) sources (4) IR detector and (5) signal processor / computer. As shown in figure 4.7 a parallel beam of radiation is directed from the source to the interferometer. It is well known that the interference patterns are obtained for monochromatic radiation.

Radiation from the source strikes the beam splitter and separates into two beams. One beam is transmitted through the beam splitter to the fixed mirror and the second is reflected off the beam splitter to the moving mirror. The fixed and moving mirrors reflect the radiation back to the beam splitter. Again, half of this reflected radiation is transmitted and half is reflected at the beam splitter, resulting in one beam passing to the detector and the second back to the source. The interference patterns (interferogram) obtained can be transferred back to the original frequency distribution. This can be achieved by a mathematical process known as Fourier Transform, nowadays; this process is carried out by a computer or microprocessor of the spectrometer. The end result of the Fourier transform is the spectrum of peaks and valleys that is displayed. The resulting absorption pattern can be compared to the millions of patterns that are stored in computer databases, both on-site and remotely via the Internet. If a matching spectrum is obtained, then the identity of the sample compound can be determined. FT-IR Spectrometer makes use of all the frequencies from the source simultaneously, rather than sequentially as in dispersive instrument (i.e. grating spectrometer). This feature is called the Multiplex or Fellgett Advantage.

There are different versions; modifications and attachments available with FT-IR. Diffuse Reflectance Infrared Fourier Transform Spectroscopy (DRIFTS) uses an effective way of obtaining infrared spectra directly on powdered samples with a minimum sample preparation [29-31]. The advantage is that it permits conventional infrared spectral data to be obtained on the samples that are not altered much from their original state.

4.3.7 Applications of FT-IR Spectroscopy

Various applications of FT-IR spectroscopy are as follows :

- Identification of simple mixtures of organic and inorganic compounds.
- Routine qualitative and quantitative FT-IR Analysis.
- Determination of functional groups in unknown materials.
- Identification of polymers and polymer blends.
- Determination of degrees of crystallinity in polymers.
- Indirect verification of trace organic contaminants on surfaces.
- Thin film analysis.
- Analysis of adhesives, coatings, adhesion promoters or coupling agents.
- Analysis of resins, composite materials and release films.
- Identification of rubbers and filled rubbers.
- Comparative chain lengths in organics.
- Extent of thermal, UV or other degradation or depolymerization of polymers and paint coatings.
- Analysis of gaseous samples using a gas cell for environmental study.
- Analysis of unknown solvents, cleaning agents and detergents.

4.3.8 Advantages of FT-IR

Some of the major advantages of FT-IR over the dispersive technique include:

- 1. Better Speed:** As noted earlier, because all of the frequencies are measured simultaneously, most measurements by FT-IR are made in a few seconds rather than several minutes. It is also referred to as the Fellgett Advantage.
- 2. Sensitivity:** Sensitivity is dramatically improved with FT-IR for many reasons. The detectors employed are much more sensitive, the optical

throughput is much higher (referred to as the Jacquinot Advantage) which results in much lower noise levels, and the fast scans enable the co-addition of several scans in order to reduce the random measurement noise to any desired level (referred to as signal averaging).

- 3. Mechanical Simplicity:** The moving mirror in the interferometer is the only continuously moving part in the instrument. Thus, there is very little possibility of mechanical breakdown.
- 4. Internally Calibrated:** These instruments employ a He-Ne laser (helium-neon laser) as an internal wavelength calibration standard (referred to as the Connes Advantage). The use of a helium - neon laser as the internal reference in many FT-IR systems provides an automatic calibration in an accuracy of better than 0.01 cm^{-1} . These instruments are self-calibrating and never need to be calibrated by the user.
- 5. Increased optical throughput (Jaquinot advantage) :** Energy-wasting slits are not required in the interferometer because dispersion or filtering is not needed. Instead, a circular optical aperture is commonly used in FT-IR systems. The beam area of an instrument is usually 75 to 100 times larger than the slit width of a dispersive spectrometer. Thus, more radiation energy is made available. This constitutes a major advantage for many samples or sampling techniques that are energy-limited.
- 6. Elimination of stray light and emission contributions:** The interferometer in FT-IR modulates all the frequencies. The unmodulated stray light and sample emissions (if any) are not detected.
- 7. Powerful data station :** Modern FT-IR spectrometers are usually equipped with a powerful, computerized data system. It can perform a

wide variety of data processing tasks such as Fourier transformation, interactive spectral subtraction, baseline correction, smoothing, integration, and library searching.

8. Resolving power of FT-IR instrument is constant over the entire spectrum, whereas it varies with frequency in the conventional technique [32].
9. IR analysis can be conducted at room temperature.
10. Equally applicable to both emission and absorption spectroscopy.

These advantages, along with several others, make measurements made by FT-IR extremely accurate and reproducible. Thus, it is a very reliable technique for positive identification of virtually any sample. The sensitivity benefits enable identification of even the smallest of contaminants. In addition, the sensitivity and accuracy of FT-IR detectors, along with a wide variety of software algorithms, have dramatically increased the practical use of infrared for quantitative analysis. Thus, FT-IR technique has brought significant practical advantages to infrared spectroscopy.

4.3.9 Analytical Capabilities of FT-IR

- Identifies chemical bond functional groups by the absorption of infrared radiation, which excites vibrational modes in the bond.
- May be used in transmission mode.
- Detects and Identifies organic contaminants.
- In attenuated total reflectance (ATR) mode, the detection depth is generally 1-2 μm deep, but can be much more or less dependent upon the material. Black, absorbing materials tend to be less.
- Especially capable of identifying the chemical bonds of organic materials.

- Characterization of compounds via FT-IR is not only limited to organic compounds. Any inorganic compound that forms bonds of a covalent nature within a molecular ion fragment, cation or anion, will produce a characteristic absorption spectrum, with associated group frequencies.
- Identifies water, phosphates, sulfates, nitrates, nitrites, carbonate ions, silicates ions, and ammonium ions.
- Detection limits vary greatly, but are sometimes $<10^{13}$ bonds/cm³ or sometimes sub monolayer.
- Useful with solids, liquids, or gases.

4.3.10 Limitations of FT-IR

- Minimal elemental information is given for most samples.
- FT-IR instrument is inherently a single-beam instrument.
- Background solvent or solid matrix must be relatively transparent in the spectral region of interest.
- Molecule must be active in the IR region. (When exposed to IR radiation, a minimum of one vibrational motion must alter the net dipole moment of the molecule in order for absorption to be observed.)
- It mainly operates in transparent or reflective mode.
- Limited surface sensitivity (typical sampling volumes are ~ 0.8 μm).
- Minimum analysis area ~ 15 micron.
- Limited inorganic information.
- IR-active atmospheric components (CO₂, H₂O) will appear in the spectrum. (However, usually, a "Background" spectrum is run, and then automatically subtracted from every spectrum.)
- Cannot detect atoms or monoatomic entities contain no chemical bonds.

- Aqueous solutions are very difficult to analyze- water is a strong IR absorber.
- Complex mixtures - samples give rise to complex spectra.



Figure : 4.8 Nicolet 6700 FT-IR spectrometer

The present author has used Nicolet 6700 FT-IR spectrometer (as shown in figure 4.8) having optical resolution of 0.09 cm^{-1} , in the range from 400 cm^{-1} to 4000 cm^{-1} in KBr disc medium. The set up used for the analysis was from Physics Department of Saurashtra University.

4.4 Thermal Studies

According to widely accepted definition of thermal analysis (Thermo analytical), it is a group of techniques in which physical properties of a substance and/or its reaction products are measured as a function of temperature whilst the substance is subjected to a controlled temperature program [1]. According to International Confederation for Thermal Analysis and Calorimetry (ICTAC), thermal analysis is defined as a group of techniques in which a property of the sample is monitored against time or temperature while the temperature of the sample, in a specified atmosphere, is programmed [33]. Nearly over a dozen thermal methods can be identified, which differ in the properties measured and temperature programs [34-36]. These methods find widespread use for both quality control and research

applications of various substances, such as, polymers, pharmaceuticals, crystals, clays, minerals, metals and alloys.

4.4.1 Brief History

Historically, Josiah Wedgwood (1730-1795) first attempted to study the thermal behaviour of a clay piece and noted that the decrease in its size due to water loss on drying then increase its size before the final decrease continuously. In 1887, Henry Louis Le Chatelier introduced the use of heating rate curves to identify clays [37]. G. Tammann introduced the term “thermal analysis” first time in 1903 [38]. In 1904, Kumakov [39] developed a versatile photographic recorder which was utilized in Differential Thermal Analysis (DTA) by the Russian school [40]. In the year 1915, Kotaro Honda [41] laid the broad foundations of modern thermogravimetry, introducing the thermo balance. The first commercial thermo-gravimeter was produced in 1945 [42]. Differential Scanning Calorimetry (DSC) technique was developed by Watson et al in 1964 [43]. However, because of advent of electronics and computer interfacing, very accurate fully automated computer controlled thermal analyzers are available.

4.4.2 Classification of Thermal Analysis Techniques

Thermal analysis techniques involve the measurement of various properties of materials subjected to dynamically changing environments under predetermined condition of heating rate, temperature range and gaseous atmosphere or vacuum. Classification of thermal analysis techniques is as shown in table 4.4. Among all the thermal methods, the most widely used techniques are TGA, DTA and DSC, which are employed in inorganic and organic chemistry, metallurgy, mineralogy and other areas.

Table : 4.4 : Classification of Thermal Analysis Techniques

Techniques Based On Variation of Physical Property	Thermal Analysis (Thermo Analytical) Techniques	
	Abbreviated Name	Full Form
Classical Techniques		
Mass	TG / TGA	Thermo-Gravimetry / Thermo Gravimetric Analysis
	DTG	Derivative Thermo-Gravimetry
		Isobaric Mass-Change Determination
	EGD	Evolved Gas Detection
	EGA • TG – FT-IR • TG – MS	Evolved Gas Analysis • Thermo Gravimetric Analysis Coupled to a Fourier Transform Infrared Spectrophotometer • Thermo Gravimetric Analysis Coupled to a Mass Spectrometer
		Emanation Thermal Analysis
		Thermo-Particulate Analysis
Temperature	DTA	Differential Thermal Analysis
	DDTA	Derivative Differential Thermal Analysis
		Heating Curve Determination • Heating Rate Curve • Inverse Heating Rate Curve
Enthalpy	DSC	Differential Scanning Calorimetry
	DSM/NC	Differential Scanning Micro / Nano Calorimetry
Dimensions	TD	Thermo- Dilatometry • Differential Dilatometry • Derivative Dilatometry
Modern Techniques		
Mechanical Characteristics	TMA	Thermo Mechanical Analysis
	DMA	Dynamic Mechanical Analysis
		Dynamic Thermomechanometry
Acoustic Characteristics		Thermosonimetry
		Thermoacoustimetry
Optical Characteristics		Thermoptometry
Electrical Characteristics		Thermoelectrometry
	DETA	Dielectric Thermal Analysis
Magnetic Characteristics		Thermomagnetometry

In certain cases, the use of a single thermo analytical technique may not provide sufficient information to solve the problem on hand and hence the use of other thermal techniques, either independently or simultaneously, for complementary information becomes necessary. For example, both differential thermal analysis (DTA) and thermo gravimetric analysis (TGA) are widely used in studies involving physicochemical changes accompanied by variation in the heat content and the weight of the material.

4.4.3 Thermo Gravimetric Analysis (TGA)

Thermo gravimetric analysis is a technique in which the mass of a substance is measured as a function of temperature or time while the substance is subjected to a controlled temperature program. The curve obtained in a thermo gravimetric analysis is called thermogram (TG) and its first derivative is called a derivative thermogram (DTG).

Modern commercial TG instrument consists of following main parts:

- A sensitive analytical balance
- A temperature programmable furnace
- A purge gas system for providing suitable gas atmosphere
- A microprocessor for instrument control, data acquisition and display

The null-point weighing mechanism is employed since the sample remains in the same zone of furnace irrespective of changes in mass. The furnace is normally an electrical resistive heater and the temperature range for most of the furnace is from ambient to 1000-2000 °C. The rate of heat exchange between the furnace and the sample depends on the heating rate which influences the TG curve in a number of ways. A slower rate gives a

better resolution of the closely lying steps, while the faster heating rate merges such steps.

One of the objectives of TG and DTA is to delineate as accurately as possible the various temperatures associated with the thermal behavior of a given substance, i.e., temperature of decomposition, stability range of an intermediate compound and the temperature at which the reaction get completed. As noted earlier that the TGA involves change in weight with respect to temperature. The acquired data obtained as a plot of mass or loss of mass in percentage as a function of temperature is considered as a thermal spectrum, or a thermogram, or a thermal decomposition curve. These thermograms characterize a system in terms of temperature dependence of its thermodynamic properties and physical-chemical kinetics. Since the TGA involves measurement of a change in weight of a system as the temperature is increased at pre-determined rate, changes in weight are a result of the rupture and/or formation of various physical and chemical bonds at elevated temperatures that lead to the evaluation of volatile products or the formation of heavier reaction products. From such curves, parameters concerning the thermodynamics and kinetics of the various chemical reactions can be evaluated, reaction mechanism, the intermediate and final reaction products can be identified. Usually, the temperature range is from ambient to 1200 °C with inert or reactive atmospheres. The derivative in TG is often used to pinpoint completion of weight- loss steps or to increase resolution of overlapping weight-loss occurrences. The shape of thermogravimetric curve of a particular compound is influenced by the heating rate of the sample and the atmosphere surrounding it [23,34,44].

Applications of TGA

- Study thermal degradation / decomposition / dehydration.
- Chemical reaction resulting in changes of mass such as absorption, adsorption, desorption.
- To check the sample purity.

4.4.4 Differential Thermal Analysis (DTA)

DTA is a technique in which the temperature difference between a substance and a reference material is measured as a function of temperature whilst the substance and reference material are subjected to a controlled temperature program [33]. DTA provides information on the chemical reactions, phase transformations, and structural changes that occur in a sample during a heat-up or a cool-down cycle. The DTA measures the differences in energies released or absorbed, and the changes in heat capacity of materials as a function of temperature. The graph of DTA signal, i.e. differential thermocouple output in micro volts on the Y-axis plotted versus the sample temperature in °C on the X-axis gives the results of DTA.

Modern thermo-balances are often equipped so as to record the DTA signal and the actual thermo-gravimetric measurement, simultaneously. In addition to showing the energetic nature of weight loss events, the DTA signal can also show thermal effects that are not accompanied by a change in mass, e.g. melting, crystallization or a glass transition. Transition temperatures are measured precisely using the DTA. The DTA identifies the temperature regions and the magnitude of critical events during a drying or firing process such as binder burnout, carbon oxidation, sulfur oxidation, structural clay collapse, Alpha to Beta quartz transition, carbonate decompositions,

recrystallizations, melting and cristobalite transitions, melting, solidification or solidus temperature, glass transition temperature (T_g), curie point, energy of reaction, heat capacity, and others. The transition enthalpy is estimated from the DTA curve using the heat capacity of the heat sensitive plate as a function of temperature.

Application of DTA

- Primarily used for detection of transition temperature.
- To check the sample purity.

4.4.5 Differential Scanning Calorimetry (DSC)

DSC is a technique in which the difference in energy inputs into a substance and a reference material is measured as a function of temperature whilst the substance and reference material are subjected to a controlled temperature program [33]. A DSC analyzer measures the energy changes that occur as a sample is heated, cooled or held isothermally, together with the temperature at which these changes occur.

The graph of heat flow in mJ/s on the Y-axis plotted versus temperature at a fixed rate of change of temperature in °C on the X-axis shows the output of the DSC. Usually, for the power compensation DSC curve, heat flow rate should be plotted on the ordinate with endothermic reactions upwards, and for the heat-flux DSC curve with endothermic reactions downwards. The energy changes enable the user to find and measure the transitions that occur in the sample quantitatively, and to note the temperature where they occur, and so to characterize a material for melting processes, measurement of glass transitions and a range of more complex events.

There are two methods of carrying out DSC, namely, (i) Power-compensated DSC, and (ii) heat-flux DSC. Power-compensated DSC is the method usually discussed in textbooks, though most practical instruments are based on heat-flux DSC. However, in practice these usually give equivalent results. In the present study the heat flux type of DSC was used.

Power-Compensated DSC : In this method, the sample and reference are in separate furnaces, each with a heater coil and a thermocouple. The aim is to maintain both at the same temperature, even during a thermal event in the sample. The difference in power supplied to the two furnaces to maintain zero temperature differential between the sample and the reference is measured.

Heat-Flux DSC : The sample and reference are both within the same furnace and are connected by a low-resistance heat-flow path. If any difference in temperature develops, heat flows in proportion to that temperature difference.

DTA and DSC are sister techniques which provide fast, convenient analysis of the glass characteristic temperatures such as T_g and temperatures of phase changes, for instance devitrification and melting. DSC is rather more versatile than DTA. DSC allows quantitative determination of heat capacity, and also the enthalpy of a phase transformation.

Application of DSC :

- Determination important transition temperatures.
- Determine heat of fusion of a crystal phase.
- Degree of crystallization and study the crystal kinetics.
- Determine heat capacity and heat of formation.
- To check the sample purity.

4.4.6 Experimental Procedure :

In the present study, the thermal analysis - TGA, DTA and DSC of the grown struvite and related crystals were carried out to determine simultaneous changes of mass and caloric reactions using PC controlled Linseis Simultaneous Thermal Analyzer (STA) PT-1600, in the atmosphere of air from 35 °C to 900 °C at a heating rate of 15 °C/min. TA-WIN and WIN-STA software used for testing and analysis. The set up for thermal analysis is shown in figure 4.9.

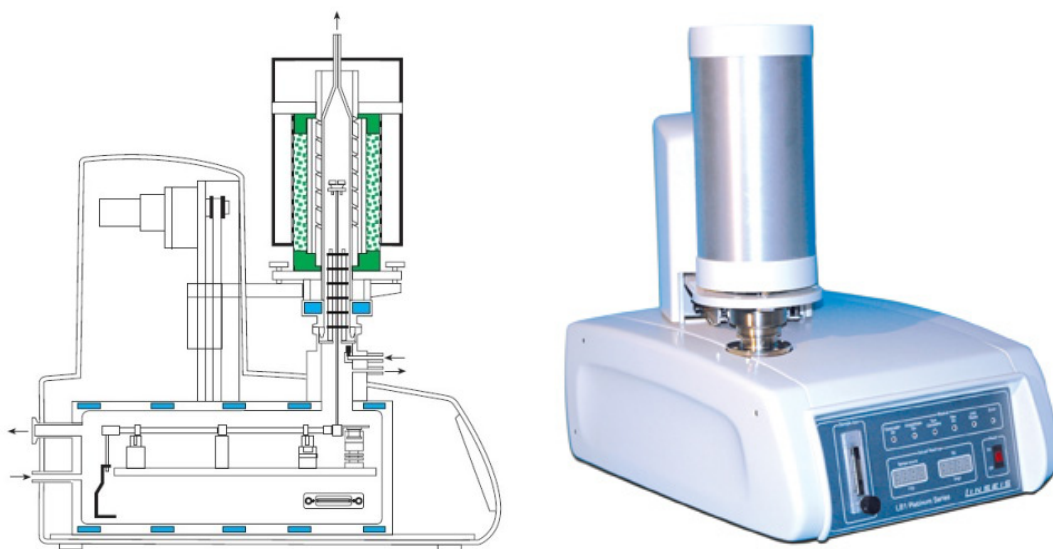


Figure : 4.9 Linseis Simultaneous Thermal Analyzer PT-1600

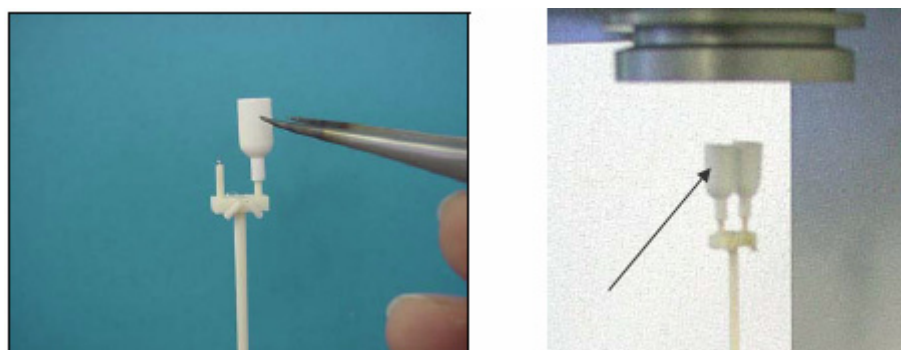


Figure : 4.10 Measuring head and crucible

After switching on computer and thermo balance, one has to open furnace using LIFT switch. As shown in the figure 4.10, the measuring head,

carries two equal crucibles, one for the reference material and one for the sample substance, each one is sitting on a thermocouple. Carefully remove used crucible and clean it thoroughly. Insert a fine powder of the grown crystals under investigation in the sample crucible in the right side. The sample is evenly distributed in the bottom of the sample crucible. Take Al_2O_3 , with equal amount in reference crucible in the left. The two thermocouples are wired such as to measure the temperature difference between the sample and the reference material. The absolute temperature is measured with the reference thermocouple. Good thermal contact between the sample and heat-flux sensor is an indispensable requirement for optimum results. Since the test parameters have a significant influence in thermo analytical investigations, the parameters such as calibration, sample preparation, sample weight, reference material, sample chamber temperature, temperature program and atmosphere should be well considered. Calibration of the instrument is a prerequisite for quantitative analysis of STA measurements.

4.5 Dielectric Studies

Every material has a unique set of electrical characteristics, which are dielectric properties, like permittivity, permeability, resistivity, conductivity, etc. A material is classified as “dielectric” if it has the ability to store energy when an external electric field is applied. In other words, materials, which are electric insulators or in which an electric field can be sustained with a minimum dissipation of power, are known as dielectric materials. Simply, dielectrics are insulating materials. In dielectrics all the electrons are bound to their parent molecules and there are no free charges. Even with normal voltage or thermal energy the electrons are not released. Dielectrics are non

metallic materials of high specific resistance and have negative temperature coefficient of resistance. The dielectric characteristics of the material are important to study the lattice dynamics in the crystal. It is important to note that permittivity and permeability are not constant. They can change with frequency, temperature, orientation, mixture, pressure, and molecular structure of the material. Many authors discussed various dielectric properties, dielectric applications and dielectric theories in details [45-49]. Classical theory of dielectric constant was given by Kachhava and Saxena [50]. Also the predecessors of the present author have described the dielectric properties in detail [51-54], therefore, it is avoided in the present thesis.

In the present investigation the dielectric study was carried out by measuring different parameters such as capacitance and dielectric loss of the pressed pellets of samples of known dimension at room temperature on Agilent 4284 A precession Inductance, Capacitance and Resistance (LCR) meter using specially designed sample holder, within the frequency range from 1 kHz to 1 MHz. Figure 4.12 (a) shows the photograph of the set up. The powdered samples were pelletized by using a die of 1 cm diameter and applying 2 tone pressure. The pellets were placed in a suitably design spring-loaded holder. Figure 4.12 (b) describes the design of the sample holder.



Figure : 4.11 (a) Agilent 4284 A precession LCR meter (b) Sample Holder

Dielectric constant (κ) or Relative Permittivity (ϵ_r) : Dielectric constant is defined as the ratio of the capacitance (C) of a capacitor filled with the given material to the capacitance (C_0) of an identical capacitor in a vacuum without the dielectric material. The dielectric constant can also be defined as the ratio of the permittivity of the dielectric material (ϵ) to the permittivity of vacuum (ϵ_0). The dielectric constant, is therefore, also known as the *relative permittivity* (ϵ_r) of the material. Some times it is also referred as the *absolute permittivity*.

$$\text{Dielectric constant, } \kappa = \epsilon_r = \frac{C}{C_0} = \frac{\epsilon}{\epsilon_0} \quad (4.3)$$

Since the dielectric constant is just a ratio of two similar quantities, it is dimensionless and is always greater than 1. It is a measure of polarization in the dielectric material. It denotes a large-scale property of dielectrics without specifying the electrical behaviour on the atomic scale. In the present study dielectric constant was calculated using following formula

$$\text{Dielectric constant, } \kappa = \epsilon_r = \frac{C d}{\epsilon_0 A} \quad (4.4)$$

Where, where C is the capacitance, d is the thickness of the pellet, ϵ_0 is the vacuum dielectric constant (permittivity of free space, $\epsilon_0 = 8.854 \times 10^{-12}$ F/m) and A is the area of the pellet.

Complex Relative Permittivity (ϵ^*) :

Permittivity is determined by the ability of a material to polarize in response to the field, and thereby reduce the total electric field inside the material. Thus, permittivity relates to the ability of material to transmit (or permit) an electric field. The response of normal materials to external fields

generally depends on the frequency of the field. This frequency dependence reflects the fact that the polarization of material does not respond instantaneously to an applied field. The response must always be causal which can be represented by a phase difference. For this reason permittivity is often treated as a complex function. The response of materials to alternating fields is characterized by a complex permittivity,

$$\varepsilon^* = \varepsilon' - j \varepsilon'' = |\varepsilon| e^{-j\delta} \quad (4.5)$$

Where ε' is the real part of the relative permittivity (i.e. the dielectric constant), which is related to the stored energy within the medium; and ε'' is the imaginary part of the relative permittivity, which is related to the dissipation (or loss) of energy within the medium. Equation (4.5) expresses the complex permittivity in two ways, as real and imaginary or as magnitude and phase.

Dielectric Loss : The dielectric loss is a loss of energy which eventually produces a rise in temperature of a dielectric placed in an alternating electrical field. In other words it is a measure of the energy absorbed by dielectric. It is the electrical energy lost as heat in the polarization process in applied AC electric field. The ratio of imaginary part to the real part of the relative permittivity is known as dielectric loss or the dissipation factor D .

$$D = \tan \delta = \frac{\varepsilon''}{\varepsilon'} \quad (4.6)$$

The dissipation factor is measured along with the capacitance at room temperature using the LCR meter.

a. c. Conductivity and a.c. Resistivity :

a.c. conductivity is one of the studies done on solids in order to characterize the bulk resistance of the crystalline sample. The values of a. c. conductivity

and a. c. resistivity were calculated for the different frequencies of the applied electric field using the following formulae,

$$\text{a. c. conductivity, } \sigma_{ac} = \frac{2 \pi f C D d}{A} \quad (4.7)$$

where, f is the frequency, C capacitance, D dissipation factor or dielectric loss or $D = \tan \delta$, d thickness of the pellet and A is the area of the pellet.

$$\text{a. c. resistivity, } \rho_{ac} = \frac{1}{\sigma_{ac}} \quad (4.8)$$

4.6 Micro-hardness Studies

Micro-hardness tests are the simplest, cheapest and non-destructive ones to assess the mechanical properties of materials, which are reviewed in detail by Mott [55]. In the present investigation, Vickers micro-hardness (i.e. micro-indentation hardness) study was carried out and related mechanical properties of the Struvite crystals were assessed. The present author has used Vaiseshika Vickers micro-hardness tester type 7005 for the measurements of Vickers micro-hardness. The details of the micro-hardness study will be discussed elaborately in the chapter VII.

4.7 Etching Studies

Etching is one of the selective tools to identify the defects in the as grown crystals, which is discussed in detail by Sangwal [56]. When the crystal is selectively dissolved in an etchant, the reversal of the growth-taking place by giving a well defined etches pits. The etching time depends on the reactivity of the crystalline material in different etchants. In the present investigation chemical etching study of the struvite crystals with the citric acid was carried out and will be discussed elaborately in the chapter VII.

References

1. D. A. Skoog, F. J. Holler, T. A. Nieman, "*Principles of Instrumental Analysis*", Saunders College Publishing, Philadelphia, (1998).
2. W. C. Roentgen, *Ann. Phys. Chem.*, **64** (1898) 1.
3. W. L. Bragg, *Nature*, **90** (1912) 410.
4. W. L. Bragg, *Proc. Cambridge Philos. Soc.*, **17** (1913) 43.
5. P. Debye, P. Scherrer, *Physik. Z.*, **27** (1917) 277.
6. A. W. Hull, *Phys. Rev. (2)*, **9** (1917) 84.
7. A. W. Hull, *J. Am. Chem. Soc.*, **41** (1919) 1168.
8. H. M. Rietveld, *Acta Cryst.*, **22** (1967) 151.
9. H. M. Rietveld, *J. Appl. Cryst.*, **2** (1969) 65.
10. <http://www.matter.org.uk/diffraction/x-ray/images/powderstatic3.jpg>
11. L. V. Azaroff, M. J. Buerger, "*The Power Method in X-ray Crystallography*", Mc Graw Hill, New York (1958).
12. H. P. Klug, L. E. Alexander, "*X-ray Diffraction Procedures*", 2nd Ed. Wiley, New York (1974).
13. D. Louer, E. Mittemeijer, "*Powder Diffraction in Material Science*", (1967).
14. H. Lipson, H. Steeple, "*Interpretation of X-ray Powder Diffraction Patterns*", Macmillan, New York (1970).
15. <http://www.lcc-toulouse.fr/lcc/IMG/jpg/XPertMPD1-2.jpg>
16. A. A. Christy, Y. Ozaki, V. G. Gregoriou, "*Modern Infrared Fourier Transform Spectroscopy*", Elsevier, New York (2001).
17. A. A. Michelson, *Philos. Mag.*, **31** (1891) 338.
18. A. A. Michelson, *Philos. Mag.*, **34** (1892) 280.
19. A. A. Michelson, *Philos. Mag.*, **45** (1898) 85.

20. J. W. Cooley, J. W. Tukey, *Math. Comput.*, **19** (1965) 297.
21. N. B. Colthup, L. H. Daly, S. E. Wiberley, "*Introduction to Infrared and Raman Spectroscopy*", Academic Press, London (1975).
22. http://en.wikipedia.org/wiki/Infrared_spectroscopy.
23. S. M. Khopkar, "*Basic Concepts of Analytical Chemistry*", Wiley Eastern, New Delhi, (1984).
24. S. I. Gupta, V. Kumar, R. C. Sharma, "*Elements of Spectroscopy*", Pragati Prakashan, Meerut, India (2007).
25. M. J. D. Lon, *Anal. Chem.*, **97A** (1969) 41.
26. <http://www2.chemistry.msu.edu/faculty/reusch/VirtTxtJml/Spectrpy/Images/irspect.gif>.
27. E. G. Brame, J. G. Grasselli, "*Infrared and Raman Spectroscopy*", Vol. 1, Practical Spectroscopy Series, Marcell Decker, New York (1977).
28. <http://chemwiki.ucdavis.edu/@api/deki/files/5122/=2.gif>
29. B. K. Sharma, "*Spectroscopy*", Goel Publ., Meerut, (1997).
30. M. P. Fuller, P. R. Griffiths; *Analy. Chem.*, **50** (1978) 1906.
31. M. P. Fuller, P. R. Griffiths; *Appl. Spectrosc.*, **34** (1980) 533.
32. B. C. Smith, "*Fourier Transform Infrared Spectroscopy*", CRC Press, Boca Raton (1996).
33. J. O. Hill, "*For Better Thermal Analysis*", 3rd Edition, International Confederation for Thermal Analysis, New Castle, Australia (1991).
34. W. W. Wendlandt, "*Thermal Analysis*", Wiley, New York (1985).
35. M. E. Brown, "*Introduction to Thermal Analysis: Techniques and Applications*". Chapman and Hall, New York (1988).
36. P. J. Haines, "*Thermal Methods of Analysis*", Blackie, London (1995).

37. H. Le Chatelier, *Bull. Soc. Fr. Min. Cristallogr.*, **10** (1887) 204.
38. G. Z. Tammann, *Z. Anorg. Chem.*, **37** (1903) 303.
39. N. S. Kurnakov, *Z. Anorg. Chem.*, **42** (1904) 184.
40. H. Saito, "*Thermobalance Analysis*", Technical Book Pub., Tokyo (1962).
41. K. Honda, *Sci. Rep. Tohoku. Univ.*, **4** (1915) 97.
42. W. W. Wendlandt, P. K. Gallagher, "*Brief history of thermal analysis*", In "*Thermal Characterization of Polymeric Materials*", Ed. E. A. Turi, Academic Press, London (1981).
43. E. Watson, M. O'Neill, J. Justin, N. Brenner, *Anal. Chem.*, **36** (1964) 1233.
44. L. Erdey, "*Gravimetric Analysis*", Pergamon Press, New York (1963).
45. H. Frohlic, "*Theory of Dielectrics*", Clarendon Press, Oxford (1949).
46. J. C. Anderson, "*Dielectric*", Chapman and Hall, London (1963).
47. P. J. Harrop, "*Dielectrics*", Butterworth, London (1972).
48. B. Tareev, "*Physics of Dielectric Materials*", Mir Publishers, Moscow (1975).
49. L. Solymar, D. Walsh, "*Lectures on the Electrical Properties of Materials*", Oxford University Press, New York (1984).
50. C. M. Kachhava, S. C. Saxena, *Indian J. Phys.*, **41** (1967) 440.
51. B. B. Parekh, *Ph.D. Thesis*, Saurashtra University, Rajkot (2005).
52. S. R. Suthar, *Ph.D. Thesis*, Saurashtra University, Rajkot (2007).
53. D. J. Dave, *Ph.D. Thesis*, Saurashtra University, Rajkot (2011).
54. K. D. Parikh, *Ph.D. Thesis*, Saurashtra University, Rajkot (2011).
55. B. W. Mott, "*Micro-indentation hardness testing*", Butterworths Scientific Publications, London (1956).
56. K. Sangwal, "*Etching of crystals: Theory, experiment, and application*", Elsevier Science, Amsterdam, North Holland, (1987).

Chapter V

Growth and Characterization of Struvite

Topic Number	Topic	Page Number
5.1	Introduction	203
5.2	Growth of Struvite Crystals	204
5.3	Gel Grown Struvite Crystals and Morphology	207
5.4	Powder X-ray Diffraction Study	217
5.5	FT-IR Spectroscopic Study	219
5.6	Thermal Studies	224
5.7	Dielectric Studies	233
5.8	Conclusions	237

5.1 Introduction

Since there are many advantages of gel growth technique as discussed explicitly earlier in section 3.13 of chapter III, many researchers have used the technique to grow urinary type crystals, such as calcium oxalate [1-5], brushite [6-9], uric acid crystals [10], hydroxyapatite crystals [11], mixed calcium phosphate and calcium oxalate [12].

However, very few attempts were made to grow struvite crystals by gel method [13-16]. Previously, Abbona and Boistelle [17] carried out the study of the growth of struvite crystals by using solution growth technique by mixing equal volumes of equi-molar solutions of $NH_4H_2PO_4$ and $MgSO_4 \cdot 7H_2O$. Whereas, struvite crystals were grown by Iruan and Ramasamy [13] using gel growth technique and the effect of impurities on the morphology of struvite crystals by adding ammonium, lead, barium, cadmium, and calcium ions were reported. Natarajan et al [14] reported the growth of platelet type struvite crystals using gel growth technique. In the present study, the author has grown struvite and related crystals using gel growth technique.

This chapter deals with the growth and characterization of struvite crystals. Struvite crystals were grown by single diffusion gel growth technique in silica hydro gel medium, which provides the simplified *in vitro* model of the highly complex growth of urinary calculi *in vivo*. The grown crystals were characterized by powder XRD, FT-IR, thermal analysis and dielectric study. The kinetic parameters as well as thermodynamic parameters were calculated by applying well known formulae.

5.2 Growth of Struvite Crystals

The single diffusion gel growth technique was used to grow struvite crystals. Distilled water and analytical reagent (AR) grade chemicals were used to grow the struvite crystals. All test tubes and glassware were cleaned as well as autoclaved at 120 °C for 15 min before use. The whole experiment was conducted at the room temperature and process was carried out in the aseptic medium in a laminar flow hood to avoid microbial contaminations.

5.2.1 Preparation of Sodium Meta-silicate Stock Solution

In the present investigation, sodium meta-silicate (SMS) - $\{Na_2SiO_3 \cdot 9H_2O\}$ powder was used for preparation of the gel medium. First of all 200 g SMS powder was added in one liter of double distilled water in a beaker. The mixture was stirred vigorously for 2 h for uniform mixing up using a magnetic stirrer. Thus, a dense milky solution of sodium meta-silicate was formed. It was then kept in undisturbed condition for a couple of days to allow sedimentation so that heavy insoluble impurities could accumulate at the bottom of a beaker. This was decanted into another beaker and filtered twice with Whatman qualitative filter paper of 11 μ m pore size and 12.5 cm diameter (Cat No 1001 125) for high-purity filtration. Then the solution was centrifuged on MSE high-speed centrifuge unit for about half an hour at 10000 revolutions per minute. Practically the solution got rid off all suspended impurities and as a result, transparent, slightly golden colored solution of SMS was obtained. Then, the filtered solution was stored in a light protected glass container with air tight cork so that the solution may not be affected by oxygen and carbon dioxide (usually to avoid absorption of carbon dioxide) in air and light. This is known as stock SMS solution, which could be preserved for quite a long

period. However, the present author has prepared fresh SMS solutions for each set of experimentation.

5.2.2 Preparation of SMS Solution with Definite Specific Gravity

The specific gravity (SG) of the stock SMS solution can be determined by pycnometer, i.e. specific gravity bottle, which is usually made of glass, with a close-fitting ground glass stopper having a capillary tube through it, so that air bubbles may escape from the apparatus. The SMS solution of desired SG was prepared by adding double distilled water of appropriate volume. The SG of each of the SMS solutions was determined by the following formula,

$$\text{Specific Gravity (SG)} = \frac{M_s - M_0}{M_w - M_0} \quad (5.1)$$

Where M_0 = Mass of the empty dry bottle, M_s = Mass of the bottle filled with SMS solution and M_w = Mass of the bottle filled with distilled water.

In the present study, the SG of SMS solutions was selected in the range of 1.04 to 1.08 for the different sets of struvite crystal growth.

5.2.3 Preparation of Gel

Aqueous solutions of Ammonium Dihydrogen Phosphate (ADP) - $\{NH_4H_2PO_4 \cdot 2H_2O\}$ of different concentration were mixed with the SMS solution of definite SG in appropriate amount so that the desired value of the pH could be set for the mixture. Here, during the procedure of adjusting the definite value of pH of the mixture, the SMS solution was added in a drop by drop manner to the ADP solution, with constant stirring to avoid excessive ion concentrations which otherwise cause premature local gelling and make the final medium inhomogeneous. The gel solution of 20 mL was transferred into the test tubes of 140 mm length and 25 mm diameter. In the present study,

the pH value of the mixture was kept in the range of 6.0 to 9.5 for the different sets of struvite crystal growth. It has been noted in chapter III that as polymerization process in the silica hydro gel is pH sensitive, the pore size distribution and hence the gel density varies with pH. It was observed that the time required for gelation was very sensitive to pH. Moreover, it was also noticed that gels of insufficient density take a long time to form and were mechanically unstable. Within 2 days, good quality gels were set in the test tubes for the above selected range of pH values. Here, the silica gel was chosen so that it remains stable and does not react with the diffusing solutions or with the product crystal formed.

5.2.4 Pouring of Supernatant Solution

After the gelation took place, 20 mL supernatant solutions (SS) of aqueous magnesium acetate [$Mg(CH_3COO)_2 \cdot 4H_2O$] with different definite concentration were gently poured on the set gels in test tubes by using pipette without damaging gel surface. Moreover, in order to avoid damage, the supernatant solution was added drop wise with a pipette as well as the drops being allowed to fall on to the side of the test tube wall. All the test tubes were capped with airtight stopples and kept undisturbed.

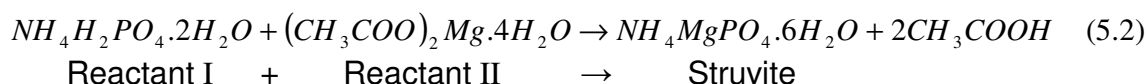
5.2.5 Different Growth Parameters

Different growth conditions, for instance, the SG of SMS solution, the gel pH, the concentrations of reactants, etc., play important role in the growth of crystals. In the present study, different growth parameters were used to grow struvite crystals. Table 5.1 shows the growth parameters of the experiment.

Table : 5.1 : Different Growth Parameters Used to Grow Struvite Crystals

Set No.	SG of SMS Solution	Concentration of ADP (Reactant I) (M)	pH Value of the Gel	Concentration of Supernatant Solution of Magnesium Acetate (Reactant II) (M)
1	1.04	1.0	6.0 to 8.75	1.0
2	1.05	0.5	6.5 to 9.5	1.0
3	1.06	0.5	4.5 to 10.0	1.0
4	1.06	0.75	6.0 to 8.0	0.75
5	1.06	1.0	6.0 to 8.0	1.0
6	1.07	0.5	6.5 to 9.5	1.0
7	1.08	0.5	6.0 to 9.0	1.0
8	1.08	1.5	6.0 to 8.0	1.5
9	1.057	0.25 to 1.0	7.5	1.0

The following reaction is expected to occur in the gel between the two reactants, namely, ADP as a reactant - I present in the gel and magnesium acetate as a reactant - II present in the SS.



As a result struvite crystals were grown in the gel media. The grown struvite crystals were carefully removed from the gel medium. The struvite crystals being sparingly soluble in water, quickly rinsed in distilled water and then dried on a filter paper. The grown crystals were kept in airtight bottles and used for further investigation.

5.3 Gel Grown Struvite Crystals and Morphology

5.3.1 Growth Period

The time involved in the formation as well as growth was found to be depended on the concentrations of the reactants involved. The time taken before crystals were seen with the naked eye varied from a few hours to a few

days. It was found that the growth of the struvite crystals completed within 10 days after the pouring of supernatant solution. It was also found that the struvite crystals grew very rapidly near the gel – liquid interface, which might be due to higher concentration gradients near the interface. Moreover, the crystals at substantial depths from gel - liquid interface were grown more slowly than those near the gel - liquid interface, it might be due to the smaller concentration gradients at higher depths.

5.3.2 Morphology

The external shape of the crystal is known as morphology. Usually, the morphology of the crystals depends on the internal and external factors. The internal factors include internal elements, periodicity and anisotropy of the bonding, which constitutes the crystal structure and dislocations; while the external factors are the growth parameters. In the past, many attempts have been made to correlate the morphological development of crystals with their internal structure. During their growth crystals adopt a variety of habits due to differences in relative growth rates of faces of which the crystals are composed. According to most crystal growth theories, the as grown crystal morphology is dominated by the slow-growing faces because the fast-growing faces may “grow-out” and not be represented in the final crystal habit, however, recently Prywer [18] reported that the morphological importance of faces is not always inversely proportional to their growth rates.

The shape of a crystal is determined by relative rates of deposition of particles on its various faces. However, the general rule is that the faces which grow slowest appear as large developed faces as already mention. However, any factor which causes an alternation in the rate of deposition at

any surface will influence crystal habit. The external factors are usually temperature, supersaturation, solvent, and impurity concentration. The habit of solution grown crystal is affected by solvent / solute interaction at the crystal / solution interface. It is assumed that the solvent affects the habit of crystals through preferential adsorption of solvent molecules on specific crystal faces. Berkovitch Yellin [19] used electrostatic potential maps at the closest approach distances to study the relative polarities of various crystal faces which found to be crucial for predicting various crystal habits.

There are several books available on crystal habits [20-22]. In the present study, the author found that the struvite crystal morphology as well as growth process were strongly dependent on growth parameters. By changing the growth parameters, struvite crystals with different morphologies like prismatic type, pyramidal type, star type, rectangular platelet type, elongated platelet type, needle type, coffin shaped and dendritic type were grown by single diffusion gel growth technique. In most of the cases grown struvite crystals were euhedral or panidiomorphic, i.e., crystals with well developed, sharp, faces (external surfaces). In many cases, it was observed that good quality crystals were eventually grew at higher depths from the gel - liquid interface, i.e., at some lower region of the tube.

Prismatic Type Crystals : Prismatic type struvite crystals with different diaphaneity and diverse apparent size were found in most of the sets put under the growth study. It was noticed that struvite crystals with prismatic morphology usually grown in the pH range of 6.8 to 7.2. However, the good quality transparent prismatic type struvite crystals with optimum apparent size were observed only for the growth parameters as SMS of SG 1.04, 1.0 M

ADP, 1.0 M magnesium acetate as SS with 7.0 pH value of the gel. Though all the crystals were that of prismatic type morphology the number densities of the grown struvite crystals under these growth parameters were found to be less.

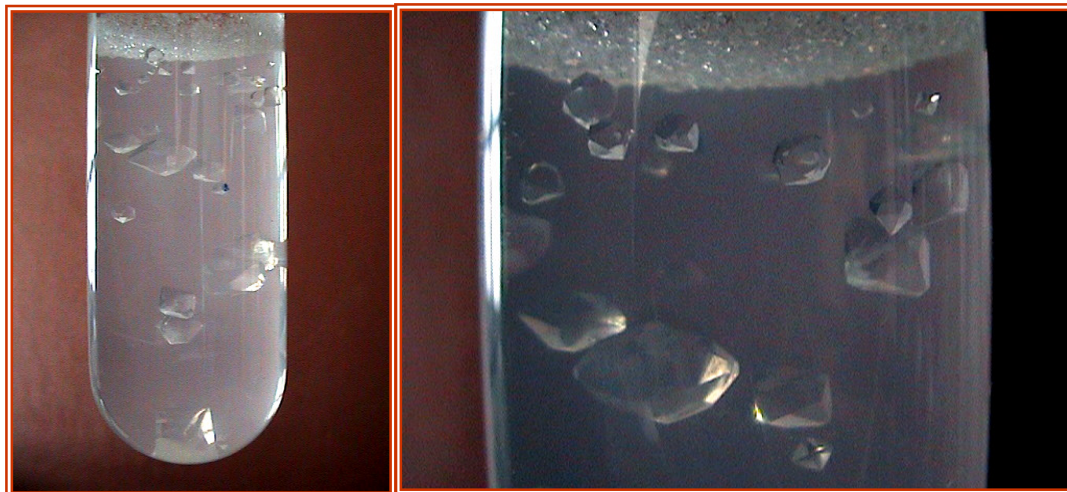


Figure : 5.1 Prismatic Type Struvite Crystals grown in Gel Media



Figure : 5.2 Prismatic Type Struvite Crystals Grown for the Growth Parameters as SMS of SG 1.04, 1.0 M ADP, 1.0 M SS with 7.0 pH Value of the Gel

Figure 5.1 shows prismatic type struvite crystals grown in gel media, and figure 5.2 depicts some of the best prismatic type euhedral struvite crystals.

Pyramidal Type Crystals : Pyramidal type struvite crystals were observed at the bottom of the test tube with the growth parameters as SMS of SG 1.04, 1.0 M ADP, 1.0 M magnesium acetate SS with 7.0 pH value of the gel. It might be due to possible growth in only one direction. Figure 5.3 shows the euhedral pyramidal type struvite crystal.

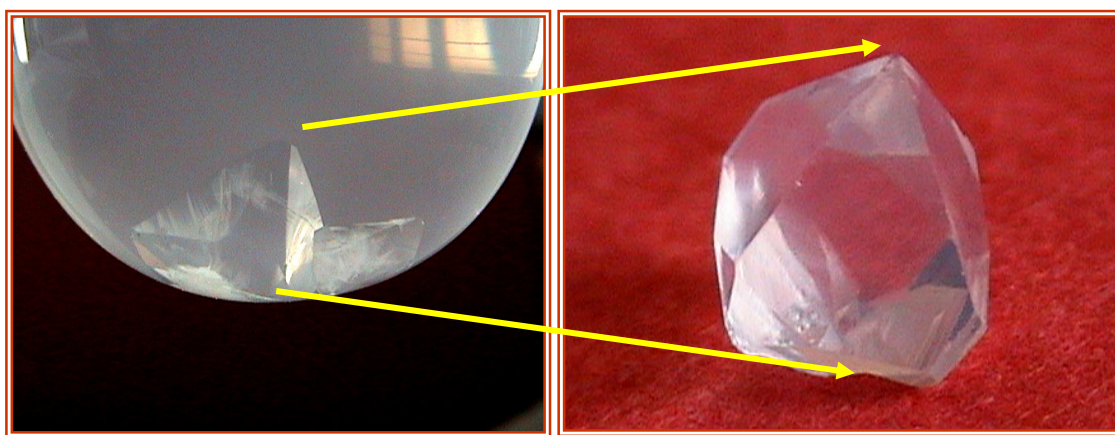


Figure : 5.3 Pyramidal Type Struvite Crystal

Star Type Crystals : Usually star type bunch of poly-crystals were found in the gel at the gel – liquid interface for the pH values of the gel up to 6.8. Figure 5.4 represents star type struvite crystals.

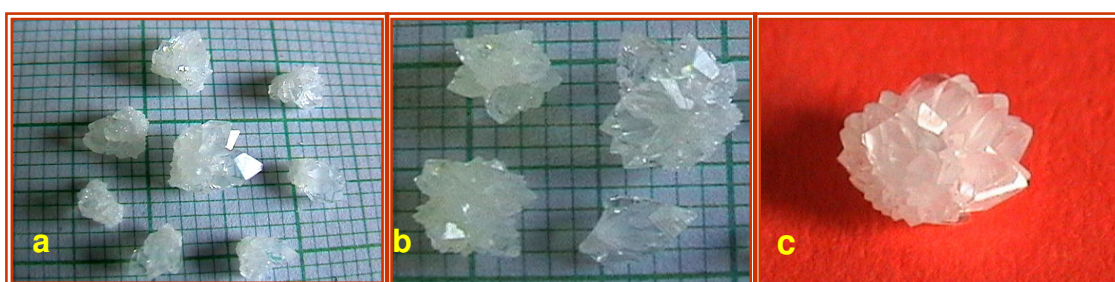


Figure : 5.4 Star type Poly-crystals of Struvite for the Growth Parameters

- (a) SMS of SG 1.06, 0.5M ADP, 1.0 M SS, 4.5 pH value of gel;
- (b) SMS of SG 1.05, 0.5 M ADP, 1.0 M SS, 6.5 pH value of gel; and
- (c) SMS of SG 1.06, 0.75 M ADP, 0.75 M SS, 6.0 pH value of gel

Platelet Type Crystals : Rectangular platelet type struvite crystals were grown for the growth parameters SMS of SG 1.06, 1.0 M ADP, 1.0 M magnesium acetate SS and the pH values of the gel in the range of 6.8 to 7.2 (See figure 5.5). Moreover, these types of crystals were also grown for the SMS of SG 1.06, 0.75 M ADP and 0.75 M magnesium acetate SS in the range of 7.2 to 7.5 pH values of the gels (see figure 5.6). Similar crystals were obtained for SMS of SG 1.08, 1.5 M ADP and 1.0 M SS with 7.5 pH of gel.

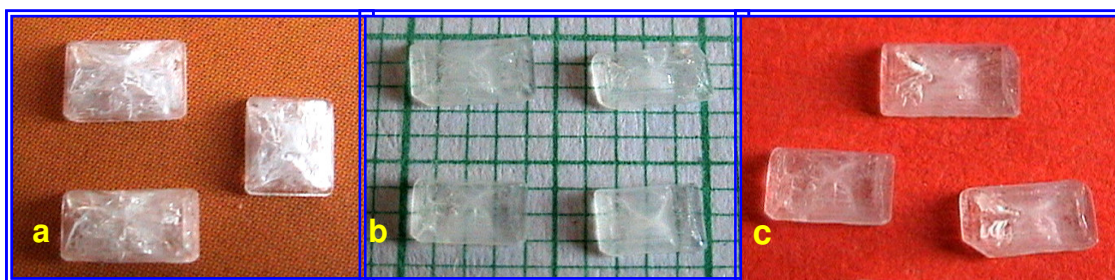


Figure : 5.5 Rectangular Platelet type Struvite Crystals with Growth Parameters SMS of SG 1.06, 1.0 M ADP, 1.0 M SS for (a) 6.8 pH; (b), (c) 7.2 pH values of gel



Figure : 5.6 Rectangular Platelet type Struvite Crystals with Growth Parameters SMS of SG 1.06, 0.75 M ADP, 0.75 M SS for (a) 7.2 pH; (b), (c) 7.5 pH values of gel

Coffin Shaped Crystals :



Figure : 5.7 Coffin Shaped Struvite Crystals for the Growth Parameters (a) and (b) SMS of SG 1.06, 1.0 M ADP, 1.0 M SS for 7.0 pH value of gel; (c) SMS of SG 1.06, 0.75 M ADP, 0.75 M SS for 8.0 pH value of gel

Usually, coffin-lid shaped crystal morphology is found to be a very typical for crystals growing in living animal and human organisms [23,24]. Figure 5.7 illustrates the coffin shaped struvite crystals, which were grown under the growth parameter as SMS of SG 1.06, 1.0 M ADP, 1.0 M magnesium acetate SS for 7.0 pH value of gel and SG 1.06, 0.75 M ADP, 0.75 M magnesium acetate SS for 8.0 pH value of gel.

Dendritic Type Crystals :

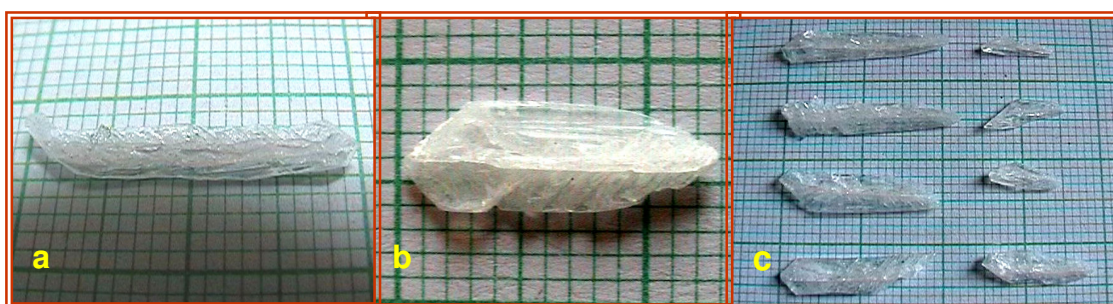


Figure : 5.8 Dendritic Type Struvite Crystals with Growth Parameters

- (a) SMS of SG 1.05, 0.5 M ADP, 1.0 M SS for 7.0 pH value of gel;
- (b) SMS of SG 1.06, 0.75 M ADP, 0.75 M SS for 7.0 pH value of gel; and
- (c) SMS of SG 1.08, 0.5 M ADP, 1.0 M SS for 7.5 pH value of gel



Figure : 5.9 Branched Dendritic type Struvite Crystals with Growth Parameters

- (a) SMS of SG 1.08, 1.5 M ADP, 1.5 M SS for 7.0 pH value of gel;
- (b) SMS of SG 1.06, 1.0 M ADP, 1.0 M SS for 6.8 pH value of gel; and
- (c) SMS of SG 1.06, 0.75 M ADP, 0.75 M SS for 7.2 pH value of gel

Dendritic type struvite crystals were observed in the upper column of the gel (see figure 5.12) in all most all the cases with higher values of gel densities, more precisely, for all the selected higher values of SG between 1.05 to 1.08 and within the pH values of the gel in the range of 6.8 to 7.5 pH. Figure 5.8 shows the feather type dendritic crystals. Some times as shown in

figure 5.9, the X-shape branched dendritic type crystals were also noticed. Also, notice X-shape dendritic crystal in figure 5.12 (b)

Needle Type Crystals : As shown in figure 5.10, the needle type struvite crystals were noticed in the case with growth parameter as SMS solution of SG 1.06, 0.5 M ADP, 10.0 pH value of the gel and SS of 1.0 M magnesium acetate. The apparent lengths of the needles were up to 0.9 cm and thickness up to 0.5 mm.



Figure : 5.10 Needle Type Struvite Crystals with Growth Parameters SMS of SG 1.06, 0.5 M ADP, 1.0 M SS for 10.0 pH value of Gel

It can be noticed that the morphology or habit of growing crystal was dependent on various parameters. Different gel densities and concentration of nutrients allowed the preferential adsorption and growth of different faces in every case, which resulted into different growth morphologies of struvite crystals.

5.3.3 Diaphaneity

The grown struvite crystals had transparent, translucent and opaque diaphaneity, depending upon the location and the growth conditions. It was observed that opaque crystals were grown at gel-liquid interface, whereas more transparent crystals were grown at the higher depth in the gel column. Figure 5.11 demonstrates different diaphaneity of the prismatic type crystals. Crystals of remarkably high optical perfection can be grown for SMS solution

of SG 1.04, 1.0 M ADP solution with 7.0 pH value of the gel and SS of 1 M magnesium acetate.



**Figure : 5.11 Different Diaphaneity of Prismatic Type Struvite Crystals
(a) Transparent, (b) Translucent and (c) Opaque**

It was also noticed that as the pH value of the gel increased, the transparency of the grown crystals decreased. For instance, transparent prismatic type crystals were more frequently observed within the pH range of 6.5 to 7.2, whereas transparency reduced for the higher values of gel pH. In the cases of higher gel pH, the transparent prismatic crystals were also noticed in the gel column at higher depth from the gel - liquid interface. Moreover, the transparency decreased with the increasing concentration of reactant solutions as well as gel density.

5.3.4 Number Density

The number densities of the grown crystals were found to be dependent on the location, concentration of reactants, gel density as well as the pH value of the gel. It was also found that as the pH of the gel increased, the number density of the grown struvite crystals increased. This may be due to high density of gel for higher pH values, which does not allow to supply nutrients readily at the growing crystals but allows large number of local nucleations followed by limited growth of crystals. For instance, figure 5.12 illustrates the photographs of 5th set in which struvite crystals were grown with

the growth parameters as SMS solution of SG 1.06, 1.0 M ADP and SS of 1.0 M magnesium acetate for the different pH values of the gel. It is clear from the figure that very few struvite crystals were grown below 7.0 pH values of the gel. It is also observed that the number density of the grown struvite crystals decreased with increase in the depth of gel column (see figure 5.12). At larger distances from the gel - liquid interface, where the number of crystals growing diminishes, since the prevailing diffusion gradients are smaller, and this is believed to be the principal explanation of the relative crystal scarcity.

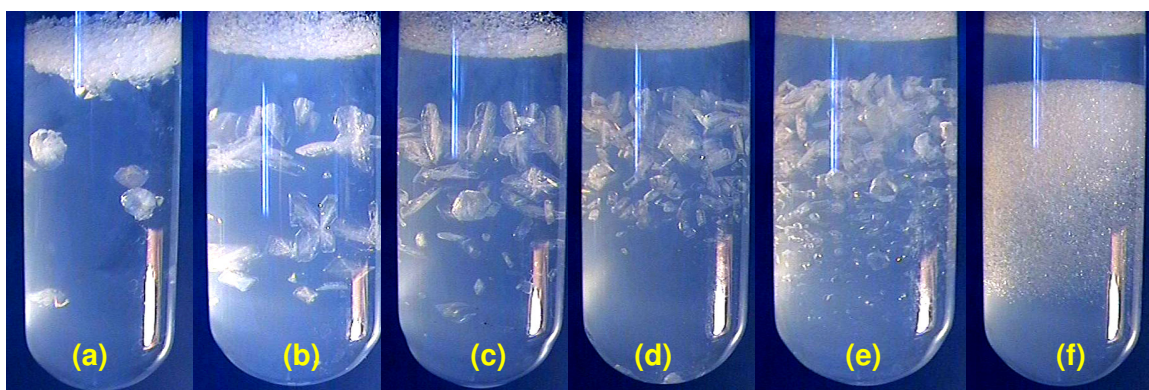


Figure : 5.12 Struvite Crystals Grown in the Gel Media for Growth Parameters as SMS Solution of SG 1.06, 1.0 M ADP and SS of 1.0 M SS with gel pH as (a) 6.0 pH, (b) 6.8 pH, (c) 7.0 pH, (d) 7.2 pH, (e) 7.5 pH and (f) 8.0 pH

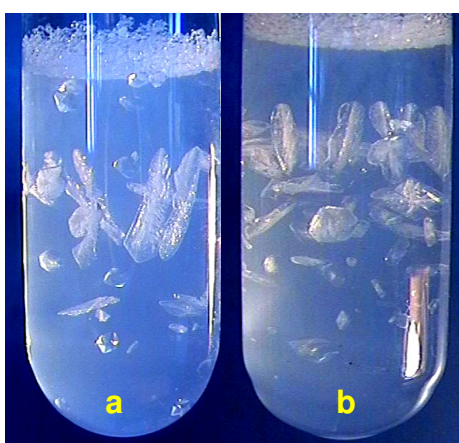


Figure : 5.13 Number Density Increased with Concentration of Reactants (a) SG 1.06, 0.75 M ADP, 0.75 M SS and 7.0 pH value of gel (b) SG 1.06, 1.0 M ADP, 1.0 M SS and 7.0 pH value of gel

The number density of the grown crystals increased with the increasing concentrations of either the reactant - I, i.e., ADP, or the reactant - II, i.e., supernatant solution of magnesium acetate. For example, figure 5.13 shows the comparison of the grown struvite crystals for the cases of the equal growth parameters as SMS of SG 1.06 and 7.0 pH values of gel, while concentration of both the reactants were increased from 0.75 M to 1.0 M and as a result the number density found to be increased.

5.3.5 Apparent Size

The size of the crystals observed during crystal growth experiments in gel medium in glass test tubes does not represent the actual size of crystals due to apparent change in the size introduced by refraction in glass and gel media. The apparent size of the grown struvite crystals was found to be dependent on the location, concentration of reactants, gel density as well as the pH value of the gel. It was observed that the average apparent size of the grown crystals was decreased with increase in the depth of gel column.

5.4 Powder X-ray Diffraction Study

Powder X-ray Diffraction (XRD) is perhaps the most widely used x-ray diffraction technique for characterizing inorganic and organic crystalline materials. As the name suggests, the sample is usually in a powder form, consisting of fine grains of single crystalline material to be studied. The term 'powder' really means that the crystalline domains are randomly oriented in the sample. Therefore, when the 2-D diffraction pattern is recorded, it shows concentric rings of scattering peaks corresponding to the various d - spacings in the crystal lattice. The positions and the intensities of the peaks are used for identifying the underlying structure or phase of the material. The method

has been traditionally used for phase identification, quantitative analysis and the determination of structure imperfections. In recent years, applications have been extended to new areas, such as the determination of crystal structures and the extraction of three-dimensional micro-structural properties. A detailed description of the powder XRD is already mentioned in the section 4.2 of Chapter-IV.

The powder XRD of grown struvite crystals was carried out to identify it as a crystalline material as well as to verify its structure. Figure 5.14 exhibits the powder XRD pattern of gel grown struvite crystals with the assigned planes indicated therein.

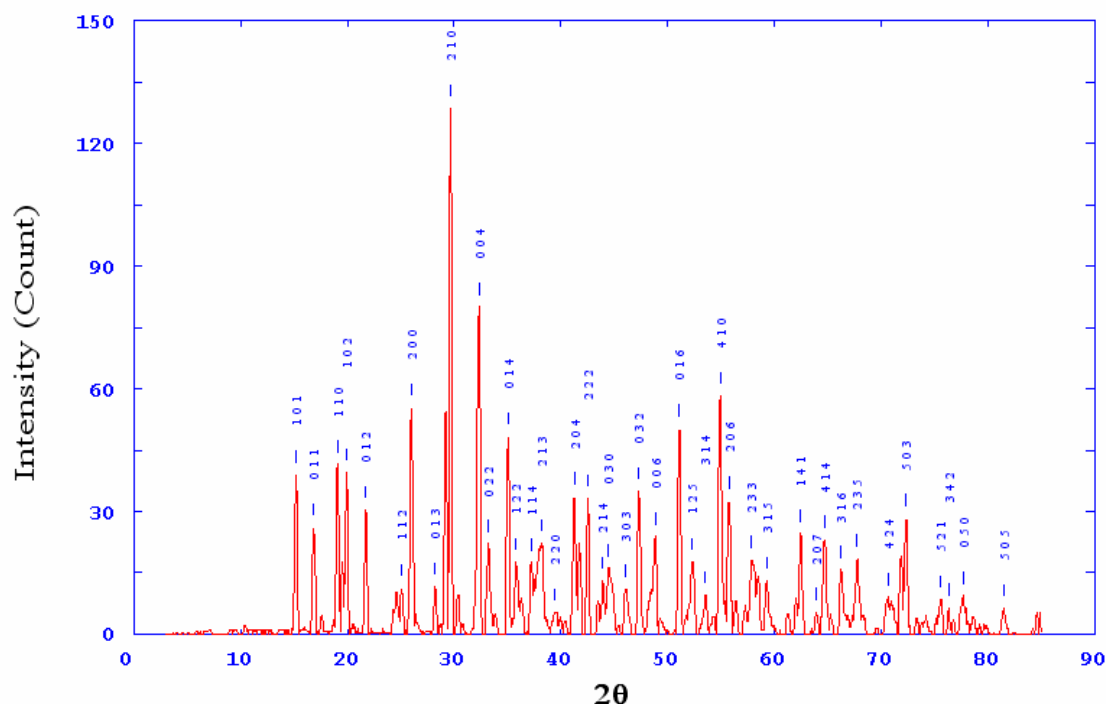


Figure : 5.14 Powder XRD Pattern of Struvite

In the present investigation it has been found that struvite crystallizes in the orthorhombic $Pmn2_1$ space group with unit cell parameters: $a = 6.954 \text{ \AA}$, $b = 6.140 \text{ \AA}$, $c = 11.216 \text{ \AA}$ and $\alpha = \beta = \gamma = 90^\circ$.

Table : 5.2 : Comparison of Unit Cell Parameters of Struvite

Reported by with Reference	Technique Used	Struvite Crystal	Unit Cell Parameters (in Å)		
			a	b	c
J. A. Bland, S. J. Basinski [25]	X-ray Reflection	Struvite found in can of Japanese crab-meat	6.13	6.92	11.19
A. Whitaker, J. W. Jeffery [26]	Single Crystal XRD	Naturally occurring specimen found in a tin of Salmon	6.941	6.137	11.199
F. Abbona, M. Calleri and G. Ivaldi [27]	XRD	Synthetic struvite	6.955	6.142	11.218
G. Ferraris, H. Fuess, W. Joswig [28]	Neutron Diffraction		6.955	6.142	11.218
T. Pi, S. L. García [29]	Powder XRD	Naturally occurring struvite found from Chalco paleolake, Mexico	6.9371	6.1294	11.1988
K. C. Joseph [15]	Powder XRD	Gel grown struvite crystals	6.965	6.166	11.228
Present Author	Powder XRD	Gel grown struvite crystals	6.954	6.140	11.216

From the table 5.2, it is clear that the values are closely matching with those reported previously [15,25-29]. The powder XRD studies confirmed the structural identity of the grown struvite crystals.

5.5 FT-IR Spectroscopic Study

Many common minerals exhibit unique spectra in the mid-infrared range, which extends from 400 cm⁻¹ to 4000 cm⁻¹. FT-IR spectroscopy has been used extensively for the identification of organic and inorganic compounds and the minerals in the urinary tracts and calculi [30-34]. Some studies have been undertaken on newberyite, i.e., $MgHPO_4 \cdot 3H_2O$ [35], and on struvite [36]. Infrared and Raman spectra of struvite were reported by Stefov et al [37]. Recently, FT-IR study of the struvite crystals found from the

Chalco paleolake, Mexico, was carried out by Pi et al [29]. Details of the FT-IR technique are discussed in section 4.3 of chapter IV.

The FT-IR spectrum of the struvite crystals is presented in figure 5.15 and the vibrational band assignments according to literature and experimental data are summarized in table 5.3.

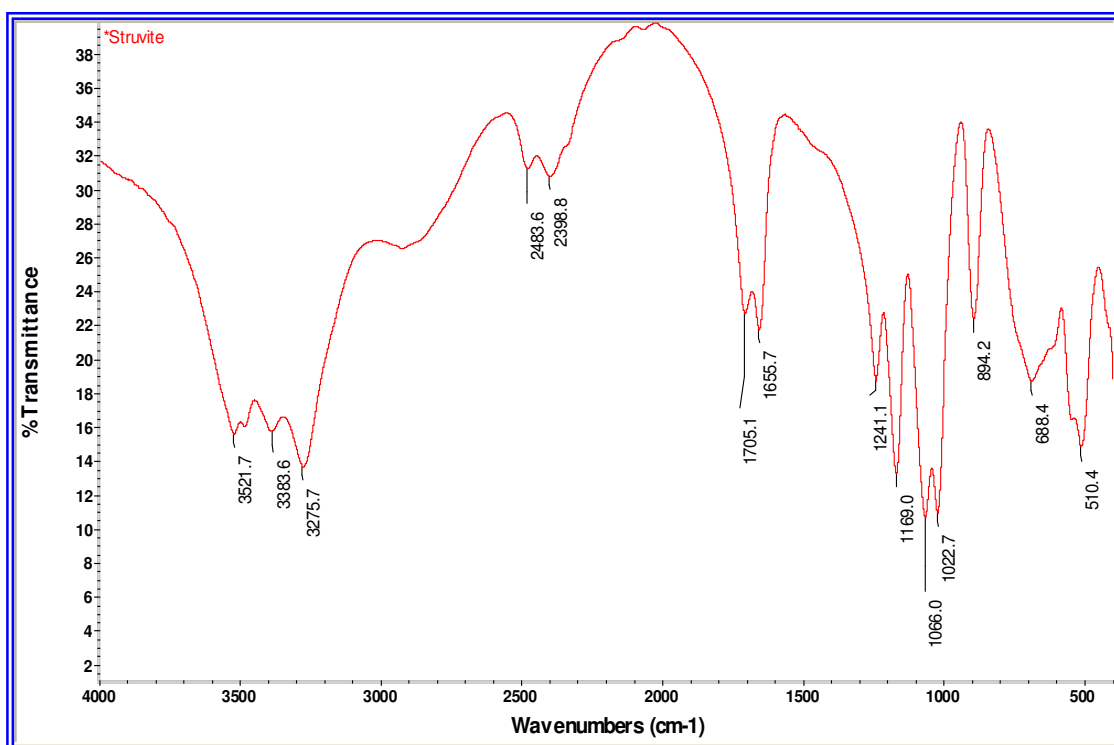


Figure : 5.15 FT-IR Spectrum of Struvite

Struvite has a characteristic FT-IR spectrum, which can be easily recognized even in mixed urinary calculi, since it has distinguishing positions of the absorption bands occurred due to various vibrations such as, water of crystallization, NH_4^+ units, tetrahedral PO_4^{3-} anions units, and metal oxygen bonds [38].

FT-IR spectroscopy provides a sensitive tool for the detection of H_2O molecules, i.e., water of crystallization in minerals and their binding states in a crystal. The FT-IR technique investigates O–H vibrations, whose absorption

bands appear at different frequencies depending on the cations directly linked to the hydroxyls. There are four regions found in the FT-IR spectrum depicting the absorptions due to water of crystallization in struvite as shown in table 5.3, which are closely matched to the previously reported absorptions in several inorganic hydrated compounds [39-46].

Table: 5.3 :Assignments of Absorption Bands in the FT-IR Spectrum of Struvite

Assignments		Reported IR frequencies wavenumbers (cm ⁻¹)	Observed IR frequencies wavenumbers (cm ⁻¹)
Absorption peaks due to water of crystallization	H–O–H stretching vibrations of water crystallization	3280 to 3550 [39-46]	3275.7, 3383.6, 3475, 3521.7
	H–O–H stretching vibrations of cluster of water molecules of crystallization	2060 to 2460 [39-46]	2398.8, 2483.6
	H–O–H bending modes of vibrations	1590 to 1650 [39-46]	1655.7, 1705.1
	Wagging modes of vibration of coordinated water	808 [39-46]	894.2
Absorption peaks due to NH₄⁺ units	ν_1 symmetric stretching vibration of N – H in NH ₄ ⁺ units	2800 to 3000 [47-50]	2921
	ν_2 symmetric bending vibration of N – H in NH ₄ ⁺ units	1630 to 1750 [47-50]	1655.7, 1705.1
	ν_3 asymmetric stretching vibration of N – H in NH ₄ ⁺ units	3130 to 3693 [47-50]	3275.7, 3383.6, 3475, 3521.7
	ν_4 asymmetric bending vibration of N – H in NH ₄ ⁺ units	1390 to 1640 [47-50]	1241.1
Absorption peaks due to PO₄³⁻ units	ν_1 symmetric stretching vibration of PO ₄ ³⁻ units	930 to 995 [51-54]	894.2
	ν_2 symmetric bending vibration of PO ₄ ³⁻ units	404 to 470 [52]	404
	ν_3 asymmetric stretching vibration of PO ₄ ³⁻ units	1017 to 1163 [36,52,54,55]	1022.7, 1066, 1169
	ν_4 asymmetric bending modes	509 to 554	510.4, 562
Metal-Oxygen bonds	Metal-Oxygen bonds	400-650	618, 688.4
	Deformation of OH linked to Mg ²⁺	847	894.2

Intense bands appeared at the 3275.7 cm^{-1} , 3383.6 cm^{-1} , 3475 cm^{-1} and 3521.7 cm^{-1} indicate H–O–H stretching vibrations of water of crystallization. Here, the position of relatively broad band peak at 3275.7 cm^{-1} suggests that the water is strongly hydrogen bonded to the Mg cations. The weak bands appeared at 2398.8 cm^{-1} and 2483.6 cm^{-1} in the spectrum can be assigned due to H–O–H stretching vibrations of cluster of water molecules of crystallization. The medium intense bands appeared at 1655.7 cm^{-1} and 1705.1 cm^{-1} in the spectrum indicate the H–O–H bending modes of vibrations suggesting the presence of water [36]. A medium absorption band at 894.2 cm^{-1} indicates the wagging modes of vibration of the coordinated water and the Metal–Oxygen bond in the complex.

NH_4^+ cation is a tetrahedron having four vibrational modes and all the four appear in FT-IR spectra due to its general position in the crystal. A medium broad band appeared at 2921 cm^{-1} can be attributed to the ν_1 symmetric stretching vibration of N–H in NH_4^+ units. Strong bands observed in the region of 3200 to 3600 cm^{-1} were ascribed to the ν_3 asymmetric stretching vibration of N–H in NH_4^+ units along with H–O–H stretching vibrations of water crystallization. Moreover, medium bands at 1655.7 cm^{-1} and 1705.1 cm^{-1} were due to the ν_2 symmetric bending vibration of N–H in NH_4^+ units overlapping with the H–O–H bending modes of vibrations. A band noticed at 1241.1 cm^{-1} may be assigned to the ν_4 asymmetric bending vibration of N–H in NH_4^+ units. All the bands, appeared due to NH_4^+ cation, are closely matched with the previously reported peaks in several inorganic NH_4^+ containing compounds [47-50].

Vibrational modes of tetrahedral XY_4 molecules are well known [50]. Julien et al [51] had described the vibrational modes of the materials containing PO_4^{3-} anions. In the FT-IR spectrum, the ν_1 symmetric stretching vibration of tetrahedral PO_4^{3-} anions units was found to be at medium band at 894.2 cm^{-1} in case of struvite, which corresponds to the previously reported values for different phosphate minerals as 930 cm^{-1} (augelite), 940 cm^{-1} (wavellite), 970 cm^{-1} (rockbridgeite), 995 cm^{-1} (dufrenite) and 965 cm^{-1} (beraunite) and 964 cm^{-1} (whitlockite) [52-54]. The position of the symmetric stretching vibrations is mainly dependent on the type of mineral, the cation present and crystal structure. While, the positions of the asymmetric stretching vibrations ν_3 of phosphate PO_4^{3-} anion units in struvite were found at the strongest peaks at 1022.7 cm^{-1} , 1066 cm^{-1} and 1169 cm^{-1} , which are in accordance with the values reported earlier [36,52,54,55]. The symmetric bending vibrations ν_2 of PO_4^{3-} units were observed at 404 cm^{-1} , which corresponds to the values reported for various phosphate minerals as 438 cm^{-1} (augelite), 452 cm^{-1} (wavellite), 440 cm^{-1} and 415 cm^{-1} (rockbridgeite), 455 cm^{-1} , 435 cm^{-1} and 415 cm^{-1} (dufrenite), 470 cm^{-1} and 450 cm^{-1} (beraunite), and 431 cm^{-1} (whitlockite) [52]. Moreover, the asymmetric bending vibrations ν_4 of PO_4^{3-} units in struvite were observed at 510.4 cm^{-1} and 562 cm^{-1} . Here, ν_1 and ν_3 involve the symmetric and asymmetric stretching mode of the P–O bonds, whereas ν_2 and ν_4 involve mainly O–P–O symmetric and asymmetric bending mode with a small contribution of P vibration. The absorption peaks at 618 cm^{-1} and 688.4 cm^{-1} ascribe the presence of oxygen-metal bond. Thus, the FT-IR spectrum proves presence of water of hydration, N – H bond, P – O bond, NH_4^+ ion and PO_4^{3-} ion and metal -oxygen bond.

5.6 Thermal Studies

Thermal analysis may help in the identification of the main components of urinary calculi. With the help of thermal analysis one can find the true number of water molecules associated to the urinary calculi, which further helps in the differentiation among the various forms of calcium oxalate such as monohydrate COM or whewellite, dihydrate COD or weddelite, and trihydrate COT. Likewise thermal analysis is also useful for the differentiation of various phosphate type urinary calculi, namely, brushite, struvite, and newberyite.

Several authors attempted to study the thermal properties of urinary type crystals either grown in laboratory [8, 53-57] or surgically removed from patients [58-61]. Moreover, some researchers reported the thermal studies of such minerals as mineralogical aspects [29, 62].

The thermal properties of gel grown brushite were reported by Joshi and Joshi [8], and Madhurambal et al [57], whereas Girija et al [63] reported that of calcium oxalate monohydrate by using the TGA technique. Recently, the thermal properties of gel grown Monosodium Urate Monohydrate (MSUM) [56] and sodium oxalate monohydrate (SOM) crystals [64] are reported. Kohutova et al [58] reported the thermal studies of COM, COD and HA urinary crystals obtained from the patients. Wilson et al reported the thermal analysis of uric acid crystals [59] and calcium phosphate stones [60], which were surgically removed from patients. Nasir [61] reported the thermal analysis of mixed phosphate type urinary calculi. Details of the techniques used for the thermal study are elaborately discussed in section 4.4 of chapter 4.

5.6.1 Thermo-Gravimetric Analysis (TGA)

In the present thermal study, thermo gravimetric analysis (TGA), differential thermal analysis (DTA) and differential scanning calorimetry (DSC) of powdered struvite were carried out simultaneously using Linseis Simultaneous Thermal Analyzer (STA) PT-1600, in the atmosphere of air from 25 °C to 900 °C at a heating rate of 15 °C/min and α -Al₂O₃ as standard reference. TGA, DTA and DSC profiles obtained for the gel grown struvite are as shown by the curves (a), (b) and (c), respectively, in figure 5.16.

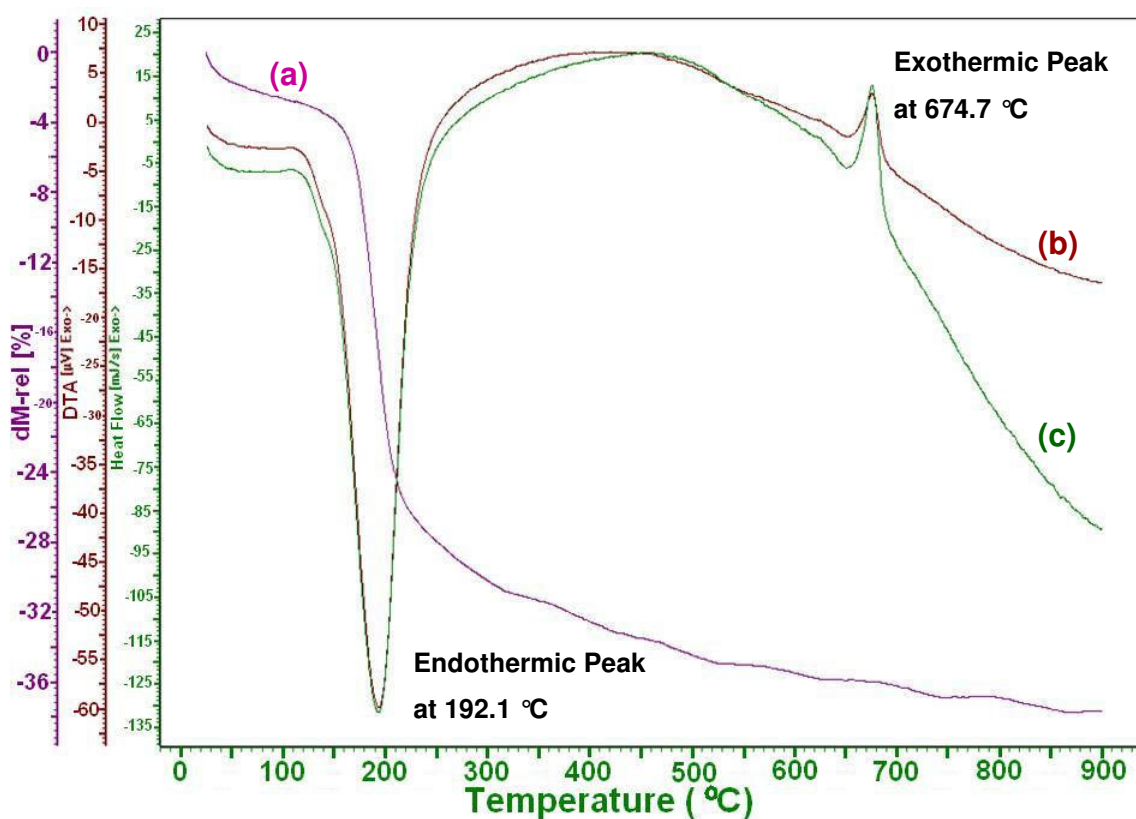


Figure : 5.16 TGA, DTA and DSC Profiles for the Gel Grown Struvite Crystal

The graph of mass loss in mg on the Y-axis plotted versus temperature at a fixed rate of change of temperature in °C, i.e., heating rate, on the X-axis gives the TGA curve (thermo-gram), which is shown as the curve (a) of figure 5.16 for struvite. From the thermo-gram, it is found that just above the room temperature, the crystal has started dehydrating and then decomposing and,

finally, at 900 °C it become 62.4 % of original weight. Total mass loss is found to be 37.6 %, which may be due to the loss of ammonia and water of crystallization. This weight loss corresponds to the following decomposition reaction for struvite :



A continuous loss of mass in the TGA curve can be attributed to the simultaneous dehydration and decomposition of the sample. From the TGA curve one can clearly notice that there must be a simultaneous loss of both NH_3 and H_2O molecules from the struvite structure and also most probably occurs gradually as a function of temperature rather than in distinct steps. Otherwise, double steps would have appeared in the TGA curve. The mass loss in the TGA analysis of sample at temperatures above 100 °C indicates association of water molecules with the struvite structure. From the thermogram, the number of water molecules associated with the crystal was estimated to be 5. The number of water molecules associated with struvite is found 5 instead of 6 from TGA, which may be due to the reasons, such as, (i) Struvite is thermodynamically unstable and starts dehydrating just above the room temperature. (ii) Struvite may loss some of the water molecules during the sample preparation in the powder form, i.e., during the crushing of struvite.

Since the decomposition of struvite starts just above the room temperature, struvite type urinary calculi can be decomposed by prolonged thermal treatment at quite low temperatures.

Table 5.4 indicates the TGA results of struvite crystals along with the theoretically calculated and experimentally obtained percentage weight.

Table : 5.4 : TGA Results of Struvite Crystals

Temperature	Substance	Theoretical weight (%) (Calculated)	Practical weight (%) (from TGA)
Room Temperature	$NH_4MgPO_4 \cdot 5H_2O$ (Struvite)	100	100
900 °C	0.05 [$MgHPO_4$] + 0.95 [NH_4MgPO_4] i.e. 5 % dehydrated newberyite + 95 % dehydrated struvite	60.03	62.4

The thermal decomposition of struvite has been found to be dependent upon the conditions of decomposition. It was found different in nitrogen or in a moist atmosphere. Previously Frost et al [36] reported the total mass loss of 42 % for struvite, but it was conducted in a flowing nitrogen atmosphere, instead of atmosphere of air, at a heating rate of 1 °C/min. Recently, it was reported by two different groups of researchers, namely Bhuiyan et al [65] and Pi et al [29], that the decomposition of struvite was found to be dependent on the rate of heating. Bhuiyan et al [65] also reported that struvite was ultimately transformed into amorphous magnesium hydrogen phosphate $MgHPO_4$ after the gradual loss of ammonia and water molecules. On the contrary Sarkar et al [66] reported that both newberyite and struvite formed when the thermally treated struvite samples were re-hydrated at room temperature in excess water. Based on these experiments, it could be predicted that upon rehydration, struvite would only form if some amount of NH_3 molecules were still present in the structure after dehydration and decomposition. Here, the formation of both struvite and newberyite in a rehydrated sample shows the complex character of thermally amorphized struvite which is probably biphasic.

5.6.2 Differential Thermal Analysis (DTA)

The plot of DTA signal, i.e. differential thermocouple output in micro volts on the Y-axis versus the sample temperature in °C on the X-axis, is as shown by curve (b) in figure 5.16. The transition temperatures were measured precisely using DTA curve. In the DTA curve a very strong endothermic peak was observed at 192.1 °C, which might be due to release of crystalline water along with ammonia. Processes involving a loss of mass usually give rise to endothermic nature in DTA trace because of the work of expansion. During this endothermic process, the amount of heat change was found to be 428.71 $\mu\text{Vs/mg}$. In the DTA curve one medium exothermic peak was also observed at 674.7 °C, which might be due to high temperature phase transition. During this exothermic process, the amount of heat change was found to be $-22 \mu\text{Vs/mg}$.

5.6.3 Differential Scanning Calorimetry (DSC)

In DSC the heat flow was measured during the course of experiment. The plot of heat flow in mJ / s on the Y-axis versus temperature at a fixed rate of change of temperature in °C on the X-axis is as shown by curve (c) in figure 5.16. The DSC curve has similar profiles, verifying the endothermic and exothermic transitions, in agreement with the DTA and TGA results. The endothermic transition refers to thermal dehydration and decomposition of struvite, whereas the exothermic transitions probably correspond to high temperature phase transition of struvite. In the thermo-gram, no remarkable change was observed for the peak which was noticed at 674.7 °C in DTA and DSC curves due to the possible phase transition, since no significant change took place in the mass of the specimen. DSC technique is not only sensitive

for the determination of enthalpy, but it is also very sensitive for the determination of heat capacities.

From the available computer software, namely, TA-WIN and WIN-STA used for thermal analysis provided with the set up STA PT-1600, various thermodynamic parameters were calculated, i.e., the enthalpy, specific heat capacity, amount of heat change, and heat flow rate. The values of these parameters are tabulated in table 5.5.

Table : 5.5 : Thermodynamic Parameters of Struvite

Reaction	Peak Temperature T	Enthalpy ΔH	Specific Heat Capacity ΔC_p	Amount of Heat Change	Heat Flow Rate
Unit →	°C	J / g	J / g °C	μVs/mg	mJ / s
Endothermic Reaction	192.1	950.62	0.72	428.71	131.51
Exothermic Reaction	674.7	- 88.49	1.59	- 22.01	- 13.14

(Note : According to the general convention the plus and minus symbols just indicate the direction of heat flow; they do not imply positive or negative energy)

5.6.4 Kinetic Parameters of Dehydration and Decomposition

The use of thermo-gravimetric data to evaluate the kinetic parameters of solid-state reactions involving weight loss has been investigated by many workers [67-69]. Usually, the kinetic parameters can be evaluated from the TGA curve by applying several equations [67-69], which were proposed by different authors on the basis of different assumptions to the kinetics of the reaction and the Arrhenius law. These equations are (i) Coats and Redfern Relation [67], (ii) Horowitz and Metzger Relation [68] and (iii) Freeman - Carroll Relation [69]. However, in the present investigation, the Coats and Redfern relation is used because it facilitates not only to evaluate the

activation energy and order of reaction but also the frequency factor. It also helps to evaluate the thermodynamic parameters further. The Coats and Redfern relation is as follows :

$$\log_{10} \left(\frac{1 - (1 - \alpha)^{1-n}}{T^2(1-n)} \right) = \left\{ \log_{10} \left(\frac{AR}{aE} \right) \left(1 - \frac{2RT}{E} \right) \right\} - \left\{ \frac{E}{2.3RT} \right\} \quad (5.4)$$

where, α is the fraction of original substance decomposed at time t , that is, $\alpha = (W_o - W) / (W_o - W_f)$; W_o is the initial weight, W is the weight at time t , W_f is the final weight; E is the activation energy of the reaction, A is the frequency factor, a is the heating rate in K/min, R is the gas constant, n is the order of reaction and T is the absolute temperature. Here, it should be noted that the equation (5.4) is valid for all values of n except $n = 1$.

The plots of $Y = -\log_{10} [\{1 - (1 - \alpha)^{1-n}\} / \{T^2(1-n)\}]$ versus $X = 1/T$, were straight lines for different values of n , however, the best linear fit plot gives the correct value of n . The value of activation energy is obtained from the slope of the best linear fit plot. Figure 5.17 shows the Coats and Redfern plot. The values of activation energy E , frequency factor A and order of reaction n are as tabulated in table 5.6.

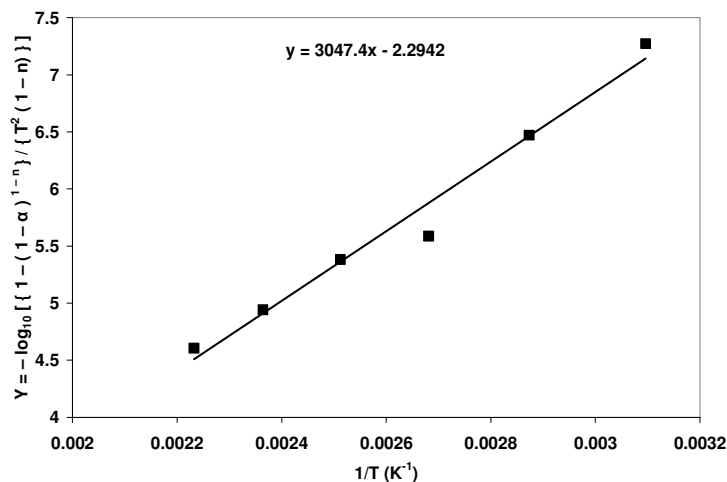


Figure : 5.17 Coats and Redfern Plot

Table : 5.6 : Kinetic Parameters of Dehydration and Decomposition of Struvite

Kinetic Parameters	Symbol	Value
Activation Energy	E	58.35 kJ Mol ⁻¹
Frequency Factor	A	2.289 x 10 ⁷
Order of Reaction	n	2

5.6.5 Thermodynamic Parameters of Dehydration and Decomposition

Various thermodynamic parameters were calculated by applying well known formulae, as described in detail by Laidler [70]. The standard entropy of activation $\Delta^\ddagger S^\circ$ (here, superscript \ddagger is for activation and superscript $^\circ$ is for standard), i.e. entropy change associated with the activation reaction, can be calculated by the formula,

$$\Delta^\ddagger S^\circ = 2.303 \times R \times \log_{10} \left(\frac{A h}{k T_m} \right) \quad (5.5)$$

where, A is the frequency factor, k Boltzmann constant, h Plank's constant, R gas constant, T_m absolute temperature in K.

The standard enthalpy of activation $\Delta^\ddagger H^\circ$ can be calculated by the formula,

$$\Delta^\ddagger H^\circ = E - 2RT \quad (5.6)$$

Enthalpy is a state function whose absolute value cannot be known. $\Delta^\ddagger H^\circ$ can be ascertained, either by direct method or indirectly. An increase in the enthalpy of a system, for which $\Delta^\ddagger H^\circ$ is positive, is referred to as an endothermic process. Conversely, loss of heat from a system, for which $\Delta^\ddagger H^\circ$ has a negative value, is referred to as an exothermic process.

The standard Gibbs energy difference between the transition state of a reaction and the ground state of the reactants is known as standard Gibbs energy of activation. The standard Gibbs energy of activation $\Delta^\ddagger G^\circ$ can be calculated by

$$\Delta^{\ddagger}G^{\circ} = \Delta^{\ddagger}H^{\circ} - T \Delta^{\ddagger}S^{\circ} \quad (5.7)$$

The standard change in internal energy of activation $\Delta^{\ddagger}U^{\circ}$ can be calculated by the following formula

$$\Delta^{\ddagger}U^{\circ} = E - RT \quad (5.8)$$

Table 5.7 gives the values of different thermodynamic parameters of dehydration and decomposition calculated at 398 K temperature.

Table : 5.7 : Thermodynamic Parameters of Dehydration and Decomposition

Thermodynamic Parameters	Symbol	Value
Standard Entropy of activation	$\Delta^{\ddagger}S^{\circ}$	$-106.43 \text{ J Mol}^{-1} \text{ K}^{-1}$
Standard Enthalpy of activation	$\Delta^{\ddagger}H^{\circ}$	$51.73 \text{ kJ Mol}^{-1}$
Standard Gibbs Energy of activation	$\Delta^{\ddagger}G^{\circ}$	$94.09 \text{ kJ Mol}^{-1}$
Standard Internal Energy of activation	$\Delta^{\ddagger}U^{\circ}$	$55.04 \text{ kJ Mol}^{-1}$

Here, negative value of $\Delta^{\ddagger}S^{\circ}$ shows that the process is non-spontaneous, whereas the positive value of $\Delta^{\ddagger}H^{\circ}$ shows that the enthalpy is increasing during the process and such process is an endothermic process. Positive value of $\Delta^{\ddagger}G^{\circ}$ shows that the struvite is thermodynamically unstable.

The enthalpy involved in the thermal dehydration and decomposition process obtained by the Coats and Redfern integration method do not correspond to the value given in table 5.5 obtained from DSC curve, which can be ascribed to certain reasons, such as, (i) the different mathematical treatments involved in both the methods, (ii) the value obtained by the Coats and Redfern method is molar enthalpy, i.e., in the units of kJ / Mol, whereas the value obtained from DSC curve is in the units of J / g. (iii) in Coats and Redfern method, the value of enthalpy is calculated from the best linear fit obtained in C. R. plot, i.e., at 398 K temperature, which is just onset

temperature of dehydration and decomposition process. Whereas in DSC method, the value of enthalpy is calculated at maximum reaction rate, i.e., at the peak of a DSC curve, which is 192 C (465 K) for dehydration and decomposition process of struvite, (iv) the programmed heating rates are generally assumed to be the actual heating rates, whereas, in reality, this may not be the case as there are many factors that would change the actual heating rates of nonisothermal thermograms.

5.7 Dielectric Studies

The value of dielectric constant (κ) of a material is usually composed of four contributions; which are from electronic, ionic, dipolar and space charge polarizations. However, all these may be active in low frequency region. The nature of variation of dielectric constant with frequency indicates which contribution is prevailing. The space - charge contribution depends on the purity and perfection of crystal. The dipolar orientational effect can be sometimes seen upto 10^{10} Hz. The ionic and electronic polarizations always exist below 10^{13} Hz [71].

Microwaves play a vital role in the diagnosis and treatment of diseases caused by the abnormal mineralization of biological fluids in human body. The first hand information regarding the dielectric behavior of these minerals facilitates to detect the relevant crystals. Issac Paul et al [72] reported a comparative study of the dielectric properties of urinary crystals grown *in vitro* by gel technique with natural stones procured from patients who had undergone stone removal surgery.

Every material has a unique set of electrical characteristics that are dependent on its dielectric properties. The dielectric constant was calculated

from the value of the capacitance of the sample using standard formula given by equation (4.4) in chapter IV.

Figure 5.18 shows the variations in the dielectric constant and dielectric loss with the frequency of applied field at room temperature. The value of dielectric constant for 1 kHz frequency was found as 75.8, which was finally reduced to 53.1 at 1 MHz frequency of applied field. It was noticed for struvite that the dielectric constant decreased with the increasing value of frequency of applied field. This may be due to dipoles do not comply with the rapidly varying electric field.

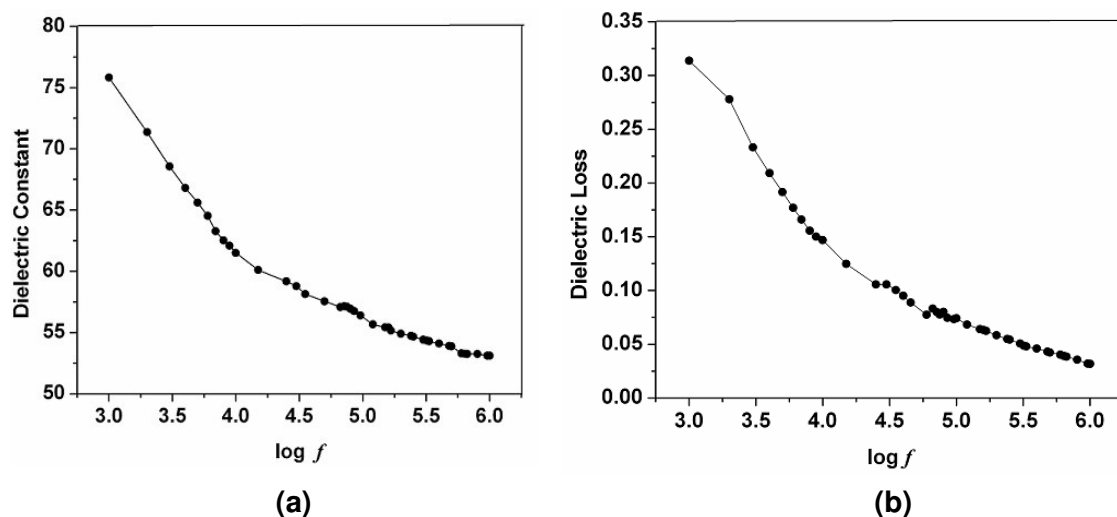


**Figure : 5.18 (a) Variation in Dielectric constant with Frequency of Applied Field
(b) Variation in Dielectric Loss with Frequency of Applied Field**

From figure 5.18 (a) one can conjecture that the space charge polarization is active in low frequency region, which is also reflected further in terms of rapid decrease in the value of dielectric constant with increase in frequency and its higher values in the low frequency region. This type of behaviour is observed in calcium pyrophosphate tetrahydrate [73], L-alanine doped KDP [74], bis-thiourea strontium chloride [75], zinc tartrate [76], and strontium tartrate [77] crystals. It was observed that the value of dielectric loss also decreased with the increasing value of frequency of applied field.

The a.c. conductivity (σ_{ac}) and a.c. resistivity (ρ_{ac}) were evaluated using well known formula as depicted by equation (4.7) and (4.8) in chapter IV. Figure 5.19 shows the nature of variation of a.c. conductivity and a.c. resistivity with frequency of applied field. It was found that a.c. conductivity increased whereas the a.c. resistivity decreased with the increasing value of frequency of applied field.

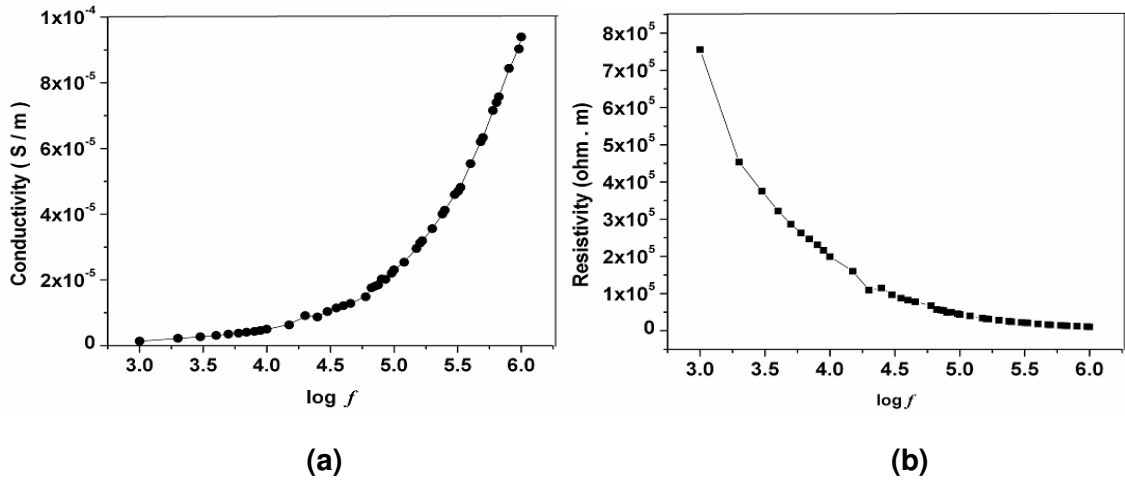


**Figure : 5.19 (a) Variation in a.c. Conductivity with Frequency of Applied Field
(b) Variation in a.c. Resistivity with Frequency of Applied Field**

In case of measuring conductivity at different frequency of applied field, i.e., $\omega = 2 \pi f$, the response that characterizes a variety of materials with various chemical compositions, either crystalline or amorphous, can be written as Jonscher's dynamical law :

$$\sigma(\omega, T) = \sigma_{DC}(T) + a(T) \omega^n \quad (5.9)$$

where, $\sigma_{DC}(T)$ is the direct current (or static, $\omega = 0$) conductivity, $a(T)$ is a factor that depends on temperature but not on ω , and n is an exponent in the range $0.6 \leq n \leq 1$. This equation predicts that at certain frequency if σ_{DC} is much less than the second term, then $\sigma(\omega, T) \propto \omega^n$, and as a result a plot of $\log \sigma$ versus $\log \omega$ describes a straight line with slope n . Whereas in the

case of σ_{DC} is larger than the second term, for example, by increasing temperature, the $\sigma(\omega, T) \propto \sigma_{DC}(T)$, in which the a.c. method renders a measurement of σ_{DC} and plot of $\log \sigma$ versus $\log \omega$ gives a horizontal straight line. This technique has been applied by Ortiz-Lopez and Gomez-Aguilar [79] for polycrystalline and amorphous C_{60} . Figure 5.20 depicts a plot of $\log \sigma$ versus $\log \omega$, which is a straight line with slope $n = 0.6297$.

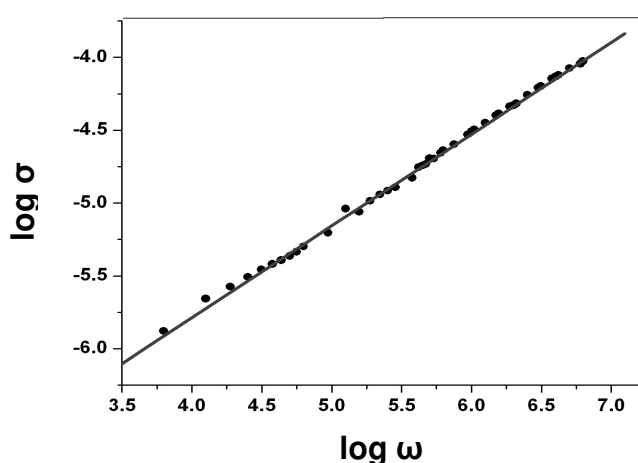


Figure : 5.20 Plot of $\log \sigma$ versus $\log \omega$

From the complex a. c. impedance spectra, Park [80] observed the impedance consisting of two regions for measuring frequency; for high frequency the proton migration in the bulk, while the low frequency region may be due to the charge transport at the surface.

Chen et al [81] studied a. c. impedance data as a function of frequency in the temperature range 40°C to 150°C . The frequency dependence of conductivity followed Jonscher's dynamical law. The obtained values of the exponent n decreased from 1 to 0.25 as temperature increased. The electrical conduction at low temperatures below 70°C is attributed to the hopping of proton on O–H–O hydrogen bonds among hydrogen vacancies. At

temperatures between 70°C to 97°C, additional defects are created by breaking the stronger hydrogen bond in ammonium groups. While above 97°C, ammonium ions in the crystal were proposed to have the contribution to the electrical conduction.

In the present study as it has been mentioned earlier, section 1.4 of Chapter I, that in struvite structure PO_4 tetrahedron, $\text{Mg.6H}_2\text{O}$ octahedron and NH_4 groups connected together by hydrogen bonding, the electrical conduction is expected to occur due to hopping of protons through hydrogen bondings through hydrogen vacancies.

5.8 Conclusions

1. Struvite crystals can be grown by single diffusion gel growth technique.
2. Growth conditions, i.e., the SG of SMS solution, gel pH, the concentrations of reactants, etc., play important role in the growth of crystals.
3. The crystal morphology of struvite was strongly dependent on growth parameters. By changing the growth parameters, struvite crystals with different morphologies like prismatic type, pyramidal type, star type, rectangular platelet type, elongated platelet type, needle type, coffin-lid shaped and dendritic type can be grown.
4. The grown struvite crystals had transparent, translucent and opaque diaphaneity, depending upon the location and the growth conditions.
5. Fine transparent prismatic type struvite crystals with optimum apparent size were observed only for the growth parameters as SMS of SG 1.04, 1.0 M ADP, 1.0 M magnesium acetate as SS with 7.0 pH value of the gel.
6. The powder XRD studies confirmed the structural identity of the grown struvite crystals. Struvite crystallized in the orthorhombic $\text{Pmn}2_1$ space

group with unit cell parameters as, $a = 6.954 \text{ \AA}$, $b = 6.140 \text{ \AA}$, $c = 11.216 \text{ \AA}$ and $\alpha = \beta = \gamma = 90^\circ$, which are closely matching with previously reported values. Every unit cell comprises of two molecules.

7. FT-IR spectrum of the struvite crystals revealed the presence of functional groups. The spectrum confirmed the presence of water of hydration, N – H bond, P – O bond, NH_4^+ ion and PO_4^{3-} ion and metal -oxygen bond.
8. The struvite crystals were found to be thermally unstable. From the TGA curve, it was found that just above the room temperature, the crystal started dehydrating and then decomposing and, finally, at 900°C it became 62.4 % of original weight, which may be due to the simultaneous loss of ammonia and water of crystallization. From the TGA, the number of water molecules associated with the crystal was estimated to be 5, which may be due to unstable nature of struvite and loss some of the water molecules during the sample preparation in the powder form, i.e., during the crushing of struvite.
9. In the DTA curve two remarkable peaks were observed. A very strong endothermic peak observed at 192.1°C attributed to release of crystalline water along with ammonia and the amount of heat change was found to be 428.31 \mu Vs/mg during this endothermic process. A medium exothermic peak observed at 674.7°C attributed to high temperature phase transition and the amount of heat change was found to be -22 \mu Vs/mg .
10. The DSC curve exhibited peaks at the same temperatures as peaks were obtained in DTA curve. In the thermo-gram, no remarkable change was noticed for the peak noticed at 674.7°C in DTA and DSC curves.

- 11.** By applying the Coats and Redfern relation to the dehydration along with decomposition stage, the values of kinetic parameters were calculated. The values of activation energy E , frequency factor A and order of reaction n were found to be $58.35 \text{ kJ Mol}^{-1}$, 2.289×10^7 and 2, respectively.
- 12.** The thermodynamic parameters for the dehydration and decomposition process were also evaluated. The values of standard entropy, standard enthalpy, standard gibbs energy and standard change in internal energy of activation were found to be $-106.43 \text{ J Mol}^{-1} \text{ K}^{-1}$, $51.73 \text{ kJ Mol}^{-1}$, $94.09 \text{ kJ Mol}^{-1}$ and $55.04 \text{ kJ Mol}^{-1}$, respectively.
- 13.** For struvite, the dielectric constant as well as dielectric loss was found to be dependent on the frequency of applied field at room temperature. It was noticed both the dielectric constant and dielectric loss were found to be decreased with the increasing value of frequency of applied field.
- 14.** It was found that a. c. conductivity increased whereas the a. c. resistivity decreased with the increasing value of frequency of applied field. The a. c. conductivity is expected due to the hopping of protons through vacancies in hydrogen bondings.

References

1. S. Bisailon, R. Tawashi, *J. Pharm. Sci.*, **64** (1975) 458.
2. V. S. Joshi, *Ph.D. Thesis*, Saurashtra University, Rajkot (2001).
3. V. S. Joshi, B. B. Parekh, M. J. Joshi, A. B. Vaidya, *J. Cryst. Growth*, **275** (2005) e1403.
4. E. V. Petrova, N. V. Gvozdev, L. N. Rashkovich, *J. Optoelectron. Adv. Mater.*, **6** (2004) 261.
5. D. Valarmathi, L. Abraham, S. Gunasekaran, *Indian J. Pure Appl. Phys.*, **48** (2010) 36.
6. T. Iruan, S. N. Kalkura, D. Arivuoli, P. Ramasamy, *J. Cryst. Growth*, **130** (1993) 217.
7. N. Srinivasan, S. Natarajan, *Indian J. Phys.*, **70B** (1996) 563.
8. V. S. Joshi, M. J. Joshi, *Cryst. Res. Technol.*, **38** (2003) 817.
9. B. B. Parekh, *Ph.D. Thesis*, Saurashtra University, Rajkot (2005).
10. S. N. Kalkura, V. K. Vaidyan, M. Kanakavel, P. Ramasamy, *J. Cryst. Growth*, **132** (1993) 617.
11. M. Ashok, N. M. Sundaram, S. N. Kalkura, *Mater.Lett.*, **57** (2003) 2066.
12. R. Vani, E. K. Girija, M. Palanichamy, S. N. Kalkura, *Mater. Sci. Eng.: C*, **29** (2009) 1227.
13. T. Iruan, D. Arivuoli, P. Ramasamy, *Cryst. Res. Technol.*, **25**(1990)K104.
14. S. Natarajan, E. Ramachandran, D. Suja, *Cryst. Res. Technol.*, **32**(1997)553.
15. K. C. Joseph, *Ph. D. Thesis*, Saurashtra University, Rajkot (2005).
16. P. Sundaramoorthi, S. Kalainathan, *Asian J. Chem.*, **19** (2007) 2783.
17. F. Abbona, R. Boistelle, *Cryst. Res. Technol.*, **20** (1985) 133.
18. J. Prywer, *Prog. Cryst. Growth Charact. Mater.*, **50** (2005) 1.

19. Z. Berkovitch-Yellin, *J. Am. Chem. Soc.*, **107** (1985) 8239.
20. I. Kostov, R. I. Kostov, "*Crystal Habit of Minerals*", Academy Publishing House and Pensoft Publishing (Bulg. Academic Monogr. 1), Sofia (1999).
21. I. Sunagawa, "*Crystals : Growth, Morphology, and Perfection*", Cambridge University Press, Cambridge (2005).
22. R. V. Gaines, H. C. W. Skinner, E. E. Foord, B. Mason, A. Rosenzweig, V. T. King, E. Dowty, "*Dana's New Mineralogy*", 8th Edition, John Wiley & Sons, New York (1997).
23. M. A. Dominick, M. R. White, T. P. Sanderson, T. V. Vleet, S. M. Cohen, L. E. Arnold, M. Cano, S. T. Gregg, J. D. Moehlenkamp, C. R. Waites, B. E. Schillin, *Toxicol. Pathol.*, **34** (2006) 903.
24. A. Wierzbicki, J. D. Sallis, E. D. Stevens, M. Smith, C. S. Sikes, *Calcif. Tissue Int.*, **61** (1997) 216.
25. J. A. Bland, S. J. Basinski, *Nature*, **183** (1959) 1385.
26. A. Whitaker, J. W. Jeffery, *Acta Cryst.*, **B26** (1970) 1429.
27. F. Abbona, M. Calleri, G. Ivaldi, *Acta Cryst.*, **B40** (1984) 223.
28. G. Ferraris, H. Fuess, W. Joswig, *Acta Cryst.*, **B42** (1986) 253.
29. T. Pi, S. L. García, M. C. Miranda, B. O. Guerrero, P. Roy, *Revista Mexicana de Ciencias Geológicas*, **27** (2010) 573.
30. M. Daudon, M. Protat, R. Reveillaud, H. Boyer, *Kidney Int.*, **23** (1983) 842.
31. A. Hesse, D. Bach, "*Stone analysis by infrared spectroscopy*", In "*Urinary Stones: Clinical and Laboratory Aspects*", Ed. R. G. Alan, University Park Press, Baltimore (1982).
32. B. Soptrajanov, G. Jovanovski, I. Kuzmanovski, V. Stefov, *Spectrosc. Lett.*, **31** (1998) 1191.

33. B. Soptrajanov, I. Kuzmanovski, V. Stefov, G. Jovanovski, *Spectrosc. Lett.*, **32** (1999) 703.
34. M. Volmer, J. C. De Vries, H. Goldschmidt, *Clin. Chem.*, **47** (2001) 1287.
35. F. A. Miller, G. L. Carlson, F. F. Bentley, W. H. Jones, *Spectrochim. Acta*, **16** (1960) 135.
36. R. L. Frost, M. L. Weier, K. L. Erickson, *J. Therm. Anal. Calorim.*, **76** (2004) 1025.
37. V. Stefov, B. Soptrajanov, F. Spirovski, I. Kuzmanovski, H. D. Lutz, B. Engelen, *J. Mol. Struct.*, **752** (2005) 60.
38. J. Bellanto, "Infrared spectroscopy of urinary calculi", In "Renal Tract Stone: Metabolic Basis and Clinical Practise", Ed. J. E. A. Wickham, A. Colinbuck, Churchill Livingstone Inc., New York (1990).
39. F. A. Miller, C. H. Wilkins, *Anal. Chem.*, **24** (1952) 1253.
40. I. Gamo, *Bull. Chem. Soc. Jpn.*, **34** (1961) 760.
41. P. J. Lucchesi, W. A. Glasson, *J. Am. Chem. Soc.*, **78** (1956) 1347.
42. J. Lecomte, *J. Chim. Phys.*, **50** (1953) C53.
43. C. Duval, *Anal. Chim. Acta*, **13** (1955) 32.
44. V. C. Farmer, "Infrared spectra of minerals", Monograph No. 4, Mineral. Soc. Pub., United Kingdom, London (1974).
45. T. Kebede, K. V. Ramana, M. S. P. Rao, *Proc. Indian Acad. Sci. (Chem. Sci.)*, **113** (2001) 275.
46. M. Dhandapani, L. Thyagu, P. A. Prakash, G. Amirthaganesan, M. A. Kandhaswamy, V. Srinivasan, *Cryst. Res. Technol.*, **41** (2006) 328.
47. J. T. Kloprogge, M. Broekmans, L. V. Duong, W. N. Martens, L. Hickey, R. L. Frost, *J. Mater. Sci.*, **41** (2006) 3535.

48. J. L. Dong, X. H. Li, L. J. Zhao, H. S. Xiao, F. Wang, X. Guo, Y.H. Zhang, *J. Phys. Chem. B*, **111** (2007) 12170.
49. M. Shashikala, S. Elizabeth, B. Chary, H. L. Bhat, *Curr. Sci.*, **56**(1987) 861.
50. K. Nakamoto, "*Infrared and Raman Spectra of Inorganic and Coordination Compounds*", 3rd ed., John Wiley & Sons, New York (1978).
51. C. M. Julien, P. Jozwiak, J. Garbarczyk, In *Proc. of the Int. Workshop "Advanced Techniques for Energy Sources Investigation and Testing"*, Sofia, Bulgaria (2004).
52. R. L. Frost, M. L. Weier, W. N. Martens, D. A. Henry, S. J. Mills, *Spectrochim. Acta*, **62** (2005) 181.
53. S. K. H. Khalil, M. A. Azooz, *J. Appl. Sci. Res.*, **3** (2007) 387.
54. S. D. Ross, "*Phosphates and Other Oxy-anions of Group V*" in "*The Infrared Spectra of Minerals*", ed. V. C. Farmer, London, (1974).
55. H. Saidou, S. B. Moussa, M. B. Amor, *Environ. Technol.*, **30** (2009) 75.
56. B. B. Parekh, S. R. Vasant, K. P. Tank, A. Raut, A. D. B. Vaidya, M. J. Joshi, *Am. J. Infectious Dis.*, **5** (2009) 232.
57. G. Madhurambal, R. Subha, S. C. Mojumdar, *J. Therm. Anal. Calorim.*, **96** (2009) 73.
58. A. Kohutova, P. Honcova, V. Podzemna, P. Bezdicka, E. Vecernikova, M. Louda, J. Seidel, *J. Therm. Anal. Calorim.*, **101** (2010) 695.
59. E. V. Wilson, M. J. Bushiri, V. K. Vaidyan, *J. Optoelectron. Biomed. Mater.*, **2** (2010) 85.
60. E. V. Wilson, M. J. Bushiri, V. K. Vaidyan, *Spectrochim Acta A Mol Biomol Spectrosc.*, **77** (2010) 442.
61. S. J. Nasir, *Qatar Uni. Sci. J.*, **18** (1999) 189.

62. T. Echigo, M. Kimata, A. Kyono, M. Shimizu, T. Hatta, *Mineral. Mag.*, **69** (2005) 77.
63. E. K. Girija, S. N. Kalkura, P. Ramasamy, *Mat. Chem. Phys.*, **52**(1998)253.
64. B. Parekh, P. Vyas, S. Vasant, M. J. Joshi, *Bull. Mater. Sci.*, **31**(2008) 143.
65. M.I.H. Bhuiyan, D. S. Mavinic, F. A. Koch, *Chemosphere*, **70**(2008)1347.
66. A. K. Sarkar, *J. Mater. Sci.*, **26** (1991) 2514.
67. A. W. Coats, J. P. Redfern, *Nature*, **201** (1964) 68.
68. H. H. Horowitz, G. Metzger, *Anal. Chem.*, **35** (1963) 1464.
69. E. S. Freeman, B. Carroll, *J. Phys. Chem.*, **62** (1958) 394.
70. K. J. Laidler, "*Chemical Kinetics*", 3rd Ed., Harper and Row, New York (1987).
71. D. Enakshi, K. V. Rao, *J. Mater. Sci. Lett.*, **4** (1985) 1298.
72. I. Paul, G. Varghese, M. A. Ittyachen, K. T. Mathew, A. Lonappan, J. Jacob and S. B. Kumar, *Microw. Opt. Technol. Lett.*, **35** (2002) 297.
73. B. B. Parekh, M. J. Joshi, *Cryst. Res. Technol.*, **42** (2007) 127.
74. K. D. Parikh, D. J. Dave, B. B. Parekh, M. J. Joshi, *Cryst. Res. Technol.*, **45** (2010) 603.
75. R. R. Hajiyani, D. J. Dave, C. K. Chauhan, P. M. Vyas, M. J. Joshi, *Mod. Phys. Lett. B*, **24** (2010) 735.
76. R. M. Dabhi, B. B. Parekh, M. J. Joshi, *Indian J. Phys.*, **79** (2005) 503.
77. S. K. Arora, V. Patel, B. Amin, A. Kothari, *Bull. Mater. Sci.*, **27**(2004) 141.
78. A. K. Jonscher, "*Dielectric Relaxation in Solids*", Chelsea Dielectric Press, London (1983).
79. J. Ortiz-Lopez, R. Gomez-Aguilar, *Rev. Mex. Fis.*, **49** (2003) 529.
80. J. Park, *Solid State Commun.*, **123** (2002) 291.
81. R. Chen, C. Yen, C. Shern, T. Fukami, *J. Appl. Phys.*, **98** (2005) 044104.

Chapter VI

Growth Inhibition Study of Struvite

Topic Number	Topic	Page Number
6.1	Introduction	246
6.2	Brief Review of Inhibition Studies of Urinary Calculi	247
6.3	Gel Growth – A Simplified <i>In Vitro</i> Model	251
6.4	Medicinal Plants Used for Growth Inhibition Studies	253
6.5	Preparation of Herbal Extracts	263
6.6	Growth Inhibition Study of Struvite by Herbal Extracts	264
6.7	Growth Inhibition Study by Fruit Juice of <i>Citrus Medica</i> Linn	277
6.8	Mechanism of Inhibition	286
6.9	Conclusions	293

6.1 Introduction

This chapter describes the growth inhibition study of struvite crystals. Struvite type urinary calculi can grow rapidly forming "staghorn-calculi", which is more painful urological disorder. It has also high degree of recurrence. As mentioned earlier in chapter II, struvite stones are among the most difficult and dangerous problems in stone disease because of the potential of life-threatening complications from infection. Epidemiological studies from various countries continue to report a frequency of the occurrence of struvite stones of between 25 % and 38 % [1,2]. Many surgical options are available as medical management options for struvite calculi. As described earlier in section 2.10 of chapter II, surgical options may include extracorporeal shock wave lithotripsy, ureteroscopic stone extraction and percutaneous nephrolithotomy. Recurrence is the core issue in the clinical management of struvite calculi. Although, surgical management has become increasingly tolerable, medical prevention of recurrent struvite calculi is feasible, easily obtained and greatly desirable. In such a condition, it is the need of society to discover such drugs, which will inhibit struvite growth, in addition to high success rates, excellent safety profile, low side effect profile, and ease of use, such a drug will be ideal for management of calculi. Therefore, it is of prime importance to study the growth and inhibition of struvite crystals *in vitro*. In the present investigation *in vitro* single diffusion gel growth technique was used to study the growth and inhibition behavior of struvite crystals by using the herbal extracts like *Boerhaavia diffusa* Linn, *Commiphora wightii* and *Rotula aquatica* Lour as well as the fruit juice of *Citrus medica* Linn. The goal of this growth inhibition study was dual: (i) to find inhibition efficiency of these herbal extracts and fruit juice

on struvite crystal growth as well as to provide a perspective for further investigation of their possible use in stone therapy, and (ii) to identify versatile and “green” inhibitors of struvite.

6.2 Brief Review of Inhibition Studies of Urinary Calculi

There are substances, which may change or modify urinary crystal formation, can be divided into three main groups: (i) Inhibitors, (ii) Promoters, and (iii) Complexors. Substances that reduce the crystallization are called inhibitors and contrary to this, which increase crystallization are termed as promoters. The details of the inhibitor and promoters are already discussed in section 2.6.6 of chapter II. Urinary inhibitors attach to the growth sites on crystalline face and retard the growth and aggregation further.

In the literature one can find information on glutamic acid, α -ketoglutaric acid [3], magnesium, ethylene diamine tetra acetic acid (EDTA), citrate [4,5], phytic acid [6], pyrophosphate [5,7], diphosphonate [7], amino acids like lysine [8], aspartic acid [4], ornithine, tryptophan [9], organic acids such as tartaric, malonic, citric, hippuric [10,11] and osteopontin (OPN) [4], which have kidney stone dissolving properties.

Many chemicals are found to be having inhibitive actions on the growth of urinary stones and crystals; for example, magnesium, citrate, pyrophosphate and nephrocalcin are the common inhibitors for calcium phosphate crystals [12], tartrates were found as a good inhibitor in natural and artificial urine media [13], some amino acids, which show the influence on the spontaneous precipitation of calcium oxalate and depend on the type and the concentration of amino acids used [14], the citrate compounds, which show the inhibition of nucleation and growth steps of COM crystallization [15], some

phosphate derivatives, such as, D fructose-1.6-diphosphate, pyrophosphate methylene diphosphonate and phytate are found to be strongly inhibiting the growth of COM seed crystallization [16]. Inhibition of calcium oxalate crystal formation is exhibited by citrate, pyrophosphate, glycosaminoglycans, RNA fragments and nephrocalcin [17,18]. Moreover, the inhibition of COM aggregation is possible by mainly two glycoproteins, namely, nephrocalcin and Tamm-Horsfall glycoprotein [19]. Certain substances that form soluble complexes with lattice ions for specific crystals and decrease the free ion activity of that particular ion and as a result effectively decrease the state of saturation for that ion system. It has been found that both citrate and magnesium not only act as inhibitors but also as complexors [20,21]. Sometimes, a substance may promote one stage of crystal formation such as growth and inhibit another stage such as aggregation, for example, glycosaminoglycans promote crystal nucleation but inhibit crystal aggregation and growth [22].

Many researchers have reported the growth inhibition study of various urinary type crystals as follows:

Inhibition of calcium oxalate : Several researchers have concentrated growth inhibition studies on calcium oxalate due to its highest epidemiological rates. Atanassova et al [3,8] showed the inhibiting effect of α -ketoglutaric acid and DL-lysine on calcium oxalates. Inhibition and dissolution of calcium oxalate crystals in solutions containing a homoeopathic medicine *Berberis Vulgaris-Q*, amino acids such as aspartic acid, glutamic acid, α -keto glutaric acid, a naturally occurring inhibitor, and juices of some fruits of citrus group such as lemon and orange were reported by Das et al [23]. Moreover, Das et

al [24] reported the use of extracts of the edible plant *Trianthema monogyna* (commonly known as pathari, ghetuli, vasu or lana sata) a naturally growing herb of north eastern Uttar Pradesh, India, and the pulse *Macrotyloma uniflorum* (commonly known as kurthi or horsegram) in the inhibition / dissolution of calcium oxalate and gallbladder stone. Qiu et al [25] reported that citrate modified the shape and inhibited the growth of COM crystals by selectively pinning step motions on the (-101) face, whereas leaving the (010) to grow uninhibited.

Recently, *in vitro* inhibition studies of COM crystal growth using various Mediterranean traditional Algerian medicinal plants such as *Ammodaucus leucotrichus*, *Ajuga iva*, *Erica multiflora* and *Stipa tenacissima*, *Globularia alypum*, *Atriplex halimus*, *Tetraclinis articulata*, *Chamaerops humilis* and *Erica arborea* were carried out by M. Beghalia et al [26] and found the extracts of these plants as potent inhibitors of COM. Among these, the two plant extracts that exhibited highest potency on calcium oxalate crystallisation, *Ammodaucus leucotrichus* was found to inhibit potently the nucleation, growth, and aggregation phases of crystallization, but *Erica multiflora* inhibited nucleation and growth of the crystals but not their aggregation [27]. Recently, Frackowiak et al [28] reported that the extract of *Humulus lupulus* L. have high potency for inhibition and dissolving synthetic calcium oxalate crystals as well as real kidney stones, obtained from patients after surgery. Farook et al [29] have estimated the inhibition efficiency of medicinal plants *Achyranthes aspera* Linn, *Passiflora leschenaultii* DC, *Solena amplexicaulis* (Lam.) Gandhi, *Scoparia dulcis* Linn and *Aerva lanata* (Linn.) on the mineralization of calcium oxalate, calcium carbonate and calcium phosphate. Aal et al [30] indicated the

inhibition of calcium oxalate by extract of *Ammi visnaga*. Bensatal and Ouharani [31] showed inhibition of crystallization of calcium oxalate by the extraction of *Tamarix gallica* L. Joshi et al [32] studied *in vitro* growth inhibition of COM crystals by herbal extracts of *Tribulus terrestris* Linn., and *Bergenia ligulata* Linn.

Inhibition of Brushite : *In vitro* growth inhibition study on brushite crystals in the presence of citric acid and lemon juice along with the artificial reference urine and natural urine was reported by Joshi and Joshi [33], which showed strong inhibition of growth of brushite crystal. Later on Joshi et al [34] reported the inhibition of the growth of brushite crystals using aqueous extracts of *Tribulus terrestris* Linn and *Bergenia ligulata* Linn, whereas Joseph et al [35] reported the inhibitory effect of tartaric acid and tamarind on brushite.

Inhibition of Hydroxyapatite : Parekh et al [36] reported the growth inhibition of hydroxyapatite crystals at physiological temperature *in vitro* by using herbal extracts of *Boswellia serrata* Roxb., *Tribulus terrestris* Linn, *Rotula aquatica* Lour, *Boerhaavia diffusa* Linn and *Commiphora wightii* herbal extract solutions and the diffusion constants were measured for Ca^{2+} ions.

Inhibition of Cystine : D. Heimbach et al [37] reported that the combination of 2% acetylcysteine with alkaline solutions, especially tris-hydroxymethylene-aminomethane (THAM) at a pH of 10.0, is an effective tool in the management of cystine stone disease.

Inhibition of Calcium Phosphates : Recently, Das and Verma [38] reported the inhibitory effect of grape extract on the tri-calcium phosphate. Parekh [39] conducted *in vitro* growth inhibition experiments for calcium pyrophosphate

tetrahydrate crystals using herbal extracts of *Rotula aquatica* Lour, *Boerhaavia diffusa* Linn, and *Commiphora wightii*.

Inhibition of Struvite : Growth inhibition reports on struvite crystals are scarce in literature. Earlier, *in vitro* inhibition of struvite crystals grown by *Proteus mirabilis* in artificial urine in the presence of acetohydroxamic acid (AHA) was reported by Downey et al [40]. The AHA primarily acts as a urease inhibitor, which may disrupt the struvite growth and formation directly through the interference with the molecular growth processes on crystal surface. Phosphocitrate was reported to inhibit *in vivo* formation of struvite [41]. Crystal growth studies and molecular modeling results indicate strong affinity of phosphocitrate to (1 0 1) faces of struvite [42]. Natarajan et al [43] carried out crystal growth experiments of some urinary crystals by incorporating the extracts or juices of some natural products in the gel media to find their inhibitory or promotory effects.

6.3 Gel Growth – A Simplified *In Vitro* Model

The growth of crystals in static solution is generally explained with the help of standard laws of physical chemistry. However, the normal urine in a human body is not a static solution, but new solutes are added and subtracted from the solution. Moreover, it is difficult to mimic the urinary tract *in vitro*; however, the growth of crystals in a gel medium under static environment helps explain the growth of urinary calculi in a body to a certain extent. Hence the growth of urinary calculi can be simulated in a laboratory by growing crystals in a silica hydro gel medium. The gel framework, though chemically inert, provides a three dimensional matrix in which the crystal nuclei are delicately held and provides a substratum for a gradual supply of nutrients for

growth. Slow and controlled diffusion of reactants in gels can mimic the condition in a body. Bio-crystallization usually occurs in the slow and steady process in the soft tissues, cavities or vessels. Growth of crystals with different morphologies is commonly found in bio-crystallization. In the gel growth technique, by changing the growth conditions, crystals with different morphologies and sizes can be obtained. The main advantage is that the crystals can be observed practically in all stages of their growth. The crystal growth by gel method provides simulation of synovial cartilage and other biological fluids [35,44]. The growth of urinary crystals in silica hydro gel can be considered as a simplified *in vitro* model of the highly complex growth of urinary calculi *in vivo*.

The *in vitro* growth inhibition or dissolution study is important as the growth of calculi continues to occur with the supply of nutrients through urine and the inhibition process has to be achieved. In the gel growth, nutrients are constantly supplied to the growing crystals and the dissolution or inhibition is to be checked for the selected solutions.

The growth of crystals from the gel, the simplest technique under ambient conditions, is suitable for the growth of bio-materials crystals, urinary type crystals and certain other compound crystals, which are sparingly soluble and decomposes at low temperatures or decomposes before melting. The gel density, pH and concentration of the reactants are important factors influencing the growth of good quality single crystals at room temperatures. This technique has been elaborately explained in Chapter-III. This technique has been employed as a simple technique to grow various urinary type crystals [45-48] and study the role of various inhibitors *in vitro* [33,35].

Recently, a modified gel growth technique has been proposed for the micro-crystal growth and *in situ* observations, which has been successfully tested for brushite micro-crystal growth inhibition in the presence of citric acid [49].

6.4 Medicinal Plants Used for Growth Inhibition Studies

The ancient Indian treatise written in Sanskrit like *Rig Veda*, *Atharva Veda* (4500-1600 BC), *Ayurveda* (sub section of *Atharva Veda*), *Charaka Samhita* (approximately 1500 BC), *Sushruta Samhita* (600 BC) and *Ashtangha Hridaya Samhita* (approximately 700 AD) mention the use of several plants as medicine. In the indigenous Indian system of medicine i.e., in the Ayurveda, many herbal medicines have been recommended for the treatment of urinary stone problem and some of them have been experimentally evaluated [24,29,33-36,43,50].

6.4.1 *Boerhaavia diffusa* Linn

Nomenclature : *Boerhaavia diffusa* Linn is a medicinal plant commonly known as *Punarnava*, *Raktapunarnava*, *Raktakanda*, *Raktapushpa*, *Kshudra*, *Varshaketu*, *Varshabhu* or *Shothaghni* in Sanskrit [51,52], Spreading Hogweed in English. It has different names in different Indian languages – *Biskhapra* in Hindi; *Gadhapurna* in Bengali; *Satodi*, *Dholia-saturdo*, *Moto-satoda* in Gujarati; *Thzhuthama* in Malayalam; *Mukaratte* in Tamil and *Itsit* in Punjabi. It is also known as *Huang Xi Xin* or *Huang Shou Dan* in China, *Pigweed* in USA, *Erva Tostao* in Brazil. The plant was named by Linnaeus in honour of Hermann Boerhaave, a famous Dutch physician of the 18th century [53]. The meaning of *diffusa* in the name is "spreading". The meaning of the name *Punarnava* in Sanskrit is "*Punah punarnava bhawati iti*" which is translated as that which becomes fresh again and again. The plant is known

as *Punarnava* due to two reasons: (i) The name probably derived from the perennial habit of the plant, which remains dry and dormant during summer and regenerates from the same old root stock in the rainy season [54], and (ii) The name *Punarnava* may derived from the Sanskrit phrase “*Karoti shariram punarnavam*” that denotes such therapeutic property which translates as “that which rejuvenates the body”.

Plant Description : *Boerhaavia diffusa* Linn (*B. diffusa*) is a herbaceous plant of the family Nyctaginaceae. It is a perennial diffuse herb with stout root stock and many branches. *B. diffusa* is up to 1 m long or more, having spreading branches. The stem is prostrate, woody or succulent, cylindrical, often purplish, hairy, and thickened at its nodes. Leaves are simple, green, thick, fleshy, hairy and arranged in unequal pairs. Leaves are ovate-oblong, acute or obtuse, rounded or subcordate at base, glabrous above, whitish beneath. Flowers pale rose in color, in irregular clusters of terminal panicles. Fruits highly viscid, easily detachable, one seeded, indehiscent with thin pericarp. It has a large root system bearing rootlets. The tap root is tuberous, cylindrical to narrowly fusiform, conical or tapering, light yellow, brown or brownish grey. It is thick, fleshy and very bitter in taste.



Figure : 6.1 *Boerhaavia Diffusa* Linn Plant, Leaves, Flowers, Fruits, Roots [55, 56]

Distribution : *B. diffusa* is found in the tropical, subtropical and temperate regions of the world. It is distributed in India, China, Australia, Pakistan, Egypt, Sudan, Srilanka, USA, South Africa and in several countries of the Middle East [57].

Chemical Composition : The plant extract contains a large number of biochemical compounds as listed in table 6.1.

Table : 6.1 : Biochemical Compounds Present in *Boerhaavia Diffusa* Linn [58-68]

Group	Biochemical Compounds Present	References
Alkaloids	Punarnavine 1-2, hypoxanthine 0-L-arabinofuranoside	[58-60]
Flavonoides	Boeravinone A to F, Flavone, 5-7-dihydroxy-3'-4'-dimethoxy-6-8-dimethyl	[61]
Xanthone	Borhavine	[62]
Steroids	β -sitosterols, Campesterol, Daucosterol, Sitosterol oleate, Sitosterol palmitate, Stigmasterol	[63]
Triterpenoides	Ursolic acid	[64]
Lipids – Organic acids	Arachidic acid, Behenic acid, Glycerol, Heptadecyclic acid, Oleaic acid, Palmitic acid, Stearic acid, Tetracosanoic, Hexacosanoic	[65]
Carbohydrates	Fructose, Galactose, Glucose, Sucrose, Xylose	
Proteids	Alanine, Aspartic acid, Glutamic acid, Glutamine, Glycoproteins, Histidine, Leucine, Methionine, Proline, Serine, Threonine, Tyrosine, Valine	
Alkane	Triacontan-1-ol, Oxalic acid; Hentriacontane, n	
Lignans	Liriodendrin, Syringaresinol-mono-beta-d-glucoside	[66]
Others	Punarnavoside, Boerhaavic acid, Potassium nitrate	[67,68]

Medicinal Properties : The whole plant or its specific parts (leaves, stem, and roots) are known to have medicinal properties. In *Ayurveda* the plant is used for the treatment of many diseases [69-74], such as diabetes, stress, dyspepsia, abdominal pain, inflammation, jaundice, hepatitis, gastro-intestinal disorders (as laxative) enlargement of spleen, congestive heart failure and bacterial infections. The plant is known to possess anti-inflammatory [75,76],

anticonvulsant [77-80], antifibrinolytic [66], diuretic [81-84], hepatoprotective [85-88], antidiabetic [89,90] and immunomodulatory [91-93] activities. It was also reported to be useful in the treatment of elephantiasis, night blindness, corneal ulcers and nephritic syndrome [94-96]. Olaleye et al [97] reported antioxidant and hepatoprotective properties of the extracts of *B. diffusa* leaves in pharmacological models. Punarnavine, an alkaloid isolated from *B. diffusa* has been shown *in vitro* anticancer [98], antiestrogenic [99] and immunomodulatory [100] activity.

6.4.2 *Commiphora wightii*

Nomenclature : The name is derived from Greek words 'kommis' and 'phora' meaning gum bearer. In Indian languages, it is known by various names like *gugal* in Gujarati, *guggul* in Hindi, *guggulu* in Sanskrit, *gukkulu* and *maishakshi* in Tamil, Indian bdellium in English, *Mo ku er mo yao* in Chinese. Detailed descriptions regarding the actions, uses, and indications as well as the varieties of *C. wightii* have been described in the Ayurvedic treatises.



Figure : 6.2 *Commiphora Wightii* Plant, Leaves, Flower, Fruit, Stem, Gum [101]

Plant Description : *C. wightii* is a flowering plant in the family Burseraceae. It is a shrub or small tree, 1.5–2 m in height, reaching a maximum height of 4 m, with thin papery bark [102]. It has a thick main stem with short, thorny

branches. The leaves are non-hairy, simple or trifoliate and the leaflets ovate. Leaves have aromatic smell. It is a slow growing, endangered medicinal tree [103,104]. Flowers are small, brownish red, occurring singly or in groups of 2-3. Fruit is an ovoid green berry like drupe, reddish and 6-8 mm in diameter. It provides yellowish oleo gum resin (commonly known as gum guggul) which is extracted from the bark by a process called tapping. A plant generally takes 10 years to reach tapping maturity under the prevailing dry climatic conditions.

Distribution : The tree is found in rocky and open hilly areas or rough terrain and sandy tracts in warm and semiarid to arid areas. It is distributed in India, Nepal, Srilanka, China, Bangladesh and Pakistan. In India it is found in arid, rocky tracts of Rajasthan (Thar Desert), Aravalli range, Gujarat (Kachchh and Saurashtra regions) [105], Maharashtra, Madhya Pradesh, Karnataka and Eastern Himalayas [106]. The plant may be found from northern Africa to central Asia, but is most common in northern India.

Chemical Composition : Many groups have studied the phytochemistry of *C. wightii* and found ferulates [107], steroids [108], guggulsterones [109] guggutetrols [110]. New antifungal flavanone, muscanone was isolated along with known naringenin from *C. wightii* by Fatope et al [111]. The golden yellow oleo-gum-resin is a complex mixture of over two dozen ketones, several phenolics, diterperoids, flavonoids and sterols [112,113].

C. wightii contains Guggulsterol-I { $C_{27}H_{44}O_4$ }, Guggulsterol-II { $C_{27}H_{46}O_3$ }, Guggulsterol-III { $C_{27}H_{44}O_3$ }, Guggulsterol-IV { $C_{27}H_{44}O_3$ }, Guggulsterol-V { $C_{29}H_{50}O_4$ }, Guggulsterol-VI { $C_{27}H_{32}O_2$ }. The active components of the plant are the guggulsterones specifically the

stereoisomers, guggulsterone-E { $C_{21}H_{28}O_2$ }, and guggulsterone-Z { $C_{21}H_{28}O_2$ }, which are potent lipid and cholesterol lowering natural agents [114,115].

Medicinal Properties : *C. wightii* is one of the most important medicinal plants used in the herbal system of medicine. A monograph of all the major citations of its use was published by Apte [116]. *C. wightii* is used as an Ayurvedic medicine for the treatment of joint pains, arthritis, hyperlipidemia, inflammation, sciatica, paralysis, convulsions, gonorrhea, chronic cough and cold, bronchitis, diabetes, urinary disorder, dysuria, calculi, fever, skin ailments, stress, ulcers, cardiovascular disease, lipid disorders, high cholesterol [117,118], obesity and other weight-related problems. *C. wightii* is effective as a weight-loss and fat burning agent. It increases white blood cell counts and possesses strong disinfecting properties. Various studies to check most of these therapeutic effects of *C. wightii* were carried out by different researchers [72,119-122]. The guggul resin has proven medicinal properties and is used to cure various diseases such as hypercholesterolemia [123], cardiovascular diseases [124] and cancerous diseases [125]. The cardiovascular therapeutic benefits of guggul and guggulsterone appear to be due to the multiple pharmacological activities, notably the hypolipidemic, anti-oxidant, and anti-inflammatory effects [124]. The main ingredients of *C. wightii* are flavonoids which have potent anti-oxidant actions [111]. It has also shown dose dependent anti-inflammatory activity and was also found to control inflammation and pain in osteoarthritis patients [126]. Recently Ishnava [127] et al reported antibacterial potential of gum resin of *C. wightii*.

6.4.3 *Rotula aquatica* Lour

Nomenclature : *Rotula aquatica* Lour (*R. aquatica*) is commonly known as *Pashanbheda* or *Ashmahabhedah* in Sanskrit and *Lun guan mu* in Chinese.

Plant Description : *R. aquatica* belonging to the family boraginaceae, is a rheophytic woody aromatic medicinal shrub. Generally, reaches a height of 2 to 3 m. The leaves are alternate, imbricate, ovate-oblong, usually 0.8 to 1.5 cm in length and short-stalked. The flowers are small, crowded and pink.



Figure : 6.3 *Rotula Aquatica* Lour Plant, Flower and Root [128]

Distribution : *R. aquatica* is distributed in India, Sri Lanka, China, tropical southeastern Asia including Indonesia, Malaysia, Myanmar, Philippines, Thailand, Vietnam, Africa, Brazil and Latin America [129]. The plant is scattered throughout peninsular and eastern India in the sandy and rocky beds of streams and rivers.

Chemical Composition : The sterol, rhabdiol, polyphenols (tannins), glycosides and ureide allantoin were isolated from the roots by researchers [50,129-131]. The plant contains Baunerol [132], steroid and alkaloids [131].

Medicinal Properties : Usually, plant root is used for medicinal purpose. It is used for treatment of cough, cardiac disorder, blood disorders, fever, ulcers, poisons, dysuria, bladder stone, cancer, piles and venereal diseases in Ayurveda [72, 133-137]. In Ayurveda, it is a well-known lithontriptic (stone-

dissolving) drug [138]. In India *R. aquatica* is one of the most extensively used medicinal plants to dissolve urinary calculi. The root tuber of *R. aquatica* is astringent, bitter, diuretic, cooling, laxative and also lithotriptic. A decoction of root is diuretic and used for treating stones in bladder [139]. The aqueous extract of the root of *R. aquatica* showed antioxidant and antiurolithiatic activity. Sterol and rhabdiol were found to be active to induce diuresis (division or separation of a structure's parts) and allantoin is responsible for diuretic activity [130]. The antiurolithiatic activity of the root extract can be attributed to its diuretic activity. The aqueous extract of *R. aquatica* root has shown crystal dissolving activity against monosodium urate monohydrate type urinary calculi [50], whereas ethyl acetate extract of *R. aquatica* root showed significant antilithic activity against struvite and calcium oxalate stones [140]. The stems were also used in diuretic decoctions and found effective in preventing cell proliferation of pancreatic cancer cell lines [131]. Christina et al demonstrated stone inhibitory effect of *R. aquatica* root decoction in male Wistar rats [141]. Recently, Mengi et al [142] investigated anti-inflammatory potential of aqueous extract of *R. aquatica* roots in acute and chronic inflammatory conditions in rats. Moreover, acute toxicity studies revealed that *R. aquatica* root extract was found safe at all doses when administered orally to rats, up to a dose of 2000 mg kg⁻¹. *R. aquatica* is well known for the treatment of urinary calculi, but its inhibitory property on struvite has not been scientifically reported previously. Therefore, in the present study the inhibitory property of the aqueous extract of *R. aquatica* root on struvite has investigated.

6.4.4 *Citrus Medica* Linn

Nomenclature : In the present growth inhibition study the author has used one of the citrus fruits - *Citrus medica* Linn., commonly known as *Baranimbu*, *Bijaura* or *Bijoru* in Hindi, *Matulunga* in Sanskrit, Citron in English, *Cidro* in Spanish, *Zitronatzitrone* in German, *Fo shou* in Chinese and as *Bushukan* in Japanese. The designation *medica*, given it by Linnaeus, is apparently derived from its ancient name "Median or Persian apple". The general descriptions, characteristics, constituents, various medicinal use were discussed by many researchers [143,144].

Plant Description : *Citrus Medica* Linn is belonging to the Rutaceae family. It is an evergreen armed shrub with straggling thorny branches and smooth yellowish brown bark. Generally, this shrub reaches a height of 2.4 to 4.5 m. Leaves are oblong or elliptic with acute or rounded apex, coriaceous (leathery; stiff and tough, but somewhat flexible), glabrous (without surface ornamentation such as hairs, scales or bristles), pellucid-punctate (tiny marked with dots in leaves visible when held in front of light), dull dark green and lemon-scented. Leaflets are 7.5 - 15 cm long. Flowers are white tinged with pink and scented. The fruit is fragrant, mostly oblong, obovoid or oval. The size of the fruit varies greatly from 9 to 30 cm. Peel is usually very thick, rough and bumpy, which becomes yellow when ripe. It contains numerous seeds.

Distribution : It grows in evergreen forests naturally or can also be cultivated. Citrus is grown in tropical and subtropical regions of the world and occupies a wide range of latitude over which it is being cultivated. The north-eastern Indian states are rich treasure of various citrus species and their varieties. It is

found in the base region of Himalaya from Gadwal to Sikkim. It is also seen in Assam, Central India and Western Ghats of India. It is now cultivated commercially in the Mediterranean region and, to a lesser extent, in the West Indies, Florida, and California.



Figure : 6.4 Citrus Medica Linn Plant, Leaves, Flowers, Fruits

Chemical Composition : The fruit juice contains good amount of citric acid - $\{C_6H_8O_7\}$ along with ascorbic acid $\{C_6H_8O_6\}$, hesperidin $\{C_{28}H_{34}O_{15}\}$, campesterol $\{C_{28}H_{48}O\}$, stigmasterol $\{C_{29}H_{48}O\}$, β -sitosterol $\{C_{29}H_{50}O\}$, malic acid $\{C_4H_6O_5\}$, phosphoric acid $\{H_3PO_4\}$, potassium citrate $\{C_6H_5K_3O_7\}$, mucilage and sugar [145]. The peels are reported to contain coumarins- $\{C_9H_6O_2\}$, limettin $\{C_{11}H_{10}O_4\}$, scoparone $\{C_{11}H_{10}O_4\}$, scopoletin $\{C_{10}H_8O_4\}$ and umbelliferone $\{C_9H_6O_3\}$ [137]. Seeds of the fruit contain limonin $\{C_{26}H_{30}O_8\}$, limonol $\{C_{26}H_{32}O_8\}$ and nomilinic acid [146].

Medicinal Properties : Various parts of this plant are widely used in Indian traditional system of medicine [69,147-149]. Ripe fruits are used in sore throat, cough, asthma, arthritis, rheumatism, thirst, hiccough, ear ache and vomiting. It is potent anti-scorbutic, stomachic, tonic, stimulant, expellant of poison, correct fetid breath; distilled water of the fruit is sedative; fruits and

seeds are cardiac tonic and useful in palpitation. Fruit juice also acts in stimulating liver for proper secretion of bile juices. Roots, flowers, seeds, peels and leaves are also used in many ailments. Fruit extracts have also shown good antioxidant activity [150]. Recently, it is reported that the analgesic activity of fruit decoction [151] and antimicrobial activity of fruit juice as well as juiceless fruit pulp extract [152] of *Citrus medica* Linn are noteworthy.

6.5 Preparation of Herbal Extracts

6.5.1 Plants Material : *B. diffusa* roots obtained from Vasai, Thane district, Maharashtra and the *R. aquatica* Lour, roots were collected from Savantwadi, Maharashtra in the Winter season and authenticated by Dr. M. R. Almeida, Taxonomist, Mumbai. *C. wightii* gum resin was obtained from Barda, Gujarat in Spring and authenticated by Dr. P. S. Nagar, Saurashtra University, Rajkot.

6.5.2 Extraction : The respective plant materials were cleaned, dried, powdered (50 g) and added to distilled water (400 mL). The mixture was heated in a boiling water bath until it reduced to half of the original volume. The extract was dried in a rotary vacuum evaporator to a syrupy consistency and then in a steam bath to thick, pasty consistency. The extracts were stored in glass vials kept in airtight plastic boxes in refrigerator and used to investigate inhibitory effect on struvite type urinary calculi. All the extracts were prepared at Bhavan's SPARC at Mumbai and were provided to the present author for the study. Two different concentrations, namely 0.5% and 1.0% of aqueous root extracts of *B. diffusa* and *R. aquatica* as well as aqueous gum resin extract of *C. wightii* were used to determine the inhibitory effect.

6.6 Growth Inhibition Study of Struvite by Herbal Extracts

6.6.1 Single Diffusion Gel Growth Technique

The single diffusion gel growth technique was used to study the growth and inhibition behavior of struvite crystals in the presence of different herbal extracts. Sodium Metasilicate (SMS)- $\{Na_2SiO_3.9H_2O\}$ solution of specific gravity 1.05 was used to prepare the gel. An aqueous solution of Ammonium Dihydrogen Phosphate (ADP)- $\{NH_4H_2PO_4.2H_2O\}$ of 0.5 M concentration was mixed with the SMS solution in appropriate amount so that the pH value 7.0 could be set for the mixture. The gel solution of 20 mL was transferred into the test tubes of 140 mm length and 25 mm diameter. All test tubes and other glassware were autoclaved at 120°C for 15 min. Here, the silica gel was chosen because it remains stable and does not react with the reacting solutions or with the product crystal formed. After the gelation took place, 20 mL supernatant solutions (SS) of pure (i.e. control solution, without inhibitor) 1.0 M magnesium acetate- $\{C_4H_6MgO_4.4H_2O\}$ and 1.0 M magnesium acetate prepared with 0.5 % and 1.0 % concentrations of the each of the herbal extracts were gently poured on the set gels in test tubes. This was done in the aseptic medium in a laminar flow hood to avoid microbial contaminations. Composition and the pH value of the SS are as shown in table 6.2. After pouring SS, the test tubes were capped with airtight stopples. The experiment was conducted at the room temperature.

The following reaction is expected to occur in the gel between the two reactants:

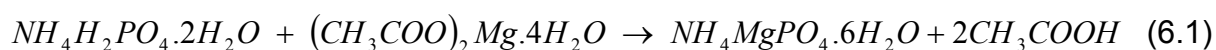


Table : 6.2 : Composition and pH of Supernatant Solution with Herbal Extracts

Concentration	pH	Composition of Supernatant Solution		
		Distilled Water (mL)	Magnesium Acetate (g)	Extract (g)
No Inhibitor	8.00	20	4.288	-
0.5 % <i>B. Diffusa</i> Linn	7.25	20	4.288	0.1 g <i>B. diffusa</i> Linn
1.0 % <i>B. Diffusa</i> Linn	7.00	20	4.288	0.2 g <i>B. diffusa</i> Linn
0.5 % <i>C. Wightii</i>	7.64	20	4.288	0.1 g <i>C. wightii</i>
1.0 % <i>C. Wightii</i>	7.60	20	4.288	0.2 g <i>C. wightii</i>
0.5 % <i>R. Aquatica</i> Lour	6.95	20	4.288	0.1 g <i>R. aquatica</i> Lour
1.0 % <i>R. Aquatica</i> Lour	6.76	20	4.288	0.2 g <i>R. aquatica</i> Lour

The apparent lengths of growing/dissolving struvite crystals in each of the test tubes were measured by using a traveling microscope of least count 0.001 cm at regular time interval. The apparent lengths of growing/dissolving struvite crystals at different depth from the gel-liquid interface in each of the test tubes were measured and mean length of the crystals at different depth was calculated. The statistical analysis of the single factor ANOVA was carried out. The total mass and total volume of struvite crystals in each test tubes were measured after removal of crystals and per test tube the yield of crystals was obtained for each concentrations with and without herbal extracts.

6.6.2 Struvite Crystals Grown in the Gel Media

The gel-grown struvite crystals exhibit different morphologies, viz. dendritic, prismatic, rectangular platelet and needle type depending upon the location of growth. As shown in figure 6.5, at gel-liquid interface, dendritic-type crystals were observed, whereas at higher depths in the gel from gel-liquid interface, prismatic-type crystals were observed. Due to higher concentrations

of reactants at the gel – liquid interface, more-or-less, a direct reaction took place, which might resulted in to dendritic type crystals.

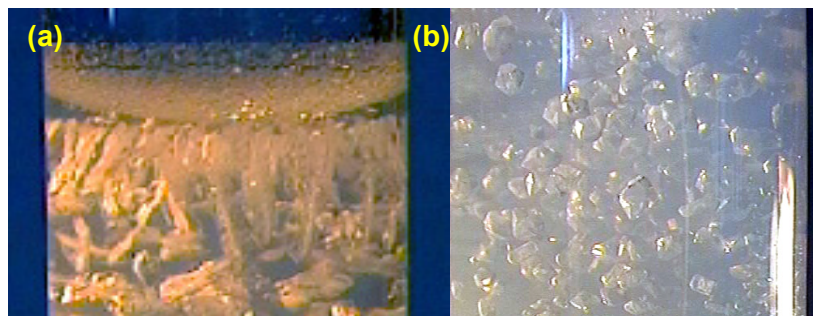


Figure : 6.5 (a) Dendritic crystals grown at the gel-liquid interface
(b) Prismatic crystal grown in the gel at higher depths

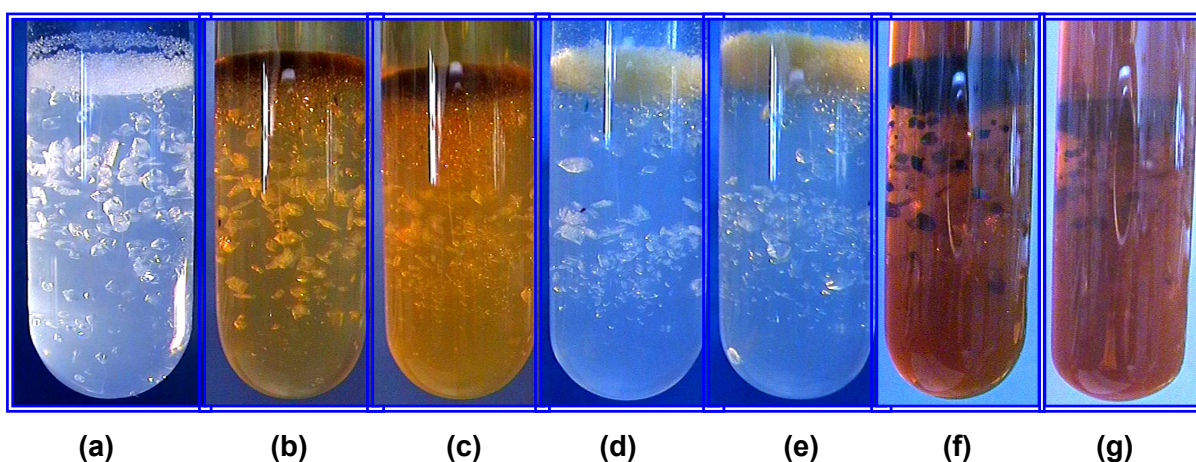


Figure : 6.6 Struvite Crystals Grown in the Gel Medium
[(a) No Inhibitor, (b) 0.5 % *B. Diffusa* Linn, (c) 1.0 % *B. Diffusa* Linn, (d) 0.5 % *C. Wightii*,
(e) 1.0 % *C. Wightii*, (f) 0.5 % *R. Aquatica* Lour, (g) 1.0 % *R. Aquatica* Lour]

It was noticed that the number of grown struvite crystals and their average apparent length in the silica-hydro gel medium decreased with the increasing concentrations of the extracts in the SS. The reduction in the number density of the grown struvite crystals in the test tubes with extracts proved the inhibitory effect of the herbal extracts experimented. It was found that the crystals grown in the test tubes without the extract were transparent to translucent diaphaneity. On the other hand, some of the crystals grown in the test tubes with the *R. aquatica* extract showed dark brown colorization which might be due to inclusion of the extract in the crystals. Figure 6.6 shows the struvite crystals grown in the gel medium for different extracts.

6.6.3 Growth of Struvite Crystals at Gel – Liquid Interface

After pouring of the SS, dendritic type struvite crystals were found to grow at the gel–liquid interface. The growth rates of crystals, at the end of first, second, third and fourth day, growing in the gel at the gel–liquid interface for different concentration of SS are as presented in table 6.3. It can be noticed from the table that the growth rates are comparatively lower for the each of the herbal extracts, whereas they are comparatively higher for the control solution without inhibitor. Moreover, the growth rates are decreased with the increasing concentration of each extract. It is also noticed that the growth rates decrease with time in each concentration. The lowest growth rate 0.638 cm/day is observed for the SS with 1.0 % *R. aquatica*, while the highest growth rate 1.185 cm/day is noticed for control solution. The average apparent lengths of the dendritic crystals growing in the gel at gel-liquid interface are increased up to first 4 days for control solution, whereas they are increased just for first 2 days in the both concentrations of *B. diffusa*; for 3 days in 0.5 % *C. wightii*, only for 1 day in 1.0 % *C. wightii*; for 2 and 1 day in 0.5% and 1% *R. aquatica* extract solutions, respectively, and followed by dissolution.

Table : 6.3 : Growth of Struvite Crystals at Gel-Liquid Interface

Growth Rate (cm/day)	Day	No Inhibitor (Control Solution)	Concentration of Herbal Extract					
			<i>B. Diffusa</i> Linn		<i>C. Wightii</i>		<i>R. Aquatica</i> Lour	
			0.5 %	1.0 %	0.5 %	1.0 %	0.5 %	1.0 %
Growth Rate (cm/day)	1	1.185	1.027	0.825	0.740	0.715	0.745	0.638
	2	0.608	0.534	0.413	0.448	D. S.*	0.425	D. S.*
	3	0.410	D. S.*	D. S.*	0.299	-	D. S.*	-
	4	0.309	-	-	D. S.*	-	-	-

* D. S. = Dissolution Started

Here, the lower values of growth rate in comparison to control solution, the reduction in growth rates with the increasing concentrations of each tested extracts as well as the reduction in growth rates with the time proved the inhibitory effect of the extracts.

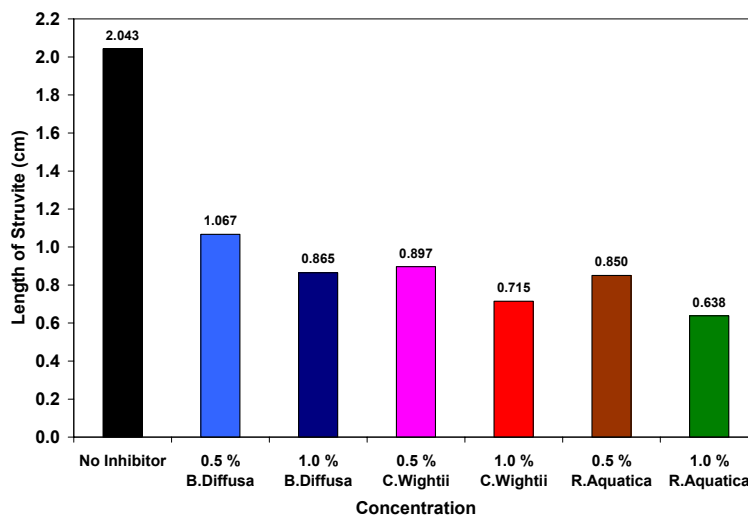


Figure : 6.7 Maximum length of Dendritic Type Struvite Crystals Grown at the Gel-Liquid Interface in Different Concentration

The histogram in figure 6.7 shows the maximum apparent lengths of the dendritic type struvite crystals at the gel – liquid interface in each concentration. It is clear from the figure that the apparent lengths of the crystals are remarkably inferior in all the cases with herbal extracts in comparison to control solution. It can also be noticed that the apparent lengths are decreased with the increasing concentration of extracts.

The extent of inhibition of growing struvite crystals at the gel – liquid interface at the end of first day are tabulated in table 6.4. Interestingly, the significant percentage of inhibition is noticed for every herbal extract studied. The maximum percentage of inhibition 46.16 % is observed for 1.0 % *R. aquatica* extract, where as minimum 13.33 % inhibition is observed for 0.5 % of *B. diffusa* extract.

Table : 6.4 : Inhibition of Struvite Crystal Growth in Gel at Gel–Liquid Interface in the Presence of Different Herbal Extracts on the First Day

Apparent Crystal Length (cm)	No Inhibitor (Control Solution)	Concentration of Herbal Extract					
		<i>B. Diffusa</i> Linn		<i>C. Wightii</i>		<i>R. Aquatica</i> Lour	
		0.5 %	1.0 %	0.5 %	1.0 %	0.5 %	1.0 %
Average Length	1.185	1.027	0.825	0.740	0.715	0.745	0.638
Reduction in Length	-	0.158	0.360	0.445	0.470	0.440	0.547
% of Inhibition	-	13.33%	30.37%	37.55%	39.66%	37.13%	46.16%

6.6.4 Growth and Dissolution of Struvite Crystals at Gel–Liquid Interface

The growth and dissolution of dendritic type struvite crystals at gel-liquid interface is shown by plots of average length versus time period in figure 6.8.

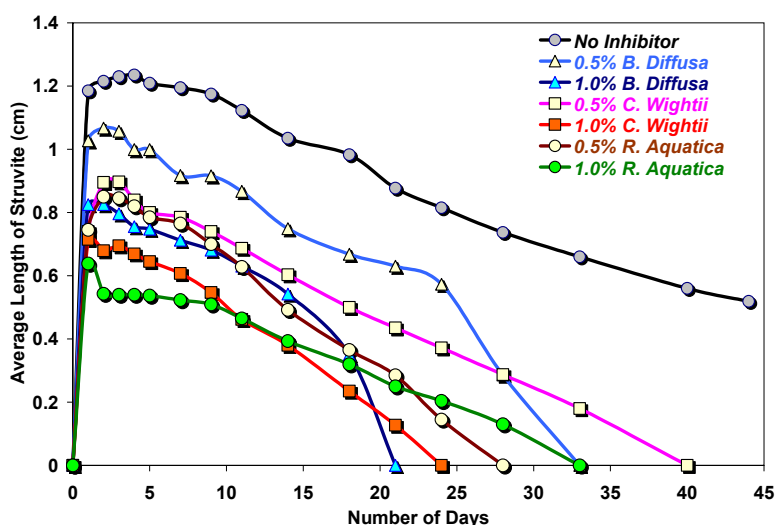


Figure : 6.8 Growth and Dissolution of Struvite Crystals at Gel-Liquid Interface

It is observed that struvite crystals grown at gel – liquid interface also dissolved to some extent even in the absence of herbal extract. It may be due to partial dissolution of the crystals in acetic acid produced as a byproduct of the chemical reaction as shown in equation (6.1), which forms the compound for crystals growth. But, at the same time the dissolution rates are enhanced in all the concentrations of herbal extracts. Table 6.5 depicts the dissolution

rates, enhanced dissolution rates as well as the percentage of enhanced dissolution rates due to the presence of herbal extracts.

Table : 6.5 : Dissolution Rate of Struvite Crystals at Gel-Liquid Interface

Dissolution Rate (cm/day)	No Inhibitor (Control Solution)	Concentration of Herbal Extract					
		<i>B. Diffusa</i> Linn		<i>C. Wightii</i>		<i>R. Aquatica</i> Lour	
		0.5 %	1.0 %	0.5 %	1.0 %	0.5 %	1.0 %
Dissolution Rate	1.8×10^{-2}	3.4×10^{-2}	4.3×10^{-2}	2.4×10^{-2}	3.1×10^{-2}	3.3×10^{-2}	2.0×10^{-2}
Enhanced Dissolution Rate	-	1.6×10^{-2}	2.5×10^{-2}	0.6×10^{-2}	1.3×10^{-2}	1.5×10^{-2}	0.2×10^{-2}
% of Enhanced Dissolution Rate	-	88.89%	138.8%	33.33%	72.22%	83.33%	11.11%
Number of Days Required for Complete Dissolution of the Dendritic Type Struvite Crystals Grown at the Gel – Liquid Interface							
Days	-	33	21	40	24	28	33

Here, the dissolution rates for all herbal extracts are remarkably higher than that of control solution. Moreover, dissolution rates are significantly increased with increasing the concentration of herbal extract, except for *R. aquatica*. Enhanced dissolution rates are observed for all the herbal extracts. It is clear from the table that the maximum percentage of enhanced dissolution rate 138.8 % is observed in the case of 1.0 % *B. diffusa*.

The number of days required for the complete dissolution of the dendritic type struvite crystals grown at the gel – liquid interface are also mentioned in table 6.5, which shows that minimum 21 days are required for the complete dissolution of crystals grown at gel – liquid interface for the concentration of SS with 1.0 % *B. diffusa*.

From the analysis of tables 6.4 and 6.5, it can be perceived that the extracts of *R. aquatica* have retarded the growth rate from the very beginning

of the crystal growth, whereas extracts of *B. diffusa* have speed up the dissolution rates once the growth of the crystals took place. Here, the percentage of enhanced dissolution rates in all the tested concentrations of herbal extracts confirmed the inhibitory effect of the extracts.

6.6.5 Depth of Growth of Struvite Crystals in Gel Column

The depth of growth, i.e., the depth from the gel-liquid interface in gel column up to which struvite crystals are growing, *versus* time period plots are shown in figure 6.9 for all concentrations of herbal extracts selected for study.

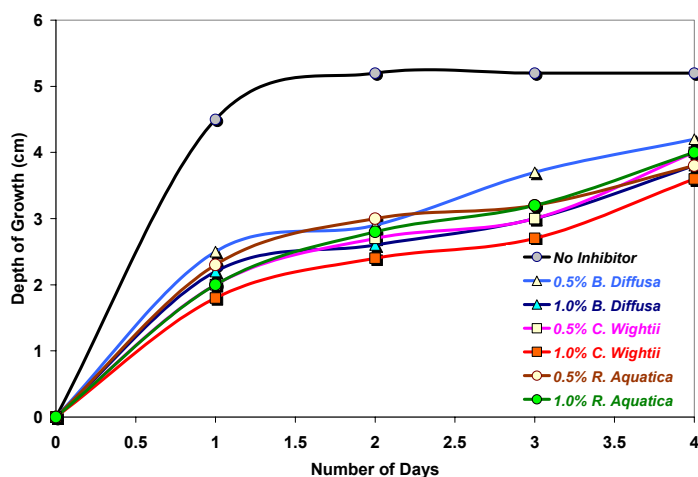


Figure : 6.9 Depth of Growth During First Four Days After Pouring of SS

From the figure it is clear that the maximum depth of growth 5.2 cm is attained in just 2 days after the pouring of SS in case of no inhibitor (control solution), where as the maximum depths of growth after 2 days are restricted to just 2.7 and 2.4 cm for 0.5 % and 1.0% concentrations of *C. wightii* extracts, respectively; 2.9 cm and 2.6 cm for 0.5 % and 1.0 % concentrations of *B. diffusa* extracts, respectively; while 3.0 cm and 2.8 cm for 0.5 % and 1.0 % concentrations of the *R. aquatica* extracts, respectively. This suggests that the extracts impede the diffusion process of reactants occurring in the gel column for the nucleation and, subsequently, the growth of crystals. Thus, the

reduction in depths of growth indicates the inhibition offered by all the three herbal extracts.

6.6.6 Growth and Dissolution of Struvite Crystals at Different Depth

Growth and dissolution of struvite crystals at different depth in gel from the gel–liquid interface in the absence of herbal extract is shown by the plots of average length *versus* time period in figure 6.10.

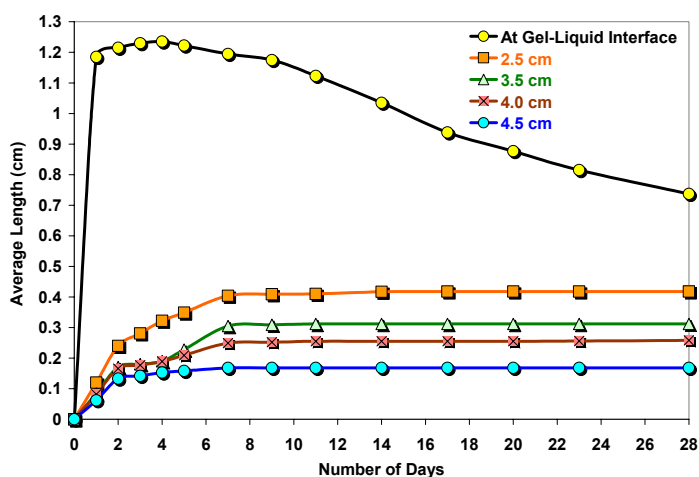


Figure : 6.10 Growth Of Struvite Crystals at Different Depth from the Gel-Liquid Interface in the Absence of Inhibitor

From this figure one can notice that the average length of growing crystals in the gel at gel–liquid interface increases up to first 4 days and then it decreases by indication of dissolution, due to the formation of acetic acid. It is noticed that the average length of growing crystals at different depth from the gel–liquid interface increases up to first 7 days and then it remains constant. As the depth of the gel column increases, the average size of the grown crystals is found to be gradually smaller.

The growth and dissolution of struvite crystals at different depths in the gel column from the gel – liquid interface in case of 0.5 % and 1.0 % concentrations of *B. diffusa*, *C. wightii*, and *R. aquatica* are studied and the

plots of average length of crystals versus time period are shown in figures 6.11 to 6.13, respectively.

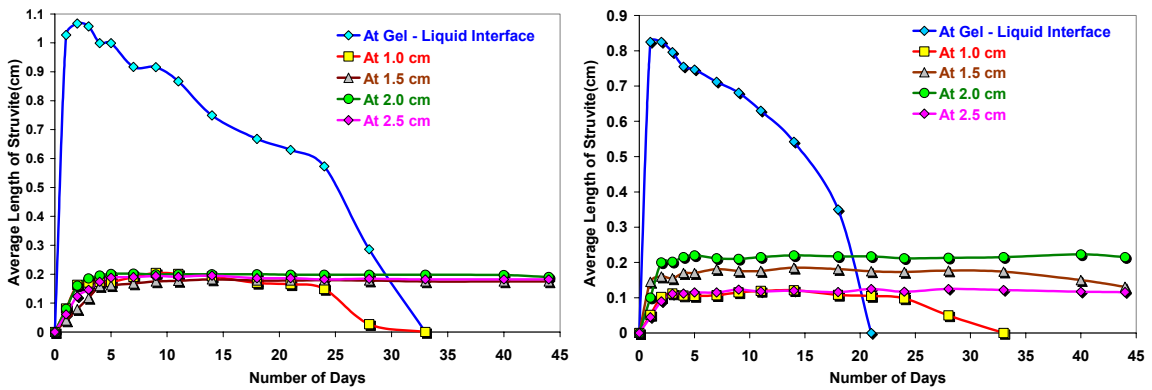


Figure :6.11 Growth and Dissolution of Struvite at Different Depth from the Gel-Liquid Interface for 0.5% *B. Diffusa Linn* (Left) and 1.0% *B. Diffusa Linn* (Right)

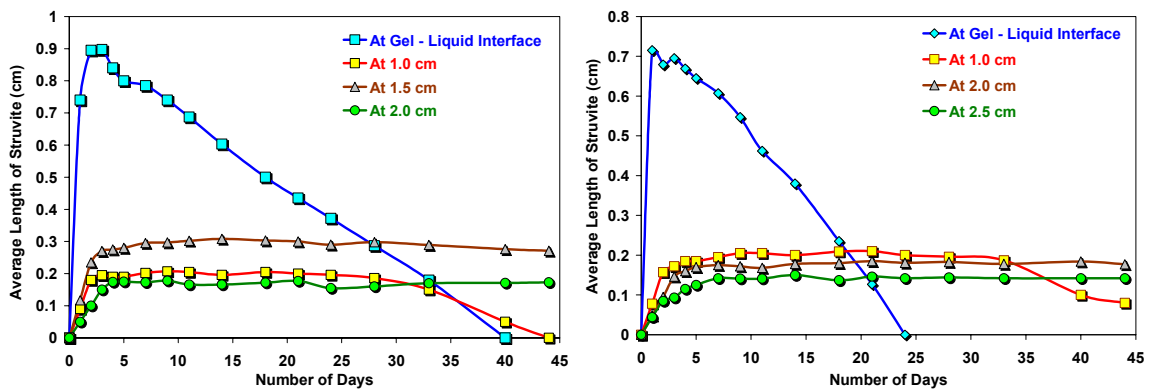


Figure : 6.12 Growth and Dissolution of Struvite at Different Depth from the Gel-Liquid Interface for 0.5% *C. Wightii* (Left) and 1.0% *C. Wightii* (Right)

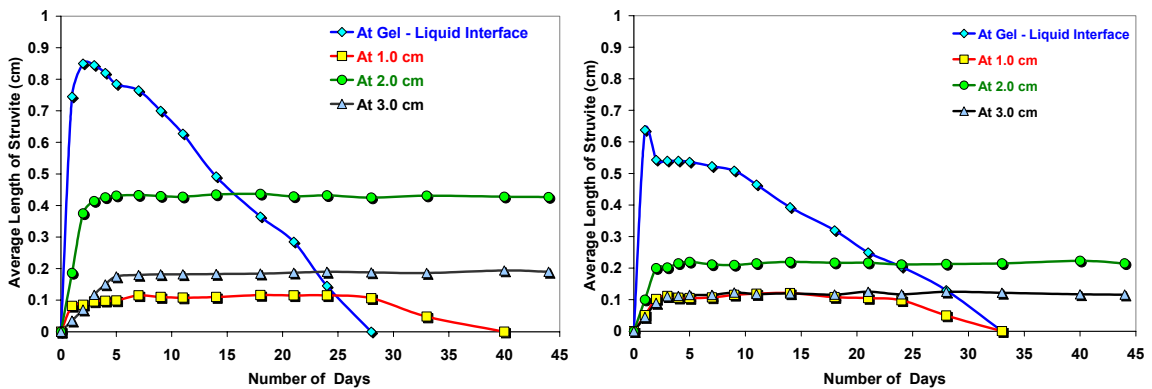


Figure : 6.13 Growth and Dissolution of Struvite at Different Depth from the Gel-Liquid Interface for 0.5% *R. Aquatica* (Left) and 1.0% *R. Aquatica* (Right)

From the above figures it is clear that the similar phenomena are observed more effectively in the presence of all the tested herbal extracts. It was

noticed that the growth rate as well as the apparent size of the crystals grown were lower, which also proved the inhibitory effect of the extracts.

6.6.7 Variation in the size of Prismatic Type Struvite Crystals

Figure 6.14 shows the dimension of the grown prismatic type struvite crystals in all the tested concentrations of SS with and without herbal extracts.

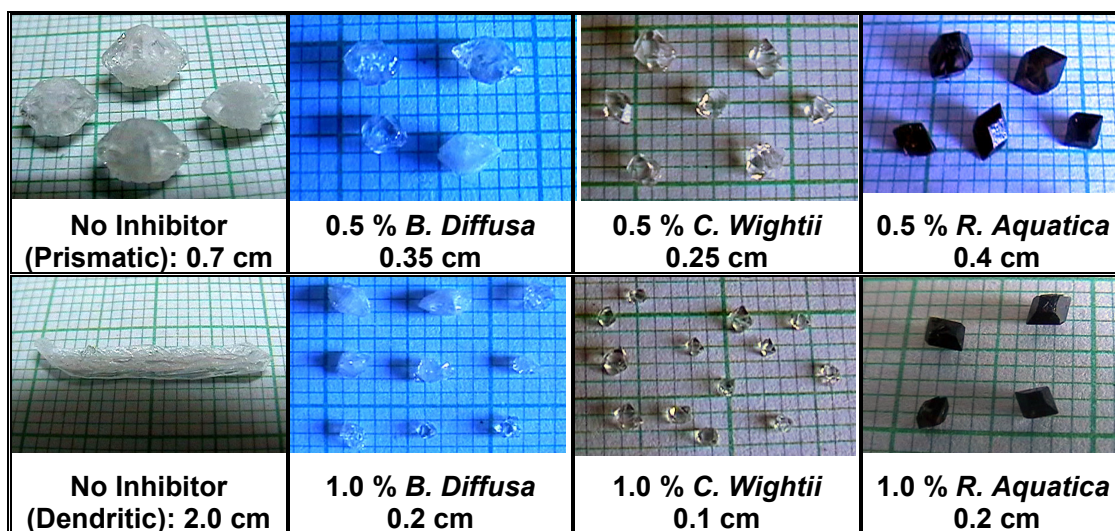


Figure : 6.14 Variation in the Size of Prismatic Type Struvite Crystals

From the figure it can be perceived that the average dimension of the prismatic type crystals grown with the herbal extracts are comparatively smaller than that of control solution, which also gives an idea of the inhibitory effect of all the three evaluated extracts. The least average dimension of prismatic crystals is found to be 0.1 cm for the 1.0 % *C. wightii* extract.

6.6.8 Fragmentation of Struvite Crystals

The phenomenon of fragmentation or fracture of the grown struvite crystals due to the presence of the herbal extract was quite interesting and deserved further attention. The incorporation of extract not only allowed the crystalline face to grow further, but presumably weakened the existing bonds, leading to cracking and further fracture into fragments. The depth of fragmentation of grown crystals, i.e., the depth from the gel-liquid interface up

to which the crystals start breaking near the gel-liquid interface was noticed for each of the concentrations of the assessed herbal extracts. Figure 6.15 shows the plots of the depth of fragmentation *versus* time interval. Initially, the concentration of extracts in the gel column was less and gradually built up due to diffusion in to the gel from the SS, which consequently increased the depth of the fragmentation with the passage of time.

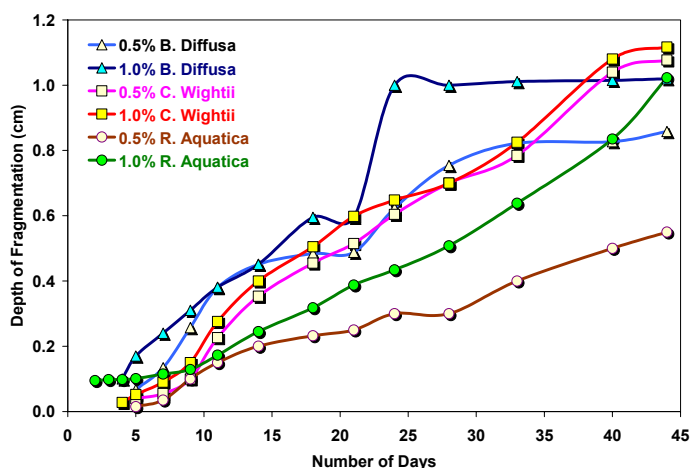


Figure : 6.15 Depth of Fragmentation *versus* Days

It was also observed that at higher depths some of the fragmented crystals retained their critical size. As the concentration of the extract was low at higher depths in the gel column than at the gel-liquid interface, it did not allow crystals to dissolve completely after the fragmentation, but retained a steady state, i.e., a balance between the growth and dissolution. The average length of crystals after fragmentation was found even less than 1 mm. After fragmentation, the dimensions of crystals remained far less than 5 mm, i.e., the maximum dimension of calculi which can pass through the urinary tract.

6.6.9 Total Mass and Volume of the Grown Struvite Crystals

After the growth and dissolution studies, the struvite crystals were gently removed from the gel and the total mass as well as the total volume of the crystals for each concentration was measured.

Figure 6.16 shows the histograms depicting the total mass and total volume of the grown crystals for each concentration of the extracts.

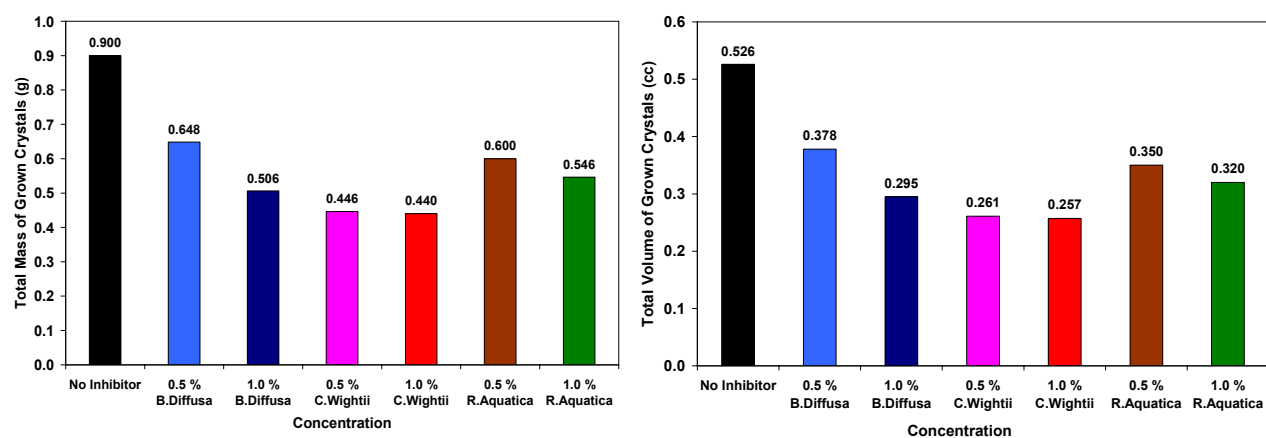


Figure : 6.16 Total Mass (Left) and Total Volume (Right) of the Grown Struvite Crystals in Different Concentration

Both total mass and volume of the grown struvite crystals are considerably lower for the extracts in comparison to the control solution depicting the inhibitory effect of the extracts. The least mass and volume are observed in the case of 1.0 % *C. wightii*.

6.6.10 Statistical Analysis

The single factor analysis of variance (ANOVA) was carried out using MS excel to check the comparison of values of apparent length of struvite crystal in the control and each extract groups. ANOVA statistical analysis confirmed that the variations in the average length of struvite crystals with concentration as well as with time for each evaluated herbal extracts were highly significant at 0.05 level. From this *in vitro* growth inhibition study, it can be concluded that all the investigated herbal extracts i.e. *B. diffusa*, *C. wightii* and *R. aquatica* are found to be a potent inhibitor for struvite crystals.

6.7 Growth Inhibition Study by Fruit Juice of *Citrus Medica* Linn

A treatment with alkali, usually in the form of magnesium potassium citrate or potassium citrate, is very common to increase urinary citrate and reduce the rates of stone formations in the patients of hypocitraturic calcium nephrolithiasis [153-155]. A critical review on preventive treatment of nephrolithiasis with alkali citrate is written by Mattle and Hess [156]. Inasmuch as the most of the earlier studies on citrate inhibition have been mainly concentrated on calcium oxalate monohydrate and brushite crystals, the present investigation has been carried out to prove the citrate inhibition in struvite crystals also. For human being Acetohydroxamic acid (AHA) is the most widely used irreversible inhibitor of bacterial urease. AHA has a high renal clearance, can penetrate the bacterial cell wall, and acts synergistically with several antibiotics. Although *in vivo* studies have demonstrated that AHA inhibition of bacterial urease decreases urinary alkalinity and ammonia levels even in the presence of infection, 20 % of patients experience associated adverse effects. These include phlebitis, deep venous thrombosis, and hemolytic anemia. In addition, the use of AHA in patients with impaired renal function (serum creatinine level > 2.5 mg/dL) limits its effectiveness and increases its toxicity [157].

Struvite type kidney stones thrive in basic conditions of urine and hence the treatment should be the acidification of the urine. It is of prime importance to carry out the search for suitable struvite inhibitor, which has probably no side effects. As one of the main chemical constituents in the juice of *Citrus medica* Linn is citric acid, it has been decided to check its inhibitive effect on struvite crystals. Therefore, the growth inhibition study of struvite

crystals was carried out by the present researcher using natural fruit juice of *Citrus medica* Linn under *in vitro* conditions to identify the potency of its inhibition, which can be further, studied *in vivo*.

6.7.1 Single Diffusion Gel Growth Technique

For this study single diffusion gel growth technique was used and up to the process of gelation the same steps were followed as described in the sub section 6.6.1 of this chapter. After gelation took place, 20 mL supernatant solutions (SS) of pure 1.0 M magnesium acetate— $\{C_4H_6MgO_4 \cdot 4H_2O\}$ prepared with different concentration of fresh and filtered juice of *Citrus medica* Linn were gently poured on the set gels in test tubes. After pouring SS, the test tubes were capped with airtight stopples. Here, for each test tube, 20 mL SS of 1.0 M magnesium acetate were prepared by taking different volumes of the juice of *Citrus medica* Linn and distilled water. Composition and the pH of the SS are as shown in table 6.6.

Table : 6.6 : Composition and pH of SS with Fruit Juice of *Citrus Medica* Linn

Number of Supernatant Solution (SS)	Composition of the Supernatant Solution (SS)			pH of the Supernatant Solution
	Volume (mL)		Powder (g)	
	Juice of <i>Citrus Medica</i> Linn	Distilled Water	Magnesium Acetate	
SS-1	00	20	4.288	7.80
SS-2	02	18	4.288	5.87
SS-3	04	16	4.288	5.40
SS-4	06	14	4.288	5.01
SS-5	08	12	4.288	4.87
SS-6	10	10	4.288	4.75
SS-7	12	08	4.288	4.67
SS-8	14	06	4.288	4.57
SS-9	16	04	4.288	4.50
SS-10	18	02	4.288	4.43
SS-11	20	00	4.288	4.35

6.7.2 Struvite Crystals Grown in the Gel Media

Figure 6.17 shows the photographs of the struvite crystals grown in the gel medium. It is observed that as the concentration of the juice of *Citrus medica* Linn is increased in the SS, the number of struvite crystals grown in the silica hydro gel medium decreases and also average size of the struvite crystals decreases. This clearly indicates inhibition due to *Citrus medica* Linn.

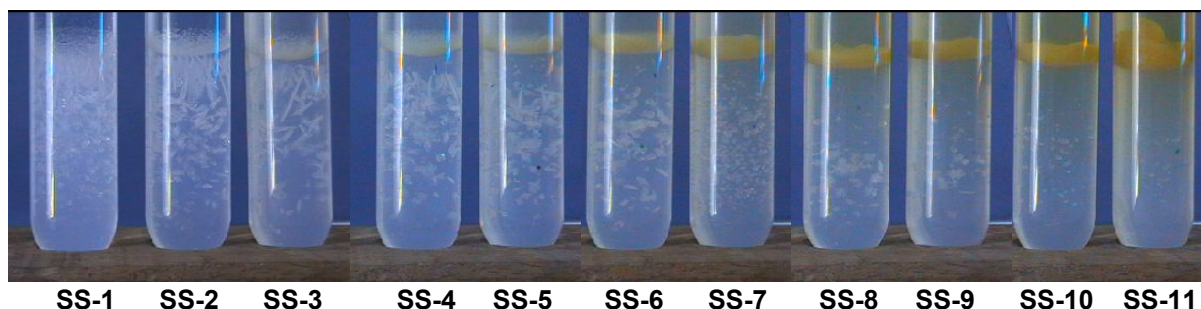


Figure : 6.17 Photographs of the Struvite Crystals Grown in Gel Medium in Test Tubes with Different Concentration of the Juice of *Citrus Medica* Linn

6.7.3 Growth of Struvite Crystals at Gel – Liquid Interface

After pouring of the SS, dendritic type crystals were grown in the gel at the gel–liquid interface. The growth rates of struvite crystals, at the end of 2nd and 4th day, growing in the gel at the gel–liquid interface for different concentration of SS are presented in table 6.7.

Table : 6.7 : Growth Rates of the Struvite Crystals Growing in the Gel at Gel–Liquid Interface for the Different Concentrations at the End of 2nd and 4th Day

Number of Supernatant Solution	Growth Rate (cm / day)	
	At the end of Day 2	At the end of Day 4
SS-1	0.608	0.309
SS-2	0.300	0.192
SS-3	0.250	0.125
SS-4	0.240	Dissolution Started
SS-5	0.225	Dissolution Started
SS-6	0.240	Dissolution Started

It can be noticed from table 6.7 that the growth rate of crystals and hence the size of the crystals are decreased with the increasing concentration of *Citrus medica* Linn. Here, the lower values of growth rate in comparison to control solution, the reductions in growth rates with increasing concentrations of the juice as well as the reduction in growth rates with time evidently proved the inhibitory effectiveness of the juice.

It was observed that the length of crystals growing in the gel at gel–liquid interface increased up to first 4 days in the cases of the SS-1 (i.e., control solution) and SS-2; and then they started dissolving. The length was increased up to first 3 days in the case of SS-3 and the dimension remained unchanged up to the end of 4th day; and then started dissolving. In the cases of the SS-4 to SS-6, length of the crystals growing in gel at gel–liquid interface increased just up to first 2 days; and then they started dissolving gradually.

It was remarkably found that in the case of SS-7 and for other higher concentrations, i.e., for SS-7 to SS-11, struvite crystals could not either nucleate or grow at the gel–liquid interface; which can be clearly noticed in the photographs in figure 6.17. This might be due to the effect of higher concentration of the juice of *Citrus medica* Linn in the SS. Thus, this study significantly proved the inhibitory potency of the *Citrus medica* Linn juice.

Figure 6.18 shows the histograms depicting the maximum apparent length of the grown struvite crystals in the gel media for different concentrations of SS. It is observed that the maximum dimensions of the grown crystals in the gel media decreases with the increasing concentration of *Citrus medica* Linn in the SS, which may be due to inhibitory effect of the juice.

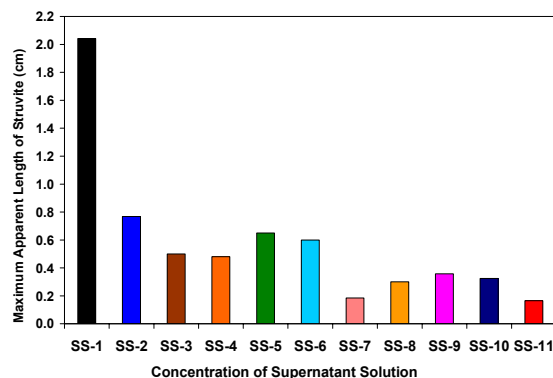


Figure : 6.18 Maximum Apparent Length of Dendritic Type Struvite Crystals

6.7.4 Growth and Dissolution of Struvite Crystals at Gel–Liquid Interface

This study is important as it is conducted under the growth conditions. The simple dissolution is tested by placing the already grown crystal in an appropriate solution. The usual aim is to achieve the inhibition and dissolution of growing calculi in a body, where the required nutrients for the growth are being continuously supplied. Altogether, the same thing is mimicked in this *in vitro* experiment. At the gel–liquid interface the concentration gradients of the nutrients are the maximum and hence it is important to study the effect of juice on the growing crystals. The growth and dissolution of struvite at the gel–liquid interface is shown by the plots of average length *versus* time period in figure 6.19.

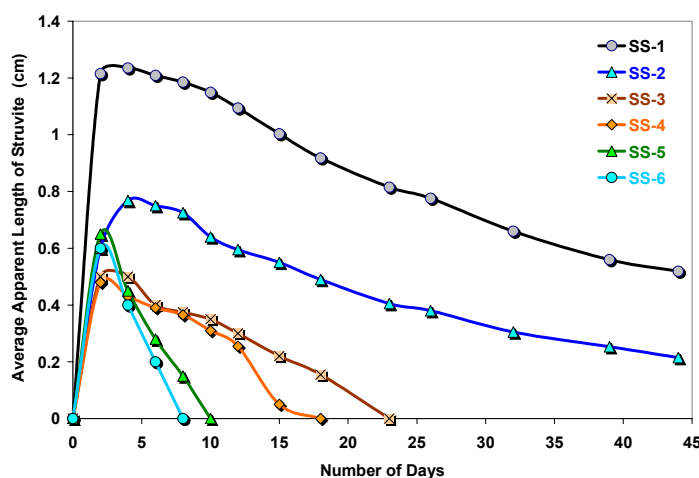


Figure : 6.19 Growth and Dissolution of Struvite at the Gel–Liquid Interface

It is found that the crystals grown at the gel-liquid interface are dissolved up to a certain extent in control solution SS-1, which may be due to the formation of acetic acid. But, at the same time, it is observed that the dissolution of the crystals grown at the gel-liquid interface takes place comparatively faster for the higher concentrations of *Citrus medica* Linn, i.e., for the SS-2 to SS-6.

The dissolution rates of grown crystals in the gel at gel-liquid interface for the different concentration of *Citrus medica* Linn are as given in table 6.8.

Table : 6.8 : Dissolution Rates of the Struvite Crystals in the Gel at Gel-Liquid Interface for the Different Concentrations

Dissolution Rates (cm / day)	No Inhibitor SS-1	Concentration of SS with Juice of <i>Citrus medica</i> Linn				
		SS-2	SS-3	SS-4	SS-5	SS-6
Dissolution Rate (cm / day)	1.79×10^{-2}	1.38×10^{-2}	2.63×10^{-2}	3.00×10^{-2}	4.51×10^{-2}	6.00×10^{-2}
Enhanced Dissolution Rate (cm / day)	-	-0.41×10^{-2}	0.84×10^{-2}	1.21×10^{-2}	2.72×10^{-2}	4.21×10^{-2}
% of Enhanced Dissolution Rate	-	-	47 %	67.59 %	151.95 %	235.19 %
Number of Days Required for Complete Dissolution of the Dendritic Type Struvite Crystals Grown at the Gel – Liquid Interface						
Days	-	70	23	18	10	08

Dissolution rates for SS-3 to SS-6 are found remarkably higher than that of control solution. Moreover, the dissolution rates are increased with the increasing concentration of juice in the SS, except the case of SS-2. Moreover, table 6.8 also represents enhanced dissolution rates as well as the percentage of enhanced dissolution rates due to the presence of juice. This further suggests that at the gel – liquid interface the already observed dissolution due to the formation of acetic acid is enhanced by the presence of juice. It is found that the percentage of enhanced dissolution rates increased appallingly with the increasing concentration of juice.

As mentioned in table 6.8, the number of days required for the complete dissolution of the dendritic type struvite crystals grown at the gel – liquid interface are reduced with the increasing concentration of juice. It is further noticed that minimum 8 days were required for the complete dissolution of crystals grown at gel – liquid interface for the concentration of SS-6.

6.7.5 Growth and Dissolution of Struvite Crystals at Different Depth

At different depths from the gel–liquid interface the grown crystals were measured and the phenomenon of the on set of dissolution was noted down. The growth and dissolution of struvite crystals grown at different depths in each cases from SS-2 to SS-11 are as shown in the plots of average length *versus* time in figures 6.20 (a-j). As the depth of the gel column increases, the average lengths of the grown crystals are decreased gradually by taking more time. It may be due to the lower concentration gradients at higher depths. Moreover, the average size of grown struvite crystals decreases with the increasing concentration of the juice in the SS. The period of dissolution, i.e., the time taken for the complete dissolution of the crystals, is found moderately less for the crystals grown near the interface, whereas it is quite longer for the crystals grown at the higher depth. At the gel–liquid interface the dissolution is faster due to the presence of sufficient amount of the juice. However, the amount of the juice decreases down towards the bottom of the gel column, which may be responsible for the delayed dissolution. It can be noticed from the figure 6.20 (j) for SS-11 that the dissolution period is the same for two different depths and average length of crystals are almost nearly same, which indicates that the higher amount of juice brings almost enough concentrations in the gel column to dissolve crystals nearly in uniform manner.

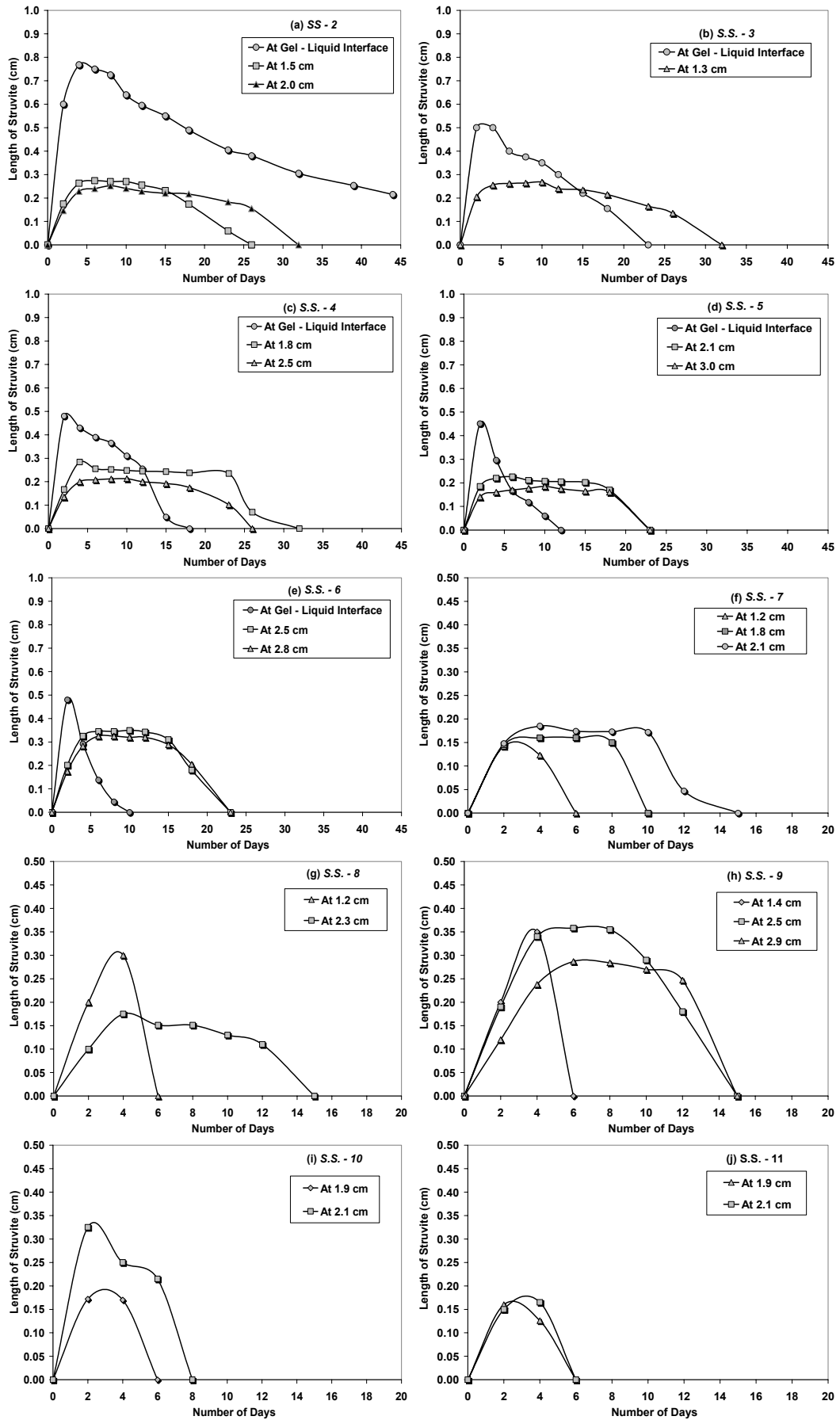


Figure : 6.20 (a) to (j) Growth and dissolution of Struvite at different depth from the gel-liquid interface

6.7.6 Depth of Dissolution

The depth of dissolution is defined as the depth from the gel – liquid interface up to which either the grown crystals are dissolved completely or no crystal can grow at all. Figure 6.21 shows the plots of depth of dissolution versus time in days. It is found that the depth of dissolution increases with time. In pure control solution SS-1, it is almost parallel to the x-axis and for solutions of higher concentrations of the juice it is pushed deeper and deeper in to the gel. The depth of dissolution is increased slowly for the lower concentration, while it is increased rapidly for the higher concentrations, e.g., the depth of dissolution of 5.00 cm is achieved in just 15 days for SS-10 and SS-11; while it is achieved in 39 days for SS-4. Single factor ANOVA was also carried out; which established that the difference in the depth of dissolution was highly significant at 0.001 level.

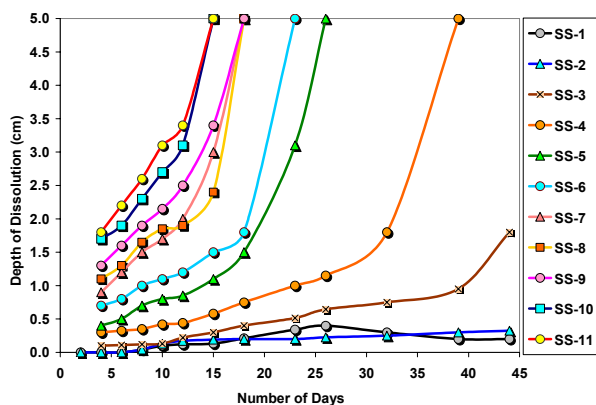


Figure : 6.21 Depth of Dissolution

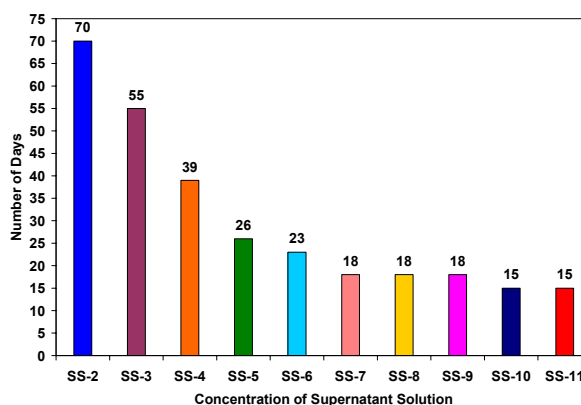


Figure : 6.22 Days for Complete Dissolution

6.7.7 Complete Dissolution

A histogram of figure 6.22 shows the numbers of days required for the complete dissolution of grown crystals in the gel media for different concentrations of SS. It is found that, the number of days required for the complete dissolution is reduced with the increasing concentration of the juice of *Citrus medica* Linn in the SS. For example, one can notice from the

histogram that it took 70 days for the complete dissolution for SS-2 and just 15 days for SS-11. Thus the reduction in the days for the complete dissolution with the increasing concentration of juice undoubtedly proved the potency of inhibition of struvite crystals.

6.8 Mechanism of Inhibition

Inhibition of crystal growth is widely studied subject and hence a collection of research papers has been edited by Amjad [158] and published in a book form. Inhibition is a complex interplay where the crystal structure, nature and bonds exposed on plane considered, adsorption the crystalline face, chemical potentials and chemical reactivity, impeding the motion of growing steps on crystalline face, forming a complex of cations required for growth in solutions etc. have their important influence.

Considering brushite crystal as a good model, Skitric et al [159] summarized following points for interaction of additives with crystal.

(1) The importance of molecular size and structure of the additive, i.e., small or macromolecules, number of functional groups in the molecule and its overall change in the growth of crystals. This may be useful in the selection of inhibiting molecule. For example, glutamate and aspartate ions have only one overall negative charge, which produce no significant effect on CHPD (brushite) crystal faces, which can be increased by attaching more negative groups like OH^- .

(2) The importance of structural fit between the organic molecule and the ionic structure of a particular crystal face. This decides the order of inhibition or reaction at particular crystalline face. This may differently affect various crystalline faces depending upon the crystalline face exposed to the solution

and as a result may change the morphology of the growing crystal. Small molecules with negatively charged groups, such as citrate ions do interact with the lateral faces of brushite crystals and slowing down the crystallization and inviting changes in the crystal morphology.

(3) The influence of the hydration layer exposed on the surface of the crystals. For polyaspartic acid and brushite crystals, such structural fit exists between distances of neighboring calcium ions from two adjacent layers constitute Ca - HPO₄ bi layer lying beneath hydrated layer parallel to the (0 1 0) plane.

Lundager Madsen and Bech Pederson [160] have found for brushite that most of the foreign metal ions are inhibitors, the only exception being Mg²⁺, which has no significant effect and Pb²⁺, which is a promoter. They have explained the inhibition and promotion mechanism as follows:

(1) Inhibition of crystal growth is due to adsorption of the inhibitor and so it is the inhibition of nucleation. The inhibitor is adsorbed to minute nuclei and preventing their further development.

(2) Promotion involves most likely the nucleation stage only, this stage being facilitated by the possibility of forming less soluble compound than that formed in the absence of additive. (For example, the promotive effect of Pb²⁺ on both crystallization and hydrolysis of brushite may be due to nucleation of less soluble hydroxypyromorphite {Pb₅OH(PO₄)₃}.)

(3) Reduction of average crystal size in comparison with the blank may be caused by promotion of nucleation, inhibition of crystal growth, or both. Growth inhibition is usually accompanied by irregular growth, because adsorption is not uniform, or growth rate fluctuates in space and time. If the

degree of adsorption is different for different faces of crystal then habit modification occurs.

Wierzbicki et al [42] studied inhibition of struvite by phosphocitrate. The presence of phosphocitrate induced crystal face specific inhibition of struvite crystals, which lead to the total cessation of crystal growth when sufficient inhibitor concentration was available. The crystal growth studies and results of molecular modeling suggested strong affinity of phosphocitrate to (1 0 1) faces of struvite. As a consequence of this an alteration in the expression of these faces was observed which led to the characteristic narrowhead struvite morphology. However, the similar changes were not observed in the presence of identical concentrations of citrate, acetohydroxamic acid, and N-sulfo-2-amino tricarballylate, indicating the unique interaction of phosphocitrate with the struvite crystal lattice.

To assess the inhibiting behaviour of phosphocitrate on struvite Wierzbicki et al [42] used Cerius molecular modeling software. The initial confirmation was positioned near the struvite surface within electrostatic interaction range and the energy minimization procedure was applied. The minimization procedure considers the contributions from electrostatic faces, van der Waal forces, hydrogen bonds, bond angles and dihedral angles to the total energy of a system. However, the application of model was complicated due hemimorphic nature of struvite [161], for which the crystal habit does not reflect the full symmetry group of the crystal. In hemimorphic character of struvite, (0 0 1) faces are accompanied by larger (0 0 $\bar{1}$) faces. Also (0 1 1) faces accompanied by smaller (0 1 $\bar{1}$) faces. The crystal morphology is

completed by a set of (1 0 1) faces accompanied by much smaller symmetry related (1 0 $\bar{1}$) faces.

There are also growth inhibition studies reported for hydroxyapatite by aspartic acid [162], heme crystals by antimalarials [163], COM crystals from human kidney tissue culture medium [164], calcium pyrophosphate crystals [165]. There are several models and mechanisms discussed by many authors, for instance, a model on complete crystal growth inhibition based on thermodynamics of interfaces [166] and computation by numerical solutions to modified fully transient 2D continuum model of crystal growth for arrest by an adsorption – inhibition mechanism [167].

The citrate inhibition theory has been widely discussed theory for urinary calculi inhibition. Citrate prevents crystallization by binding with calcium as well as citric acid brings the pH of solution to 3.0 to 4.0. Citrate is the most important complexor of calcium in urine and reduces ionic calcium concentration [15, 168-170].

As mentioned earlier in section 2.7.3 of chapter II, hypocitraturia, a low amount of citrate in urine, is considered to be an important risk factor for urinary stone formation. Generally urinary citrate is considered as important inhibitor of the crystallization of stone forming calcium salts. The mean normal urinary citrate excretion is 640 mg / day in healthy individuals.

In the pathophysiology, the excretion of citrate in urine is a function of filtration, re-absorption, peritubular transport, and synthesis by the renal tubular cell. The proximal tubule reabsorbs most (70-90%) of the filtered citrate and as a result the citrate secretion is negligible. Altogether, acid-base status plays the most significant role in citrate excretion. Alkalosis enhances

citrate excretion, whereas acidosis decreases it. In acidosis, increased citrate utilization by the mitochondria in the tricarboxylic acid cycle occurs. This results in lower intracellular levels of citrate, facilitating citrate-re-absorption and hence reducing citrate excretion. Citrate excretion is generally impaired by acidosis, hypokalemia, a high–animal protein diet, and urinary tract infection [171].

Citrate plays several important roles in the mechanism of urinary calculi formation. First of all citrate binds with calcium ions in the urine and reduces calcium ion activity, consequently, the lowering the urinary supersaturation of calcium phosphate and calcium oxalate. Second, citrate has a direct inhibitory effect on the crystallization and precipitation of calcium salts. In addition, citrate may also enhance the effectiveness of protein inhibitors of crystallization. For example, inhibition of aggregation of COM crystals by Tamm-Horsfall protein (THP) is increased by citrate. Citrate also expected to reduce the urinary osteopontin, which is an important component of the protein matrix of urinary calculi [172]. Moreover, urinary citrate excretion also increases urinary pH, which is a factor in uric acid crystallization and uric acid stone formation [171].

De Yoreo et al [173] carried out the combination of two investigative tools, namely, AFM and molecular modeling and discussed both the physical and stereochemical factors responsible for COM inhibition by citrate. Molecular modeling investigations of interactions of citrate with steps and faces on COM crystal surfaces provided links between the stereochemistry of interaction and the binding energy levels that underlie mechanisms of growth modification and changes in overall crystal morphology.

The citrate inhibition suggests that sodium citrate, citric acid and other citrate compounds are acting as alkalization agents indicated for systematic metabolic acidosis (renal tubular acidosis), while urinary alkalization or hypocitraturia contains di-sodium citrate. Pak et al [168] reported successful management of uric acid nephrolithiasis with potassium citrate. Potassium citrate reduces urinary saturation of calcium salts by complexing calcium and reducing ionic calcium concentration. Later on Pak [174] preferred potassium citrate because it appeared to decrease urinary calcium excretion at least transiently. Similarly, sodium citrate [175], potassium citrate [176], sodium potassium citrate [177], and potassium-magnesium citrate [178] were studied. In present author's lab, earlier workers studied *in vitro* growth inhibition of brushite crystals by citric acid [49,179,180].

Many juices have been tried to study the risk factor of urolithiasis. The effect of cranberry juice on urinary risk factor for calcium oxalate stones has been investigated by McHary et al [181], which exhibited antilithogenic properties. Effect of acute load of grapefruit juice on urinary excretion of citrate and urinary risk factors for renal stone formation has been discussed by Trinchieri et al [182]. Moreover, effect of blackcurrant, cranberry and plum juice consumption on risk factors associated with kidney stone has been reported [183]. As cranberry juice acidifies urine it could be useful in the treatment of brushite and struvite stones. Blackcurrant juice can support the treatment and metaphylaxis of uric acid stone disease because of its alkalizing effect. Lemon juice [180] and lemonade [184] have been found useful in management of urolithiasis. A comparative study of orange juice versus lemonade in reducing stone forming risk is reported [185].

In the present investigation of growth inhibition of struvite crystals by selected herbal extracts, the present author proposes two stage inhibition hypothesis. These herbal extracts contains several forms of sterol, lipids, organic acids etc. and they are expected to inhibit the growing struvite crystals in two different stages:

- (1) By forming stable complexes with Mg^{2+} ion and thus impeding the supply of Mg^{2+} ions for the growth of struvite crystals. (For instance, Magnesium-L-Aspartate Dihydrate $\{C_8H_{12}O_8N_2Mg.2H_2O\}$ is the magnesium salt of aspartic acid and like other magnesium salts of organic acids, is highly water soluble.)
- (2) By adsorption on the growing crystalline surface. The large amount of adsorption of organic compound may induce desorption of complex formed by Mg^{2+} ions and thereby weakening the bonds of crystals leading to fragmentation.

These herbal extracts contain different types of organic compounds and it is difficult to pin point directly which compound is responsible for growth inhibition of struvite crystals.

It is proposed by the present author that the citric acid present in the *Citrus medica* Linn is responsible for growth inhibition of struvite crystals. The other acids and sterols may be responsible for forming complexes of Mg^{2+} and thereby not allowing it for growth of struvite crystals. The higher concentration of juice contains higher concentration of citric acid which may dissolve struvite by forming a soluble magnesium citrate. Thus the present study may also support citrate inhibition theory for struvite crystals, which has been already proved for calcium oxalate and brushite crystals.

6.9 Conclusions

1. The comparative lower values of growth rate, reductions in the growth rates with the increasing concentrations of extracts as well as the reduction in the growth rates with the time proved the inhibitory effect of all the three evaluated extracts, i.e. *Boerhaavia diffusa* Linn, *Commiphora wightii* and *Rotula aquatica* Lour.
2. The maximum apparent lengths of the dendritic type struvite crystals grown at the gel – liquid interface were reduced with the increasing concentration of each tested extract.
3. Significant percentage of inhibition of growing struvite crystals at gel – liquid interface at the end of first day was noticed in each of the herbal extracts, clearly demonstrating the inhibitory effect of all the three extracts used for the investigation. The maximum percentage of inhibition 46.16 % was observed for 1.0 % *R. aquatica* extract, where as minimum 13.33 % of inhibition was observed for 0.5 % of *B. diffusa* extract.
4. Dissolution rates for all the cases with the herbal extracts were found remarkably higher than that of control solution. Moreover, dissolution rates significantly increased with the increasing concentration of herbal extract, except for *R. aquatica*. Enhanced dissolution rates were observed for all the herbal extracts. Maximum percentage of enhanced dissolution rate 138.8 % was observed in the case of 1.0 % *B. diffusa* Linn.
5. The dendritic type struvite crystals grown at the gel – liquid interface were found to be dissolved completely within 21 to 40 days in all the cases with herbal extract. Minimum 21 days were required for the complete dissolution for 1.0 % *B. diffusa*.

6. From the analysis of growth and dissolution rates, it was found that extracts of *R. aquatica* have retarded the growth rate from the very beginning of the crystal growth, whereas extracts of *B. diffusa* have speed up the dissolution rates once the growth of the crystals took place.
7. All the extracts impeded the diffusion process of reactants occurring in the gel column for the nucleation and, subsequently, the growth of crystals. The reduction in depths of growth indicated the inhibition offered by all the three herbal extracts.
8. Growth rates as well as the apparent size of the crystals grown at the higher depths were lower for all the cases with herbal extracts.
9. The average dimensions of the prismatic type crystals grown with the herbal extracts were comparatively smaller than that of control solution, which also gave an idea of the inhibitory effect of all the three evaluated extracts. The least average dimension of prismatic crystals was found to be 0.1 cm for the 1.0 % *C. wightii* extract.
10. The remarkable phenomenon of fragmentation of the grown struvite crystals was observed for all the three tested herbal extracts. The average length of crystals after fragmentation was found even less than 1 mm.
11. Both the total mass and volume of the grown struvite crystals were considerably lower for the cases with extracts depicting the inhibitory effect of all the evaluated herbal extracts. The least mass and volume observed for 1.0 % *C. wightii*.
12. As the concentration of the juice of *Citrus medica* Linn was increased in the SS, the number of struvite crystals grown in the gel medium decreased and also average size of the struvite crystals decreased.

- 13.** Lower values of growth rate in comparison to control case, reductions in the growth rates with the increasing concentrations of the juice as well as the reduction in growth rates with the time evidently proved the inhibitory effectiveness of the juice.
- 14.** Struvite crystals could not either nucleate or grow at the gel–liquid interface for the higher concentration of juice in the SS (e.g. SS-7 to SS-11), which significantly proved the inhibitory potency of the *Citrus medica* Linn juice.
- 15.** Maximum dimensions of the grown crystals in the gel media decreased with the increasing concentration of the juice in the SS, which might be due to inhibitory effect of the *Citrus medica* Linn juice.
- 16.** Dissolution rates of the crystals grown at gel-liquid interface for SS-3 to SS-6 were found remarkably higher than that of control solution. Moreover, the dissolution rates were increased with the increasing concentration of the juice in the SS, except the case of SS-2.
- 17.** Enhanced dissolution rates were observed for all the concentration with the *Citrus medica* Linn juice.
- 18.** The period of dissolution of the crystals was found moderately less for the crystals grown near the gel–liquid interface, whereas it was quite longer for the crystals grown at the higher depth from the gel–liquid interface.
- 19.** The depth of dissolution was increased slowly for the lower concentration, while it was increased rapidly for the higher concentration of the juice. Single factor ANOVA statistical analysis established that the difference in the depth of dissolution was highly significant at 0.001 level.

20.All the struvite crystals grown in the gel were found to be dissolved completely within 15 to 55 days in all the cases with the juice. Minimum 15 days were required for the complete dissolution in the cases of SS-10 and SS-11. Moreover, reduction in the number of days required for the complete dissolution with the increasing concentration of the juice undoubtedly proved the potency of inhibition of struvite crystals.

From this *in vitro* growth inhibition study of struvite crystals, it can be concluded that all the investigated herbal extracts i.e. *B. diffusa*, *C. wightii* and *R. aquatica* as well the juice of *Citrus medica* Linn are found to be potent inhibitors for struvite crystals.

References

1. M. Daudon, B. Bounxouei, C. F. Santa, S. S. Leite, B. Diouf, F. F. Angwafoo, J. Talati, G. Desrez, *Prog. Urol.*, **14** (2004) 1151.
2. Z. Djelloul, A. Djelloul, A. Bedjaoui, Z. K. Omar, A. Attar, M. Daudon, A. Addou, *Prog. Urol.*, **16** (2006) 328.
3. S. Atanassova, K. Neykov, I. Gutzow, *J. Cryst. Growth*, **160** (1996) 148.
4. L. Wang, W. Zhang, S. R. Qiu, W. J. Zachowicz, X. Guan, R. Tang, J. R. Hoyer, J. J. De Yoreo, G. H. Nancollas, *J. Cryst. Growth*, **291** (2006) 160.
5. H. Sidhu, R. Gupta, S. K. Thind, R. Nath, *Urol. Res.*, **14** (1986) 299.
6. A. Millan, O. Sohnel, F. Grases, *J. Cryst. Growth*, **179** (1997) 231.
7. H. Fleisch, *Kidney Int.*, **13** (1978) 361.
8. S. Atanassova, K. Neykov, I. Gutzow, *J. Cryst. Growth*, **212** (2000) 233.
9. F. Grases, J. March., F. Bibiloni, E. Amat, *J. Cryst. Growth*, **87** (1988) 299.
10. F. Grases, H. Millan, A. Gracia-Raso, *J. Cryst. Growth*, **89** (1988) 496.
11. I. Gutzow, S. Atanassova, G. Budevsky, K. Neykov, *Urol. Res.*, **21**(1993)181.
12. H. Ito, F. L. Coe, *Am. J. Physiol.*, **233** (1977) F 455.
13. K. Croft, J. H. Adair, R. Bowyer, J. G. Brockis, "Urinary Stones", Proc. of the 11th Int. Urinary Stone Conf., Singapore (1983). Eds. R. L. Ryall, J. G. Brockis, V. R. Marshall, Cheurchill Livingstone Co., Melbourne (1984).
14. D. Skrtic, H. F. Milhofer, *J. Cryst. Growth*, **129** (1993) 449.
15. P. A. Antinozzi, C. M. Brown, D. L. Purich, *J. Cryst. Growth*, **125** (1992) 215.
16. F. Grases, P. March, *J. Cryst. Growth*, **96** (1989) 993.
17. J. Garside, "Biological Mineralization and Demineralization", Ed. G. H. Nancollas, Springer Verlag, New York (1982).
18. S. R. Khan, P. N. Shevock, R. L. Hackett, *J. Urol.*, **139** (1988) 418.

19. J. Asplin, S. Gannelli, Y. Nakagawa, F. Coe, *Am. J. Physiol.*, **260**(1991)569.
20. R. S. Malek, W. H. Boyce, *J. Urol.*, **109** (1973) 551.
21. M. H. Malagodi, H. A. Moye, *Urol. Surv.*, **31** (1981) 8132.
22. R. S. Malek, W. H. Boyce, *J. Urol.*, **117** (1977) 336.
23. I. Das, S. Gupta, V. Pandey, S. Ansari, *J. Cryst. Growth*, **267** (2004) 654.
24. I. Das, S. K. Gupta, S. A. Ansari, V. N. Pandey, R. P. Rastogi, *J. Cryst. Growth*, **273** (2005) 546.
25. S. R. Qiu, A. Wierzbicki, E. Salter, S. Zepeda, C. A. Orme, J. R. Hoyer, G.H. Nancollas, A. M. Cody, J.J. De Yoreo, *J. Am. Chem. Soc.*,**127**(2005) 9036.
26. M. Beghalia, S. Ghalem, H. Allali, A. Belouatek, A. Marouf, *J. Med. Plants Res.*, **2** (2008) 66.
27. M. Beghalia, S. Ghalem, H. Allali, A. Belouatek, A. Marouf, *Malaysian J. Biochem. Mol. Biol.*, **16** (2008) 11.
28. A. Frackowiak, T. Kozlecki, P. Skibinski, W. Gawel, E. Zaczynska, A. Czarny, K. Piekarska, R. Gancarz, *J. Cryst. Growth*, **312** (2010) 3525.
29. N. A. M. Farook, S. Rajesh, M. Jamuna, *E-J. Chem.*, **6** (2009) 938.
30. E. A. A. Aal, S. Daosukho, H. E. Shall, *J. Cryst. Growth*, **311** (2009) 2673.
31. A. Bensatal, M. R. Ouharani, *Urol. Res.*, **36** (2008) 283.
32. V. S. Joshi, B. B. Parekh, M. J. Joshi, A. D. B. Vaidya, *J. Cryst. Growth*, **275** (2005) e1403.
33. V. S. Joshi, M. J. Joshi, *Indian J. Pure Appl. Phys.*, **41** (2003) 183.
34. V. S. Joshi, B. B. Parekh, M. J. Joshi, A. B. Vaidya, *Urol. Res.*, **33**(2005) 80.
35. K. C. Joseph, B. B. Parekh, M. J. Joshi, *Curr. Sci.*, **85** (2005) 1232.
36. B. B. Parekh, M. J. Joshi, A. D. B. Vaidya, *J. Cryst. Growth*, **310**(2008)1749.
37. D. Heimbach, D. Jacobs, S. C. Muller, A. Hesse, *Urology*, **55** (2000) 17.

38. I. Das, S. Verma, *J. Sci. Ind. Res.*, **67** (2008) 291.
39. B. B. Parekh, *Ph.D. Thesis*, Saurashtra University, Rajkot (2005).
40. J. Downey, J. Nickel, L. Claphom, R. J. McLean, *Br. J. Urol.*, **70** (1992) 355.
41. J. D. Sallis, R. Thomson, B. Rees, R. Shankar, *J. Urol.*, **140** (1998) 1063.
42. A. Wierzbicki, J. D. Sallis, E. D. Stevens, M. Smith, C. S. Sikes, *Calcif. Tissue Int.*, **61** (1997) 216.
43. S. Natarajan, E. Ramachandran, D. Suja, *Cryst. Res. Technol.*, **32** (1997)553.
44. W. Archilles, R. Freitag, B. Kiss, H. Riedmiller, *J. Urol.*, **154** (1995) 1552.
45. V. S. Joshi, M. J. Joshi, *Cryst. Res. Technol.*, **38** (2003) 817.
46. N. Srinivasan, S. Natarajan, *Indian J. Phys.*, **70A** (1996) 563.
47. K. R. Babu, M. Deepa, M. Nair, V. K. Vaidyan, *Bull. Mater. Sci.*, **21**(1998)121.
48. G. R. Shivkumar, E. Girija, S. N. Kalkura, *Cryst. Res. Technol.*, **33**(1998)197.
49. B. B. Parekh, M. J. Joshi, A. D. B. Vaidya, *Curr. Sci.*, **93** (2007) 373.
50. A. A. Raut, S. Sunder, S. Sarkar, N. S. Pandita, A. D. B. Vaidya, *Fitoterapia*, **79** (2008) 544.
51. A. B. Rendle, "*The Classification of Flowering Plants: Dicotyledons*", Vol.2, Cambridge University Press, London, UK (1925).
52. B. M. Goyal, P. Bansal, V. Gupta, S. Kumar, R. Singh, M. Maithani, *Int. J. Pharm. Sci. Drug Res.*, **2** (2010) 17.
53. G. L. Chopra, "*Angiosperms: Systematics and Life Cycle*", S. Nagin & Co., Jalandhar, Punjab, India (1969).
54. A. Singh, *Curr. Sci.*, **93** (2007) 446.
55. <http://botany.csd.tamu.edu/FLORA/imaxxny.htm>
56. D. N. Milic, *Ph.D. Thesis*, University of Naples Federico II, Napoli (2007).

57. V. H. Heywood, "*Flowering Plants of the World*", Oxford University Press, London, UK (1978).
58. S. R. Surange, G. S. Pendse, *Indian J. Med. Res.*, **7** (1972) 1.
59. T. N. Basu, M. B. Gupta, P. K. Seth, K. P. Bhargava, *J. Pharm. Pharmacology*, **12** (1968) 37.
60. K. Ahmad, A. Hossain, *J. Agric. Biol. Sci.*, **11** (1968) 41.
61. N. Lami, S. Kadota, Y. Tezuka, T. Kikuchi, *Chem. Pharm. J.*, **38** (1990) 1558.
62. B. Ahmed, C. P. Yu, *Phytochem.*, **31** (1992) 4382.
63. R. Bharali, M. R. H. Azad, J. Tabassum, *Indian J. Physiol. Pharmacol.*, **47** (2003) 459.
64. A. N. Mishra, H. P. Tiwari, *Phytochem.*, **10** (1971) 3318.
65. R. R. Agarwal, S. S. Dutt, *Chem. Abstr.*, **30** (1936) 44.
66. G. K. Jain, N. M. Khanna, *Indian J. Chem.*, **28** (1989) 163.
67. R. K. Seth, M. Khamala, M. Chaudhury, S. Singh, J. P. S. Sarin, *Indian Drugs*, **23** (1986) 583.
68. Web site: <http://www.rain-tree.com/ervatostao.htm>
69. K. M. Nadkarni, "*Indian Materia Medica*", 3rd edition, Popular Book Depot, Mumbai (1954).
70. K. R. Kirtikar, B. D. Basu, "*Indian Medicinal Plants*", 2nd edition, Lalit Mohan Basu Publications, Allahabad, India (1933).
71. R. W. Chopra, I. C. Chopra, K. L. Handa, L. D. Kapur, "*Medicinal plants in diabetes*", In : "*Indigenous Drugs of India*", Ed. P. Gupta, 2nd Edition, Dhar and Sons Ltd, Calcutta, India (1958).
72. R. N. Chopra, S. L. Nayar, I. C. Chopra, "*Glossary of Indian Medicinal Plants*", Council of Scientific and Industrial Research (CSIR), New Delhi, India (1996).

73. M. Aslam, "Asian medicine and its practise in Britain". In: "Pharmacognosy", Ed. W. C. Evans, Saunders Company Ltd, London, UK (1996).
74. D. K. Olukoya, N. Tdika, T. Odugbemi, *J. Ethnopharmacol.*, **39** (1993) 69.
75. T. N. Bhalla, M. B. Gupta, K. P. Bhargava, *Indian J. Med. Res.*, **6** (1971) 11.
76. C. A. H. Lima, J. S. Gracioso, E. J. Bighetti, R. L. Germonsén, B. A. R. Souja, *J. Ethnopharmacol.*, **71** (2000) 267.
77. V. Mudgal, *Planta Med.*, **28** (1975) 62.
78. S. K. Adesina, *J. Crude Drug Res.*, **17** (1979) 84.
79. M. Kaur, R. K. Goel, *Evidence-Based Complementary and Altern. Med.*, **2011** (2011) 7 pages, Article ID 310420, doi:10.1093/ecam/nep192.
80. P. A. Akah, A. I. Nwambie, *Fitoterapia*, **64** (1993) 42.
81. R. P. Singh, K. P. Shokala, B. L. Pandey, R. G. Singh, U. R. Singh, *Indian J. Med. Res.*, **11** (1992) 29.
82. B. B. Gaitonde, H. J. Kulkarni, S. D. Nabar, *Bull. Haffkine Inst.*, (Bombay, India), **2** (1974) 24.
83. E. Jarald, N. Nalwaya, E. Sheeja, S. Ahmad, S. Jamalludin, *Indian Drugs*, **47** (2010) 20.
84. M. V. Devi, S. Satyanarayana, A. S. Rao, *J. Res. Edu. Ind. Med.*, **5** (1986) 11.
85. K. K. Chakraborty, S. S. Handa, *Indian Drugs*, **27** (1989) 161.
86. B. K. Chandan, A. K. Sharma, K. K. Anand, *J. Ethnopharmacol.*, **31**(1991)299.
87. G. Rajukumari, A. Sarla, S. S. Agarwal, *Ind. J. Pharmacol.*, **23** (1991) 264.
88. A. K. Rawat, S. Mehrotra, S. C. Tripathi, U. Shome, *J. Ethnopharmacol.*, **56** (1997) 61.
89. L. Pari, M. A. Satheesh, *J. Ethnopharmacol.*, **91** (2004) 109.
90. L. Pari, M. A. Satheesh, *J. Med. Food.*, **7** (2004) 472.

91. S. Mehrotra, K. P. Mishra, R. Maurya, R. C. Srimal, V. K. Singh, *Int. Immunopharmacol.*, **2** (2002) 987.
92. S. Mehrotra, V. K. Singh, S. S. Agarwal, R. Maurya, R. C. Srimal, *Exp. Mol. Pathol.*, **72** (2002) 236.
93. R. Pandey, R. Maurya, G. Singh, B. Sathiamoorthy, S. Naik, *Int. Immunopharmacol.*, **5** (2005) 541.
94. J. Mishra, R. Singh, *Indian J. Pharmacol.*, **12** (1980) 59.
95. R. H. Singh, K. N. Udupa, *Indian J. Med. Res.*, **7** (1972) 1.
96. R. H. Singh, K. N. Udupa, *Indian J. Med. Res.*, **7** (1972) 17.
97. M. T. Olaleye, A. C. Akinmoladun, A. A. Ogunboye, A. A. Akindahunsi, *Food Chem. Toxicol.*, **48** (2010) 2200.
98. K. A. Manu, G. Kuttan, *Asia-Pac. J. Cancer Prev.*, **10** (2009) 1031.
99. S. Sreeja, *J. Ethnopharmacol.*, **126** (2009) 221.
100. K. A. Manu, G. Kuttan, *Immunopharmacol. Immunotoxicology*, **31**(2009) 377.
101. V. Soni, "Final Project Report of In-situ conservation of *Commiphora wightii* a red-listed medicinal plant species of Rajasthan state", IUCN, SSC Project, Jaipur (2008).
102. S. Kumar, V. Shankar, *Arid Environ.*, **5** (1982) 1.
103. V. Soni, *Conservation Evidence*, **7** (2010) 27.
104. I. Haque, R. Bandopadhyay, K. Mukhopadhyay, *Mol. Biol. Rep.*, **37**(2010)847.
105. G. L. Shah. "Flora of Gujarat State", University press, Sardar Patel University, Vallabh Vidhyanagar (1978).
106. S. D. Sabnis, K. S. S. Rao, "Proceedings of National Seminar on Resources", Ed. S. K. Jain, R. R. Rao, Botanical Survey of India, Dehradun (1983).

107. N. Zhu, M. M. Rafi, R. S. DiPaola, J. Xin, C. K. Chin, V. Badmaev, G. Ghai, R. T. Rosen, C. T. Ho, *Phytochem.*, **56** (2001) 723.
108. A. G. Bajaj, S. Dev, *Tetrahedron*, **38** (1982) 2949.
109. S. Swaminathan, R. K. Bakshi, S. Dev, *Tetrahedron*, **43** (1987) 3827.
110. V. Kumar, S. Dev, *Tetrahedron*, **43** (1987) 5933.
111. M. O. Fatope, K. S. Suad, J. O. Ochei, M. Z. Salma, Y. Takeda, *Phytochem.*, **62** (2003) 1251.
112. S. Dev, "A Selection of Prime Ayurvedic Plant Drugs", Anamaya Pub., New Delhi (2006).
113. S. Dev, *Pure Appl.Chem.*, **61** (1989) 353.
114. S. Shishodia, K. B. Harikumar, S. Dass, K. G. Ramawat, B. B. Aggarwal, *Anticancer Res.*, **28** (2008) 3647.
115. E. I. Ashry, N. Rashed, O. M. Salama, A. Saleh, *Pharmazie*, **58** (2003) 163.
116. V. Apte, "Monograph on Guggul and Guggul kalpa", Mumbai (1998).
117. N. L. Urizar, D. D. Moore, *Annu. Rev. Nutr.*, **23** (2003) 303.
118. X. Wang, J. Greilberger, G. Ledinski, G. Kager, B. Paigen, G. Jurgens *Atherosclerosis*, **172** (2004) 239.
119. G. V. Satyavati, C. Dwarakanath, S. N. Tripathi, *Indian J. Med. Res.*, **57** (1969) 1950.
120. S. C. Malhotra (Ed.), "Pharmacological & Clinical Studies of Guggulu in Hyperlipidaemia/Lipid Metabolism", Cent. Counc. for Res. in Ayurveda and Siddha, Ministry of Health & Family Welfare, Govt. of India, New Delhi (1992).
121. S. Nityanand, N. K. Kapoor, *Indian J. Exp. Biol.*, **9** (1971) 376.
122. N. L. Urizar, A. B. Liverman, D. T. Dodds, F. V. Silva, P. Ordentlich, Y. Yan, *Science*, **296** (2002) 1703.

123. R. B. Singh, M. A. Niaz, S. Ghosh, *Cardiovasc. Drugs Ther.*, **8** (1994) 659.
124. R. Deng, *Cardiovasc. Drug Rev.*, **25** (2007) 375.
125. D. Xiao, S. V. Singh, *Mol. Cancer Ther.*, **7** (2008) 171.
126. A. R. Chopade, N. S. Naikwade, W. A. Mulla, F. J. Sayyed, *Int. J. PharmTech Res.*, **3** (2011) 349.
127. K. B. Ishnava, Y. N. Mahida, J. S. S. Mohan, *J. Pharmacogn. Phytotherapy*, **2** (2010) 91.
128. www.phytoimages.siu.edu/users/pelserpb/4_4_11/4apr11/rotulaaquatica.jpg
129. K. P. Martin, *Plant Cell Rep.*, **21** (2003) 415.
130. S. Patil, C. I. Jolly, S. Narayanan, *Indian drugs*, **40** (2003) 328.
131. S. Patil, S. Narayanan, G. Eibl, C. I. Jolly, *Indian J. Exp. Biol.*, **42** (2004) 893.
132. R. P. Rastogi, B. N. Mehrotra, "*Compendium of Indian Medicinal Plant*", Vol. 1, National Institute of Science Communication, New Delhi (1959).
133. V. P. K. Nambiar, A. Jayanthi, T. K. Sabu, *Aryavaidyan*, **17** (2003) 73.
134. V. Narayanaswami, U. S. Ali, *Indian J. Med. Res.*, **1** (1967) 242.
135. D. P. Sebastian, S. Benjamin, M. Hariharan, *Phytomorphol.*, **52** (2002) 137.
136. T. Pullaiah, "*Encyclopedia of World Medicinal Plants*", Vol. 4, Regency Publication, New Delhi (2006).
137. C. P. Khare, "*Indian Medicinal Plants: An Illustrated Dictionary*", Springer, Berlin (2007).
138. A. P. Singh, *Ethno. Bot. Leaflets*, **11** (2007) 206.
139. M. Chithra, K. P. Martin, C. Sunandakumari, P. V. Madhusoodanan, *Indian J. Biotechnol.*, **3** (2004) 418.
140. K. V. S. R. G. Prasad, K. Bharathi, K. Srinivasan, *Indian Drugs*, **30**(1993) 398.

141. A. J. M. Christina, M. M. Priya, P. Moorthy, *Meth. Find. Exp. Clin. Pharmacol.*, **24** (2002) 357.
142. S. S. Mengi, V. J. Bakshi, *Pharma. Biol.*, **47** (2009) 491.
143. A. K. Meena, A. Kandale, M. M. Rao, P. Panda, G. Reddy, *Int. Res. J. Pharm.*, **2** (2011) 14.
144. H. Panda, “*Medicinal Plants Cultivation and their Uses*”, Asia Pacific Business Press, Delhi (2004).
145. Web site: www.ayushveda.com
146. T. R. Govindachari, *Fitoterapia*, **71** (2000) 317.
147. Anonymous, “*The Ayurvedic Pharmacopoeia of India*”, Part I, Vol III, Govt. of India, New Delhi, (2001).
148. Anonymous, “*The Wealth of India-Raw Materials*”, Vol III, National Inst. of Sci. Commun. and Inf. Resour., New Delhi (1992).
149. E. Peter, J. Peter, B. Nes, G. Asukwo, *Turk. J. Bot.*, **32** (2008) 161.
150. G. K. Jayaprakash, B. S. Patil, *Food Chem.*, **101** (2007) 410.
151. A. N. Sah, V. Juyal, A. B. Melkani, *J. Pharm. Res.*, **3** (2010) 2119.
152. A. N. Sah, V. Juyal, A. B. Melkani, *Pharmacogn. J.*, **3** (2011).
153. C. Y. Pak, *Am. J. Kidney Dis.*, **17** (1991) 420.
154. B. Hamm, S. Jordi, L. Zipperle, E. Ettinger, R. Giovanoli, *Nephrol. Dial. Transplant.*, **15** (2000) 366.
155. L. L. Hamm, K. S. Smith, *Endocrinol. Metab. Clin. North Am.*, **31** (2002) 885.
156. D. Mattle, B. Hess, *Urol. Res.*, **33** (2005) 73.
157. M. Meng, (2009) Struvite and Staghorn calculi, Web site:
<http://emedicine.medscape.com/article/439127-overview#showall>

158. Z. Amjad (Ed.), *“Advances in Crystal Growth Inhibition Technologies”*, Kluwer Academic Publishers, New York (2002).
159. M. Skitric, S. Sarig, H. Füredi-Milhofer, *Prog. Colloid Polym. Sci.*, **110** (1998) 300.
160. H. E. Lundager Madsen, Jo Bech Pedersen, *“Influence of Foreign Metal Ions on Crystal Morphology and Transformation of Brushite”*, In *“Advances in Crystal Growth Inhibition Technologies”*, Z. Amjad (Ed.), Kluwer Academic Publishers, New York (2002).
161. F. Abbona, R. Boistelle, *J. Cryst. Growth*, **46** (1979) 339.
162. S. P. Huang, K. C. Zhou, Z. Y. Li, *Trans. Nonferrous Met. Soc. China*, **17** (2007) 612.
163. C. R. Chong, D. J. Sullivan Jr., *Biochem Pharmacol.*, **66** (2003) 2201.
164. Y. Nakagawa, H. C. Margolis, S. Yokoyama, F. J. Kezdy, E. T. Kaiser, F. L. Coe, *J. Biological Chem.*, **256** (1981) 3936.
165. J. D. Sallis, A. Wierzbicki, H. S. Cheung, *“Calcium Pyrophosphate Crystal Salt forms and the Influence of Phosphocitrate”*, In *“Advances in Crystal Growth Inhibition Technologies”*, Z. Amjad (Ed.), Kluwer Academic Publishers, New York (2002).
166. M. R. Anklam, A. Firoozabadi, *J. Chem. Phys.*, **123** (2005) 144708.
167. L. N. Brush, E. Le, *Cryst. Growth Des.*, **6** (2006) 643.
168. C. Y. Pak, K. Sakhaee, C. Fuller, *Kidney Int.*, **30** (1986) 422.
169. J. L. Mayer, L. H. Smith, *Invest. Urol.*, **13** (1975) 36.
170. C. Y. C. Pak, *J. Urol.*, **128** (1982) 1157.

171. E. V. Lerma, "Hypocitraturia", Eds. B.F. Schwartz, L.G. Gomella, F. Talavera, website: <http://emedicine.medscape.com/article/444968-overview>, Updated: Mar 29, 2011.
172. B. Hess, L. Zipperl, P. Jaeger, *Am. J. Physiol.*, **265** (1993) F784.
173. J. J. De Yoreo, S. R. Qiu, J. R. Hoyer, *Am. J. Physiol. Renal Physiol.*, **291** (2006) F1123.
174. C. Y. Pak, *Miner. Electrolyte Metab.*, **13** (1987) 257.
175. K. Sakhaee, J. A. Harvey, P. K. Padalino, P. Whitson, C. Y. Pak, *J. Urol.*, **150** (1993) 310.
176. P. Barcelo, O. Wuhl, E. Servitge, A. Rousaud, C. Y. Pak, *J. Urol.*, **150** (1993) 1761.
177. J. Hofbauer, K. Höbarth, N. Szabo, M. Marberger, *Br. J. Urol.*, **73** (1994) 362.
178. B. Ettinger, C. Y. Pak, J. T. Citron, C. Thomas, B. Adams-Huet, A. Vangessel, *J. Urol.*, **158** (1997) 2069.
179. B. B. Parekh, M. J. Joshi, *Indian J. Pure Appl. Phys.*, **43** (2005) 675.
180. V. S. Joshi, M. J. Joshi, *Indian J. Pure Appl. Phys.*, **41** (2003) 183.
181. T. McHarg, A. Rodgers, K. Charlton, *BJU Int.*, **92** (2003) 765.
182. A. Trinchieri, R. Lizzano, P. Bernardini, M. Nicola, F. Pozzoni, A. L. Romano, M. P. Serrago, S. Confalanieri, *Dig. Liver Dis.*, **34** (2002) S 160.
183. T. Kessler, B. Jansen, A. Hesse, *Eur. J. Clin. Nutr.*, **56** (2002) 1020.
184. M. A. Seltzer, R. K. Low, M. McDonald, G. S. Shami, M. L. Stoller, *J. Urol.*, **156** (1996) 907.
185. C. V. Odvina, *Clin. J. Am. Soc. Nephrol.*, **1** (2006) 1269.

Chapter VII

Vickers Micro-hardness and Etching Study of Struvite

Topic Number	Topic	Page Number
7.1	Introduction	309
7.2	Hardness	311
7.3	Classification of Hardness Testing	312
7.4	Dynamic Hardness Tests	314
7.5	Static Indentation Hardness Tests	316
7.6	Brief Review of Hardness Studies of Urinary Calculi	328
7.7	Vickers Micro-hardness Study of Struvite	329
7.8	Chemical Etching Study of Struvite	342
7.9	Conclusions	351

7.1 Introduction

The presence of urinary calculi in the kidney causes discomfort and some times acute pain to patients. Hence, the removal of such calculi is important, which is commonly done, nowadays, non-destructively with lithotripters without surgery as discussed in section 2.10 of chapter II. The treatment of urinary stone diseases has been revolutionized since the introduction of lithotripters like extra-corporeal shock wave lithotripters (ESWL) in the early 1980s [1,2]. The introduction of ESWL has greatly reduced the need for surgical intervention. Because of the differences in chemical compositions and structural features of urinary calculi [3], the shock wave-stone interaction during ESWL [4], and thus the efficacy of stone fragmentation, may vary significantly. Stone hardness and brittleness are important variables to be considered when planning lithotripsy. Calculi of varying composition respond differently to shockwave fragmentation. Thus, accurate prediction of response to lithotripsy remains a challenge to the urologist. Certain factors such as the chemical composition, size, hardness and position of the calculus are known to be important in determining the success rate. Moreover, this treatment may cause collateral damage to the surrounding tissues. Most of the side effects and discomfort experienced after ESWL treatment are mild and temporary, on the other hand the more extreme side effects includes hemorrhage, edema, tubular necrosis as well as renal fibrosis [5]. Since the limited data on the material strength of kidney stones have been reported [6-9], it is, therefore, very much essential to find the hardness and related mechanical properties of these urinary calculi as well as urinary type crystals. The hardness values of these calculi can help

physicians to determine the appropriate intensity levels during the ESWL, so as to minimize the side effects inflicted. Zhong et al [10] advocated the use of micro-hardness test as it provides a simple and convenient way to characterize complex mechanical properties of renal calculi. Moreover, to determine the mechanical properties of renal calculi for better understanding the efficiency of stone fragmentation during ESWL, Zhang et al [10] used Knoop and Vickers hardness measurements to study the resisting capacity of a stone against a penetrating load. To improve the efficiency of ESWL management, it is desirable to identify the physical properties of urinary calculi which can offer direct correlation with their fragilities during ESWL and thus can be used to guide management procedures for more effective stone fragmentation.

In the present investigation, Vickers micro-hardness study was carried out and related mechanical properties of the struvite crystals were assessed. The study of different mechanical properties of *in vitro* gel grown struvite crystals will be useful in designing and optimizing the ESWL parameters for the management of struvite type calculi.

This chapter mainly describes two different facets - Vickers micro-hardness study as well as chemical etching study of struvite crystals. The first half of the chapter explains the concept of hardness, classification of various hardness measurement techniques, classical micro-indentation hardness techniques and the Vickers micro-hardness study along with related mechanical properties of struvite crystals. Whereas the later part of the chapter deals with the etching studies of struvite crystals using citric acid. The kinetic as well as thermodynamic parameters are also reported.

7.2 Hardness

Literally the meaning of hardness is the state or quality of being hard. The hardness of a material measures how tightly the atoms are held together within it. Hardness of material is ability of a body to resist permanent deformation. The term 'hardness' can have various meanings in different contexts, for example implying resistance to elastic deformation in the case of elastomeric materials or resistance to groove formation in scratching. The term hardness may also refer to resistance to bending, abrasion or cutting. However, according to the modern interpretation, hardness is the property of a material that enables it to resist plastic deformation on indentation by a comparatively strong and stiff indenter of well defined geometry. Stillwell [11] defined hardness as resistance against lattice destruction, whereas Ashby [12] stated it as the resistance offered by a solid to permanent deformation. It is now accepted that hardness is a measure of the resistance that the lattice offers to the motion of dislocations. Also, the chemical forces in a crystal resist the motion of dislocation as it involves the displacement of atoms. This resistance is termed as the intrinsic hardness of a crystal.

Initially metallurgists and mineralogists were interested in hardness. However, in the last several decades, physicists, chemists, material scientists, biologists, pharmacists, and many others also have involved themselves in studies of hardness. Discussion of various aspects of hardness and data on a large number of materials are found in books [13-15], compilations [16-18] and also in several articles strewn over many scientific journals.

Hardness tests are no longer limited to metals, but the currently available tools and procedures cover a vast range of materials including

polymers, elastomers, thin films, semiconductors, ceramics and also biomaterials.

Hardness testing is perhaps the simplest and the least expensive method for mechanical characterization of materials, since it does not require an elaborate specimen preparation, involves rather inexpensive testing equipment, and is relatively quick. The theoretical and empirical investigations have resulted in fairly accurate quantitative relationships between hardness and other mechanical properties of materials such as ultimate tensile strength, yield strength and strain hardening coefficient [19,20].

7.3 Classification of Hardness Testing

A variety of classical hardness test methods exist to determine hardness of materials. A comprehensive review of various hardness tests and its applications are available in the publications by Tabor [13], Mott [15], Shaw [18], Vander Voort [21], O'Neill [22], Williams [23] and Lysaght [24].

The hardness tests may be classified using various criteria, including type of measurement, magnitude of indentation load, and nature of the test (i.e., static, dynamic, or scratch). The many hardness tests listed here measure hardness under different experimental conditions, for instance, indenters of different sizes, shapes and materials with appropriate applied loads and reduce their data using different formulae. A broad classification of hardness tests is given in table 7.1.

Hardness tests can be classified as dynamic hardness test or static indentation hardness tests. Dynamic test methods measure hardness as related to elastic behaviour of materials, whereas static methods measure hardness as related to plastic behaviour of materials.

Table : 7.1 : Classification of Hardness Testing

Classification By		Hardness Testing Methods	
Class	Sub Class		
Attrition or Indentation Method	Dynamic Hardness Testing	Scratch Hardness Test	Reaumur Scratch Test (1722) Mohs Hardness Test (1822) Turner-Sclerometer Test (1896)
		Rebound Hardness Test	Scleroscope Hardness Test Shore Scleroscope Hardness Test (1907) Leeb Hardness Test (1975)
		Plowing Hardness Test	Bierbaum Sclerometer Test
		Cutting Hardness Test	
		Damping Hardness Test	Herbert Pendulum Test (1923) Kusnezow Pendulum Test
		Abrasion Hardness Test	Sandblast Type Test
		Erosion Hardness Test	
		Cloudburst Hardness Test	
	Static Hardness Testing	Static Indentation Hardness Test	Brinell Hardness Test (1900) Rockwell Hardness Test (1920) Vickers Hardness Test (1925) Knoop Hardness Test (1939)
	Size of Indentation (Magnitude of Indentation Load)	Macro	Macro-Indentation Hardness Test (Higher Loads)
Micro		Micro-Indentation hardness Test	Vickers Hardness Test (1 g to 200 g) Knoop Hardness Test (1 g to 200 g)
Nano		Nano-Indentation hardness Test	Nano-hardness Test (0.1mN Load, depth h < 200 nm)
Type of Measurement	Dimensions	Measurement of the dimensions of the indentation	Brinell Test (Curved Area) Vickers Test (Pyramidal contact area) Knoop Test (Pyramidal contact area)
	Depths	Measurement of the depths of the indentation	Rockwell Hardness Test (1920) Martens Hardness Test Nano-Indentation Method
Type of Indenter	Ball	Ball Indenter	Brinell Hardness Test Rockwell Hardness Test (For all the Scale other than A, C, D, N)
	Pyramidal	Pyramidal Diamond Indenter	Vickers Test (Face Angle 136°) Knoop Test (Rhombohedral shape with face angles 172° 30' and 130°)
	Spheroconical Diamond	Spheroconical Diamond Indenter	Rockwell Hardness Test (For Scale A, C, D and N)
	Berkovich Tip	Berkovich Nano Indenter	Nano-Indentation Hardness Test

Hardness tests are broadly classified as macro, micro or nano-hardness tests according to the forces applied and displacements obtained. The conventionally used terms like 'micro-hardness' or 'nano-hardness' are actually misnomers and there is nothing like 'micro' or 'nano' about the hardness of the material being tested. Only the sizes of the resulting indentations are either of micro or nano scale. So, terms 'micro-indentation hardness' or 'nano-indentation hardness' are perhaps better descriptions.

7.4 Dynamic Hardness Tests

In this type of test an indenter is dropped from a given height on the surface and the depth of the impression produced is measured. The hardness is expressed in terms of energy of the impact, the depth and size of the indentation. As different test methods are already summarized in table 7.1, the detailed discussions are avoided.

7.4.1 Scratch Hardness Test : Scratch hardness is the measure of how resistant a sample is to fracture or plastic (permanent) deformation due to friction from a sharp object. This test is the oldest form of hardness measurement and was probably developed by mineralogists. In the first test one merely observes whether the selected material is capable of scratching another. In the second form of this method, the hardness number is expressed in terms of width or depth of a scratch made with a diamond or a steel indenter, under a definite load traversing the surface at a steady rate. The scratch hardness is related to the breaking of the chemical bonds in the material, creation of micro-fractures on the surface, or displacing atoms (in metals) of the mineral. Generally, minerals with covalent bonds are the hardest, while minerals with ionic, metallic, or van der Waals bonding are

much softer. Reaumur test, Mohs test and Turner-sclerometer test are the examples of scratch hardness test.

7.4.2 Rebound Hardness Test : An object of standard mass and dimensions is bounced from the surface of the work piece being tested, and either the height or velocity of rebound is the measure of hardness. The test relates more closely to the elastic limit of the material than to the work-hardening and tensile strength characteristics of indentation tests. The Scleroscope, Shore Scleroscope and Leeb tests are examples of rebound hardness test.

7.4.3 Plowing Hardness Test : In which a blunt element (usually diamond) is moved across a surface of the specimen being tested under controlled conditions of load and geometry and the width of the groove is the measure of hardness. The Bierbaum test is of this type.

7.4.5 Cutting Hardness Test : Sharp tool of a given geometry is caused to remove a chip of standard dimensions.

7.4.6 Damping Hardness Test : In this test, change in amplitude of a pendulum having hard pivot resting on test surface is the measure of hardness. The Herbert pendulum test, Kusnezow pendulum test are the examples.

7.4.7 Abrasion Hardness Test : Specimen is loaded against a rotating disk and the rate of wear is taken as a measure of hardness.

7.4.8 Erosion Hardness Test : Sand or abrasive gram is caused to impinge upon the test surface under standard conditions and loss of material in given time is taken as the measure of hardness.

7.4.9 Cloudburst Hardness Test : A procedure in which a shower of steel balls, dropped from a predetermined height, dulls the surface of a hardened part in proportion to its softness and thus reveals defective areas.

Some of the above relative hardness tests are limited in practical use and do not provide accurate numeric data or scales particularly for modern day materials. The usual method to achieve a hardness value is to measure the depth or area of an indentation left by an indenter of a specific shape, with a specific force applied for a specific time. There are four main standard scientific methods like Brinell, Rockwell, Vickers, and Knoop tests. For practical reasons, each of these methods is divided into a range of scales, defined by a combination of applied load and indenter geometry. These tests are discussed briefly hereby.

7.5 Static Indentation Hardness Tests

7.5.1 Brinell Hardness Test

Brinell hardness test was devised in 1900 by Johan August Brinell, Swedish metallurgist [25,26]. It is perhaps the first scientific technique to measure hardness of materials and uses a desk top machine.

Brinell Ball Indenter : In a standard Brinell test 10 mm diameter hardened steel ball is used as an indenter. On tests of extremely hard metals a tungsten carbide ball is substituted for the steel ball. Ball indenter of tungsten carbide with 1 mm, 2 mm, 2.5 mm, 5 mm and 10 mm are being used for Brinell tests according to the needs of measurements.

Load Range : The Brinell test can be conducted for a wide load range usually starting from 1 kg to 3000 kg to cover all testing requirements. The full load is normally applied for 10 to 30 seconds depending on nature of sample.

Procedure of Measurement : In a standard Brinell test a ball indenter is pressed normally with the predefined load on the surface of metal under examination for a standard period as shown in figure 7.1(a, b, c). After the removal of the load, the diameters d_1 and d_2 of the indentation impression are

measured with a low powered microscope and mean value of diameter d is calculated. To reduce various errors, usually, the geometrical similarity of indentation marks should be preserved and hence the diameter of the impression mark should be kept within the range of 0.25 to 0.50 times the diameter of the ball.

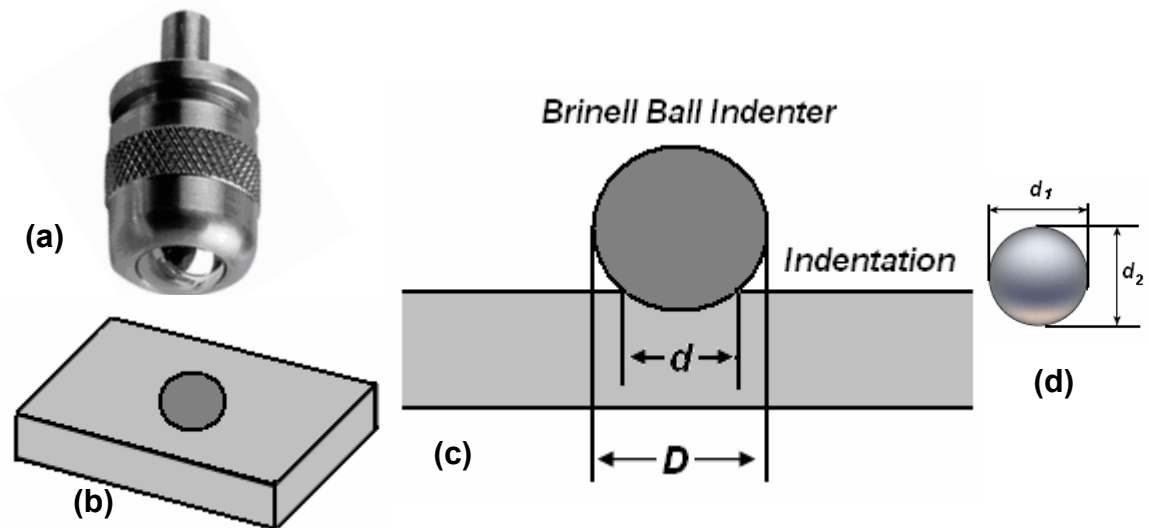


Figure : 7.1 (a) Brinell Ball Indenter, (b) Indentation Impression on Test Specimen, (c) Brinell Indentation on Test Specimen, (d) Measurement of Indentation Diameter

The Brinell hardness number (BHN) or H_B , or simply the Brinell number can be calculated using following formula

$$BHN = \frac{2 P}{\pi D \left\{ D - \sqrt{D^2 - d^2} \right\}} \quad (7.1)$$

Where P = applied load (in kg), D = diameter of an indenter (in mm) and d = diameter of an indentation impression (in mm). Computer aided automatic optical Brinell scopes are used for accurate measurements.

Baby Brinell Tests : It is common in Europe to perform Brinell tests on small parts using a 1 mm carbide ball and a test force as low as 1 kg. These low load tests are commonly referred to as baby Brinell tests.

Advantages : Among the three hardness tests, the Brinell ball makes the deepest and the widest indentations, so the test averages hardness over a wider amount of material, which is more accurate to be account for multiple grain structures and any irregularities in the uniformity of the alloy. By varying the test force and ball size, nearly all metals can be tested using a Brinell test.

Disadvantage : The impression may not be perfectly circular due to some reasons necessitating the measurement of two diagonals at right angles and using the mean value for estimating the hardness number. Though BHN widely and universally accepted in manufacturing practice, is not considered a satisfactory concept, since it does not represent the mean pressure over the curved area. An ultrasonic hardness tester – a modified version of the Brinell test has been developed to enable instantaneous and automatic read out by Szilard [27].

Application : Because of the wide test load range the Brinell test can be used on almost any metallic material. This method is the best for achieving the bulk or macro-hardness of a material, particularly those materials with heterogeneous structures. Brinell test is frequently used to determine the hardness of forgings and castings that have a grain structure too.

7.5.2 Rockwell Hardness Test

The concept of differential depth hardness measurement was first visualized by Paul Ludwik [28] in his book *Die Kegelprobe* (The Cone Trial) in 1908. The Rockwell hardness tester, a differential-depth machine, was co-invented by H. M. Rockwell and S. P. Rockwell [29], for which a patent filed in 1914 [30] and first used commercially in early 1920s.

Rockwell Hardness Scales : Several different Rockwell scales were defined, each with its own indenter geometry and maximum load, and each

appropriate for the testing of metals with a particular range of hardness. Rockwell hardness scales are divided into two main categories, (i) Regular Rockwell Scales, and (ii) Superficial Rockwell Scales.

Rockwell Indenter : Different types of indenter were developed for the Rockwell test to be used in conjunction with a range of standard force levels and scales. Spheroconical diamond indenters are used for A, C and D scale, whereas for all other scales Rockwell ball indenters are used. The diamond tip is specified by test method standards to have sphero-conical geometry with a 120° included cone angle and 0.2 mm radius tip, with the cone and radial tip blending in a tangential manner as illustrated in figure 7.2 [31].

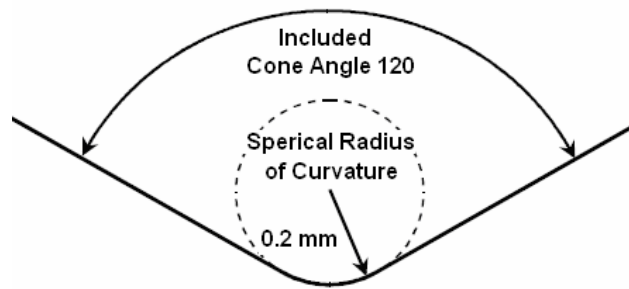


Figure : 7.2 Cross-Sectional View of Spheroconical Diamond Indenter Tip

Procedure of Measurement : In the case of the Rockwell hardness test, two levels of force are applied to the indenter at specified rates and with specified dwell times. Rockwell hardness of the material is based on the difference in the depth of the indenter at two specific times during the testing cycle. The value of regular Rockwell hardness H_R is calculated using following formula

$$H_R = 100 - \frac{h}{0.002} \text{ (for spheroconical indenter), } H_R = 130 - \frac{h}{0.002} \text{ (for ball indenter) (7.2)}$$

The superficial Rockwell hardness H_{RS} is calculated using following formula

$$H_{RS} = 100 - \frac{h}{0.001} \text{ (for spheroconical indenter and ball indenter) (7.3)}$$

Where h = difference in indentation depths measured in mm

Advantages : The test is fast, inexpensive, and relatively non-destructive, leaving only a small indentation in the material. The simplicity in the operation of a Rockwell hardness machine has provided the added advantage that Rockwell hardness testing usually does not require a highly skilled operator. One of the main strengths of the Rockwell is the small area of indentation needed. The advantage of this method lies in the rapidity with which it can be carried out and also because it does not involve optical measurements; which makes it very favorable in industries.

Disadvantage : Each Rockwell scale is an arbitrarily defined range of numbers from 0 to 100 covering a specific range of material hardness. Although, theoretically, the entire scale can be used for hardness testing, there are practical limitations on the range of testing for many of the Rockwell scales. The indenter is a major contributor to Rockwell hardness measurement error. Both the spheroconical diamond indenter and the ball indenter have characteristics that can cause significant measurement biases. The main disadvantage of this test lies with the piling up, sinking in and the elastic recovery upon removal of the load. A possible solution is due to the area of the indentation formed under the load is deduced from the acoustic impedance of the indenter-metal interface [32]. Again the dial reading is taken for hardness number, but it is based on the area of the indentation not on its recovered depth.

Applications : The hardness of plastics is most often measured by the Rockwell hardness test. Rockwell hardness is generally chosen for harder plastics such as nylon, polycarbonate, polystyrene, and acetal where the resiliency or creep of the polymer is less likely to affect the results.

7.5.3 Vickers Hardness Test

The Vickers hardness test was first described in 1922 [33] and developed in 1925 [34] by Smith and Sandland at Vickers Ltd, England, as an alternative to the Brinell method to measure the hardness of materials. It was formally also known as the Diamond Pyramid Hardness (DPH) test. The Vickers method is based on an optical measurement system.

Vickers Pyramidal Diamond Indenter : For the Vickers Hardness test, indenter should be such that, (i) indenter shape should be capable of producing geometrically similar impressions, irrespective of size; (ii) the impression should have well-defined points of measurement; and (iii) the indenter should have high resistance to self-deformation. A diamond in the form of a square-based pyramid whose opposite sides meet at the apex at an angle of 136° satisfies all of these conditions.

Reason for 136° Apex Angle of Vickers Indenter : From the Brinell test it is known that only indent diameters may be evaluated which lie within 0.25 to 0.5 times the diameter of Brinell ball indenter. The mean value of these two values is 0.375. If now the tangents are approached to the ball which touches the point of the 0.375 times ball diameter, then the tangents have an apex (apical) angle of 136° . Figure 7.3 explains the geometry of the apex angle of diamond indenter used in the Vickers hardness studies.

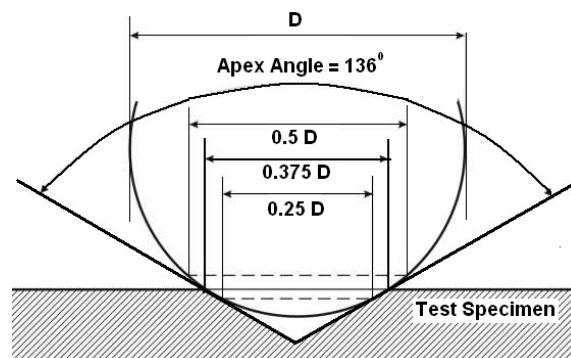


Figure : 7.3 Schematic Explanation of 136° Apex Angle of Vickers Indenter

Load Range : The Vickers test can be conducted for a wide load range usually starting from 5 g to 100 kg to cover all testing requirements. Although for the micro indentation hardness measurement load range must be kept within 5 g to 200 g.

Procedure of Measurement :

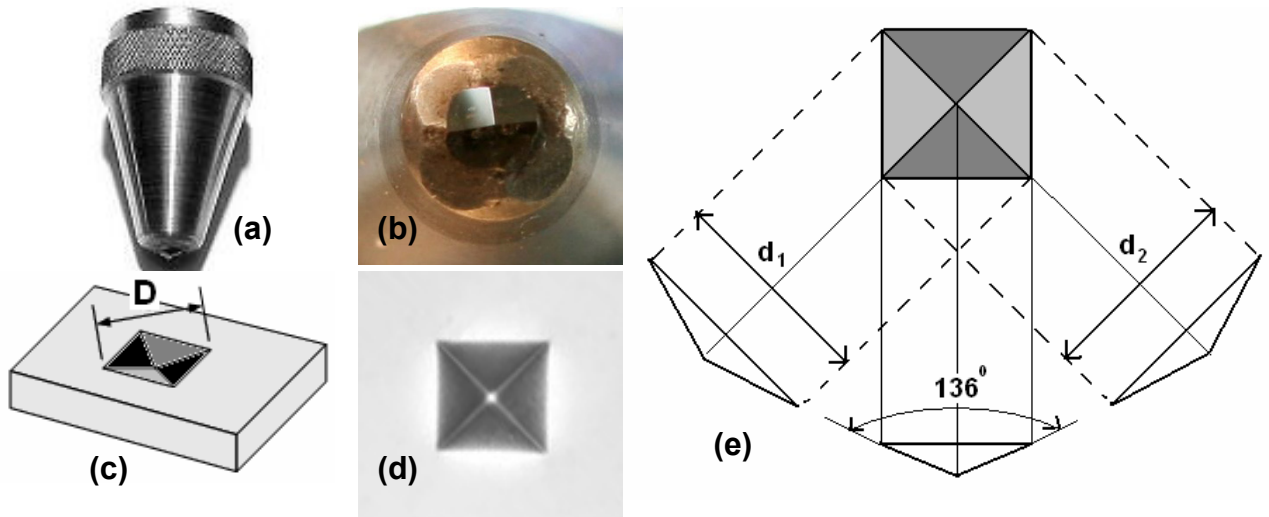


Figure : 7.4 (a) Vickers Square-based Pyramidal Diamond Indenter (b) End View, (c) Indentation Impression Side View (d) Indentation Impression Top View (e) Schematic Diagram of the Vickers Indentation Impression

The test samples with smooth surface should be kept perpendicular to the indenter on the horizontal specimen table of the tester. Indentations are made on the specimen by applying appropriate loads for definite time period usually 5 s. The impression left by the Vickers indenter is a rhombus look like a dark square on a light background. The indenter creates indentation of the order of microns. Figure 7.4 shows the Vickers square-based pyramidal diamond indenter, end on view of indenter [35], indentation impression and the schematic diagram of the Vickers indentation impression. The diagonals of indentation d_1 and d_2 are measured by means of an optical microscope

with filar eye piece, which is usually an integral part of the Vickers tester and mean arithmetic value d is calculated.

The Vickers micro-hardness number H_v (where H = hardness and subscript V = Vickers) is defined as the ratio of the applied load to the pyramidal contact area of the indentation and is calculated using the following formula:

$$H_v = \frac{P}{A} = \frac{2 P \sin\left(\frac{\theta}{2}\right)}{d^2} = \frac{2 P \sin 68^\circ}{d^2} = 1.854 \times \frac{P}{d^2} \quad (7.3)$$

Where, P is the applied indentation load in kg, A is the pyramidal contact area in sq mm, θ is the angle between the flat faces of the opposite sides of the indentation, which is 136° for Vickers micro-indenter, $1.854 (\approx 2 \sin 68^\circ)$ is a constant geometrical factor for the Vickers diamond type pyramidal indenter, d is the average diagonal length of the indented impressions in mm, and H_v is in kg / mm², conventionally, which can be converted in SI units MPa or GPa.

It is widely claimed in the literature that H_v remains constant with the change in load in the macro applied load range, whereas for micro-indentation tests, the Vickers hardness is not constant over the entire range of test loads. This phenomenon will be discussed later in this chapter.

Advantages : The advantages of the Vickers hardness test are as follows :

- It is a nondestructive method.
- Just one type of diamond indenter can be used for all types of surfaces irrespective of hardness.
- The indentation impression, produced by the Vickers indenter is clearer, than that of Brinell indenter and hence this method is more accurate.
- The indentations are geometrically similar, irrespective of size.

- Extremely accurate readings can be taken. Since determining the diagonal of a square impression is easier than determining the diameter of a circular impression, the hardness obtained by the Vickers test may be more accurate than the Brinell test.
- Microscopic regions can be investigated using much lower loads.
- The test is very precise and adaptable for testing the softest to hardest of materials, under the varying loads. One can use a wide range of test forces to suit every application.
- The biggest advantage of Vickers is its scale, which comprises the smallest and the highest hardness values in one scale, i.e. just one scale covers the entire hardness range. It is thus very suitable for laboratory tests. Vickers test can be used for all metals.
- Due to a wide range of applied force, the Vickers tester is useful for measuring the hardness of very thin as well as thick specimens.
- Indenter deformation is negligible on hard material.

Disadvantage : The main drawback is the need to optically measure the indentation size. To overcome this limitation, computer aided automatic optical instruments are used.

Applications : Since the test indentation is very small in Vickers test, it is useful for a variety of applications, such as testing very thin materials like foils or measuring the surface of a part, small parts or small areas, measuring individual microstructures, or measuring the depth of case hardening by sectioning a part and making a series of indentations to describe a profile of the change in hardness. It is also used for measuring the micro-hardness of many biomaterials.

7.5.4 Knoop Hardness Test

Frederick Knoop et al [36] developed his elongated pyramidal indenter as an alternative to the square base pyramidal Vickers indenter, in large part to overcome the cracking observed in brittle materials. It is a pure micro-hardness test.

Knoop Rhombohedral Diamond Indenter:

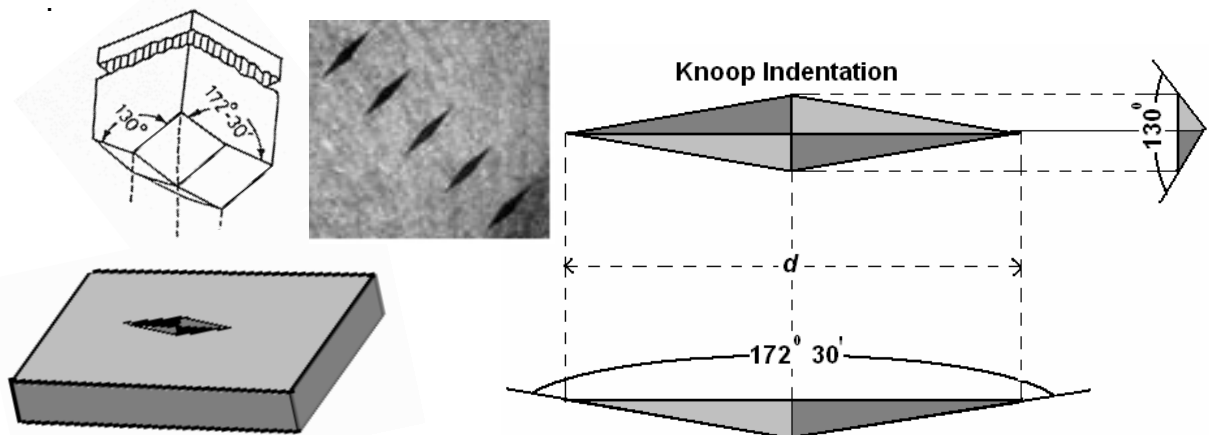


Figure : 7.5 Schematic Diagram of the Knoop Indentation Impression

The Knoop indenter has a polished diamond with rhombohedral shape with an included longitudinal angle of $172^{\circ} 30'$ and an included transverse angle of 130° . The narrowness of the indenter makes it ideal for testing specimens with steep hardness gradients. The depth of the indenter can be approximated as $1/30$ of the long dimension. The resulting indentation have long-to-short axis ratio of 7:1. Knoop indentations are about 2.8 times longer and shallower than the Vickers indentations made at the same load. Figure 7.5 shows the Knoop indenter, indentation impression and the schematic diagram of the Knoop indentation.

Load Range : Usually, Knoop tests are carried out for the load range of 10 g to 1000 g.

Measurement Procedure : The Knoop indenter is used in the same machine (with high powered microscope) as the Vickers indenter, and the test is conducted in exactly the same manner, except that the Knoop hardness (H_K) is calculated based on the measurement of the long diagonal only and calculation of the projected area of the indent rather than the surface area of the indent. The Knoop micro-hardness number H_K is calculated using the following formula:

$$H_K = \frac{P}{c d^2} = \frac{P}{\left[\frac{\tan\left(\frac{\beta}{2}\right)}{2 \tan\left(\frac{\alpha}{2}\right)} \right] d^2} = 14.229 \frac{P}{d^2} \quad (7.4)$$

Where, c is the Knoop indenter constant, $\alpha = 172^\circ 30'$, $\beta = 130^\circ$, P is the applied load in kg and d is the long diagonal length of the indentation measured in mm and H_K is in kg / mm².

Advantage : The advantages of the test are that only a very small sample of material is required. One scale covers the entire hardness range. Cracking problems are also less severe than with Vickers indentations.

Disadvantages : Knoop hardness varies with test load and results are more difficult to convert to other test scales. Optical microscope resolution may limit the application of the Knoop hardness test due to the resulting shallow indentations. The magnifications required to measure Knoop indents dictate a highly polished test surface. To achieve this surface, the samples are normally mounted and metallurgically polished; therefore Knoop is almost always a destructive test.

Application : This method is suitable for thin plastic as well as metal sheets, brittle materials, or materials where the applied load must never exceed 3.6

kg. The Knoop test is better suited for testing thin coatings, since the depth of indentation is only 1/30 of the long diagonal. The Knoop hardness test is a better choice for hard brittle materials such as glass and ceramics where indentation cracking would be more extensive using the Vickers indenter at the same load. It is also preferred for testing hardness of tooth structure.

7.5.5 Nano-Hardness Test

The nano-indentation hardness test technique was developed in the mid-1970s. This technique is also known as instrumented indentation testing, Depth-Sensing Indentation (DSI), continuous recording indentation and ultra-low-load indentation, which is a relatively new form of mechanical testing that significantly expands on the capabilities of traditional hardness testing. The name given to the technique is DSI, since the penetration depth is continuously monitored as a function of load during the instrumented indentation test. This technique has been largely used to evaluate mechanical properties of materials at the nano-scale level, especially hardness and elastic modulus. As shown in figure 7.6 three-sided, pyramid-shaped diamond indenter tip with a total included angle of 142.3° developed by Berkovich is used for testing. Nano-indenting is performed in conjunction with atomic force microscopy (AFM) or scanning electron microscopy (SEM). The selection of area for testing as well as indentations and scratching mark measurements are carried out by AFM.

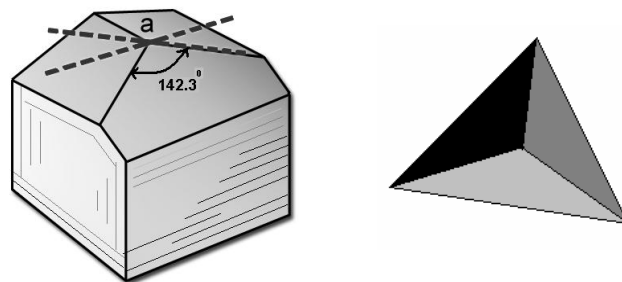


Figure : 7.6 Berkovich Indenter and Indentation Mark

Indentation loads ranging from 0.01 g to 1 g (1 μ N to 100 mN) can be made to measure material hardness. This technique provides the ability to measure the indenter penetration h under the applied force F throughout the testing cycle and is therefore capable of measuring both the plastic and elastic deformation of the material under test. Mechanical properties are derived from the indentation load-displacement curve (data) obtained in the test. Features less than 100 nm across, as well as thin films less than 5 nm thick, can be evaluated. Nano indentation hardness tests can be used to study dislocation behaviour in metals, fracture behaviour in ceramics, mechanical behaviour of thin films and bone, residual stresses and time dependent behavior in soft metals and polymers [37].

Micro-hardness study has been discussed in detail by various authors in their books [38-40], and thesis [41-46] and hence the detailed discussion is avoided hereby.

7.6 Brief Review of Hardness Studies of Urinary Calculi

There are very few reported data on the mechanical properties like ultimate strength in compression, fracture toughness, Knoop hardness, Vickers micro-hardness and Modulus of Toughness of urinary calculi [6-9, 47-53]. Earlier, Vickers micro-hardness studies on ammonium acid urate crystals were carried out [54]. Micro-hardness results of 52 urinary calculi are reported in one study. It has been found that micro-hardness increases from struvite to brushite [8]. Girija et al [55] reported Knoop micro-hardness studies of various urinary calculi like COM, COD, HAP, UA removed from patients after surgery and synthesized COM crystals. Micro-hardness studies of COM crystal has reported by Girija et al [56]. Bouropoulos et al [57] carried out Vickers

hardness studies of COM and brushite urinary stones. They have found that COM is having more hardness than brushite. Recently, micro-hardness study of COM urinary stone was carried out by Ali et al [58]. They estimated micro-hardness, fracture toughness and brittleness index for various loads. Recently, Kumar and Kalainathan [59] reported Vickers (H_V) and Knoop (H_K) micro-hardness numbers for brushite crystals grown by single diffusion gel method in the presence of different magnetic field strengths. Very few attempts were made to study the hardness of struvite crystals.

7.7 Vickers Micro-hardness Study of Struvite

7.7.1 Experimental Technique

In the present study, Vickers micro-indentation hardness test of struvite was carried out, since it is one of the predominate types of micro-hardness testing and is the standard, reliable, well established and practical method for measuring the micro-hardness of many biomaterials. As shown in figure 7.7 an opto-mechanical instrument, namely, Vaiseshika Vickers micro-hardness tester type 7005 with specifications as depicted in table 7.2 was used for the measurements of Vickers micro-hardness of struvite crystals.

The instrument comprises of microscope with a filar micrometer eyepiece mounted on stand. A loading and unloading mechanism is attached to the microscope for taking indentation of a diamond indenter on a specimen surface under certain load. An illumination system is mounted on the microscope and a rotating table brings the indented surface under the objective lens.

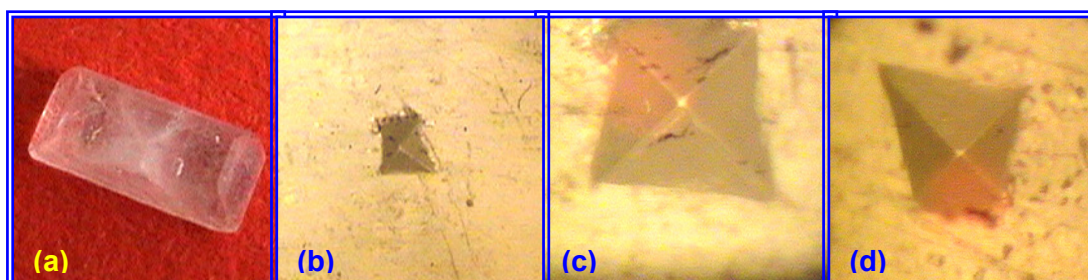
Platelet type struvite single crystals of size 6 mm × 3 mm × 1.5 mm and having smooth faces as depicted in figure 7.8 (a) were selected for the study.

Table : 7.2 : Specifications of Vickers Micro-hardness Tester Type 7005



**Figure : 7.7
Vaiseshika
Vickers
Micro-hardness
Tester Type 7005**

Part of The Instrument		Details
Viewing System of Microscope	Objective lens	40 X
	Micrometer Eyepiece	10 X
	Total Magnification	400 X
	Working Distance	1 mm
	Least count	0.0001428 mm
Illumination System	Lamp	6 V, 20W halogen
	Power Supply	230 V, A.C.
Indentation System	Indenter	Vickers Pyramidal Diamond Indenter with an angle of 136°.
	Loading / Unloading Mechanism - weights	5, 10, 20, 50, 100, 200 g
Specimen Table	Angle of Turn	0 to 180°
	Longitudinal Travel	0 to 10 mm
	Crosswire Travel	0 to 10 mm
	Micrometer Feed Scale	0.01 mm / div
Results	Range with accuracy	5 to 1500 Vickers, ± 20 Vickers



**Figure : 7.8 (a) Platelet Type Struvite Single Crystal (6 mm × 3 mm × 1.5 mm)
(b) to (d) Vickers Indentation Impressions having Average Diagonal Length
of 35.557 μm for Applied Load of 0.005 kg**

The study was carried for different indentation loads varying from 0.005 to 0.125 kg. The test samples were kept on the horizontal specimen table of the tester. Indenter is pressed normally with the predefined loads on the surface of crystal. Loading and unloading was done very slowly and carefully to avoid impact. For each test load dwell time, i.e., the duration of indentation was kept constant at 5 s. Indentations were made at room temperature. Five

indentations were performed at different points and at desirable distances on the selected as grown smooth surface of the struvite crystals for each load. The distances between the indents were kept more than five times the size of the largest indentation impression. Here, the crystal size was much larger than the indentation size, thus eliminating the boundary effects on the results. The crystal thickness was relatively large such that the indenter did not sense the lower surface [15]. The specimen table of microscope was swung over the sample to measure the diagonal of the square indentation mark. The aperture diaphragms were adjusted to obtain optimum indentation tip clarity. Indentation impressions obtained on smooth {1 0 0} surfaces of the platelet type crystals for each of the test loads were very much clear and sharp. Figure 7.8 (b) to (d) show the photographs of the indentation impressions obtained for applied load of 0.005 kg. Figure 7.8 (b) illustrates the photograph taken with lower magnification to show the surface features near the indentation mark. It is clear from the figure that no cracks are observed near the indentation mark. The diagonals of indentation d_1 and d_2 were measured with an optical microscope having total magnification of 400 X. Readings were taken using a filar micrometer eyepiece drum having least count of 0.0001428 mm. The mean arithmetic value d of the measured two diagonals was used for the calculation of the micro-hardness. Averages of 5 indentation readings were taken for each test load. The Vickers micro-hardness number (H_V) was calculated using equation (7.3). Average hardness number was calculated for each test load. The experimental data were analyzed using different theoretical models to obtain load independent hardness of the struvite crystals.

7.7.2 Load dependence of Vickers Micro-hardness Number H_v

Hardness is independent of load but it is true only for large indentations. The micro-hardness number may increase with decreasing load for small loads, since fewer numbers of dislocations become operative for slip in such small volumes of the crystal. If more than one slip system exists, increasing the load may activate a secondary system, thereby decreasing the hardness. In some other cases the micro-hardness decreases with decrease in load, which may be due to the relative contributions of plastic and elastic deformations in the indentations processes.

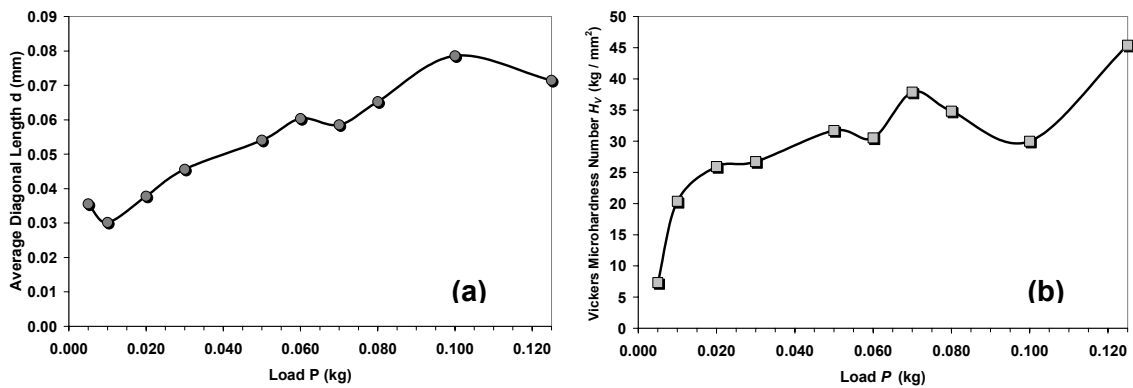
The variation of Vickers micro-hardness with load has been studied on a large number of materials. Some of the reports indicate that the micro-hardness of a given material is constant above a critical size of penetration of the indenter impression, but below this size a steady increase in micro-hardness occurs as the load decreases [60-63]. However, according to Patel and Arora [64] the Vickers hardness increases as load increases for strontium tartrate crystals. On the other hand, in the case of Vickers micro-hardness variation with load in bismuth (1 1 1) cleavage [65] and also the variation of Vickers micro-hardness with load in adamantane [66] exhibit a dip and a hump in the variation, which can be explained as generation of new dislocations resulting in a dip and then interaction within them to give further rise in the hardness and then work-hardening may give constant hardness. Also, the authors argued that different slip systems become operative at different loads for studied crystals.

Table 7.3 presents the average value of the diagonal length d of the indentation impressions for each load, and the Vickers micro-hardness

number H_V for struvite crystals in the conventional as well as in SI units. The mean diagonal length d of the indentation impressions was found to be increased with certain variations with the increasing indenter load P .

Table : 7.3 : Vickers Micro-hardness Number H_V data for Struvite crystals

Sr No.	Applied Load P kg	Mean Diagonal Length d of Indentation Impressions Mm	Vickers Micro-Hardness Number H_V	
			In Conventional Units kg / mm^2	In SI Units MPa
1	0.005 kg	0.03556 mm	7.33 kg / mm^2	71.91 MPa
2	0.010 kg	0.03017 mm	20.36 kg / mm^2	199.71 MPa
3	0.020 kg	0.03781 mm	25.93 kg / mm^2	254.32 MPa
4	0.030 kg	0.04561 mm	26.74 kg / mm^2	262.20 MPa
5	0.050 kg	0.05406 mm	31.71 kg / mm^2	311.03 MPa
6	0.060 kg	0.06035 mm	30.55 kg / mm^2	299.56 MPa
7	0.070 kg	0.05855 mm	37.86 kg / mm^2	371.30 MPa
8	0.080 kg	0.06526 mm	34.83 kg / mm^2	341.54 MPa
9	0.100 kg	0.07860 mm	30.01 kg / mm^2	294.31 MPa
10	0.125 kg	0.07145 mm	45.40 kg / mm^2	445.23 MPa



**Figure : 7.9 (a) Variation in the Mean Diagonal Length d with Indenter Load P
(b) Variation in Vickers Micro-Hardness Number H_V with Indenter Load P**

The variation in mean diagonal length with the indenter load is as shown in figure 7.9 (a). The measured Vickers micro-hardness number was seen to vary in increasing order from 7.33 kg / mm^2 (71.91 MPa) to 45.40 kg / mm^2 (445.23 MPa), with certain variations, over the increasing indenting load

range from 0.005 to 0.125 kg. The variation in Vickers micro-hardness number with indenter load is as shown in figure 7.9 (b).

It was observed that the value of Vickers hardness number increased with increasing value of load and a first peak value of 37.86 kg / mm² was observed at 0.070 kg load and subsequently the value of Vickers hardness number decreased as the load increased up to 0.100 kg, afterwards it was again increased up to 45.40 kg / mm². The initial increase in hardness with the load might be due to the continued increase in the dislocation interactions resulting in a tangled forest of dislocation lines (work hardening). The subsequent decrease in hardness with increase in load was due to “work softening” process which resulted from the activation of cross slip and the movement of piled-up dislocations [67]. Thus observed peak might be due to the possible work hardening and the subsequent decrease in the value of hardness might be due to operative slip systems. From this hardness study in the micro-indentation load range, Vickers micro-hardness number for struvite was found to be load dependent. Earlier investigations on various materials have also observed load dependent micro-hardness number [68-72]. It is well known that the load dependence of hardness in non-metals is often indicative of a major change in micro-structural response to loading.

Usually, it is believed that the measured hardness should be independent of the applied load, since the Vickers indenter gives geometrically similar indentations. But this is true only for the hardness measurements with macro-indentations and higher values of applied load. Several investigations have confirmed that for many solid materials the apparent (i.e. measured) micro-hardness number is load dependent. In such

cases generally three types of phenomena, namely, (i) normal indentation size effect (normal ISE), (ii) reverse indentation size effect (reverse ISE), and (iii) complex variations were observed. A decrease in the apparent micro-hardness with increasing applied test load is known as normal ISE, while increase in the apparent micro-hardness with increasing applied test load is known as reverse ISE. For this micro-hardness study of urinary type struvite crystals the phenomenon of reverse ISE was observed. The phenomena of normal and reverse ISE were reported in the literature and much research work has been carried out to explain the origin of the ISE and several possible explanations exist [54, 73-79]. Undoubtedly, the existence of the ISE may hamper or preclude plausible hardness measurements. Furthermore, using a load dependent hardness number in material characterization may result in some unreliable conclusions.

7.7.3 Application of Kick's Law and Phenomenon of Reverse ISE

The load-dependence of the measured Vickers micro-hardness values can also be described quantitatively through the application of the Kick's law [80] for pyramidal indenter, which is same as that of classical Meyer's power law for spherical indenter [15, 70, 71, 81]. Later on Kick's law was modified by Hays and Kendall [82], which is discussed in the next section of this chapter. For pyramidal indenter Kick's law is given as,

$$P = a d^n \tag{7.5}$$

where, **P** is the applied indentation load, **a** is the material constant; **d** is the average diagonal length of the indented impressions and **n** is Meyer index number or work hardening coefficient or strain hardening index.

From the relation (7.5), one can write

$$\log P = \log a + n \log d \quad (7.6)$$

The values of a and n can be found out from the plot of $\log P$ versus $\log d$ as shown in figure 7.10.

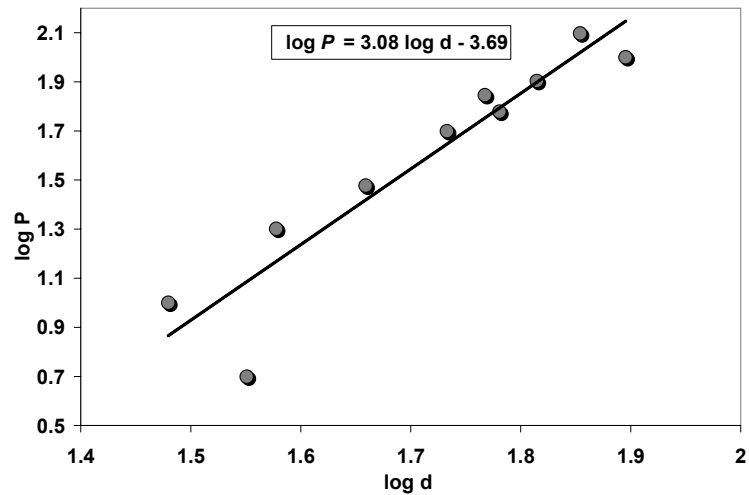


Figure : 7.10 The graph of $\log P$ versus $\log d$

Since the relation between $\log P$ and $\log d$ is linear, the slope of this straight line gives the value of constant n and the intercept on $\log P$ axis gives the value of $\log a$. The behaviour of the change in micro-hardness with the applied load can be studied by obtaining the value of n . The value of n indicates the extent of ISE. By combining the equations (7.3) and (7.5), we get

$$H_V = b d^{n-2} \quad (7.7)$$

There exist three different possibilities for the value of n . In case of $n = 2$, no ISE is observed. In case of $n < 2$, normal ISE is observed, i.e., Vickers micro-hardness number H_V decreases with the increasing applied test load. While in case of $n > 2$, reverse ISE is observed, i.e., Vickers micro-hardness number H_V increases with the increasing applied test load.

Grodzinski [83] found variation of n values from 1.3 to 4.9 in various materials. Knoop [84] observed an increase in hardness with decrease in load, whereas Campbell et al [85] and Mott et al [86] observed a decrease in hardness with decrease in load. Notwithstanding, some studies have suggested more than one value of coefficient n . Saraf [87] obtained two different values of n for higher and lower load regions in the case of baryte ($BaSO_4$) crystals. Moreover, according to Onitsch [88] for hard materials, the value of n lies in the range of 1 to 1.6 and for the soft materials the value of n is above 1.6.

In the present study, the Mayer's index number, i.e., the value of work hardening coefficient was found to be $n = 3.08$. Hence, from the value of work hardening coefficient the phenomenon of the reverse ISE was confirmed. It can be also demonstrated in the curve of figure 7.9 (b), i.e., in plot of H_v versus load P . In case of reverse ISE, a specimen does not offer resistance or undergo elastic recovery, as postulated in some of the models, but undergoes relaxation involving a release of the indentation stress along the surface away from the indentation site. This leads to a large indentation size and hence to a lower hardness at low loads. It was found that the reverse ISE phenomenon occurs only in materials in which plastic deformation is predominant. Since, $n > 1.6$ for struvite, according to Onitsch it can be considered to be soft material.

7.7.4 Application of Hays and Kendall's Model

Hays and Kendall [82] proposed that the load dependence of micro-hardness may be explained by

$$P = W + K d^2 \quad (7.8)$$

Where, W is the minimum load required to initiate plastic (permanent) deformation and K is a load-independent constant. Below the value of W plastic deformation does not initiate, but only elastic deformation occurs. The values of W and K may be calculated by plotting the graph of P versus d^2 using the experimental data as shown in figure 7.11. The linear relationship between P and d^2 implies that the Hays and Kendall's model is suitable for describing the micro-indentation data of struvite crystals.

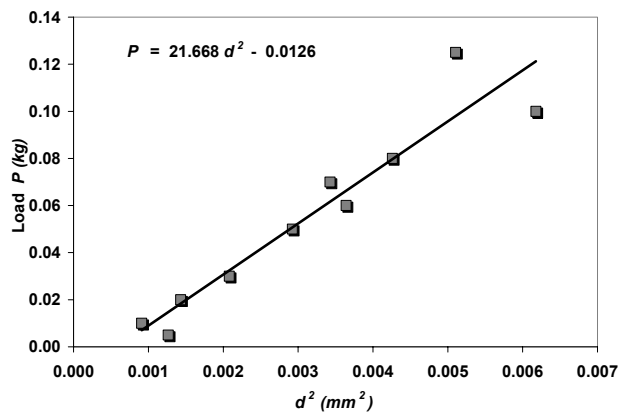


Figure : 7.11 Hays and Kendall's plot of P versus d^2 for Struvite Crystal

The load independent Vickers micro-hardness H_0 can be calculated using the following formula:

$$H_0 = 1.854 \times \frac{(P - W)}{d^2} = 1.854 \times K \quad (7.9)$$

The calculated values of W , K and H_0 are as given in table 7.4.

Table : 7.4 : The values of W , K and H_0 from Hays and Kendall's Model

For Struvite Crystals	In Conventional Units	In SI Units
Minimum Load Required to Initiate Plastic Deformation W	- 0.0126 kg	- 0.1235 N
Load-Independent Constant K	21.67 kg / mm ²	212.52 MPa
Load Independent Vickers Micro-Hardness H_0	40.18 kg / mm ²	394.05 MPa

The values of W and K depend on the chemical composition of the sample.

The value of W was found negative, which indicates that any value of load

except zero load is capable of generating plastic deformation. From Hays and Kendall's model, the value of load independent Vickers micro-hardness H_0 was obtained as 40.18 kg / mm² (\approx 394.05 MPa).

7.7.5 Application of Proportional Specimen Resistance (PSR) Model

Li and Bradt [81] explained the ISE with help of general model of Proportional Specimen Resistance (PSR). According to PSR model the micro-hardness can be described with two components: (i) the indentation load-dependent part or the ISE regime and (ii) the indentation load-independent part. Indentation test load P is related to indentation size d as,

$$P = a_1 d + a_2 d^2 \quad (7.10)$$

Where, coefficient a_1 is the contribution of proportional specimen resistance to the load dependent apparent micro-hardness, and coefficient a_2 is related to the load independent micro-hardness.

The first term $a_1 d$ was attributed to the specimen surface energy [40,89], the deformed surface layer [90,91], the indenter edges acting as plastic hinges [92], and the proportional specimen resistance [81,93]. Li and Bradt [81] suggested that a_1 / a_2 can be considered as a measure of the residual stress and these are connected with defect.

$$\frac{P}{d} = a_1 + \left(\frac{P_c}{d_0^2} \right) d \quad (7.11)$$

Where, P_c is the critical applied test load above which micro-hardness becomes load independent and d_0 is the corresponding diagonal length of the indentation. The applicability of the PSR model to describe the observed ISE in relatively wide range of applied test loads can be examined by the linearity between P/d and d .

The term α_2 is not related to the ISE, which is

$$a_2 = \left(\frac{P_C}{d_0^2} \right) \quad (7.12)$$

It is quite clear from equation (7.11), that the plot of the P/d against d must be a straight line and slope of which gives the value of α_2 . The load independent Vickers micro-hardness H_0 can be calculated using the following formula

$$H_0 = 1.854 \times \left(\frac{P_C}{d_0^2} \right) \quad (7.13)$$

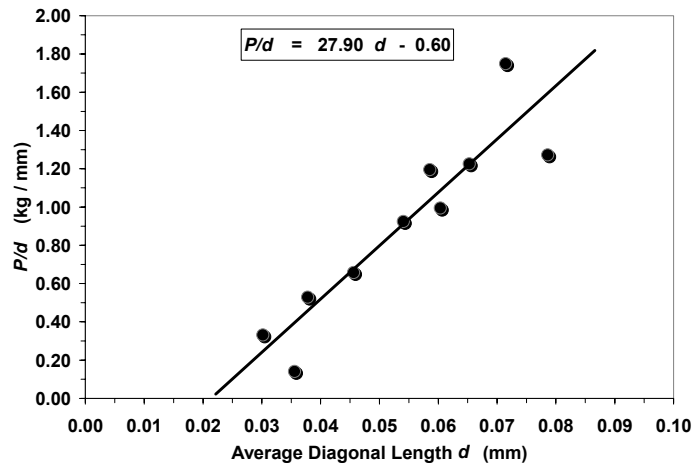


Figure : 7.12 PSR Plot of P/d versus d for Struvite Crystal

Applying the PSR model of Li and Bradt to struvite, it was observed that a plot of P/d against d gave straight line as shown in figure 7.12. This linear relationship confirmed the applicability of PSR model to struvite. The value of slope, i.e. α_2 and load independent micro-hardness H_0 were calculated from the plot of P/d versus d . The values of α_1 , α_2 and H_0 for *in vitro* gel grown urinary type struvite crystals were obtained as shown in table 7.5. According to PSR model, the value of load independent Vickers micro-hardness H_0 was calculated as 51.72 kg / mm^2 ($\approx 507.22 \text{ MPa}$). The difference in the values of load independent micro-hardness H_0 in case of PSR model and Hays and

Kendall's model may be due to different mathematical treatments and assumptions made.

Table : 7.5 : The values of α_1 , α_2 and H_0 from PSR Model

For Struvite Crystals	In Conventional Units	In SI Units
α_1	- 0.60 kg / mm	- 5884.20 N / m
α_2	27.90 kg / mm ²	273.62 MPa
Load Independent Vickers Micro-Hardness H_0	51.72 kg / mm ²	507.22 MPa

7.7.6 Yield Stress and First order Elastic Stiffness Constant

Yield stress or strength of a material is defined as the stress applied to the material at which permanent or plastic deformation starts to occur while the material is loaded. The yield stress may be noted as the point of departure from linearity in the stress-strain curve. Since the Meyer's Index n is greater than 2, yield stress can be calculated from the micro-hardness value using the following equation [94]

$$\sigma_y = \left(\frac{H_v}{2.9} \right) \{1 - (n - 2)\} \left[\frac{12.5 (n - 2)}{\{1 - (n - 2)\}} \right]^{n-2} \quad (7.14)$$

Stiffness is the measure of resistance of plastics to bending. It includes both plastic and elastic behavior, so it is an apparent value of elastic modulus rather than a true value. The first order elastic stiffness constant (C_{11}) was evaluated for struvite crystals using Wooster's empirical relation [95] as follow

$$\log C_{11} = \frac{7}{4} \log H_v \quad (7.15)$$

Table 7.6 depicts the values of yield stress and first order elastic stiffness constant, which were calculated from above respective equations.

Table : 7.6 : The values of Yield Stress and First order Stiffness constant

Model	Hays and Kendall's Model		PSR model	
	In Conventional Units kg / mm ²	In SI Units MPa	In Conventional Units kg / mm ²	In SI Units MPa
Yield Stress	281.92	2764.82	362.89	3558.87
First order Stiffness constant	641.24	34850.23	997.48	54211.77

7.8 Chemical Etching Study of Struvite

Chemical etching through a simple and widely adopted technique for the study of imperfections in a large variety of crystalline materials, the process is still not very well understood. An etching technique in association with optical microscopy can be used alternatively to x-ray method for the detection as well as quantitative analysis of defects in crystalline solids [96-99]. The high resolution imaging capability achievable with AFM has enabled the initial stages of the process of etch pit nucleation to be monitored on a scale previously unattainable [100,101].

The dissolution of crystals is a complex heterogeneous catalytic process, which attracts much attention because of its importance for many practical applications [96]. When the crystal is dissolved in a solvent, the reversals of the growth taking place by giving the well defined etch pits. The etching patterns observed at the initial stages of the dissolution of crystals are manifestation of the anisotropy of the crystal structure and of the interactions in this structure. The etching patterns result from a complex interplay of several stages of the dissolution process. The location of the etch pits is usually correlated with the defect sites in the crystals – most commonly, with dislocations, but also with surface defects, vacancy or impurity clusters.

Crystallographic etch pits do not always coincide with the dislocations. Their walls are formed by faces with low hkl - indices. Usually, the shapes of the crystallographic etch pits are correlated with the anisotropy of crystal structure [102].

There are several etching technique [103] which are listed as follows:

- (1) Chemical Etching
- (2) Electrolytic Etching
- (3) Thermal Etching
- (4) Ionic Etching

The etching process has been explained in detail by several authors. It has been briefly outlined by the present author.

When the rate of dissolution of a solid is rapid, the process is controlled by the rates of chemical and thermal diffusion in the solvent. As the dissolution rate or the under saturation of solvent becomes smaller, the surface imperfections of the solid play prominent role [104].

The unit process in dissolution can be considered as a removal of a molecule from the corner of a kink in a surface step; however, the process occurs only if: (a) a step exists on the surface, (b) the step contains kinks and (c) the solvent is under saturated at a particular kink under consideration. Any one or combination of these factors controls the dissolution.

It is important to note that the dislocation lines are quite effective in acting as nucleation centers for dissolution steps. The effect of dislocation lines on dissolution nucleation is due to their elastic energies or the chemical potential of the material near by [105].

The surface layer around a screw dislocation that lies normal to a free surface is stress free except at the core of the dislocation. However, for an edge dislocation that intersects a free surface, the most of the strain energy remains with the edge. The surface steps associated with screw dislocations are thought to be important; the dissolution takes place at moderate under-saturations. However, both the screw and the edge dislocations are etched in nearly the same manner and nearly the same rate in many crystals. Different theories of dissolution, thermodynamic and topo-chemical adsorption are of interest since they deal with the formation of dislocation etch pits on a crystal surface [106,107]. The topo-chemical theories suggest the dissolution rate in terms of chemical reactions on the crystal surface. It is considered that etch pits at the sites of dislocations are formed as a result of enhanced dissolution caused by the preferred adsorption of a reactant at that site because of the strain associated with the dislocation. The topo-chemical theories are attractive for crystalline substances. The dissolution of crystals involves the formation of reaction products, however, they poses certain limitations. One limitation is that each etching system has to be treated independently. Whereas, the thermodynamic theories are based on the postulate that the energy localized in the vicinity of a dislocation lowers the free energy needed for the nucleation of unit depth in the surface at the site of the dislocation.

Etching techniques have been successfully employed by several investigators to work out the configuration of dislocation within the body of a given crystal. Various authors have reported dislocation and etch pits by using different etchant on various crystals. It is very laborious to compile all details of etching; however, Joshi [41] has attempted to compile the details up to a certain extent. In the present author's laboratory dislocation etching has been

studied extensively on various crystals, for examples, Bismuth single crystals [108-112], antimony single crystal [113-116], anthracene single crystals [117,118], calcite crystal cleavages [119-124], Mn^{+2} and Cu^{+2} doped calcium L- tartrate crystals [44], pure and amino acids (L-histidine, L-threonine, DL-methionine) doped KDP crystals [45], pure and amino acids (L-arginine, L-lysine, L-alanine) doped KDP crystals [46]. Hence, the detailed discussion of chemical etching is avoided.

However, some limited study of etching has been carried out on urinary type crystals. Monolayer deep, triangular etch pits formation occur spontaneously on brushite (0 1 0) surfaces in undersaturated aqueous solution [125]. Also, in the case of brushite crystals *HCl* reveals various types of etch pattern, which includes spiral, dendrites, allies, straight, etc. [126]. The etch pits on as grown faces of brushite crystals have also been reported [127]. Apart from brushite crystals some studies have been reported on COM crystals. In undersaturated aqueous solution, COM develops hexagonal pits oriented along the [0 0 1] directions having perimeters defined by {0 1 0} and {0 2 1} planes [128]. The selective dissolution gives etch pits on the crystalline faces; on the other hand selective inhibition gives etch hillocks, which are complementary to etch pits. The dissolution hillocks on (0 1 0) face have been observed on COM [129]. To best of present author's knowledge no major work on chemical etching of struvite is reported.

7.8.1 Experimental Technique

Struvite crystals were grown by single diffusion gel growth technique as described in section 5.2 of chapter V. The (1 1 1) faces of the prismatic type struvite single crystals with transparent diaphaneity were selected for the

chemical etching study. The successful use of etch pits to study dislocations in crystals depends appreciably on the selection of etchant. Since the citric acid is known to be a good inhibitor of the growth of urinary crystals, dilute citric acid was chosen as an etchant for the etching study. AR grade citric acid $\{C_6H_8O_7\}$ was used for the study. The chemical etching study was carried out, using a mixture of 1 mL 0.05 M citric acid and 9 mL distilled water as an etchant solution, for different temperatures from 30° C to 70° C at the interval of 5° C temperature. The crystal was dipped into the etchant for 60 s and, thereafter, removed and air dried before observation under microscope. Etchant produced triangular etch pits on (1 1 1) surface of the crystal. In each case, the etching time was kept constant.

The widths of the etch pits were measured with the help of filar eyepiece of optical microscope attached with Vaiseshika Vickers micro-hardness tester 7005 having total magnification of 400 X. The photographs of the triangular etch pits observed on (1 1 1) face of the crystals for each temperature are as shown in figure 7.13. For each temperature, the widths of 50 etch pits were measured precisely, then the average etch pit width (W) was calculated. Figure 7.14 shows the histogram of average etch pit width *versus* temperature, which clearly depicts that the average etch pit width increased with the increasing temperature of the etchant. Moreover, the shape of the etch pits did not vary upon the change of temperature from 30 °C to 70 °C. The tests were carried out to verify that the etch pits were at the site of dislocations. Amelinckx [130] suggested several tests to establish correspondence between etch pits and dislocations. The estimation of kinetic and thermodynamic parameters for the etching process were also carried out.



Figure : 7.13 Triangular Etch Pits Observed on (111) Face of the Struvite Crystals

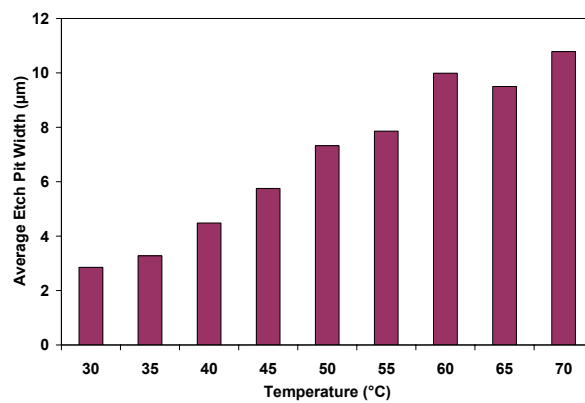


Figure : 7.14 Histogram of Etch Pit Width Versus Temperature

7.8.2 Kinetic Parameters

Several empirical relations are well reported and discussed in details by Laidler [131,132]. The Arrhenius equation is usually used today to interpret kinetic data, since it provides the quantitative basis of the relationship between the activation energy and the rate at which a reaction proceeds.

$$W = A e^{-E/RT} \quad (7.16)$$

Where, **W** = Average width of etch pit, **A** = Pre-exponential factor or frequency factor for the reaction, **E** = Activation energy of the reaction, **R** = Universal gas constant, **T** = Absolute temperature in Kelvin.

The Pre-exponential factor or frequency factor is related to the collision frequency and the steric factor. Boikess and Edelson [133] describe that the value of **A** increases if the steric factor increases or collisions frequency increases. In other words, a reaction will be faster if there is more collision or a higher percentage of the collisions which have the proper orientation required for product formation. The specific rate constant or the value of average etch pit width is high for fast reactions. It is evident from the above expression that as **E**, the activation energy, increases, the value of **W** decreases and consequently the reaction rate decreases. The activation energy is considered as a barrier to be surmounted to form the reaction product. Therefore, the higher values of activation energy show slower reaction rates.

The values of activation energy at dislocation **E** and frequency factor **A** may be calculated from the Arrhenius plot, i.e., the plot of $\log_{10} W$ versus $1/T$ as shown in figure 7.15. Since the relation between $\log_{10} W$ and $1/T$ is linear, the slope of this straight line gives the value of $\{ - E / 2.303 R \}$ and the

intercept on $\log_{10} W$ axis gives the value of $\log_{10} A$. The value of activation energy at dislocation E can be determined by

$$E = - 2.303 \times R \times (\text{slope of Arrhenius plot}) \quad (7.17)$$

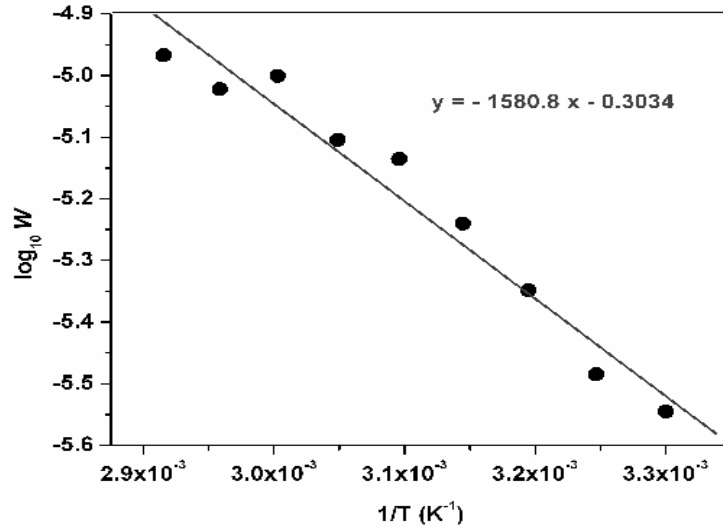


Figure : 7.15 Arrhenius Plot of $\log_{10} W$ versus $1/T$

From the Arrhenius plot, the values of activation energy at dislocation E and frequency factor A were found as $30.267 \text{ kJ Mol}^{-1}$ and 0.4972 , respectively.

7.8.3 Thermodynamic Parameters

The thermodynamic parameters can be estimated for the motions of ledges of dislocation etch pits. Various thermodynamic parameters were calculated from the well known standard formulae as described in detail by Laidler [132]. The value of standard enthalpy of activation $\Delta^\ddagger H^\circ$ was found positive and varied between 25.23 to 24.56 kJ/mole with decreasing nature for increasing etching temperature as shown in figure 7.16 (a). The positive values of $\Delta^\ddagger H^\circ$ depicted that the enthalpy was increasing during the etching process and can be said to be an endothermic process. The standard internal energy of activation $\Delta^\ddagger U^\circ$ during the etching process was found to have decreasing nature from 27.75 to 27.42 kJ/mole with the increasing etching temperature as illustrated in figure 7.16 (b). The standard entropy of activation

$\Delta^\ddagger S^\circ$ was calculated at different temperatures of etching and the plot of $\Delta^\ddagger S^\circ$ versus temperature is shown in figure 7.16 (c). Here, negative values of $\Delta^\ddagger S^\circ$ indicates that the etching process is non-spontaneous. Figure 7.16 (d) demonstrates increasing nature of the standard Gibbs free energy of activation $\Delta^\ddagger G^\circ$ from 156.89 to 166.17 kJ/mole with the increasing etching temperature.

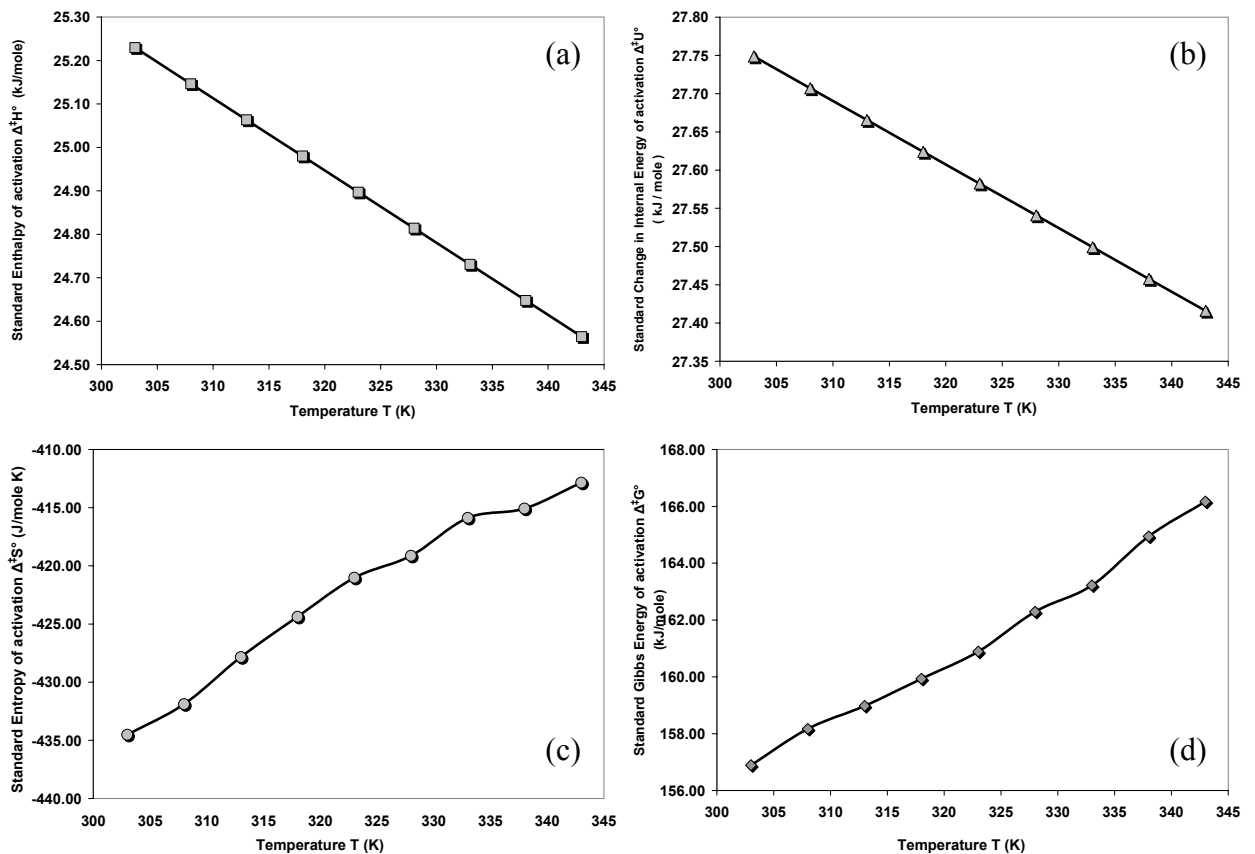


**Figure : 7.16 (a) Standard Enthalpy of activation $\Delta^\ddagger H^\circ$ versus Temperature
 (b) Standard Internal Energy of activation $\Delta^\ddagger U^\circ$ versus Temperature
 (c) Standard Entropy of activation $\Delta^\ddagger S^\circ$ versus Temperature
 (d) Standard Gibbs Free Energy of activation $\Delta^\ddagger G^\circ$ versus Temperature**

7.9 Conclusions

1. Vickers micro-indentation impressions obtained on as grown smooth surfaces of the platelet type struvite crystals for each of the test loads were very much clear and sharp.
2. The mean diagonal length d of the indentation impressions was found to be increased with certain variations with the increasing indenter load P from 0.005 to 0.125 kg.
3. The Vickers micro-hardness number H_V was found to be load dependent and phenomenon of reverse ISE was observed for struvite crystals.
4. The measured Vickers micro-hardness number H_V was seen to vary in increasing order from 7.33 kg/mm² (71.91 MPa) to 45.40 kg/mm² (445.23 MPa), with certain variations, over the increasing indenting load range from 0.005 to 0.125 kg.
5. Analysis of the experimental data on hardness as a function of indentation size from the standpoint of Kick's Law, Hays-Kendall's model and the proportional specimen resistance model revealed that these models satisfactorily explain the reverse ISE phenomena observed in the *in vitro* gel grown urinary type struvite crystals.
6. The load-dependence of the measured Vickers micro-hardness values can be quantitatively described through the application of the Kick's law. Mayer's index number, i.e. the value of work hardening coefficient was found as $n = 3.08$, which proved predominant plastic deformation and confirmed the phenomenon of reverse ISE as well.
7. The values of load independent Vickers micro-hardness H_0 were obtained as 40.18 kg/mm² (\approx 394.05 MPa) and 51.72 kg/mm² (\approx 507.22 MPa)

according to Hays-Kendall's model and the PSR model, respectively. The difference in the values may be due to different approaches in these models.

8. This study of Vickers micro-hardness and related mechanical properties for gel grown struvite crystals may provide useful information for the fragmentation of the struvite type urinary calculi by using appropriate parameters in ESWL management without causing any damage to the kidney and urinary tract.
9. Citric acid as an etchant produced triangular etch pits on as grown (1 1 1) surface of the prismatic type struvite crystals. Several standard tests confirmed the correspondence of etch pits to the emergence of dislocations.
10. The average etch pit width was found to be increased with the increasing temperature of the etchant in the range from 30 °C to 70 °C. Moreover, the shape of the etch pits did not vary upon the change of temperature.
11. The values kinetic parameters - activation energy of the reaction E and frequency factor A were found as 30.267 kJ Mol⁻¹ and 0.4972, respectively for etching process on struvite crystals.
12. The values of standard enthalpy of activation $\Delta^\ddagger H^\circ$ and standard internal energy of activation $\Delta^\ddagger U^\circ$ during the etching process were found to be positive and have decreasing nature with the increasing etching temperature. The positive value of $\Delta^\ddagger H^\circ$ explained etching process as an endothermic process, where as negative values of $\Delta^\ddagger S^\circ$ proved that the etching process was non-spontaneous.

References

1. C. Chaussy, E. Schmiedt, D. Jocham, *Lancet*, **11** (1980) 1265.
2. C. Chaussy, *J. Urol.*, **249** (1982) 417.
3. D. J. Sutor, "Physical Aspects", in "Urolithiasis", Ed. B. L. Finlayson, L. L. Hench, L. H. Smith, National Academy of Science, Washington (1972).
4. P. Zhong, *Ph.D. Dissertation*, University of Texas, Arlington (1992).
5. J. E. Lingeman, J. Newmark, "Adverse Bio Effects of Shock-Wave Lithotripsy", In: "Kidney Stones: Medical and Surgical Management", Ed. F. L. Coe, Lippincott-Raven, Philadelphia (1996).
6. R. Agarwal, V. R. Singh, *Ultrasonics*, **29** (1991) 89.
7. V. R. Singh, J. B. Dhawan, *Biomed. Mater. Eng.*, **2** (1992) 79.
8. N. P. Cohen, H. N. Whitfield, *World J. Urol.*, **11** (1993) 13.
9. P. Zhong, G. M. Preminger, *J. Endourol.*, **8** (1994) 263.
10. P. Zhong, C. Choung, R. Goolsby, *J. Biomed. Mater. Res.*, **26** (1992) 1117.
11. C. W. Stillwell, "Crystal Chemistry", McGraw Hill, New York (1983).
12. N. A. Ashby, *NZ Eng.*, **6** (1951) 33.
13. D. Tabor, "Hardness of Metals", Clarendon, Oxford (1951).
14. J. H. Westbrook, H. Conrad, "The Science of Hardness Testing and its Research Applications", American Society of Metals, Ohio (1973).
15. B. W. Mott, "Micro-hardness Indentation Testing", Butterworth Scientific Publications, London (1956).
16. J. N. Plendl, P. J. Gielisse, *Phys. Rev.*, **125** (1962) 828.
17. D. B. Sirdeshmush, K. G. Subhadra, K. Rao, T. Rao, *Cryst. Res. Technol.*, **30** (1995) 861.

18. M. C. Shaw, "The Fundamental Basis of The Hardness Test", In "The Science of Hardness Testing and Its Research Applications", Eds. J. H. Westbrook, H. Conrad, Am. Soc. for Metals, Cleveland, Ohio (1973).
19. S. Chang, M. Jahn, C. Wan, J. Wan, T. Hsu, *J. Mater. Sci.*, **11**(1976) 623.
20. M. O. Lai, K. B. Lim, *J. Mater. Sci.*, **26** (1991) 2031.
21. G. F. Vander Voort, "Metallography, Principles and Practice", ASM International, McGraw Hill, New York (1984).
22. H. G. O'Neill, "The Hardness of Metals and its Measurement", Chapman and Hall Ltd., London (1934).
23. S. R. Williams, "Hardness and Hardness Measurements", Am. Soc. of Metals, Cleveland, Ohio (1942).
24. V. E. Lysaght: "Indentation Hardness Testing", Reinhold Pub., NY, (1949).
25. J. A. Brinell, *Teknisk Tidskrift.*, **5** (1900) 69.
26. J. A. Brinell, "Congres International des Methodes d'Essai des Materiaux de Construction", Paris (1901).
27. J. Szilard, *Ultrasonics*, **22** (1984) 174.
28. P. Ludwik, *Die Kegelprobe (The Cone Trial)*, J. Springer, Berlin, (1908).
29. S. P. Rockwell, *Transactions Am. Soc. for Steel Treating*, **2** (1922) 1013.
30. H. M. Rockwell, S. P. Rockwell, Hardness-tester, U.S. Patent No. 1294171, (1914).
31. S. R. Low, "Rockwell Hardness Measurement of Metallic Materials", Natl. Inst. Stand. Technol., Washington (2001).
32. C. Kleesattel, *J. Acoust. Soc. Am.* **39** (1966) 404.
33. R. L. Smith, G. E. Sandland, *Proceedings of the Institution of Mechanical Engineers*, **1** (1922) 623.

34. R. L. Smith, G. E. Sandland, *J. Iron Steel Inst.*, London (1925).
35. http://core.materials.ac.uk/repository/mech_test/jpg/vickers_33.jpg
36. F. Knoop, C. Peters, W. Emerson, *J. Res. Nat. Bur. Stand.* **23** (1939) 39.
37. M. R. VanLandingham, *J. Res. Natl. Inst. Stand. Technol.*, **108** (2003) 249.
38. D. B. Sirdeshmukh, L. Sirdeshmukh, K. G. Subhadra, “*Micro- and Macro - Properties of Solids - Thermal, Mechanical and Dielectric Properties*”, Springer, Heidelberg (2006).
39. D. B. Sirdeshmukh, L. Sirdeshmukh, K. G. Subhadra, “*Alkali Halides - A Hand Book of Physical Properties*”, Springer, Heidelberg (2001).
40. W. C. Oliver, R. Hutchings, J. B. Pethica, In “*Microindentation Techniques in Materials Science and Engineering*”, Eds. P. J. Blau, B. R. Lawn, ASTM, Philadelphia, PA, (1986).
41. M. J. Joshi, *Ph. D. Thesis*, Saurashtra University, Rajkot (1986).
42. R. K. Marwaha, *Ph. D. Thesis*, Saurashtra University, Rajkot (1992).
43. N. Vaidya, *Ph. D. Thesis*, Saurashtra University, Rajkot (1998).
44. S. R. Suthar, *Ph. D. Thesis*, Saurashtra University, Rajkot (2007).
45. D. J. Dave, *Ph. D. Thesis*, Saurashtra University, Rajkot (2011).
46. K. D. Parikh, *Ph. D. Thesis*, Saurashtra University, Rajkot, (2011).
47. P. Zhong, C. Chuong, G. Preminger, *J. Mater. Sci. Lett.*, **12** (1993) 1460.
48. J. R. Burns, B. E. Shoemaker, J. F. Gauthier, B. Finlayson, “*Hardness Testing of Urinary Calculi*”. In “*Urolithiasis and Related Clinical Research*”, Ed. P. O. Schwille, Plenum Press, New York (1985).
49. F. Ebrahimi, F. Wang, *J. Biomed. Mater. Res.*, **23** (1989) 507.
50. S. Wang, M. Yip, Y. Hsu, K. Lai, S. Wang, *J. Biomech. Eng.*, **124** (2002)133.
51. L. G. Johrde, F. H. Cocks, *Mat. Lett.*, **3** (1985) 111.

52. L. G. Johrde, F. H. Cocks, *J. Mat. Sci. Lett.*, **4** (1985) 1264.
53. M. Uchida, Y. Imaide, H. Watanabe, "Chemical Components and Mechanical Properties of Urinary Calculi", In "Biomaterials' Mechanical Properties ASTM STP", Eds. H. E. Kambic, A. T. Yokobori, Vol. 1173, Am. Soc. for Testing and Materials, Philadelphia (1994).
54. T. Irusan, D. Arivuoli, P. Ramasamy, *J. Mater. Sci. Lett.*, **12** (1993) 405.
55. E. K. Girija, G. R. Sivakumar, S. N. Kalkura, P. Ramasamy, D. R. Joshi, P. B. Sivaraman, *Mater. Chem. Phys.*, **63** (2000) 50.
56. E. K. Girija, S. C. Latha, S. N. Kalkura, S. Subramanian, P. Ramasamy, *Mater. Chem. Phys.*, **52** (1998) 253.
57. N. Bouropoulos, D. E. Mouzakis, G. Bithelis, E. Liatsikos, *J. Endourol.*, **20** (2006) 59.
58. A. Ali, N. Raj, S. Kalainathan, P. Palanichamy, *Mater. Lett.*, **62** (2008) 2351.
59. A. R. Kumar, S. Kalainathan, *J. Phys. Chem. Solids*, **71** (2010) 1411.
60. J. R. Pandya, L. J. Bhagiya, A. J. Shah, *Bull. Mater. Sci.*, **5** (1983) 79.
61. C. C. Desai, J. L. Rai, *Bull. Mater. Sci.*, **5** (1983) 453.
62. M. S. Joshi, V. V. Joshi, A. L. Choudhari, R. G. Kanitkar, *J. Mater. Sci.*, **19** (1984) 3337.
63. M. J. Joshi, B. S. Shah, *Cryst. Res. Technol.*, **19** (1984) 1107.
64. A. R. Patel, S. K. Arora, *J. Mater. Sci.*, **12** (1977) 2124.
65. P. C. Shah, B. S. Shah, *Indian J. Pure Appl. Phys.*, **31** (1993) 845.
66. B. S. Shah, *Cryst. Res. Technol.*, **17** (1982) K27.
67. W. Hayden, W. Mofatt, J. Wulff, "The Structure and Properties of Materials", Vol. III, Mechanical Behaviour, Wiley Eastern, New Delhi, (1971).
68. D. Chakraborty, J. Mukerji, *J. Mater. Sci.*, **15** (1980) 3051.

69. K. Hirao, M. Tomozawa, *J. Am. Ceram. Soc.*, **70** (1987) 497.
70. G. N. Babini, A. Bellosi, C. Galassi, *J. Mater. Sci.*, **22** (1987) 1687.
71. A. K. Mokhopadhyay, S. K. Datta, D. Chakraborty, *J. Eur. Ceram. Soc.*, **6** (1990) 303.
72. J. B. Quinn, G. D. Quinn, *J. Mater. Sci.*, **32** (1997) 4331.
73. K. Sangwal, *Mater. Chem. Phys.*, **63** (2000)145.
74. S. Anbukumar, S. Vasudevan, P. Ramasamy, *J. Mater. Sci. Lett.*, **5** (1986) 223.
75. J. B. Charles, F. D. Gnanam, *J. Mater. Sci. Lett.*, **9** (1990) 165.
76. R. C. Dhas, J. Charles, F. D. Gnanam, *J. Mater. Sci. Lett.*, **12** (1993) 1395.
77. P. N. Kotru, A. K. Razdan, B. M. Wanklyn, *J. Mat. Sci.*, **24** (1989) 793.
78. S. Sengupta, S. P. Sengupta, *Bull. Mater. Sci.*, **15** (1992) 333.
79. J. Gong, J. Wu, Z. Guan, *J. Eur. Ceram. Soc.*, **19** (1999) 2625.
80. F. Kick, “*Das Gesetz der Proportionalen Widerstande and Science Anwendung*”, Leipzig, Felix (1885).
81. H. Li, R. C. Bradt, *J. Mater. Sci.*, **28** (1993) 917.
82. C. Hays, E. G. Kendall, *Metallography*, **6** (1973) 275.
83. P. Grodzinski, *Schweiz. Arch. Angew. Wiss.*, **18** (1952) 282.
84. F. Knoop, *Tech. Blatter.*, **27** (1937) 472.
85. R. F. Campbell, Q. Henderson, M. Donleavy, *Trans. ASM*, **40** (1948) 954.
86. W. B. Mott, S. D. Ford, I. R. W. Jones, *AERE Harwell Report*, **1** (1952)945.
87. C. L. Saraf, *Ph. D. Thesis*, M. S. University of Baroda, Vadodara, (1971).
88. E. M. Onitsch, *Mikroskopie*, **2** (1947) 131.
89. F. Fröhlich, P. Grau, W. Grellmann, *Phys. Stat. Sol. (a)*, **42** (1977) 79.
90. K. Sangwal, *J. Mater. Sci.*, **24** (1989) 1128.

91. P. M. Sargent, in: *"Micro-indentation Techniques in Materials Science and Engineering"*, Eds. P. J. Blau, B. R. Lawn, ASTM, Philadelphia, PA (1986).
92. Q. Ma, D. R. Clarke, *J. Mater. Res.*, **10** (1995) 853.
93. H. Li, Y. H. Han, R. C. Bradt, *J. Mater. Sci.*, **29** (1994) 5641.
94. J. P. Cahoon, W. H. Broughton, A. R. Kutzak, *Metall. Mater. Trans. B.*, **2** (1971) 1979.
95. W. A. Wooseter, *Rep. Prog. Phys.*, **1C** (1953) 62.
96. K. Sangwal, *"Etching of Crystals: Theory, Experiments and Applications"*, Series: *"Defects in Solids"*, Vol. 15, Elsevier Science Pub., Amsterdam, North Holland (1987).
97. W. G. Johnson, *"Dislocations etch pits in nonmetallic crystals"*, In *"Progress in Ceramic Science"*, Ed. J. E. Burke, Vol. 2, Pergamon Press, Oxford (1962).
98. R. B. Heimann, *"Principles of Chemical Etching- The Arts and Science of Etching Crystals"*, In *"Crystal Growth, Properties and Applications"*, Ed. J. Grabmaier, Vol. 8, Springer Verlag, Berlin (1982).
99. J. W. Faust, *"The Surface Chemistry of metals and semiconductors"*, John Wiley, New York (1960).
100. D. Rugar, P. K. Hansma, *Phys. Today*, **43** (1990) 23.
101. A. J. Gratz, S. Manne, P. K. Hansma, *Science*, **251** (1991) 1343.
102. M. A. Mikhailenko, T. N. Drebuschak, T. P. Shakhtsneider, V. V. Boldyrev, *ARKIVOC*, **12** (2004)156.
103. B. D. Cuming, A. J. W. Moore, *J. Aust. Inst. Met.*, **3** (1958) 124.
104. W. K. Burton, N. Cabrera, F. C. Frank, *Phil. Trans. Roy. Soc. London*, **A243** (1951) 299.

105. N. Cabrera, M. M. Levine, *Phil. Mag.*, **1** (1956) 458.
106. K. Sangwal, *J. Mater Sci.* **17** (1982) 2227.
107. R. B. Heimann, "Auflösung von Kristallen (Dissolution of Crystals)", Springer-Verlag, Wien, New York, (1975).
108. L. K. Maniar, B. J. Mehta, B.S. Shah, *Surf. Technol.*, **15** (1982) 287.
109. B. S. Shah, M. J. Joshi, L. K. Maniar, *Cryst. Latt. Def. Amorph Mat.*, **17** (1988) 417.
110. B. S. Shah, M. J. Joshi, L. K. Maniar, *Indian J. Phys.*, **65A** (1991) 113.
111. P. C. Shah, B. S. Shah, *Indian J. Pure Appl. Phys.* **30** (1992) 176.
112. K. C. Poria, M. J. Joshi, B. S. Shah, *Indian J. Phys.*, **71A** (1997) 593.
113. A. H. Raval, M. J. Joshi, *Indian J. Phys.*, **68A** (1994) 113.
114. A. H. Raval, M. J. Joshi, B. S. Shah, *Cryst. Res. Technol.*, **30** (1995) 1003.
115. A. H. Raval, M. J. Joshi, B. S. Shah, *Indian J. Phys.*, **70A** (1996) 569.
116. C. P. Maniar, A. H. Raval, M. J. Joshi, *Indian J. Phys.*, **75A** (2001) 525.
117. R. M. Vaishnav, B. J. Mehta, B. S. Shah, *Rev. Latin. de Metaly Mater.*, **2** (1982) 153.
118. R. M. Vaishnav, L. K. Maniar, M. J. Joshi, R. M. Dabhi, *Indian J. Phys.*, **74A** (2000) 581.
119. B. J. Mehta, *Surf. Technol.*, **11** (1980) 301.
120. B. J. Mehta, *Surf. Technol.*, **12** (1981) 253.
121. B. J. Mehta, *Surf. Technol.*, **13** (1981) 33.
122. B. J. Mehta, *Cryst. Res. Technol.*, **16** (1981) 1097.
123. B. T. Thumar, B. J. Mehta, *Cryst. Res. Technol.*, **19** (1984) K57.
124. B. J. Mehta, G. R. Sidapara, *Cryst. Res. Technol.*, **25** (1990) 81.
125. L. Scudiero, S. C. Longford, J. T. Dickinson, *Tribology Lett.*, **6** (1999) 41.

126. G. Kanchana, P. Sundermoorthi, R. Santhi, S. Kalainathan, G. P. Jeyanthi, *J. Miner. & Mater. Charact. & Eng.*, **7** (2007) 49.
127. M. Ohta, M. Tsutsumi, S. Ueno, *J. Cryst. Growth*, **47** (1979) 135.
128. S. Guo, M.D. Ward, J. A. Wesson, *Langmuir*, **18** (2002) 4248.
129. E. V. Petrova, N. V. Gvozdev, L. N. Reshkovich, *J. Optoelectron. & Adv. Mater.*, **6** (2004) 261.
130. S. Amelinckx, "*The Direct Observation of dislocations*", Academic Press, London (1964).
131. K. J. Laidler, *Chem. Edu.* **49** (1972) 343.
132. K. J. Laidler, "*Chemical Kinetics*", 3rd Ed., Harper & Row, New York (1987).
133. R. S. Boikess, E. Edelson, "*Chemical Principle*", Harper & Row, New York (1978).

Chapter VIII

Growth and Characterization of Struvite Family Crystals

Topic Number	Topic	Page Number
8.1	Introduction	362
8.2	Struvite Family Crystals	362
8.3	Growth of Struvite Family Crystals	365
8.4	Powder XRD study	375
8.5	FT-IR Spectroscopic Study	377
8.6	Thermal Studies	380
8.7	Dielectric Studies	387
8.8	Conclusions	391

8.1 Introduction

This chapter deals with the growth and characterization of two struvite family crystals, namely, Potassium Magnesium Phosphate Hexahydrate (PMPH) or struvite-K and Sodium Magnesium Phosphate Heptahydrate (SMPH) or struvite-Na. Both struvite-K and struvite-Na crystals were grown by single diffusion gel growth technique in silica hydro gel medium. The grown crystals were characterized by powder XRD, FT-IR, Thermal analysis and dielectric study. The kinetic parameters as well as thermodynamic parameters were calculated by applying well known formulae. The results are discussed.

8.2 Struvite Family Crystals

Struvite type compound can be represented by $X^+Y^{2+}PO_4 \cdot nH_2O$, where $n = 6$ to 8 . It contains one monovalent cation X^+ and one divalent cation Y^{2+} . Among phosphate containing bio-minerals, struvite has attracted considerable attention, because of its common occurrence in a wide variety of environments. Some of the struvite type compounds and their structural relationships have been reported by Dickens and Brown [1].

Struvite analog $X^+Y^{2+}PO_4 \cdot nH_2O$ compounds with $X = Rb$ and Tl and $Y = Mg$ were obtained by means of the gelatine-gel diffusion technique by Weil [2]. Moreover, struvite type compounds $M[Mg(H_2O)_6](XO_4)$, where $M = Rb, Tl$ and $X = P, As$ were reported by the same author [3]. Crystal chemistry of struvite analog $X^+Y^{2+}PO_4 \cdot 6H_2O$ compounds with $X = K, Rb, Cs, Tl, NH_4$ and $Y = Mg$ were reported by Banks et al [4]. Erdmann and Kothner [5] prepared rubidium magnesium phosphate hexahydrated $\{RbMgPO_4 \cdot 6H_2O\}$, by mixing solutions of magnesium sulphate and of

rubidium phosphate. Struvite analogs with $Y^{2+} = \text{Co}$ and Ni were also reported by various researchers [6-10].

Recently, Yang and Sun [11] reported the formation of new struvite type phosphate compound hazenite $\{\text{KNaMg}_2(\text{PO}_4)_2 \cdot 14\text{H}_2\text{O}\}$, which contains both K and Na as univalent cations. Recently, Yang et al [12] found hazenite mineral on completely dried-out or decomposed green algae (cyanobacteria) on porous calcium-carbonate (mainly calcite and aragonite) substrates on the shoreline in Mono Lake, California. There are many structural similarities between hazenite and struvite-type materials, which have been of great interest because of their broad and important biological, agricultural, and industrial implications [2, 4, 9, 10, 13-16]. Takagi et al [17] synthesized struvite-type compound $\text{Mg}_2\text{KH}(\text{PO}_4)_2 \cdot 15\text{H}_2\text{O}$ using different combinations of magnesium salts, concentrations (0.05-0.20 M), temperature (278-298 K) and pH (6.5-7.5).

Very few attempts were made to grow struvite-K and struvite-Na crystals in laboratory conditions. Earlier only needle type struvite-K crystals were grown by gel diffusion technique by Banks et al [4].

8.2.1 Struvite-K Crystals

Potassium magnesium phosphate hexahydrate $\{\text{KMgPO}_4 \cdot 6\text{H}_2\text{O}\}$, also known as struvite-K, is new inorganic phosphate mineral approved by the Commission on New Minerals and Mineral Names, International Mineralogical Association (CNMMN-IMA) in the year 2003 [18]. Struvite-K is the natural potassium equivalent to struvite $\{\text{NH}_4\text{MgPO}_4 \cdot 6\text{H}_2\text{O}\}$, since the crystals of struvite-K are rich in potassium and similar to struvite.

Struvite-K is a well-defined potassium analogue of struvite; where monovalent cation K^+ replaces the NH_4^+ ammonium cations. This ion replacement is possible, as the ionic radii of K^+ (1.33 Å) and NH_4^+ (1.43 Å) are almost identical [19]. Earlier, both the struvite and struvite-K were reported as iso-structural compounds [20,21].

Struvite-K was identified as a mineral at two different locations [22]: (i) at the famous sulphosalt locality of Lengenbach in Binntal, Switzerland, in a dolomitic rock of Triassic age, (ii) at Rossblei, Austria, in an abandoned galena mine. The mineral occurs as pseudomorphous aggregates of dirty white colour reaching up to several millimeter in size. The aggregates represent close intergrowths of fine-grained struvite-K and newberyite. Moreover, struvite-K was also found as urinary calculi in the animals like dogs [23], goats [24] and buffalo calves [25] fed with the high-level cottonseed meal diet. Recently, Zheng-Shun Wen et al [26] checked the effect of dietary cottonseed meal on the occurrence of urolithiasis in Chinese merino sheep and concluded that addition of high level cottonseed meal increased remarkably the levels of blood magnesium, potassium, phosphorus which further promoted the formation of struvite-K. Tay et al [27] reported that nonporous struvite-K can be used in teeth root-end filling material as the primary ceramicrete binder phase.

8.2.2 Struvite-Na Crystals

Sodium magnesium phosphate heptahydrate $\{NaMgPO_4 \cdot 7H_2O\}$, also known as struvite-Na is the sodium analog to struvite in spite of the excess of water molecule. In struvite-Na, the monovalent Na^+ cations replace the NH_4^+ (ammonium) cations. Previously the struvite structure was thought to be

unable to accommodate univalent cations smaller than K^+ ion (1.33 Å). But a sodium analog of struvite was first synthesized by Mathew et al [28]. In fact, the natural formation of the struvite analog hazenite $\{KNaMg_2(PO_4)_2 \cdot 14H_2O\}$ from Mono Lake, California, and synthesis of struvite-Na invalidates this hypothesis. One explanation for this is that the smaller ionic size of Na^+ in struvite-Na is effectively compensated by the $Na^+ - H_2O$ pair.

Alkemper and Fuess [29] synthesized sodium magnesium phosphate crystals with orthorhombic structure by heating an equimolar mixture of $NaPO_3$ and MgO to 1273 K, cooling to 873 K (5 K / min) and holding for 10 h. Whereas, Mathew et al [28] synthesized $MgNaPO_4 \cdot 7H_2O$ crystals with tetragonal structure from a batch initially set up for the preparation of $Mg_3(PO_4)_2 \cdot 8H_2O$ by following the procedure of Kanazawa et al [30], where the crystals of $Mg_3(PO_4)_2 \cdot 22H_2O$ were allowed to stand in water and the pH was adjusted to 9.0 by the addition of Na_2CO_3 .

8.3 Growth of Struvite Family Crystals

The gel growth technique and its advantages are described in great detail in chapter III. The single diffusion gel growth technique was used to grow both the struvite-K as well as struvite-Na crystals. To grow these crystals almost same steps – such as (i) preparation of sodium meta-silicate (SMS) stock solution, (ii) preparation of SMS solution with definite specific gravity (SG), (iii) preparation of gel, and (iv) the pouring of supernatant solutions (SS) were followed as precisely described in section 5.2 of chapter V and hence repetitions are avoided in this chapter. The only change was diverse selection of reactant - I during the preparation of gel. Reactant – I, i.e. ADP was replaced by potassium dihydrogen phosphate (KDP) – $\{KH_2PO_4\}$ and sodium

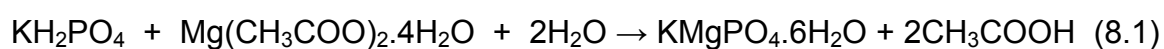
dihydrogen orthophosphate (SDO) – {NaH₂PO₄.2H₂O} for the growth of struvite-K and struvite-Na, respectively. Since the growth conditions, for instance, the SG of SMS solution, the gel pH, the concentrations of reactants, etc., play important role in the growth of crystals; in the present study, different growth parameters were used to grow struvite-K and struvite-Na crystals. Table 8.1 and 8.2 show the growth parameters for struvite-K and struvite-Na crystals, respectively.

8.3.1 Growth Parameters for Struvite-K

Table : 8.1 : Different Growth Parameters Used to Grow Struvite-K Crystals

Set	Specific Gravity of SMS	Concentration of KDP (Reactant I) (M)	pH value of the Gel	Concentration of supernatant solution of magnesium acetate (Reactant II) (M)	Liesegang Rings observed having pH values
1	1.04	1.00	6.0 to 8.0	1.00	8.0
2	1.04	1.50	6.0 to 8.0	1.50	-
3	1.05	0.25	6.0 to 8.5	1.00	> 7.0
4	1.05	0.50	6.0 to 7.5	1.00	> 7.5
5	1.05	1.00	5.5 to 8.5	1.00	> 8.0
6	1.05	1.50	6.0 to 8.0	1.00	> 7.5
7	1.05	0.50	6.0 to 9.0	0.50	-
8	1.06	0.50	6.0 to 8.5	1.00	> 8.0
9	1.06	1.00	6.0 to 8.0	1.00	8.0
10	1.07	1.50	5.8 to 7.0	1.00	-

The following reaction is expected to occur in the gel between the two reactants, namely, KDP as a reactant - I present in the gel and magnesium acetate as a reactant - II present in the SS.

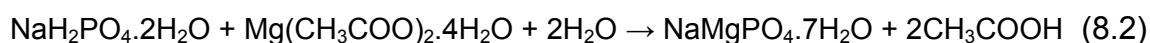


8.3.2 Growth Parameters for Struvite-Na

Table : 8.2 : Different Growth Parameters Used to Grow Struvite-Na Crystals

Set	Specific Gravity of SMS	Concentration of SDO (Reactant I) (M)	pH value of the Gel	Concentration of supernatant solution of magnesium acetate (Reactant II) (M)	Liesegang Rings observed having pH values
1	1.04	1.00	5.5 to 8.0	1.00	8.0
2	1.04	1.50	5.5 to 8.0	1.50	-
3	1.05	0.50	6.0 to 8.0	0.50	> 7.5
4	1.06	0.75	6.0 to 8.0	0.75	> 6.8
5	1.06	1.00	6.0 to 8.5	1.00	> 7.0
6	1.06	1.50	6.0 to 7.5	1.00	> 7.0

The following reaction is expected to occur in the gel between the two reactants, namely, SDO as a reactant - I present in the gel and magnesium acetate as a reactant - II present in the SS.



As a result of reactions (8.1) and (8.2) struvite-K and struvite-Na crystals were grown in the gel media of respective test tubes. It was found that the growth of these struvite type crystals completed within 12 days after the pouring of supernatant solution. It was also observed that both the struvite-K and struvite-Na types of crystals grew very rapidly near the gel - liquid interface, whereas they grew slowly at substantial depths from the gel - liquid interface which might be due to decreasing nature of concentration gradients with depth. The grown crystals were carefully removed from the gel medium, quickly rinsed in distilled water and then dried on a filter paper. The grown crystals were kept in airtight bottles and used for further investigation.

8.3.3 Morphology of Gel Grown Struvite-K Crystals

It was noticed that morphology of gel grown struvite-K crystals was dependent on growth parameters. By changing the growth parameters, struvite-K crystals with different morphologies like prismatic type, star type, rectangular platelet type, elongated platelet type, coffin shaped and dendritic type were grown by single diffusion gel growth technique.

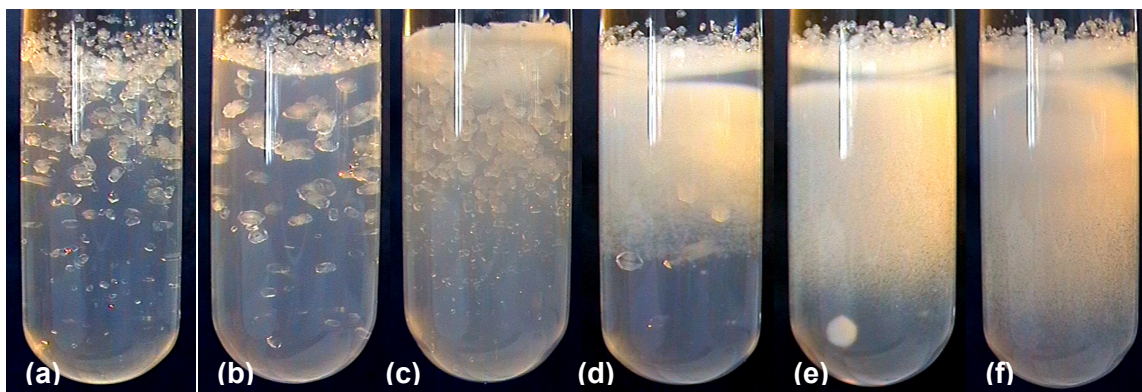


Figure : 8.1 Struvite-K Crystals Grown in Gel Medium for 1.05 SG of SMS, 0.5 M KDP and SS of 0.5 M Magnesium Acetate with different pH values as (a) 6.5 pH, (b) 7.0 pH, (c) 7.5 pH, (d) 8.0 pH, (e) 8.5 pH and (f) 9.0 pH

It was observed that pH values of the gel played an important role in the growth of the struvite-K crystals. Figure 8.1 shows the photographs of the struvite-K crystals grown in the gel medium for the growth parameters as 1.05 SG of SMS solution, 0.5 M KDP solution as reactant - I and SS of 0.5 M magnesium acetate with different pH values. As shown in figure 8.1 (a) transparent prismatic type struvite-K crystals are observed for 6.5 pH. Here, it is noticed that number density and the apparent size of the grown crystals decreases, whereas transparency increases with increasing depth of gel column. For 7.0 pH of the gel, the number density of the grown prismatic struvite-K crystals are decreased, whereas the apparent crystal size increases as shown in figure 8.1 (b). For higher values of the gel pH, the settled gels were found denser and as a result comparatively poor crystals were grown.

The dense gels have small pore sizes and do not readily facilitate the movements of supernatant solution ions for the reaction and also the dense gel put constraints on the growth of crystals.

It was also observed that the number density of the grown crystals increased with the increasing concentrations of either the first reactant, i.e. KDP or the second reactant magnesium acetate in SS. For instance, figure 8.2 shows the photographs of the test tubes with fixed values of 1.05 SG and 7.0 pH of gel with diverse concentration of both the reactants. Moreover, as shown in figure 8.2 (d), for certain higher concentrations of reactants star type bunch of poly-crystals are found to grow in the gel instead of prismatic single crystals.

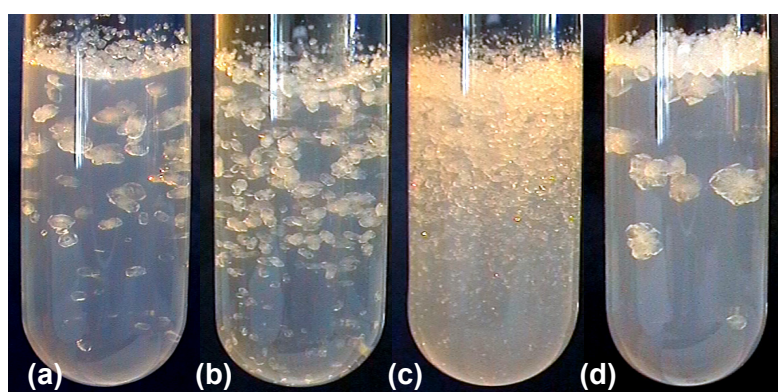


Figure : 8.2 Struvite-K Crystals Grown in Gel Medium for 1.05 SG of SMS and at 7.0 Gel pH for Different Concentration of Reactants as (a) 0.5 M KDP, 0.5 M SS, (b) 0.5 M KDP, 1.0 M SS, (c) 1.0 M KDP, 1.0 M SS and (d) 1.5 M KDP, 1.0 M SS

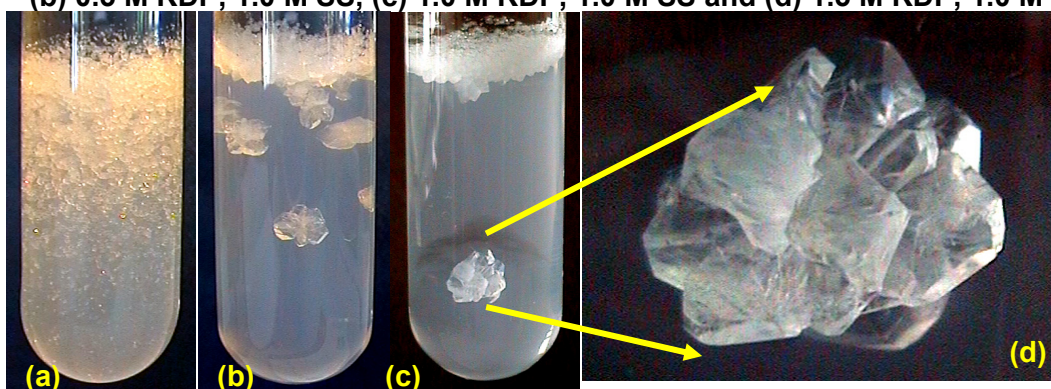


Figure : 8.3 Struvite-K Crystals Grown in Gel Medium for 1.0 M KDP, 1.0 M Magnesium Acetate in SS, 7.0 pH of Gel with Different Specific Gravity of Gel as (a) 1.05 SG, (b) 1.06 SG and (c) 1.04 SG, (d) Grown Poly-Crystal of Struvite-K

The variation in the specific gravity of the gel also played important role in the growth phenomenon of the struvite-K crystals. For example figure 8.3 shows the photographs of the test tubes with the fixed growth parameters as 1 M concentration of each of the reactants and 7.0 pH of gel but the SG of the gel was varied. As shown in figure 8.3 (b) and (c), very few star type poly-crystals are noticed in the case of 1.04 and 1.06 SG of gel, whereas the maximum number of single crystals were grown in the case of 1.05 SG of gel as seen in figure 8.3 (a).

As shown in figure 8.4 (a), the dendritic type growth is observed for the SMS solution of SG 1.04, 1.5 M KDP solution, 1.5 M magnesium acetate SS and 6 pH value of the gel, which might be due to the higher concentration of the reactants. But when gel pH was increased from 6.0 to 6.5, few poly-crystals were observed instead of dendritic crystals as can be seen in figure 8.4 (b).

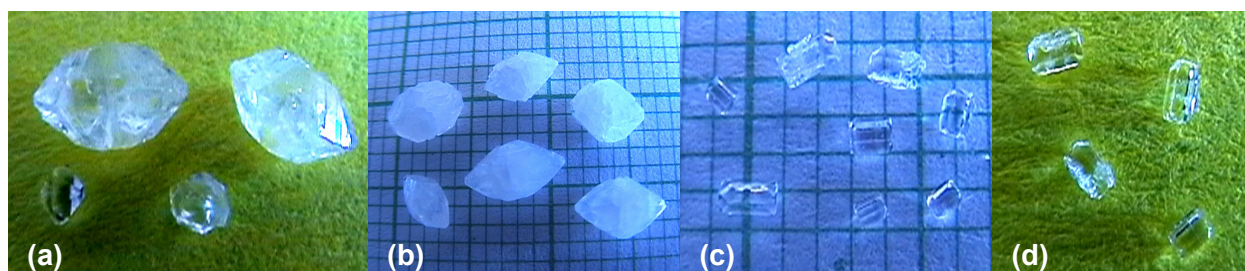
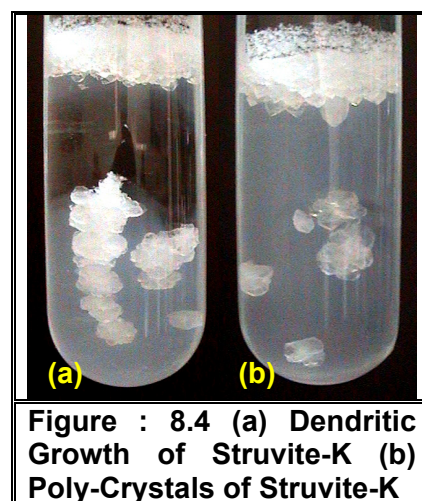


Figure : 8.5 Gel Grown Struvite-K Crystals (a) Transparent Prismatic (b) Opaque Prismatic (c) Rectangular Platelet (d) Coffin Shaped Crystals

Prismatic type struvite-K crystals with different diaphaneity and diverse apparent size ranging from 1 to 8 mm were found in all the sets (set number - 3 to 7) with 1.05 SG of SMS solutions with the pH range of 6.5 to 8.0. However, the good quality transparent prismatic type struvite-K crystals with

optimum apparent size were observed only for the growth parameters as SMS of SG 1.05, 0.5 M KDP, 0.5 M SS with 6.5 pH value of the gel. It was remarkably noticed that as the pH value of the gel increased, the transparency of the grown crystals decreased. Moreover, transparent prismatic crystals were also noticed in the gel column at higher depth from the gel liquid interface. Figure 8.5 (a) and (b) shows transparent and opaque prismatic type struvite crystals, respectively. Comparatively large, opaque, prismatic type crystals having apparent size of 5 to 9 mm were observed for the growth parameters as 1.06 SG of SMS, 1 M KDP, 1 M SS and 7.5 pH value of the gel.

As mentioned earlier, pH values of the gel played an important role in the growth morphology of the crystals, for example, with the growth parameters having 1.05 SG of SMS solution, 0.25 M KDP and 1 M SS, the rectangular platelet type {figure 8.5 (c)} as well as coffin shaped crystals {figure 8.5 (d)} were observed for 6.0 pH, the star type crystals were observed for 6.5 pH and prismatic type crystals were observed for 7.0 and 7.5 pH.

8.3.4 Morphology of Gel Grown Struvite-Na Crystals

Struvite-Na crystals were grown by changing different growth parameters as mentioned in table 8.2. Figure 8.6 shows the photographs of Struvite-Na crystals grown in the gel medium.

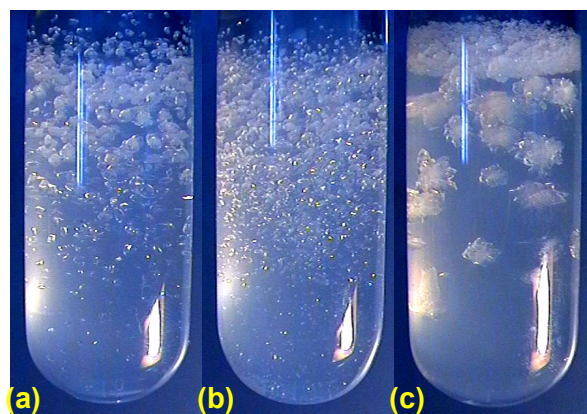


Figure : 8.6 Struvite-Na Crystals Grown in Gel Medium for growth conditions as

(a) 1.05 SG of SMS, 0.5 M SDO, 0.5 M SS and 6.5 pH of gel,

(b) 1.05 SG of SMS, 0.5 M SDO, 0.5 M SS and 7.0 pH of gel,

(c) 1.06 SG of SMS, 1.0 M SDO, 1.0 M SS and 6.5 pH of gel

Crystals with different morphologies like prismatic type, star type and dendritic type were grown in the gel. More or less, most of the findings for the growth of struvite-Na crystals were identical to those obtained for struvite and struvite-K crystals, and hence reported briefly to avoid repetitions.



Figure : 8.7 Prismatic Type Struvite-Na Crystals Grown with the Conditions as 1.05 SG of SMS, 0.5 M SDO, 0.5 M SS and pH Value of Gel as (a) 6.0 pH, (b) 6.5 pH, (c) 7.0 pH and (d) 7.5 pH

Crystallization of struvite-Na was found to be possible within the range of 6 to 7.5 pH of gel, whereas crystallization was not obtained below 6 pH and Liesegang rings were obtained along with few crystals above 7 pH of the gel. The grown struvite-Na crystals had transparent, translucent and opaque diaphaneity, depending upon the location and the growth conditions. As illustrated in figure 8.7, prismatic type struvite-Na crystals with different diaphaneity and diverse apparent size ranging from 1 to 5 mm were found in the cases with 1.05 SG of SMS solutions within the pH range of 6.0 to 7.5. It was noticed that transparency of the grown crystals gradually decreased with the increasing pH value of the gel. Moreover, good quality transparent prismatic crystals were noticed at higher depth from the gel - liquid interface as shown in figure 8.8.



Figure : 8.8 Prismatic Type Struvite-Na Crystals

As shown in figure 8.6 (c), star type poly-crystals were noticed in the cases of 1.04 and 1.06 SG of gel, whereas the maximum number of single crystals was grown in the case of 1.05 SG of gel. Star type clustered patterns of crystals were developed as a result of diffusion of highly concentrated nutrients near the gel-liquid interface.

8.3.5 Formation of Liesegang Rings

The Liesegang rings are typical periodic precipitation pattern of rings or bands formed during diffusion process of chemical reactants in gel. A brief introduction including the formation, types and the parameters affecting the development of Liesegang rings are previously discussed in section 3.11 of the chapter III.

The Liesegang rings were observed for 7.0 and higher pH values of the gel in case of struvite-K crystal growth. Such patterns arise from the interplay between the reaction kinetics and the diffusion of chemical species. Table 8.1 demonstrates the cases for which Liesegang rings are observed. Figure 8.9 (a to c) shows the formation of Liesegang rings in the test tubes with the growth parameters as 1.05 SG of SMS solution, 0.25 M KDP, 1.0 M magnesium acetate for 7.0 pH, 7.5 pH and 8.0 pH values of the gel, respectively. It was observed that as the pH of the gel increased, the number of Liesegang rings increased. The spacing between the Liesegang rings in the gel column increased with the depth. Moreover, the thickness of the Liesegang rings also increased with the depth. Joseph and Joshi [31] have discussed the effect of various parameters on the formation of Liesegang rings during the growth of calcium hydrogen phosphate dihydrate crystals. The crystals in the Liesegang rings are of the order of micrometer size. It is clear from the figure 8.9 (a) that

struvite-K crystals were grown with prismatic morphology having apparent length of 3 to 5 mm; and they also formed a ring structure under the last Liesegang ring.

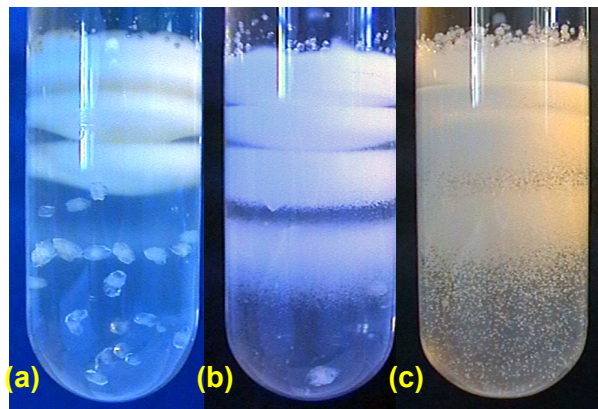


Figure : 8.9 Formation of Liesegang Rings in the experiments of Struvite-K with growth parameters : 1.05 SG of SMS, 0.25 M KDP, 1.0 M SS and Gel pH as (a) 7.0 pH, (b) 7.5 pH and (c) 8.0 pH

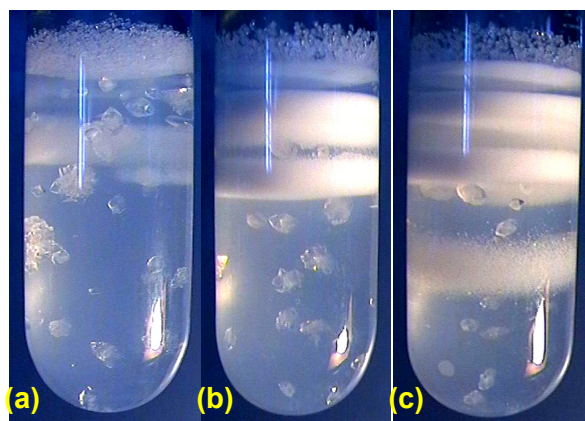


Figure : 8.10 Formation of Liesegang Rings in the experiments of Struvite-Na with growth parameters : 1.06 SG of SMS, 1.0 M SDO, 1.0 M SS and Gel pH as (a) 7.0 pH, (b) 7.5 pH and (c) 8.0 pH

The Liesegang rings were also observed for 6.8 and higher pH values of the gel for the experiments of struvite-Na crystal growth. Table 8.2 illustrates the cases for which Liesegang rings were observed. Figure 8.10 (a to c) shows the formation of distinct thick Liesegang rings at the top of the gel column near the gel-liquid interface in the test tube with the growth parameters as 1.06 SG of SMS solution, 1.0 M SDO, 1.0 M SS for 7.0 pH, 7.5 pH and 8.0 pH

values of the gel, respectively. Struvite-Na crystals with star as well as prismatic morphology were also observed along with Liesegang rings.

8.4 Powder XRD study

A detailed description of the powder XRD is already mentioned in the section 4.2 of Chapter-IV. The powder XRD study of grown struvite family crystals was carried out to confirm the crystalline material as well as to verify the structure. It was found that both of the struvite analogues under investigation, i.e., struvite-K and struvite-Na, exhibited orthorhombic crystal structure similar to struvite crystal structure.

8.4.1 Powder XRD of Struvite-K

Figure 8.11 exhibits the powder XRD pattern of struvite-K crystals. The crystal structure of struvite-K was found to be orthorhombic with unit cell parameters as, $a = 6.893 \text{ \AA}$, $b = 6.141 \text{ \AA}$, $c = 11.222 \text{ \AA}$ and $\alpha = \beta = \gamma = 90^\circ$. The values are closely matching with the reported values by Mathew and Schroeder [20], and recently reported values by Graeser et al [22].

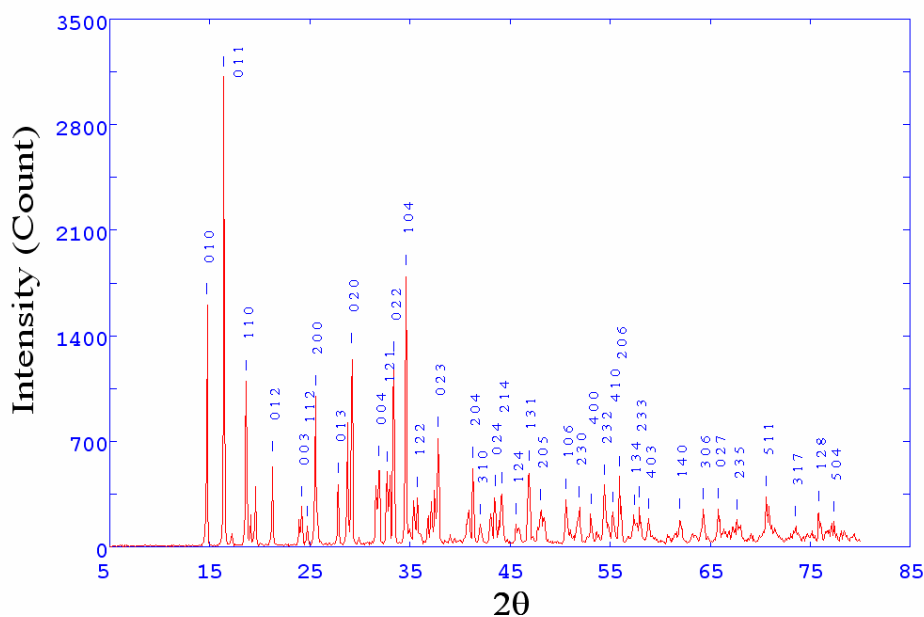


Figure : 8.11 Powder XRD Pattern of Struvite-K Crystals

The struvite-K crystal structure consists of two structural units (functional groups), namely, (i) PO_4 tetrahedron, and (ii) $\text{Mg} \cdot 6\text{H}_2\text{O}$ octahedron. Figure 8.12 shows the structural units of struvite-K. Mg^{2+} cations are all coordinated octahedrally by six H_2O molecules whose H atoms are strongly bonded to oxygen atoms in $(\text{PO}_4)^{3-}$ groups. Figure 8.13 demonstrates the crystal structure of struvite-K as explained by Graeser et al [22].

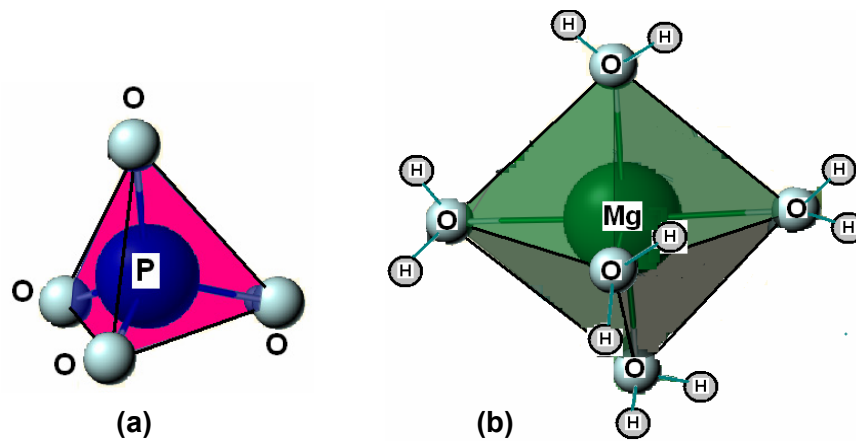


Figure : 8.12 Structural Units of Struvite-K
(a) Tetrahedra PO_4 , (b) Octahedra $\text{Mg} \cdot 6\text{H}_2\text{O}$

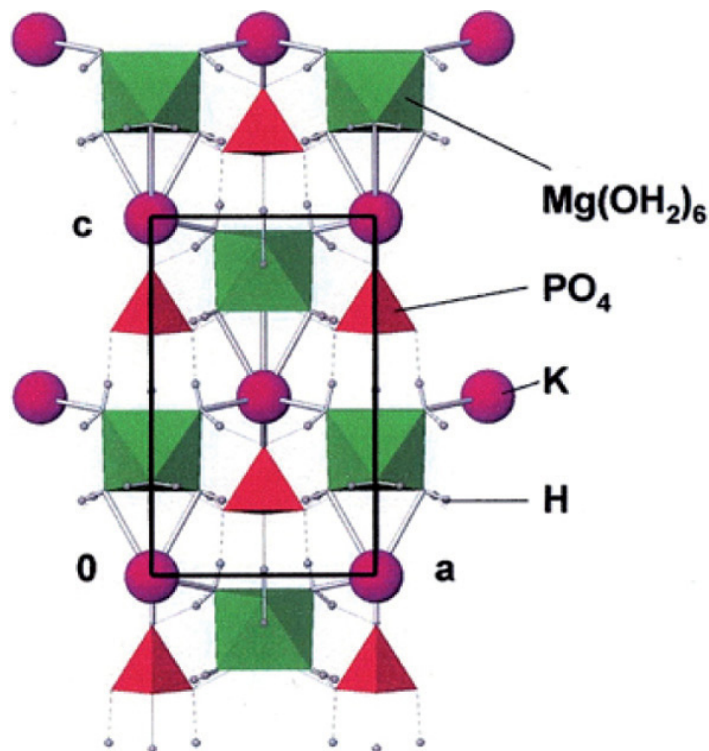


Figure : 8.13 Struvite-K Crystal Structure [22]

8.4.2 Powder XRD of Struvite-Na

Crystal structure of $\text{KNaMg}_2(\text{PO}_4)_2 \cdot 14\text{H}_2\text{O}$ has been recently reported. However, no major work on struvite-Na is reported. Figure 8.14 exhibits the powder XRD pattern of struvite-Na crystals. The crystal structure of struvite-Na was found to be orthorhombic with cell parameters as, $a = 6.893 \text{ \AA}$, $b = 6.124 \text{ \AA}$, $c = 11.150 \text{ \AA}$ and $\alpha = \beta = \gamma = 90^\circ$.

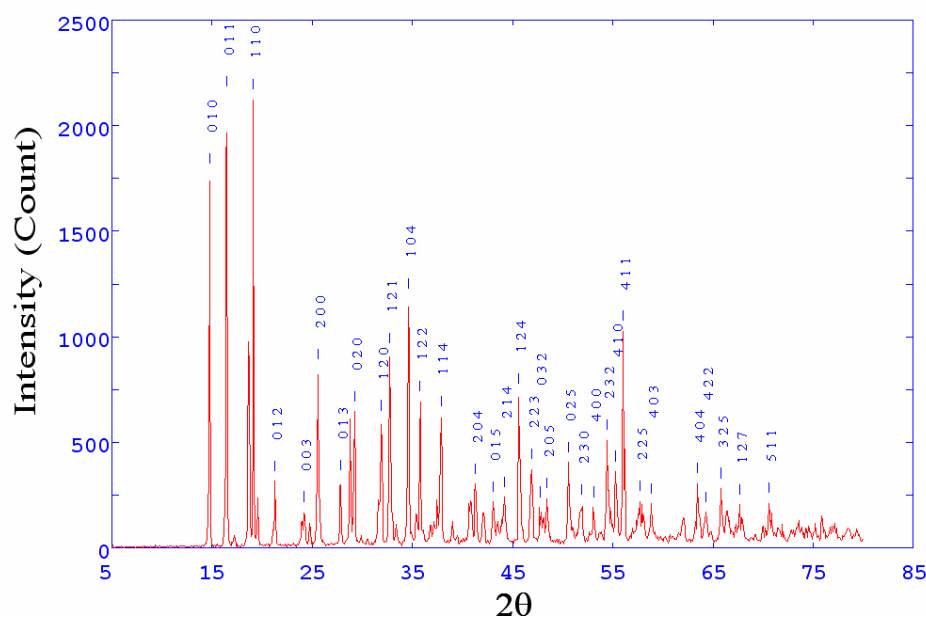


Figure : 8.14 Powder XRD Pattern of Struvite-Na Crystals

8.5 FT-IR Spectroscopic Study

Many common minerals exhibit unique spectra in the mid-infrared range, which extends from 400 cm^{-1} to 4000 cm^{-1} . Details of the FT-IR technique are previously discussed in section 4.3 of chapter IV. The FT-IR spectra of both the struvite analogue crystals are presented in figure 8.15, which depict that both the struvite-K and struvite-Na have more or less identical spectrum. The vibrational band assignments according to literature and experimental data are summarized in table 8.3.

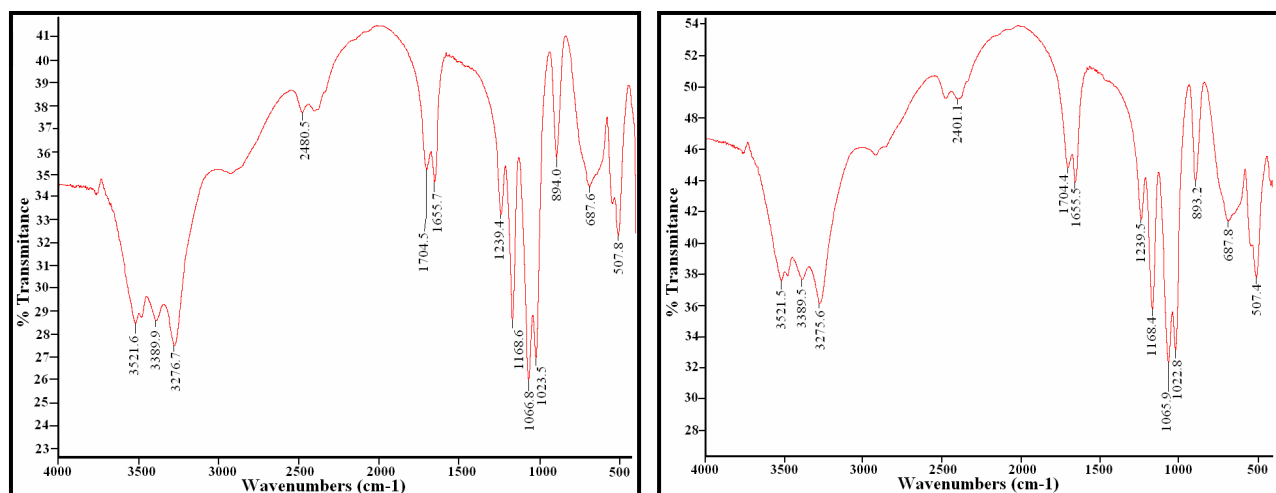


Figure : 8.15 (a) FT-IR Spectrum of Struvite-K (b) FT-IR Spectrum of Struvite-Na

Table :8.3: Assignments of Absorption Bands in the FT-IR Spectrum of Struvite

Assignments		Reported IR frequencies From Other Minerals wavenumbers (cm ⁻¹)	Observed IR frequencies wavenumbers (cm ⁻¹)	
			Struvite-K	Struvite-Na
Absorption peaks due to water of crystallization	H–O–H stretching vibrations of water crystallization	3280 to 3550	3276.7, 3389.9, 3521.6	3275.6, 3389.5, 3521.5
	H–O–H stretching vibrations of cluster of water molecules of crystallization	2060 to 2460	2375, 2480.5	2401.1, 2478
	H–O–H bending modes of vibrations	1590 to 1650	1655.7, 1704.5	1655.5, 1704.4
	Wagging modes of vibration of coordinated water	808	894	893.2
Absorption peaks due to PO ₄ ³⁻ units	ν ₁ symmetric stretching vibration of PO ₄ ³⁻ units	930 to 995	1023.5	1022.8
	ν ₂ symmetric bending vibration of PO ₄ ³⁻ units	404 to 470	421.8	407
	ν ₃ asymmetric stretching vibration of PO ₄ ³⁻ units	1017 to 1163	1066.8, 1168.6, 1239.4	1065.9, 1168.4, 1239.5
	ν ₄ asymmetric bending modes	509 to 554	507.8	507.4
Metal-Oxygen bonds	Metal-Oxygen bonds	400-650	687.6	687.8
	Deformation of OH linked to Mg ²⁺	847	894	893.2

It was found that both the struvite analogs have characteristic FT-IR spectra, since they have distinguishing positions of the absorption bands occurred due to vibrations of water of crystallization, tetrahedral PO_4^{3-} units and metal oxygen bonds.

There are four regions found in the FT-IR spectrum depicting the absorptions due to water of crystallization in both the struvite analog crystals under investigation as shown in table 8.3, which closely matched to the previously reported peaks in several inorganic hydrated compounds [32-39].

Intense bands appeared between the 3275 cm^{-1} and 3522 cm^{-1} indicate H–O–H stretching vibrations of water of crystallization. Here, the position of relatively broad band peak near 3275 cm^{-1} suggests that the water is strongly hydrogen bonded to the Mg cations. The weak bands appeared within 2375 cm^{-1} to 2480.5 cm^{-1} in the spectrum can be assigned due to H–O–H stretching vibrations of cluster of water molecules of crystallization. The medium intense bands appeared nearly at 1655 cm^{-1} and 1704 cm^{-1} in the spectrum indicate the H–O–H bending modes of vibrations suggesting the presence of water [40]. A medium absorption band at 894 cm^{-1} indicates the wagging modes of vibration of the coordinated water and the Metal–Oxygen bond in the complex.

Vibrational modes of tetrahedral XY_4 molecules are well known [41]. Julien et al [42] had described the vibrational modes of the materials containing PO_4^{3-} anions. In the FT-IR spectrum, the ν_1 symmetric stretching vibration of tetrahedral PO_4^{3-} anions units was found to be at medium band at 894 cm^{-1} in case of struvite-K and 893.2 cm^{-1} in case of struvite-Na correspond to the previously reported values for different phosphate minerals

[43-45]. The position of the symmetric stretching vibrations is mainly dependent on the type of mineral, the cation present and crystal structure. While, the positions of the asymmetric stretching vibrations ν_3 of phosphate PO_4^{3-} anion units in struvite were found at the strongest peaks between 1065.9 cm^{-1} and 1239.5 cm^{-1} , which are in accordance with the values reported earlier [40, 43, 45, 46]. The symmetric bending vibrations ν_2 of PO_4^{3-} units were observed nearly at the starting points of spectrum correspond to the previously reported values for various phosphate minerals [43]. Moreover, the asymmetric bending vibrations ν_4 of PO_4^{3-} units in struvite were observed around 507 cm^{-1} . Here, ν_1 and ν_3 involve the symmetric and asymmetric stretching mode of the P–O bonds, whereas ν_2 and ν_4 involve mainly O–P–O symmetric and asymmetric bending mode with a small contribution of P vibration. The absorption peaks near 687 cm^{-1} ascribe the presence of oxygen-metal bond.

Thus, the FT-IR spectra of both struvite-K and struvite-Na prove the presence of water of hydration, P – O bond, NH_4^+ ion and PO_4^{3-} ion and metal-oxygen bond.

8.6 Thermal Studies

The thermal studies, such as TGA, DTA and DSC of powdered samples of struvite-K as well as struvite-Na were carried out using Linseis Simultaneous Thermal Analyzer (STA) PT-1600, in the atmosphere of air from $25 \text{ }^\circ\text{C}$ to $900 \text{ }^\circ\text{C}$ at a heating rate of $15 \text{ }^\circ\text{C}/\text{min}$ using $\alpha\text{-Al}_2\text{O}_3$ as standard reference. Details of the techniques used for the thermal study are elaborately discussed in section 4.4 of chapter IV as well as section 5.6 of chapter V.

8.6.1 Thermal Study of Struvite-K

Figure 8.16 shows the TGA, DTA and DSC profiles obtained for the gel grown struvite-K as curves (a), (b) and (c), respectively. The graph of mass loss in mg on the Y-axis plotted versus temperature at a fixed rate of change of temperature in °C on the X-axis gives the TGA curve (thermo-gram).

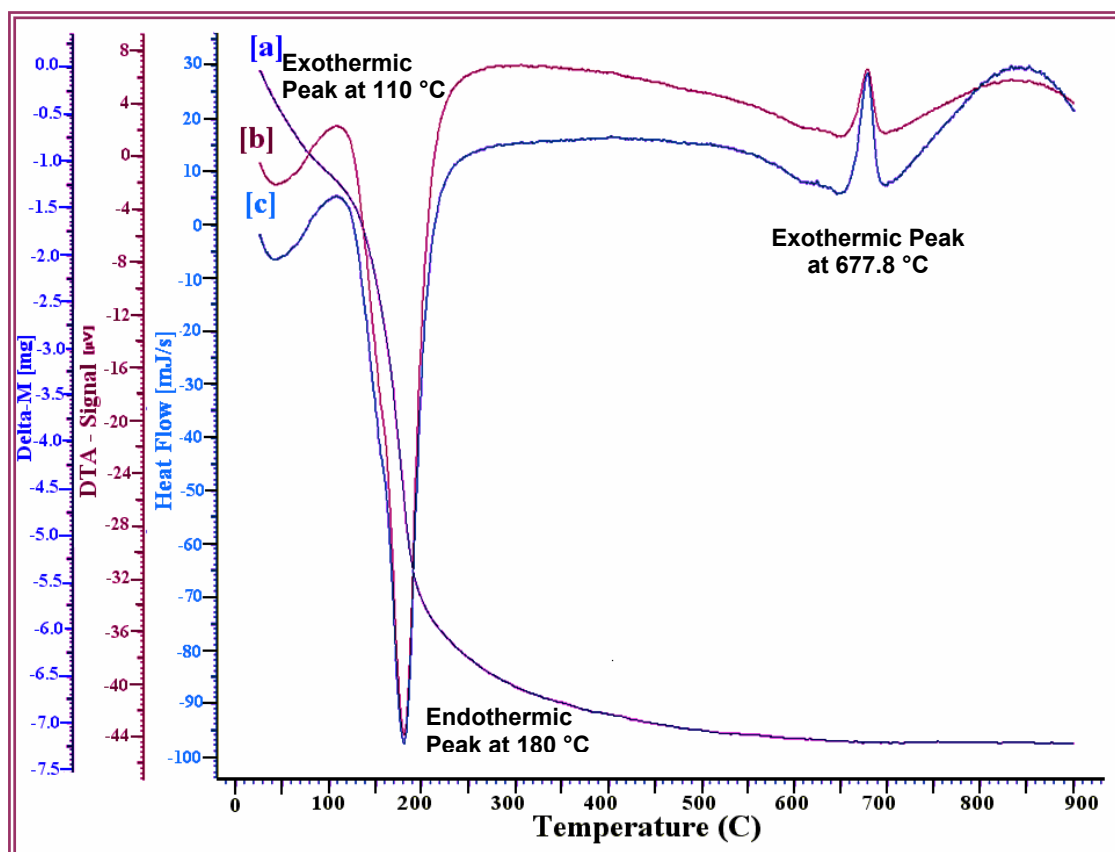


Figure : 8.16 TGA, DTA and DSC Profiles for the Gel Grown Struvite-K Crystal

From TGA curve it was found that the struvite-K started dehydrating and decomposing from just above the room temperature and finally at 600 °C it became 64.14% of the original weight and remained almost constant up to the end of analysis. Mass loss in a TGA analysis of sample at temperatures above 100 °C indicates association of water molecules with the Struvite-K chemical structure. A continuous loss of mass in the TGA curve can be attributed to the dehydration of the sample. From the TGA curve, the number

of water molecules associated with the crystal was estimated to be 5. In the temperature range 650–900 °C, no further weight loss occurred and the sample remained almost stable.

From the TGA, total mass loss is found to be 35.86 %, which may be due to the loss of water of crystallization. This weight loss corresponds to the following reaction for struvite-K :



Table 8.4 indicates the TGA results of struvite-K crystals along with the theoretically calculated and experimentally obtained percentage weight.

Table : 8.4 : TGA Results of Struvite-K Crystals

Temperature	Substance	Theoretical weight (%) (Calculated)	Practical weight (%) (from TGA)
Room Temperature	KMgPO ₄ ·6H ₂ O (Struvite-K)	100	100
900 °C	KMgPO ₄ (Dehydrated Struvite-K)	63.76	64.14

The graph of DTA signal, i.e. differential thermocouple output in micro volts on the Y-axis plotted versus the sample temperature in °C on the X-axis gives the results of DTA. The transition temperatures were measured precisely using DTA curve. In the DTA curve an endothermic peak was observed at 180 °C, which might be due to release of crystalline water. Processes involving a loss of mass usually give rise to endothermic nature in DTA trace because of the work of expansion. During this endothermic process, the amount of heat change was found to be 406.75 μVs/mg. On further heating at higher temperatures, anhydrate struvite-K was obtained. In the DTA curve of struvite-K crystals, two exothermic peaks were observed, one medium peak at 110 °C and the second strong one at 677.8 °C. Second

exothermic peak might be due to high temperature phase transition. During this exothermic process at 677.8 °C, the amount of heat change was found to be – 22.63 μVs/mg.

The graph of heat flow in mJ/s on the Y-axis plotted versus temperature at a fixed rate of change of temperature in °C on the X-axis shows the output of the DSC. The DSC curve exhibited peaks at the same temperatures as peaks were obtained in DTA curve. In the TGA curve, no remarkable change was observed for the peak which was noticed at 677.8 °C in DTA and DSC curves due to the possible phase transition, since no change took place in the mass of the specimen.

8.6.2 Thermal Study of Struvite-Na

Figure 8.17 shows the TGA, DTA and DSC profiles obtained for the gel grown struvite-Na by the curves (a), (b) and (c), respectively. From the TGA curve, it was found that the struvite-Na started dehydrating and decomposing just above the room temperature and finally at 600°C it became 63.9 % of the original weight and remained almost constant up to the end of analysis.

Mass loss in a TGA analysis of sample at temperatures above 100°C indicates association of water molecules with the struvite-Na chemical structure. A continuous loss of mass in the TGA curve can be attributed to the dehydration of the sample. From TGA, the number of water molecules associated with the crystal was estimated to be 5. In the temperature range 600–900°C, no further weight loss occurred and the sample remained stable.

From the TGA, total mass loss is found to be 36.1 %, which may be due to the loss of water of crystallization. This weight loss corresponds to the following reaction for struvite-Na :

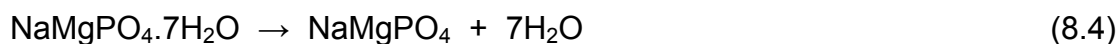


Table 8.5 indicates the TGA results of struvite-Na crystals along with the theoretically calculated and experimentally obtained percentage weight.

Table : 8.5 : TGA Results of Struvite-Na Crystals

Temperature	Substance	Theoretical weight (%) (Calculated)	Practical weight (%) (from TGA)
Room Temperature	NaMgPO ₄ ·7H ₂ O (Struvite-Na)	100	100
900 °C	NaMgPO ₄ (Dehydrated Struvite-Na)	61.25	63.9

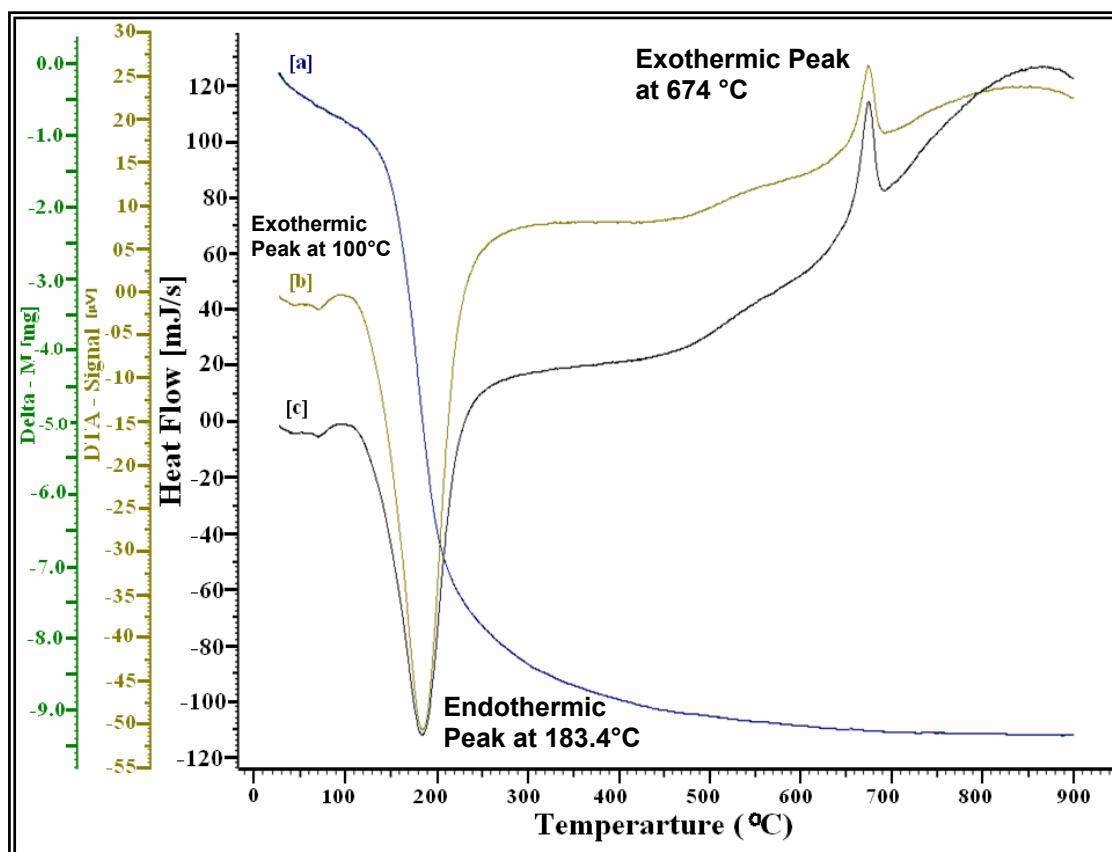


Figure : 8.17 TGA, DTA and DSC Profiles for the Gel Grown Struvite-Na Crystal

In the DTA curve an endothermic peak was observed at 183.4°C, which might be due to release of crystalline water. Processes involving a loss of mass usually give rise to endothermic nature in DTA trace because of the work of expansion. During this endothermic process, the amount of heat change was found to be 403.10 μVs/mg. On further heating at higher

temperatures, anhydrate struvite-Na was obtained. In the DTA curve of struvite-Na crystals, two exothermic peaks were observed, one medium peak at 100°C and the second strong one at 674°C. Second exothermic peak might be due to high temperature phase transition. During this exothermic process at 674 °C, the amount of heat change was found to be – 28.40 μVs/mg.

The DSC curve exhibited peaks at the same temperatures as peaks were obtained in DTA curve. In TGA curve, no remarkable change was observed for the peak which was noticed at 674°C in DTA and DSC curves due to the possible phase transition, since no change took place in the mass of the specimen.

The thermodynamic parameters obtained from the thermal analysis of both the struvite-K and struvite-Na are tabulated in table 8.6.

Table : 8.6 : Thermodynamic Parameters of Struvite-K and Struvite-Na

Compound	→	Struvite-K		Struvite-Na	
Reaction →	Unit ↓	Endothermic Reaction	Exothermic Reaction	Endothermic Reaction	Exothermic Reaction
Temperature	°C	180	677.8	183.4	674
Enthalpy (ΔH)	J / g	917.32	– 96.19	889.68	– 143.11
Specific Heat Capacity	J / g °C	0.6356	0.3415	0.9703	1.6173
Amount of Heat Change	μVs/mg	406.75	– 22.63	403.10	– 28.40
Heat Flow Rate	mJ / s	97.55	– 28.67	111.70	– 114.72

8.6.3 Kinetic Parameters of Dehydration and Decomposition

The kinetic parameters of both the struvite-K and struvite-Na were evaluated from the respective TGA curves by applying Coats and Redfern relation [47] as depicted by equation (5.4) in chapter V. Figure 8.18 (a) and (b) illustrate the Coats and Redfern plot for struvite-K and struvite-Na

respectively. The values of activation energy were obtained from the slope of the best linear fit plot. The values of activation energy E , frequency factor A and order of reaction n were obtained as tabulated in table 8.7.

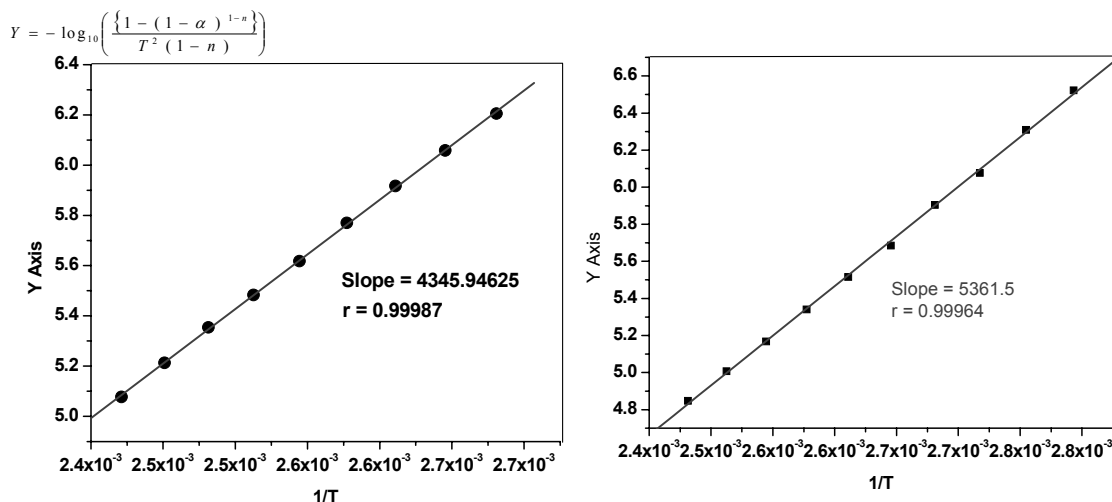


Figure : 8.18 Coats and Redfern Plots for (a) Struvite-K, (b) Struvite-Na

Table : 8.7 : Kinetic Parameters of Struvite-K and Struvite-Na

Kinetic Parameters	Symbol	Struvite-K	Struvite-Na
Activation Energy	E	83.21 kJ Mol ⁻¹	102.66 kJ Mol ⁻¹
Frequency Factor	A	4.64 x 10 ¹⁰	4.17 x 10 ¹³
Order of Reaction	n	2	2

It is noticed that the values of activation energy is slightly higher in struvite-Na than struvite-K. Which indicates that struvite-Na is slightly more stable than struvite-K. This is also reflected from DTA and DSC curves where first endothermic reaction is observed at 183.4°C for struvite-Na and for struvite-K at 180°C. This clearly suggests slightly higher stability of struvite-Na.

8.6.4 Thermodynamic Parameters of Dehydration and Decomposition

Various thermodynamic parameters such as standard entropy of activation $\Delta^\ddagger S^\circ$, standard enthalpy of activation $\Delta^\ddagger H^\circ$, standard Gibbs energy of activation $\Delta^\ddagger G^\circ$ and standard internal energy of activation $\Delta^\ddagger U^\circ$ were calculated by applying well known formulae, as described in detail by

Laidler [48] and mentioned in section 5.6.5 of chapter V. Table 8.8 gives the values of thermodynamic parameters of dehydration and decomposition for both the struvite analog crystals under present investigation.

Table : 8.8 : Thermodynamic Parameters of Dehydration and Decomposition

Thermodynamic Parameters	Symbol	Struvite-K	Struvite-Na
Standard Entropy of activation	$\Delta^\ddagger S^\circ$	$-43.00 \text{ J Mol}^{-1} \text{ K}^{-1}$	$13.76 \text{ J Mol}^{-1} \text{ K}^{-1}$
Standard Enthalpy of activation	$\Delta^\ddagger H^\circ$	$76.67 \text{ kJ Mol}^{-1}$	$96.28 \text{ kJ Mol}^{-1}$
Standard Gibbs Energy of activation	$\Delta^\ddagger G^\circ$	$93.57 \text{ kJ Mol}^{-1}$	$91.02 \text{ kJ Mol}^{-1}$
Standard Internal Energy of activation	$\Delta^\ddagger U^\circ$	$79.94 \text{ kJ Mol}^{-1}$	$99.47 \text{ kJ Mol}^{-1}$

Here, negative value of $\Delta^\ddagger S^\circ$ for struvite-K shows that the process is non-spontaneous, whereas positive value of the struvite-Na depicts spontaneous process. For both the struvite analog crystals the values of standard enthalpy of activation $\Delta^\ddagger H^\circ$ are positive, which show that the enthalpy is increasing during the process and such process is an endothermic process. Positive values of $\Delta^\ddagger G^\circ$ demonstrate that both the struvite-K and struvite-Na are thermodynamically unstable.

8.7 Dielectric Studies

Every material has a unique set of electrical characteristics which are dependent on its dielectric properties. The dielectric constant of a material is associated with the energy storage capability in the electric field in the material and the loss factor is associated with the energy dissipation, conversion of electric energy to heat energy in the material. The experimental technique used for the dielectric study was described earlier in section 4.5 of the chapter IV. The dielectric constants, dielectric loss, a.c. conductivity (σ_{ac}) and a.c. resistivity (ρ_{ac}) were evaluated with the frequency of applied field at

room temperature using well known formulae as depicted by equations (4.4), (4.6), (4.7) and (4.8) in section 4.5 of chapter IV.

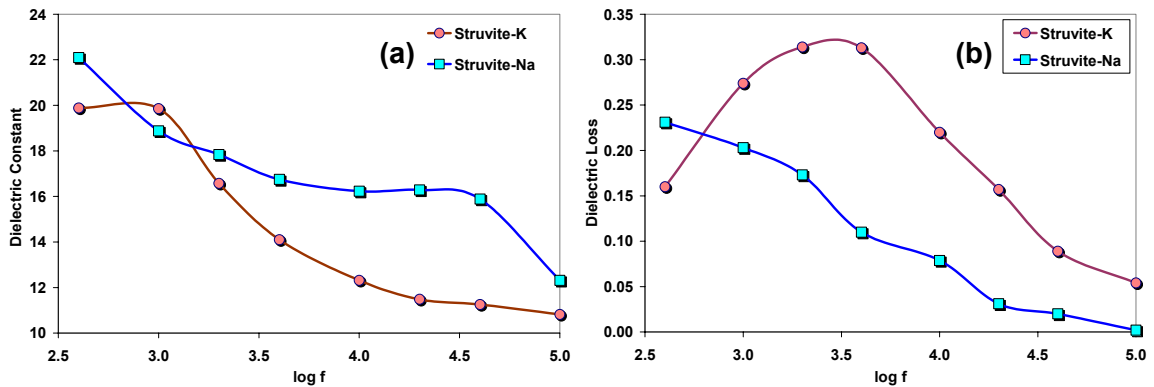


Figure : 8.19 (a) Variation in Dielectric constant and (b) Dielectric Loss with Frequency of Applied Field

Figure 8.19 (a) shows the variations in the dielectric constant of both the struvite-K and struvite-Na with the frequency of applied field from 400 Hz to 100 kHz at room temperature. The value of dielectric constant for struvite-K at 400 Hz frequency was found as 19.88, which was finally reduced to 10.82 at 100 kHz frequency of applied field. Initially, the dielectric constant remained almost constant up to 1 kHz frequency, there after it decreased rapidly with increasing frequency up to 20 kHz and then slowly decreased at higher frequency. This type of behavior indicated higher space charge polarizability of the material in the low frequency region. As the frequency increased, a point was reached where the space charge could not sustain and complied with the external field, and hence the polarization decreased and exhibited the reduction in the values of dielectric constant as frequency increased. This was discussed in detail elsewhere [49-51]. For struvite-Na the value of dielectric constant at 400 Hz frequency was found as 22.09, which was decreased rapidly initially then reduced slowly and finally reduced to 12.31 at 100 kHz frequency of applied field rapidly. It was noticed for both the struvite analog

crystals that the dielectric constant decreased with the increasing value of frequency of applied field.

It is noticed that the value of dielectric constant is maximum at lower frequencies for both the struvite-K as well as struvite-Na, since all mechanisms such as space charge, orientation, ionic and electronic polarizations are operative at lower frequencies of applied electric field. But at higher frequencies, these mechanisms cannot follow the frequency of applied electric field and hence the values of dielectric constant are low.

Figure 8.19 (b) shows the variations in the dielectric loss for both the struvite analog with the frequency of applied field. From the data of the variation of dielectric loss ($D = \tan \delta$) with frequency of applied field for struvite-K, it was surprisingly observed that dielectric loss increased up to 2 kHz and followed by decreasing nature with higher frequency, whereas in case of struvite-Na the value of dielectric loss decreased with the increasing value of frequency of applied field. Dielectric loss behaviour of struvite-K is unusual. Similar nature of dielectric loss is reported for plasticized polymer nanocomposite electrolytes by Pradhan et al [52]. Some of the possible reasons for such frequency response to dielectric loss are as under:

- (i) Such increase of dielectric loss at lower frequencies is attributed to oscillation of dipoles. Moreover, since at higher frequencies all the polarization mechanisms are not operative; hence energy need not to be spent to rotate dipoles, and consequently the dielectric loss also decreases.
- (ii) It is known that the dielectric loss is defined as ϵ'' / ϵ' . A maximum in dielectric loss at a certain frequency can be observed when ϵ' has a minimum value i.e. a minimum stored energy at that frequency.

(iii) The occurrence of peak in the frequency response of dielectric loss can be observed when the hopping frequency is approximately equal to that of the externally applied electric field, i.e., when resonance phenomena takes place.

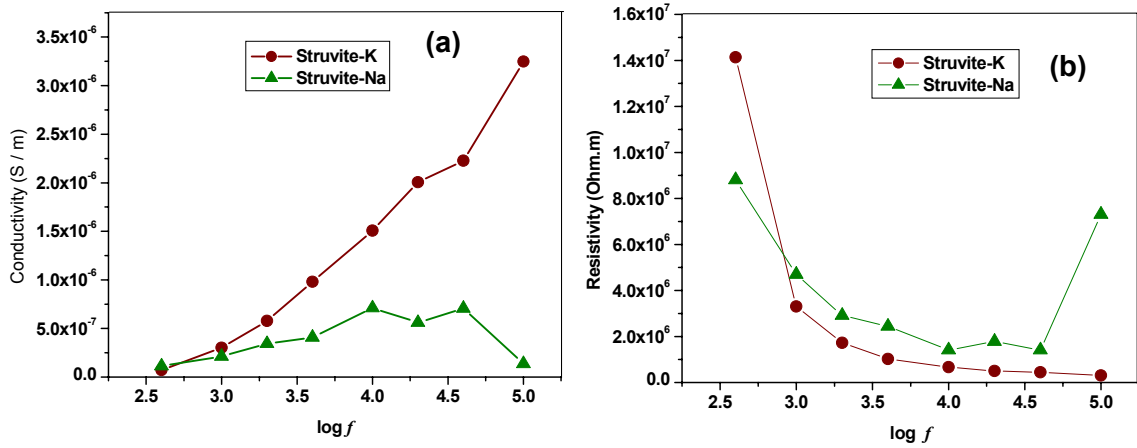


Figure : 8.20 (a) Variation in a.c. Conductivity and (b) a.c. Resistivity with Frequency of Applied Field

Figure 8.20 (a) and (b) show the nature of variation of a.c. conductivity and a.c. resistivity with frequency of applied field for both the material. It was found that for struvite-K a.c. conductivity increased and consequently the a.c. resistivity decreased with the increasing value of frequency of applied field. The frequency dependence of a.c. conductivity of struvite-K follows the Jonscher's [53] universal power law, known as "Universal Dielectric Response" (UDR).

Whereas for struvite-Na initially a.c. conductivity increased with the increasing frequency but it was reduced after 40 kHz frequency, which may be due to the mismatch of dipole frequency and applied field frequency. The a.c. resistivity of struvite-Na decreased up to 40 kHz of applied frequency followed by increasing nature.

8.8 Conclusions

1. Both the struvite analogs struvite-K and struvite-Na can be grown by using single diffusion gel growth technique.
2. Growth conditions, i.e., the SG of SMS solution, gel pH, the concentrations of reactants, etc., play important role in the growth of struvite-K as well as struvite-Na crystals.
3. The crystal morphology of both the struvite analogs was strongly dependent on growth parameters. By changing the growth parameters, struvite-K crystals with different morphologies like prismatic type, star type, rectangular platelet type, elongated platelet type, coffin-lid shaped and dendritic type can be grown. Whereas struvite-Na crystals of prismatic type, star type and dendritic type can be grown.
4. The grown struvite-K and struvite-Na crystals had transparent, translucent and opaque diaphaneity, depending upon the location and the growth conditions.
5. The phenomenon of the formation of Liesegang rings were observed in the gel growth experiments of both the struvite analogs. The numbers of formation of Liesegang rings were increased with the increasing value of the gel pH. The thickness as well as spacing between the Liesegang rings in the gel column increased with the depth.
6. The powder XRD studies confirmed the structural similarity of the grown struvite-K and struvite-Na crystals with struvite. It was found that both struvite-K and struvite-Na crystallized in the orthorhombic $Pmn2_1$ space group with unit cell parameters as follows

Struvite-K : $a = 6.893 \text{ \AA}$, $b = 6.141 \text{ \AA}$, $c = 11.222 \text{ \AA}$, $\alpha = \beta = \gamma = 90^\circ$

Struvite-Na : $a = 6.893 \text{ \AA}$, $b = 6.124 \text{ \AA}$, $c = 11.150 \text{ \AA}$, $\alpha = \beta = \gamma = 90^\circ$.

7. FTIR spectra of both the struvite analog crystals revealed the presence of functional groups. The spectra confirmed the presence of water of hydration, P – O bond and PO_4^{3-} ion and metal -oxygen bond.
8. Both the struvite-K and struvite-Na crystals were found to be thermally unstable. From the TGA curves of struvite-K and struvite-Na, it was found that these struvite analogs started dehydrating and decomposing just above the room temperature and, finally, at 600°C it became 64.14 % and 63.9 % of the original weight, respectively. A continuous loss of mass in the TGA curve depicted the simultaneous dehydration and decomposition of the material. Mass loss in a TGA analysis at temperatures above 100°C proved the association of water molecules with these crystals. From the TGA, the numbers of water molecules associated with both the crystal were estimated to be 5.
9. In the DTA curve of struvite-K, two remarkable peaks were observed. A very strong endothermic peak observed at 180°C attributed to release of crystalline water and the amount of heat change was found to be $406.75 \mu\text{Vs/mg}$ during this endothermic process. A medium exothermic peak observed at 677.8°C attributed to high temperature phase transition and the amount of heat change was found to be $-22.63 \mu\text{Vs/mg}$. Similarly in the DTA curve of struvite-Na two remarkable peaks were observed. A very strong endothermic peak observed at 183.4°C attributed to release of crystalline water and the amount of heat change was found to be $403.10 \mu\text{Vs/mg}$. A medium exothermic peak observed at 674°C attributed to high

temperature phase transition and the amount of heat change was found to be $-28.40 \mu\text{Vs/mg}$.

10. By applying the Coats-Redfern relation to the dehydration along with decomposition stage in the respective thermograms, the values of kinetic parameters were calculated. For struvite-K the values of activation energy E , frequency factor A and order of reaction n were found to be $83.21 \text{ kJ Mol}^{-1}$, 4.64×10^{10} and 2, respectively. While for struvite-Na the values of E , A and n were found to be $102.66 \text{ kJ Mol}^{-1}$, 4.17×10^{13} and 2, respectively. The high value of activation energy indicated more stable nature of struvite-Na which can also be confirmed from the thermograms.
11. The thermodynamic parameters for the dehydration and decomposition process were also evaluated for both struvite-K and struvite-Na. For both the struvite analog crystals the values of standard enthalpy of activation $\Delta^\ddagger H^\circ$ are positive, which show that the enthalpy is increasing during the process and such process is an endothermic process. Positive values of $\Delta^\ddagger G^\circ$ demonstrate that both the struvite-K and struvite-Na are thermodynamically unstable.
12. For both struvite-K and struvite-Na, the dielectric constant as well as dielectric loss was found to be dependent on the frequency of applied field at room temperature. It was noticed for both the struvite analog crystals that the dielectric constant decreased with the increasing value of frequency of applied field. For struvite-K the variation of dielectric loss increased up to 2 kHz and followed by decreasing nature with higher frequency. Such increase of dielectric loss at lower frequencies may be attributed to oscillation of dipoles as well as the matching of hopping

frequency and the frequency of the externally applied electric field. In case of struvite-Na the value of dielectric loss decreased with the increasing value of frequency of applied field.

- 13.** It was found that for struvite-K a.c. conductivity increased and consequently the a.c. resistivity decreased with the increasing value of frequency of applied field. The frequency dependence of a.c. conductivity of struvite-K follows the Jonscher's universal power law. Whereas for struvite-Na initially a.c. conductivity increased with the increasing frequency but it was reduced after 40 kHz frequency, which may be due to the mismatch of dipole frequency and applied field frequency. The a.c. resistivity of struvite-Na decreased up to 40 kHz of applied frequency followed by increasing nature.

References

1. B. Dickens, W. E. Brown, *Acta Crystallogr. B*, **25** (1972) 1159.
2. M. Weil, *Cryst. Res. Technol.*, **43** (2008) 1286.
3. M. Weil, *ChemInform*, **40** (2009). doi: 10.1002/chin.200907016.
4. E. Banks, R. Chianelli, R. Korenstein, *Inorg. Chem.*, **14** (1975) 1634.
5. H. Erdmann, P. Kothner, *Liebigs. Ann Chem.*, **294** (1896) 71.
6. R. Blachnik, T. Wiest, A. Dulmer, H. Reuter, *Z. Kristallogr.*, **212**(1997) 20.
7. M. Touaiher, M. Bettach, K. Benkhouja, M. Zahir, M. A. G. Aranda, S. Bruque, *Ann. Chim. Sci. Mat.*, **26** (2001) 49.
8. B. Bali, R. Essehli, F. Capitelli, M. Lachkar, *Acta Crystallogr.*, **61** (2005) i52.
9. C. Trobajo, M. A. Salvado, P. Pertierra, B. F. Alfonso, J. A. Blanco, S. A. Khainakov, J. R. Garcia, *Z. Anorg. Allg. Chem.*, **633** (2007) 1932.
10. G. Haferburg, G. Kloess, W. Schmitz, E. Kothe, *Chemosphere*, **72**(2008)517.
11. H. Yang, H. J. Sun, *J. Solid State Chem.*, **177** (2004) 2991.
12. H. Yang, H. J. Sun, R. T. Downs, *Am. Mineral.*, **96** (2011) 675.
13. B. Dickens, W. E. Brown, *Acta Crystallogr. B*, **28** (1972) 3056.
14. K. Angoni, J. Popp, W. Kiefe, *Spectrosc. Lett.*, **31** (1998) 1771.
15. J. D. Doyle, S. A. Parsons, *Water Res.*, **36** (2002) 3925.
16. L. Chen, Y. Shen, A. Xie, F. Huang, W. Zhang, S. Liu, *Cryst. Growth Des.*, **10** (2010) 2073.
17. S. Takagi, M. Mathew, W. E. Brown, *Acta Cryst. B*, **38** (1982) 44.
18. E. A. J. Burke, G. Ferraris, *Am. Mineral.*, **89** (2004) 1566.
19. J. E. Huheey, E. A. Keiter, R. L. Keiter, "Inorganic Chemistry", 4th Ed., Harper Collins, New York (1993).
20. M. Mathew, L. W. Schroeder, *Acta Cryst. B*, **35** (1979) 11.

21. A. Whitaker, J. W. Jeffery, *Acta Cryst. B*, **26** (1970) 1429.
22. S. Graeser, W. Postl, H. P. Bojar, P. Berlepsch, T. Armbruster, T. Raber, K. Ettinger, F. Walter, *Eur. J. Mineral.*, **20** (2008) 629.
23. J. Dunlevey, M. Laing, *South Afr. J. Sci.*, **104** (2008) 471.
24. W. D. Sun, J. Y. Wang, K. Zhang, X. Wang, *Res. Vet. Sci.*, **88** (2010) 461.
25. X. Wang, K. Huang, J. Gao, X. Shen, C. Lin, G. Zhang, *Res. Vet. Sci.*, **62** (1997) 275.
26. Z. S. Wen, X. L. Pan, Z. R. Xu, X. T. Zou, *J. Anim. Veterinary Adv.*, **10** (2011) 1383.
27. K. C. Y. Tay, B. A. Loushine, C. Oxford, R. Kapur, C. M. Primus, J. L. Gutmann, R. J. Loushine, D. H. Pashley, F. R. Tay, *J. Endod.*, **33** (2007) 1438.
28. M. Mathew, P. Kingsbury, S. Takagi, W. E. Brown, *Acta. Crystallogr. B*, **38** (1982) 40.
29. J. Alkemper, H. Fuess, *Z. Kristallogr.*, **213** (1998) 282.
30. T. Kanazawa, T. Umegaki, E. Wasai, *Gypsum Lime*, **140** (1976) 4.
31. K. C. Joseph, M. J. Joshi, *Indian J. Phys.*, **76A** (2002) 159.
32. F. A. Miller, C. H. Wilkins, *Anal. Chem.*, **24** (1952) 1253.
33. I. Gamo, *Bull. Chem. Soc. Jpn.*, **34** (1961) 760.
34. P. J. Lucchesi, W. A. Glasson, *J. Am. Chem. Soc.*, **78** (1956) 1347.
35. J. Lecomte, *J. Chim. Phys.*, **50** (1953) C53.
36. C. Duval, *Anal. Chim. Acta*, **13** (1955) 32.
37. V. C. Farmer, "Infrared spectra of minerals", Monograph No. 4, Mineral. Soc. Pub., United Kingdom, London (1974).

38. T. Kebede, K. V. Ramana, M. S. P. Rao, *Proc. Indian Acad. Sci. (Chem. Sci.)*, **113** (2001) 275.
39. M. Dhandapani, L. Thyagu, P. A. Prakash, G. Amirthaganesan, M. A. Kandhaswamy, V. Srinivasan, *Cryst. Res. Technol.*, **41** (2006) 328.
40. R. L. Frost, M. L. Weier, K. L. Erickson, *J. Therm. Anal. Calorim.*, **76** (2004) 1025.
41. K. Nakamoto, "*Infrared and Raman Spectra of Inorganic and Coordination Compounds*", 3rd ed., John Wiley & Sons, New York (1978).
42. C. M. Julien, P. Jozwiak, J. Garbarczyk, *Proc. of the Int. Workshop "Advanced Techniques for Energy Sources Investigation and Testing"*, Sofia, Bulgaria (2004).
43. R. L. Frost, M. L. Weier, W. N. Martens, D. A. Henry, S. J. Mills, *Spectrochim. Acta*, **62** (2005) 181.
44. S. K. H. Khalil, M. A. Azooz, *J. Appl. Sci. Res.*, **3** (2007) 387.
45. S. D. Ross, "*Phosphates and Other Oxy-anions of Group V*" in "*The Infrared Spectra of Minerals*", Ed. V. C. Farmer, London, (1974).
46. H. Saidou, S. B. Moussa, M. B. Amor, *Environ. Technol.*, **30** (2009) 75.
47. A. W. Coats, J. P. Redfern, *Nature*, **201** (1964) 68.
48. K. J. Laidler, "*Chemical Kinetics*", 3rd Ed., Harper and Row, New York (1987).
49. R. M. Dabhi, B. B. Parekh, M. J. Joshi, *Indian J. Phys.*, **79** (2005) 503.
50. S. K. Arora, V. Patel, B. Amin, A. Kothari, *Bull. Mater. Sci.*, **27** (2004) 141.
51. F. M. Reicha, M. El-Hiti, A. El-Sonabati, M. Diab, *J. Phys. D*, **24** (1991) 369.
52. D. K. Pradhan, R. N. P. Choudhary, B. K. Samantaray, *Int. J. Electrochem. Sci.*, **3** (2008) 597.
53. A. K. Jonscher, *Nature*, **253** (1975) 717.

Chapter IX

Conclusions

Topic Number	Topic	Page Number
9.1	Introduction	399
9.2	General Conclusions	401
9.3	Scope of the Future Work	409

9.1 Introduction

Biom mineralization or Biocrystallization is the formation of minerals by living organisms, which is quite common in the world of living being and occurs in single-celled organisms to complex multi-cellular plants and animals. Biom mineralization can be defined as the process by which mineral crystals are deposited in an organized fashion in the matrix, either cellular or extracellular, of living organisms [1]. In Biom mineralization, the formation of inorganic crystalline structures takes place in association with biological macromolecules. Biom mineralization is a hot topic in the area of materials science, which can be described as the widespread and fascinating process by which living organisms produce inorganic phases like carbonates, phosphates, oxalates, silicates, sulfates, oxides, etc. [2] In this process, a living organism provides a chemical and physical environment that controls the nucleation and growth of a unique mineral phase. Since biom mineralization seems to be an important phenomenon in topics ranging from space science to medicine, from biology to geology, and every aspect of life, additional focused research is required. Biom mineralization in humans is a physiological process regulated by interactions of minerals and organic extracellular molecules. The study of synthetic minerals in simplified solution lays the foundation for an understanding of mineralization processes in more complex environments found in the body. Mineral analysis using various modern techniques provides insights into the mechanism of biom mineralization [3].

Biom mineralization is helpful to living organisms when it occurs in the correct location in the body, but often this process occurs in the wrong place at the wrong time (bad biom mineralization..!). Humans need biom mineralization

for the formation of bone, teeth, otoconia (also known as otoliths - tiny calcium carbonate crystals within the utricle and saccule of the inner ear that are critical for the perception of gravity, linear acceleration and necessary to maintain normal balance) etc., but unfortunately, the body also produces various harmful biominerals (as listed in chapter II) responsible for kidney stones in the urinary system; basic calcium phosphate (BCP), calcium pyrophosphate dihydrate (CPPD), monosodium urate (MSU) crystals responsible for rheumatic diseases like arthritis, uric acid responsible for gout etc.

The better and higher quality of life of individual as well as the society depends on the physical health of the individual, which requires rigorous and extensive research work related to the various diseases, their cost effective medical management as well as precautionary measures. Urolithiasis is one of such diseases, which requires better attention. For a better understanding of formation of urinary type crystals, its effective medical management including diagnosis, treatment and its possible prevention, a more systematic physical chemical study of urinary type crystals is needed. Inhibitors of biocrystallization are of interest in drug design efforts against urolithiasis.

In order to contribute to the present knowledge regarding urinary type struvite crystals, the present author have put his humble efforts to study some of the aspects related to struvite crystals as it has been already discussed in the present thesis.

9.2 General Conclusions

The summary of the study carried out by the present author on the growth and characterization studies of struvite and related struvite family crystals are as follows :

1. Struvite crystals can be grown by single diffusion gel growth technique. Growth conditions played important role in the growth of crystals.
2. The crystal morphology of struvite was strongly dependent on growth parameters. By changing the growth parameters, struvite crystals with different morphologies like prismatic type, pyramidal type, star type, rectangular platelet type, elongated platelet type, needle type, coffin-lid shaped and dendritic type can be grown.
3. The grown struvite crystals had transparent, translucent and opaque diaphaneity, depending upon the location and the growth conditions. Fine transparent prismatic type struvite crystals with optimum apparent size were observed only for the growth parameters as SMS of SG 1.04, 1.0 M ADP, 1.0 M SS with 7.0 pH value of the gel.
4. The powder XRD studies confirmed the structural identity of the grown struvite crystals. It was found that struvite crystallized in the orthorhombic $Pmn2_1$ space group with unit cell parameters as $a = 6.954 \text{ \AA}$, $b = 6.140 \text{ \AA}$, $c = 11.216 \text{ \AA}$ and $\alpha = \beta = \gamma = 90^\circ$, which are closely matching with previously reported values. Every unit cell comprises of two molecules.
5. FTIR spectrum of the struvite crystals revealed the presence of functional groups. The spectrum confirmed the presence of water of hydration, N – H bond, P – O bond, NH_4^+ ion and PO_4^{3-} ion and metal -oxygen bond.

6. The struvite crystals were found to be thermally unstable from thermal studies. From the TGA, the number of water molecules associated with the crystal was estimated to be 5.
7. In the DTA curve of struvite two remarkable peaks were observed. A very strong endothermic peak observed at 192.1 °C attributed to release of crystalline water along with ammonia. A medium exothermic peak observed at 674.7 °C attributed to high temperature phase transition.
8. The DSC curve of struvite exhibited peaks at the same temperatures as peaks were obtained in DTA curve.
9. By applying the Coats and Redfern relation to the dehydration along with decomposition stage in the thermogram of struvite, the values of kinetic parameters were calculated.
10. The thermodynamic parameters for the dehydration and decomposition process of struvite were also evaluated. The process is non-spontaneous and endothermic. Struvite is thermodynamically unstable.
11. For struvite, the dielectric constant as well as dielectric loss was found to be dependent on the frequency of applied field at room temperature. It was noticed both the dielectric constant and dielectric loss were found to be decreased with the increasing value of frequency of applied field. It was found that a.c. conductivity increased whereas the a.c. resistivity decreased with the increasing value of frequency of applied field.
12. In the *in vitro* growth inhibition studies of struvite crystals, comparative lower values of growth rate, reductions in the growth rates with the increasing concentrations of extracts as well as the reduction in the growth rates with the time proved the inhibitory effect of all the three evaluated

extracts, i.e. *Boerhaavia diffusa* Linn, *Commiphora wightii* and *Rotula aquatica* Lour.

13. Significant percentage of inhibition of growing struvite crystals at gel – liquid interface at the end of first day was noticed in each of the herbal extracts, clearly demonstrating the inhibitory effect of all the three extracts used for the investigation. The maximum percentage of inhibition 46.16 % was observed for 1.0 % *R. aquatica* extract, where as minimum 13.33 % of inhibition was observed for 0.5 % of *B. diffusa* extract.
14. Dissolution rates of struvite crystals for all the cases with the herbal extracts were found remarkably higher than that of control solution.
15. The dendritic type struvite crystals grown at the gel – liquid interface were found to be dissolved completely within 21 to 40 days in all the cases with herbal extract. Minimum 21 days were required for the complete dissolution for 1.0 % *B. diffusa*.
16. From the analysis of growth and dissolution rates of struvite crystal, it was found that extracts of *R. aquatica* have retarded the growth rate from the very beginning of the crystal growth, whereas extracts of *B. diffusa* have speed up the dissolution rates once the growth of the crystals took place.
17. All the extracts impeded the diffusion process of reactants occurring in the gel column for the nucleation and, subsequently, the growth of struvite crystals. The reduction in depths of growth indicated the inhibition offered by all the three herbal extracts.
18. Growth rates as well as the apparent size of the struvite crystals grown at the higher depths were lower for all the cases with herbal extracts.

19. The remarkable phenomenon of fragmentation of the grown struvite crystals was observed for all the three tested herbal extracts. The average length of crystals after fragmentation was found even less than 1 mm.
20. Both the total mass and volume of the grown struvite crystals were considerably lower for the cases with extracts depicting the inhibitory effect of all the evaluated herbal extracts. The least mass and volume observed for 1.0 % *C. wightii*.
21. As the concentration of the juice of *Citrus medica* Linn was increased in the SS, the number of grown struvite crystals in the gel medium decreased and also average size of the struvite crystals decreased.
22. Lower values of growth rate in comparison to control case, reductions in dimension as well as the growth rates with the increasing concentrations of juice, and the reduction in the growth rates with the time evidently proved the inhibitory effectiveness of the juice on struvite.
23. Struvite crystals could not either nucleate or grow at the gel–liquid interface for the higher concentration of juice in the SS, which significantly proved the inhibitory potency of the *Citrus medica* Linn juice.
24. Enhanced dissolution rates for struvite crystals were observed for all the concentration with the *Citrus medica* Linn juice.
25. All the struvite crystals grown in the gel were found to be dissolved completely within 15 to 55 days in all the cases with juice. Moreover, reduction in the number of days required for the complete dissolution with the increasing concentration of juice undoubtedly proved the potency of inhibition of struvite crystals.

26. From this *in vitro* growth inhibition study of struvite crystals, it can be concluded that all the investigated herbal extracts i.e. *B. diffusa*, *C. wightii* and *R. aquatica*, and the juice of *Citrus medica* Linn are found to be potent inhibitors for struvite crystals.
27. The Vickers micro-hardness number H_V was found to be load dependent and phenomenon of reverse ISE was observed for struvite crystals.
28. The measured Vickers micro-hardness number H_V for struvite was seen to vary in increasing order from 7.33 kg/mm² (71.91 MPa) to 45.40 kg/mm² (445.23 MPa), with certain variations, over the increasing indenting load range from 0.005 to 0.125 kg.
29. Analysis of the experimental data on hardness as a function of indentation size from the standpoint of Kick's Law, Hays-Kendall's model and the proportional specimen resistance model revealed that these models satisfactorily explain the reverse ISE phenomena observed in the *in vitro* gel grown urinary type struvite crystals.
30. The values of load independent Vickers micro-hardness H_0 for struvite were obtained as 40.18 kg/mm² (\approx 394.05 MPa) and 51.72 kg/mm² (\approx 507.22 MPa) according to Hays-Kendall's model and the PSR model, respectively. The difference in the values may be due to different approaches as well as mathematical treatments in these models.
31. This study of Vickers micro-hardness and related mechanical properties for gel grown struvite crystals may provide useful information for the fragmentation of the struvite type urinary calculi by using appropriate parameters in ESWL management without causing any damage to the kidney and urinary tract.

- 32.** Citric acid as an etchant produced triangular etch pits on as grown (1 1 1) surface of the prismatic type struvite crystals.
- 33.** The values kinetic parameters - activation energy of the reaction E and frequency factor A were found as $30.267 \text{ kJ Mol}^{-1}$ and 0.4972 , respectively for etching process on struvite crystals.
- 34.** The values of standard enthalpy of activation $\Delta^\ddagger H^\circ$ and standard internal energy of activation $\Delta^\ddagger U^\circ$ during the etching process were found to be positive and have decreasing nature with the increasing etching temperature. The positive value of $\Delta^\ddagger H^\circ$ explained etching process as an endothermic process, where as negative values of $\Delta^\ddagger S^\circ$ proved that the etching process was non-spontaneous.
- 35.** Both the struvite analogs struvite-K and struvite-Na can be grown by using single diffusion gel growth technique. Growth conditions played important role in the growth of struvite-K as well as struvite-Na crystals.
- 36.** The crystal morphology of both the struvite analogs was strongly dependent on growth parameters. By changing the growth parameters, struvite-K crystals with different morphologies like prismatic type, star type, rectangular platelet type, elongated platelet type, coffin-lid shaped and dendritic type can be grown. Whereas struvite-Na crystals of prismatic type, star type and dendritic type can be grown.
- 37.** The grown struvite-K and struvite-Na crystals had transparent, translucent and opaque diaphaneity, depending upon the location and the growth conditions.
- 38.** The phenomenon of the formation of Liesegang rings were observed in the gel growth experiments of both the struvite analogs. The numbers of

formation of Liesegang rings were increased with the increasing value of the gel pH. The thickness as well as spacing between the Liesegang rings in the gel column increased with the depth.

- 39.** The powder XRD studies confirmed the structural similarity of the grown struvite-K and struvite-Na crystals with struvite. It was found that both the struvite analogs crystallized in the orthorhombic $Pmn2_1$ space group with unit cell parameters as follows

Struvite-K : $a = 6.893 \text{ \AA}$, $b = 6.141 \text{ \AA}$, $c = 11.222 \text{ \AA}$, $\alpha = \beta = \gamma = 90^\circ$

Struvite-Na : $a = 6.893 \text{ \AA}$, $b = 6.124 \text{ \AA}$, $c = 11.150 \text{ \AA}$, $\alpha = \beta = \gamma = 90^\circ$.

- 40.** FTIR spectra of both the struvite analog crystals revealed the presence of functional groups. The spectra confirmed the presence of water of hydration, P – O bond and PO_4^{3-} ion and metal -oxygen bond.
- 41.** Both the struvite-K and struvite-Na crystals were found to be thermally unstable. Mass loss in a TGA analysis at temperatures above 100°C proved the association of water molecules with these crystals. From the TGA, the numbers of water molecules associated with both the crystal were estimated to be 5.
- 42.** In the DTA curve of struvite-K two remarkable peaks were observed. A very strong endothermic peak observed at 180°C attributed to release of crystalline water. A medium exothermic peak observed at 677.8°C attributed to high temperature phase transition. Similarly in the DTA curve of struvite-Na two remarkable peaks were observed. A very strong endothermic peak observed at 183.4°C attributed to release of crystalline water. A medium exothermic peak observed at 674°C attributed to high temperature phase transition.

- 43.** By applying the Coats-Redfern relation to the dehydration along with decomposition stage in the thermograms of respective struvite analogs, the values of kinetic parameters were calculated.
- 44.** The thermodynamic parameters for the dehydration and decomposition process were also evaluated for both struvite-K and struvite-Na. For both the struvite analog crystals the values of standard enthalpy of activation $\Delta^\ddagger H^\circ$ are positive, which show that the enthalpy is increasing during the process and such process is an endothermic process. Positive values of $\Delta^\ddagger G^\circ$ demonstrate that both the struvite-K and struvite-Na are thermodynamically unstable.
- 45.** For both struvite-K and struvite-Na, the dielectric constant as well as dielectric loss was found to be dependent on the frequency of applied field at room temperature. It was noticed for both the struvite analog crystals that the dielectric constant decreased with the increasing value of frequency of applied field. For struvite-K the variation of dielectric loss increased up to 2 kHz and followed by decreasing nature with higher frequency. Such increase of dielectric loss at lower frequencies may be attributed to oscillation of dipoles as well as the matching of hopping frequency and the frequency of the externally applied electric field. In case of struvite-Na the value of dielectric loss decreased with the increasing value of frequency of applied field.
- 46.** It was found that for the struvite-K a.c. conductivity increased and consequently the a.c. resistivity decreased with the increasing value of frequency of applied field. The frequency dependence of a.c. conductivity of struvite-K follows the Jonscher's universal power law. Whereas for

struvite-Na initially a.c. conductivity increased with the increasing frequency but it was reduced after 40 kHz frequency, which may be due to the mismatch of dipole frequency and applied field frequency. The a.c. resistivity of struvite-Na decreased up to 40 kHz of applied frequency followed by increasing nature.

9.3 Scope of the Future Work

The future work in continuation to the present work may be pursued as follows:

1. It will be exciting to carry out the studies to grow micro and nano crystalline form of struvite and related crystals.
2. In the continuation of growth inhibition studies, it is also required to apply the results of the growth inhibition studies of all the investigated herbal extracts i.e. *B. diffusa*, *C. wightii* and *R. aquatica* on animal model and check the *in vivo* inhibitory potency of extracts.
3. It is necessary to go for design effective “green antilithic drug” based on medicinal herbal plants.
4. It will be intriguing to go for multi-technique spectroscopic investigations by Raman, infrared absorption, X-ray photoelectron spectroscopy (XPS), and photoluminescence to have insight on the effects of the investigated herbal extracts on the growth inhibition of struvite crystals.
5. It will be fascinating to explore the micro crystal growth technique to struvite crystals and apply it to *in vitro* the growth inhibition study.
6. It will be also interesting to compare the properties of pure synthetic struvite crystals grown in laboratory, struvite crystals grown in nature and the struvite stones removed surgically from the patients.
7. One can study for micro-hardness studies of struvite-K and struvite-Na.

8. It may be also enthralling to carry out growth and characterization studies of other struvite related crystals.
9. It will be also interesting to study the surface of struvite crystals using AFM after removal from growth inhibition experiments using various herbal extracts.
10. To develop a dynamical model for crystal growth, where the continuous flow of nutrients is available alike the urinary system.

References

1. A. L. Boskey, *J. Cell. Biochem.*, **72** (1998) 83.
2. A. Sigel, H. Sigel, R. K. Sigel (Eds), "*Biom mineralization: From Nature to Application*", Series : "*Metal Ions in Life Sciences*", Vol. 4, Wiley, Chichester (2008).
3. A. L. Boskey, *Calcif. Tissue Int.*, **72** (2003) 533.

Annexure : 1 : Research Paper Publication

1. **“Growth and characterization of Struvite crystals”**
Chetan K. Chauhan, K. C. Joseph, B. B. Parekh, M. J. Joshi
National Journal : Indian Journal of Pure & Applied Physics
Volume 46, July 2008, Page No. 507-512.

2. **“Growth inhibition of Struvite crystals in the presence of juice of Citrus medica Linn.”**
C. K. Chauhan, M. J. Joshi
International Journal : Urological Research
Volume 36, Issue 5, October, 2008, Page No. 265-273.
DOI No: 10.1007/s00240-008-0154-4
URL : <http://www.springerlink.com/content/w262602060150x00/fulltext.pdf>

3. **“Growth inhibition of Struvite crystals in the presence of herbal extract Commiphora wightii”**
C. K. Chauhan, M. J. Joshi, A. D. B. Vaidya
International Journal : Journal of Materials Science: Materials in Medicine
Volume 20 (Supplement 1), December 2009, Page No. 85-92
DOI No: 10.1007/s10856-008-3489-z
URL : <http://www.springerlink.com/content/frt22817108181wx/>

4. **“Growth Inhibition of Struvite Crystals in the presence of Herbal extract Boerhaavia diffusa Linn.”**
C. K. Chauhan, M. J. Joshi, A. D. B. Vaidya
International Journal : American Journal of Infectious Diseases
Volume 5, Issue 3, 2009, Page No. 170-179.
ISSN 1553-6203.
URL : <http://scipub.org/fulltext/ajid/ajid53170-179.pdf>

5. **“Growth and Characterization of Bis-Thiourea Strontium Chloride Single Crystals”**
R. R. Hajiyani, D. J. Dave, **C. K. Chauhan**, P. M. Vyas, M. J. Joshi
International Journal : Modern Physics Letters B
Volume 24, Issue 8, March 2010, Page No. 735-747.
DOI No: 10.1142/S0217984910022810

6. “Growth and characterization of Struvite-K crystals”

C. K. Chauhan, P. M. Vyas, M. J. Joshi

International Journal : Crystal Research and Technology

Volume 46, Issue 2, February 2011, Page No. 187–194.

DOI No: 10.1002/crat.201000587

URL : <http://www.crystalresearch.com/crt/ab46/ab460187.html>

7. “Growth Inhibition of Struvite Crystals in the Presence of Herbal Extract *Rotula aquatica Lour*”

C. K. Chauhan, M. J. Joshi, A. D. B. Vaidya

National Journal : Indian Journal of Biochemistry and Biophysics.

Volume 48, Issue 3, June 2011, Page No. 202 – 207.

ISSN: 0975-0959 (Online); 0301-1208 (Print)

URL:<http://nopr.niscair.res.in/bitstream/123456789/11990/1/IJBB%2048%283%29%20202-207.pdf>

8. “Growth, FT-IR Spectroscopy, Thermogravimetry and Chemical Etching Studies of Potassium Pentaborate Crystals”

Hirenkumar S. Jani, Poorvesh M. Vyas, Sonal R. Vasant, Kashmira P. Tank, **Chetan K. Chauhan**, B. B. Parekh and M. J. Joshi

Proceedings of XV National Seminar on Crystal Growth, PSNCET, Tirunelveli.
NSCG 2011 – 152 (23-25 February 2011)

9. “Struvite Crystals : A Brief Review of Mineral Properties, Bio-mineralization in Urinary Calculi, Crystal Growth and Growth Inhibition Studies”

C. K. Chauhan

VAK, Saurashtra University Publication.

Volume 4, 2009, Page No. 114 – 141

10. “In Vitro Crystallization, Characterization and Growth-Inhibition Study of Urinary Type Struvite Crystals”

C. K. Chauhan, M. J. Joshi

International Journal : Journal of Crystal Growth

Communicated.

Annexure : 2
Research Paper Presented at
International and National Level Conferences

1. ***“Growth Inhibition of Struvite crystals in the presence of the juice of Citrus medica Linn”***

Chetan K. Chauhan, R. M. Vaishnav, L. K. Maniar, Poorvesh Vyas,
Kashmira Tank, Dhaval Khunti and M. J. Joshi

11th NSCG – 11th National Seminar on Crystal Growth – 2006
(With International Participation)

SSN College of Engineering, SSN Nagar, Kalavakkam, Tamil Nadu, India
7 – 9 December, 2006.

2. ***“Micro-hardness Study of Struvite”***

Chetan K. Chauhan and M. J. Joshi

National Seminar on Recent Trends in Materials Science,
Department of Physics, Saurashtra University, Rajkot, India
25th March, 2007.

3. ***“Dielectric Study of Mixed Crystals of Mn-Fe-Co Tartrate”***

Kashmira P. Tank, S. J. Joshi, B. B. Parekh, **C. K. Chauhan**, M. J. Joshi

National Seminar on Recent Trends in Materials Science,
Department of Physics, Saurashtra University, Rajkot, India
25th March, 2007.

4. ***“Growth Inhibition of Struvite Crystals in the presence of Herbal extract Roulta Aquqtica Lour”***

C. K. Chauhan, M. J. Joshi, A. D. B. Vaidya

15th ICCG – International Conference on Crystal Growth – 2007

Salt Lake City, Utah, USA. (Presented by M. J. Joshi)

12 – 17 August, 2007.

5. ***“Growth Inhibition of Struvite crystals in the presence of Herbal extract Commiphora Wightii”***

C. K. Chauhan, M. J. Joshi, A. D. B. Vaidya

IUMRS–ICAM– 2007 (International Conference on Advanced Materials – 2007)

Hotel Grand Ashok, Bangalore, India

8 – 13 October, 2007.

6. **“Growth Inhibition of Struvite Crystals in the presence of Herbal extract *Boerhaavia diffusa* Linn.”**

C. K. Chauhan, M. J. Joshi, A. D. B. Vaidya

MolMed – 2009 : International Conference on Molecular Medicine – 2009
IIT – Madras, Chennai.
18 – 20 January, 2009.

7. **“Vickers Micro-hardness Study of Urinary Type Struvite Crystals”**

C. K. Chauhan, M. J. Joshi

ICMAT – 2009 : International Conference on Materials for Advanced Technologies - 2009
Suntec City, Singapore
28 June to 3 July 2009.

8. **“Growth and Characterization of Potassium Magnesium Phosphate Crystals”**

C. K. Chauhan, M. J. Joshi

16th ICCG – 2010 : 16th International Conference on Crystal Growth – 2010
Beijing, China
8 – 13 August, 2010.

9. **“Growth, Powder XRD, Thermal and Dielectric Studies of Cholesterol Crystals”**

Poorvesh M. Vyas, S. R. Vasant, **Chetan K. Chauhan**, H. S. Joshi, M. J. Joshi
39th NSC-2010 : 39th National Seminar on Crystallography – 2010
Department of Physics, University of Jammu, Jammu
25 – 27 October, 2010.

10. **“Synthesis and Characterization of *n*-Butyl 4-(3,4-dimethoxyphenyl –6-methyl –2-thioxo–1,2,3,4 tetrahydropyrimidine–5– carboxylate nanoparticles using w/o microemulsion technique”**

Poorvesh M. Vyas, Akshay M. Pansuriya, Yogesh T. Naliapara, **Chetan K. Chauhan** and Mihir J. Joshi

15th ISCB International Conference – 2011 : “Bridging Gaps in Discovery and Development: Chemical and Biological Sciences for Affordable Health, Wellness and Sustainability”
Department of Chemistry, Saurashtra University, Rajkot and Indian Society of Chemists & Biologists, Lucknow
The Grand Bhagwati Hotel, Rajkot
4 – 7 February, 2011.

11. “Growth, FT-IR Spectroscopy, Thermogravimetry and Chemical Etching Studies of Potassium Pentaborate Crystals”

Hirenkumar S. Jani, Poorvesh M. Vyas, Sonal R. Vasant, Kashmira P. Tank, **Chetan K. Chauhan**, B. B. Parekh and M. J. Joshi

15th National Seminar on Crystal Growth – 2011

PSN College of Engineering and Technology, Tirunelveli

23 – 25 February, 2011.

12. “In Vitro Crystallization, Characterization and Growth-Inhibition Study of Urinary Type Struvite Crystals”

Chetan K. Chauhan (*Invited Talk*)

ICMAT – 2011 : International Conference on Materials for Advanced Technologies - 2011

Suntec City, Singapore

26 June to 1 July 2011.